Design, Synthesis and Characterisation of Inhibitors of 3-Deoxy-D-*arabino*-Heptulosonate 7-Phosphate Synthase

A thesis

submitted in partial fulfilment

of the requirements for the degree

of

Doctor of Philosophy in Chemistry

at the

University of Canterbury

by

Scott Raymond Walker

UNIVERSITY OF CANTERBURY
Te Whare Wānanga o Waitaha
CHRISTCHURCH NEW ZEALAND

December 2007

Acknowledgments

I would like to thank my supervisor Emily Parker; from my earliest days in the lab you were always ready to give me independence when I wanted it, and a hand up when I needed it. Over four years and many litres of coffee, I have learnt volumes about chemistry, academia and life in general.

I would like to acknowledge the helpful discussions I have had with other staff members through the years, both at Massey and Canterbury. Thanks particularly to Pat Edwards for always being happy to share your knowledge of NMR spectroscopy, and Geoff Jameson for helping me understand the finer points of X-ray crystallography.

Thanks must also go to the various agencies that have provided me with financial support; to Massey University for a Vice-Chancellors Doctoral Scholarship and the University of Canterbury for a Canterbury Doctoral Scholarship. Thanks also to the Royal Society of New Zealand and the New Zealand Institute of Chemistry for providing financial help with travel to conferences here and abroad.

Thanks to all of my labmates over the years; especially Matthias, Ben, Celia, Leonardo (Massey), Aidan, Hemi, Muscroft and Sarah (Canterbury). Having people to laugh with makes the lab a great place to be. Big thanks also to Linley and Fiona (Massey) for keeping the freezer stocked with enzymes, and Marie (Canterbury) for helping me out with your magical mass-spec powers.

Thanks also to my family, for always being supportive of me throughout my time at university. Finally, thanks to Alice for always being there for support and companionship, whether we are separated by a few metres or hundreds of kilometres. Having you around has made these years all the more worthwhile.

Abstract

The enzyme 3-deoxy D-*arabino*-heptulosonate 7-phosphate (DAH7P) synthase catalyses the first step of the shikimate pathway. This pathway lies at the heart of bacterial metabolism, and is responsible for the synthesis of a variety of compounds essential to the chemistry of life; from the aromatic amino acids phenylalanine, tyrosine and tryptophan, to a number of aromatic and non-aromatic natural products.

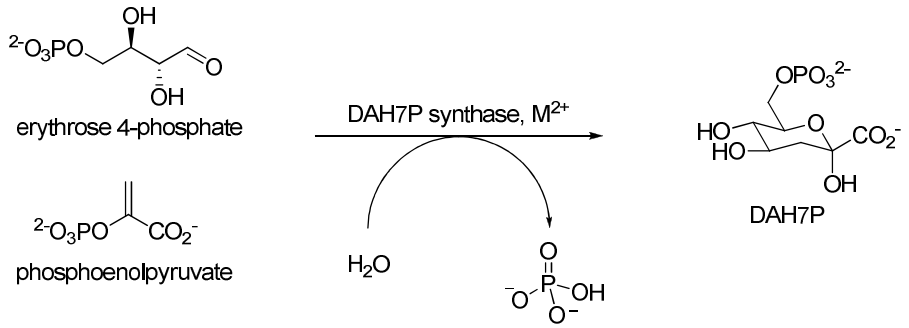

This thesis describes the design, synthesis and evaluation of inhibitors of DAH7P synthase. These inhibitors exploit a variety of strategies to interrupt the activity of DAH7P synthase, ranging from simple substrate mimicry to inhibitors that mimic unstable reaction intermediates; inhibitors that exploit metal coordination and entropic effects, and inhibitors that gain improved potency by interacting with multiple sites.

In Chapter Two, the synthesis of a mimic for a proposed unstable reaction intermediate is described, and its interaction with DAH7P synthase characterised. The compound was prepared in twelve steps from D-arabinose, and was found to be a slow-tight binding inhibitor of *Escherichia coli* DAH7P synthase.

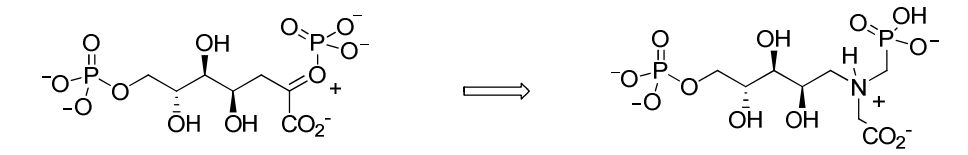

proposed DAH7P synthase intermediate *slow-tight DAH7P synthase inhibitor*

In Chapter Three, a number of compounds are prepared that were designed to bind to the phosphoenolpyruvate subsite of the DAH7P synthase active site. The binding of these compounds to the enzyme is investigated in order to gain an understanding of

the factors involved in DAH7P synthase inhibition. The enantiomeric phospholactates were prepared, and the extent of inhibition of *E. coli* DAH7P synthase was shown to be dependent on compound chirality. Several other phosphoenolpyruvate-like molecules were prepared, and were also shown to be effective DAH7P synthase inhibitors.

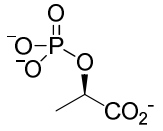

(*R*)-phospholactate
K_i: 49 ± 8 μM

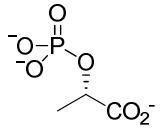

(*S*)-phospholactate
K_i: 670 ± 120 μM

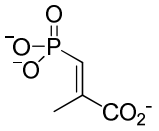

(*E*)-2-methyl-3-phosphonatoacrylate
K_i: 4.7 ± 0.7 μM

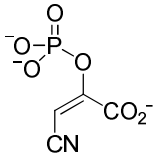

(*E*)-cyanophosphoenopyruvate
K_i: ≤75± 25 μM

In Chapter Four extended compounds are designed that will bind the enzyme by multiple interactions at both substrate binding sites. Four compounds were prepared, and an increase in inhibitory potency was observed.

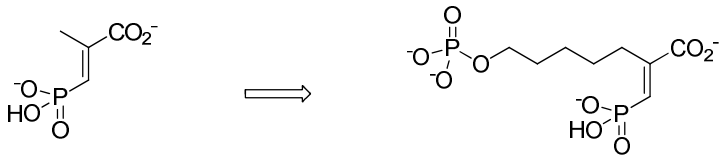

K_i: 4.7 ± 0.7 μM

K_i: ~2.5 μM

In Chapter Five computational techniques are explored to aid the interpretation of the inhibition of DAH7P synthase by the compounds prepared in these studies. Several approaches for more potent inhibition of this enzyme are outlined and discussed.

Table of Contents

Chapter Four Novel, Dual-Site Inhibitors of DAH7P synthase

Chapter Five: Discussion, Modelling and Future Directions

Chapter Six: Experimental

Abbreviations

A5P:	arabinose 5-phosphate
Ac:	acetyl
AEC:	anion exchange chromatography
aq:	aqueous
Bn:	benzyl
BTP:	1,3-bis(tris(hydroxymethyl)methylamino)propane
COSY:	correlation spectroscopy
Cy:	cyclohexyl
DABCO:	1,4-diazabicyclo[2.2.2]octane
DAH7P:	3-deoxy D-*arabino*heptulosonate 7-phosphate
DBU:	1,8-diazabicyclo[5.4.0]undec-7-ene
DEAD:	diethyl azodicarboxylate
DEPT:	distortionless enhancement by polarisation transfer
DIBAL:	diisobutylaluminium hydride
DMAP:	4-(dimethylamino)pyridine
DMSO:	dimethylsulfoxide
E4P:	erythrose 4-phosphate
EI:	electron impact ionisation
ESI:	electrospray ionisation
Et:	ethyl
FAB:	fast atom bombardment ionisation
GI:	Grubbs first generation catalyst
GII:	Grubbs second generation catalyst
HGI:	Hoveyda-Grubbs first generation catalyst
HGII:	Hoveyda-Grubbs second generation catalyst
HMQC:	heteronuclear multiple quantum coherence
HRMS:	high resolution mass spectrometry
HSQC:	heteronuclear single quantum coherence
HWE:	Horner-Wadsworth-Emmons
IBX:	2-iodoxybenzoic acid
Im:	imidazole

*i*Pr:	isopropyl
k_{cat}:	turnover number
KDO8P:	3-deoxy D-*manno* 2-octulosonate 8-phosphate
K_i:	inhibition constant
K_m:	Michealis constant
LDA:	lithium di(isopropyl)amide
Me:	methyl
NaHMDS:	sodium bis(trimethylsilyl)amide
NBS:	*N*-bromosuccinimide
NMO:	*N*-methylmorpholine *N*-oxide
NMR:	nuclear magnetic resonance
NOESY:	nuclear Overhauser effect spectroscopy
PEP:	phosphoenolpyruvate
Ph:	phenyl
ppm:	parts per million
Py:	pyridine
SEP:	sulfoenolpyruvate
TBAF:	tetrabutylammonium fluoride
TBDMS:	*tert*-butyl dimethyl silyl
TBDPS:	*tert*-butyl diphenyl silyl
Tf:	triflate
THF:	tetrahydrofuran
THP:	tetrahydropyranyl
TLC:	thin layer chromatography
TMS:	trimethylsilyl
TOCSY:	total correlation spectroscopy

Amino acid one-letter codes

A	alanine	E	glutamate	L	leucine	S	serine
R	arginine	Q	glutamine	K	lysine	T	threonine
N	asparagine	G	glycine	M	methionine	W	tryptophan
D	aspartate	H	histidine	F	phenylalanine	Y	tyrosine
C	cysteine	I	isoleucine	P	proline	V	valine

Chapter One: Introduction

1.1 The shikimate pathway

The shikimate pathway is a biosynthetic pathway responsible for producing a variety of organic compounds necessary for life. The pathway converts D-erythrose 4-phosphate (E4P), a product of the pentose phosphate pathway, and two molecules of phosphoenolpyruvate (PEP) to chorismate (Figure 1.1).[1]

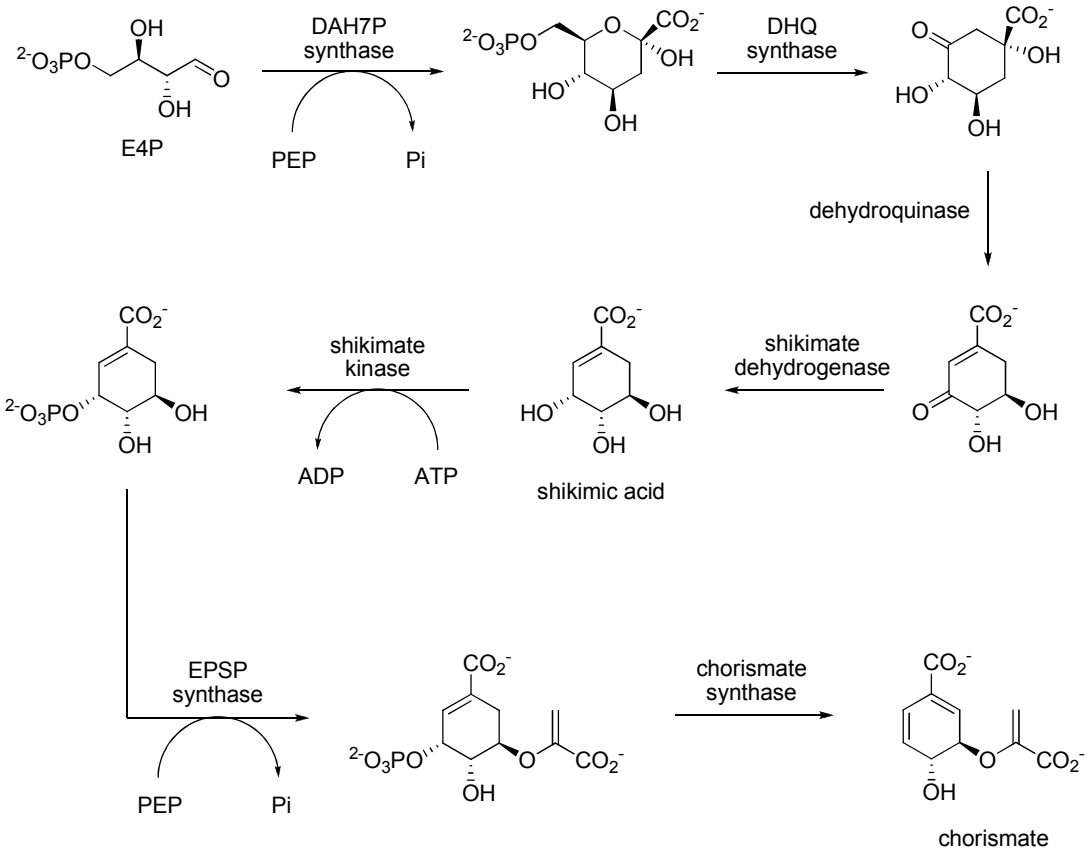

Figure 1.1 The shikimate pathway, and a selection of downstream products

Chorismate is at a metabolic branch point, and is converted into a variety of compounds of utility in the cell (Figure 1.2).

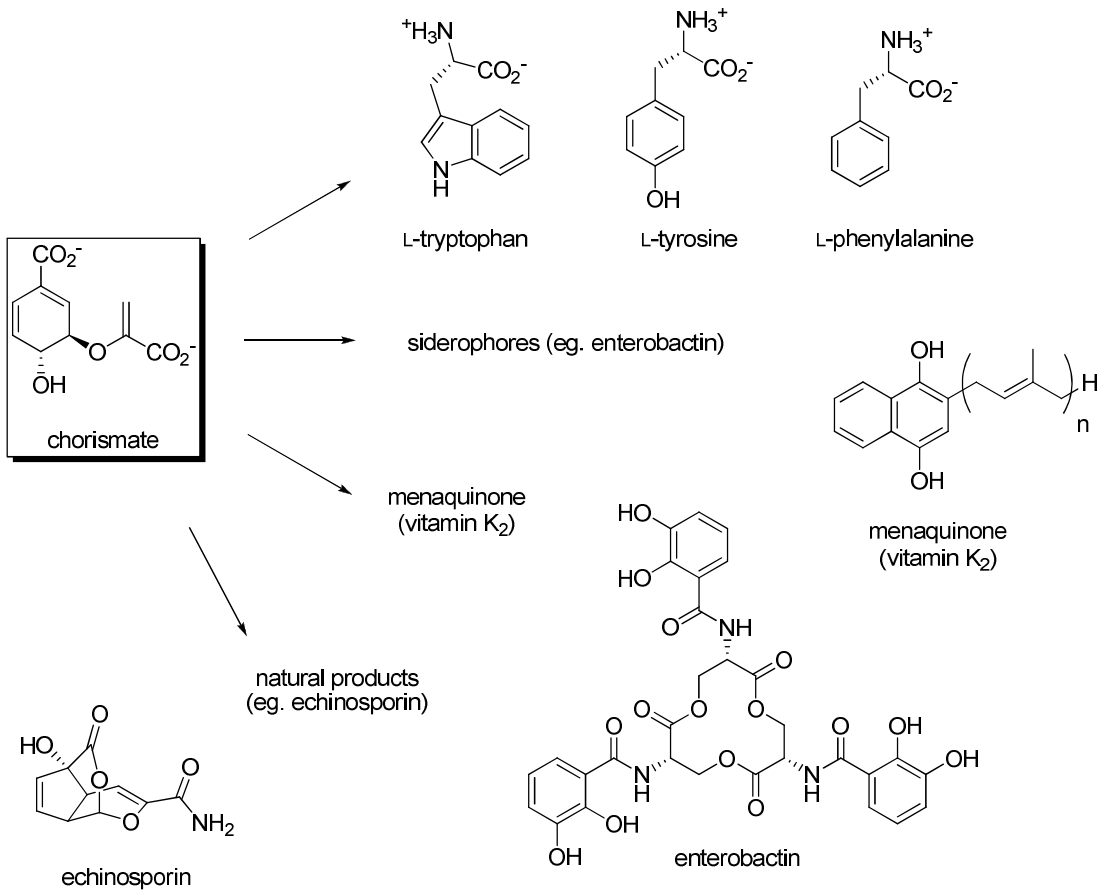

Figure 1.2: The diverse fates of chorismate

In a series of enzymatic steps, chorismate is converted into the three aromatic amino acids tyrosine, phenylalanine and tryptophan. These compounds are required not only for the synthesis of proteins, but a variety of other aromatic compounds. In addition to serving as a feedstock for amino acid biosynthesis, chorismate is converted directly into other compounds performing diverse roles in life, such as the antibiotic natural product echinosporin[2], a defensive antibiotic produced by some *Streptomyces* species; the electron transfer agent menaquinone[3]; a necessity for bacterial aerobic metabolism, and enterobactin[4], a siderophore which allows bacteria to scavenge iron(III) from the low iron environments found inside other organisms.

The shikimate pathway is present in plants, bacteria, fungi and apicomplexan parasites[5]; such as *Toxoplasma gondii*, *Cryptosporidium parvum* and *Plasmodium falciparum*; responsible for the human diseases toxoplasmosis, cryptosporidiosis and malaria, respectively. The pathway is absent in animals, and consequently the pathway has attracted interest as a target for medicines and herbicides.[6, 7] This

pathway has been shown to be essential in some disease causing organisms; for example gene disruption studies have shown that the pathway is essential for the viability of *Mycobacterium tuberculosis*.[8] The pathway has also recently attracted interest as a target for bioengineering for the industrial scale synthesis of chiral pool compounds such as (-)-shikimic acid[9]; the starting material for the Roche industrial synthesis of the anti-viral neuraminidase inhibitor oseltamivir phosphate (Tamiflu®) (Figure 1.3). The availability of shikimic acid from natural sources is low, and Roche already consumes 95% of the annual harvest of Chinese star anise (the most cost effective natural source) at current oseltamivir production levels.[10]

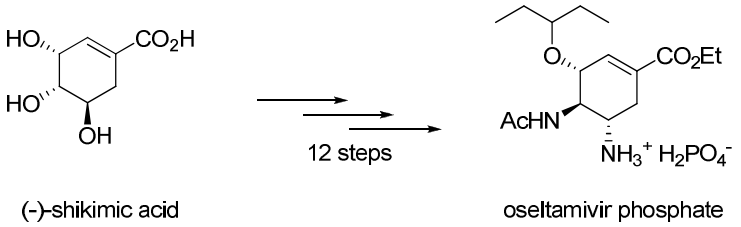

Figure 1.3: The utility of shikimate pathway compounds as chiral pool materials: shikimic acid and oseltamivir phosphate (Tamiflu®)

The herbicide glyphosate, a molecule of enormous commercial and agricultural value, is an inhibitor of the sixth step of the pathway, 5-enolpyruvyl-shikimate 3-phosphate (EPSP) synthase[11] (Figure 1.4). In addition to its success as a herbicide, glyphosate shows limited antimicrobial activity[12]; and inhibits the growth of apicomplexan parasites *in vivo*.[5] The success of this compound demonstrates the potential of shikimate pathway inhibitors as herbicidal and antimicrobial agents.

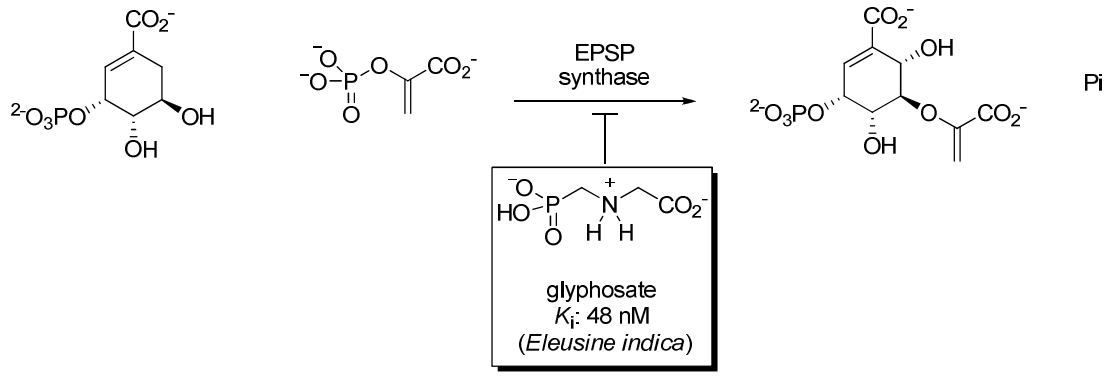

Figure 1.4: Glyphosate, and the target of its action. Inhibition data is shown for the EPSP synthase from the weed goosegrass (*Eleusine indica*).[13]

1.2 DAH7P synthase

1.2.1 Enzyme mechanism

The first step of the shikimate pathway is catalysed by the enzyme 3-deoxy-D-*arabino*-heptulosonate 7-phosphate (DAH7P) synthase, which catalyses an aldol-like reaction between E4P and PEP to form the seven carbon sugar DAH7P (Figure 1.5)[1].

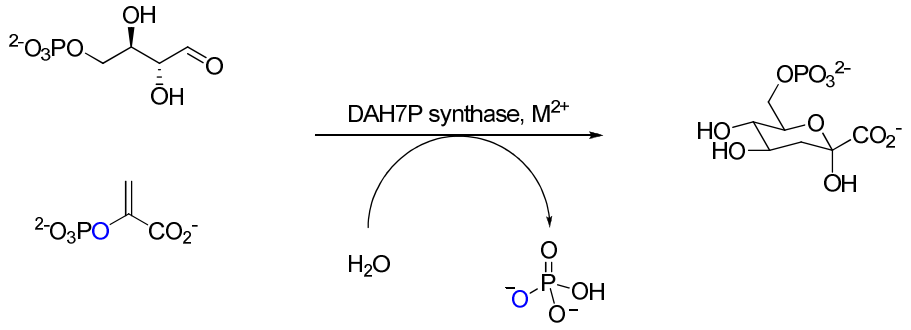

Figure 1.5: The reaction catalysed by DAH7P synthase

An analogous reaction with the five carbon sugar D-arabinose 5-phosphate is catalysed by 3-deoxy-D-*manno*-octulosonate 8-phosphate (KDO8P) synthase. This enzyme is discussed in detail in Section 1.3. DAH7P synthase is known to exist as three isozymes in *Escherichia coli*, which are each subject to feedback inhibition by phenylalanine, tyrosine or tryptophan.[1] This feedback inhibition mechanism has been shown to be the major regulatory mechanism for the entire shikimate pathway.[14] In addition, the shikimate pathway is responsible for up to 30% of the total carbon flux within the cell, so this makes DAH7P synthase a vital part of the overall control of cellular carbon flux.[1] Consequently, being able to interrupt the activity of this enzyme could have widespread cellular effects, making inhibitors of DAH7P synthase of particular interest for development as antibiotics or herbicides.

DAH7P synthase(phe), the phenylalanine inhibited isozyme of DAH7P synthase, is responsible for approximately 80% of the DAH7P synthase activity in *E. coli*, and remainder is made up by DAH7P synthase(tyr) (~20%) with very little contribution from DAH7P synthase(trp) (<1% total activity).[1]

The mechanism of DAH7P synthase has been investigated by a number of groups, and a number of key observations have been made. Unusually, DAH7P synthase catalyses the cleavage of the C-O bond of PEP[15] (Figure 1.5); typically enzymes utilising PEP make use of the high energy contained in the phosphate ester bond ($\Delta G° = -62$ kJ mol^{-1}) by cleavage of the oxygen-phosphorus bond of PEP.

All DAH7P synthases require a divalent metal ion for activity, and reactivation studies of the three *E. coli* apoenzymes has shown activity is dependent on the metal present, with the order of activity $Mn^{2+} > Cd^{2+}$, $Fe^{2+} > Co^{2+} > Ni^{2+}$, Cu^{2+}, $Zn^{2+} >> Ca^{2+}$.[16] The nature of the metal ion bound *in vivo* is a matter of dispute, since the highly active Mn^{2+} complex is also rather labile, and prone to displacement by other ions, particularly Fe^{2+}, Co^{2+} and Zn^{2+}, which form more stable metal-enzyme complexes. The metal dependencies of DAH7P synthases from other organisms have been studied; while the metal ions that provide activity are generally the same, the relative order of activity varies from species to species.[17-21]

Analysis of the product of the reaction utilising stereospecifically deuterated PEP shows that the addition proceeds in a stereospecific manner, with the *si* face of PEP attacking the *re* face of E4P[22] (Figure 1.6).

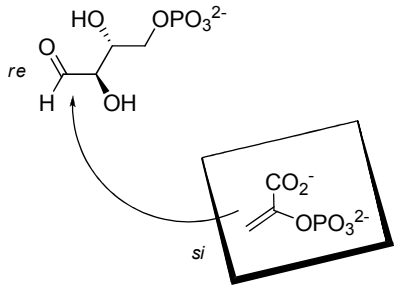

Figure 1.6: Stereospecificity of the DAH7P synthase reaction

Detailed kinetic studies have shown that the reaction proceeds through an ordered sequential mechanism, where PEP binds to the enzyme first, followed by E4P, followed by phosphate release, followed by DAH7P release.[23] The reaction is also irreversible under physiological conditions, based on the failure of DAH7P synthase to exchange ^{32}P-labelled phosphate into PEP, and the failure of DAH7P synthase to exchange ^{14}C into DAH7P from [U-^{14}C]-PEP.[23]

The mechanism of DAH7P synthase has been the subject of some debate, and the most chemically plausible mechanism is shown in Figure 1.7.

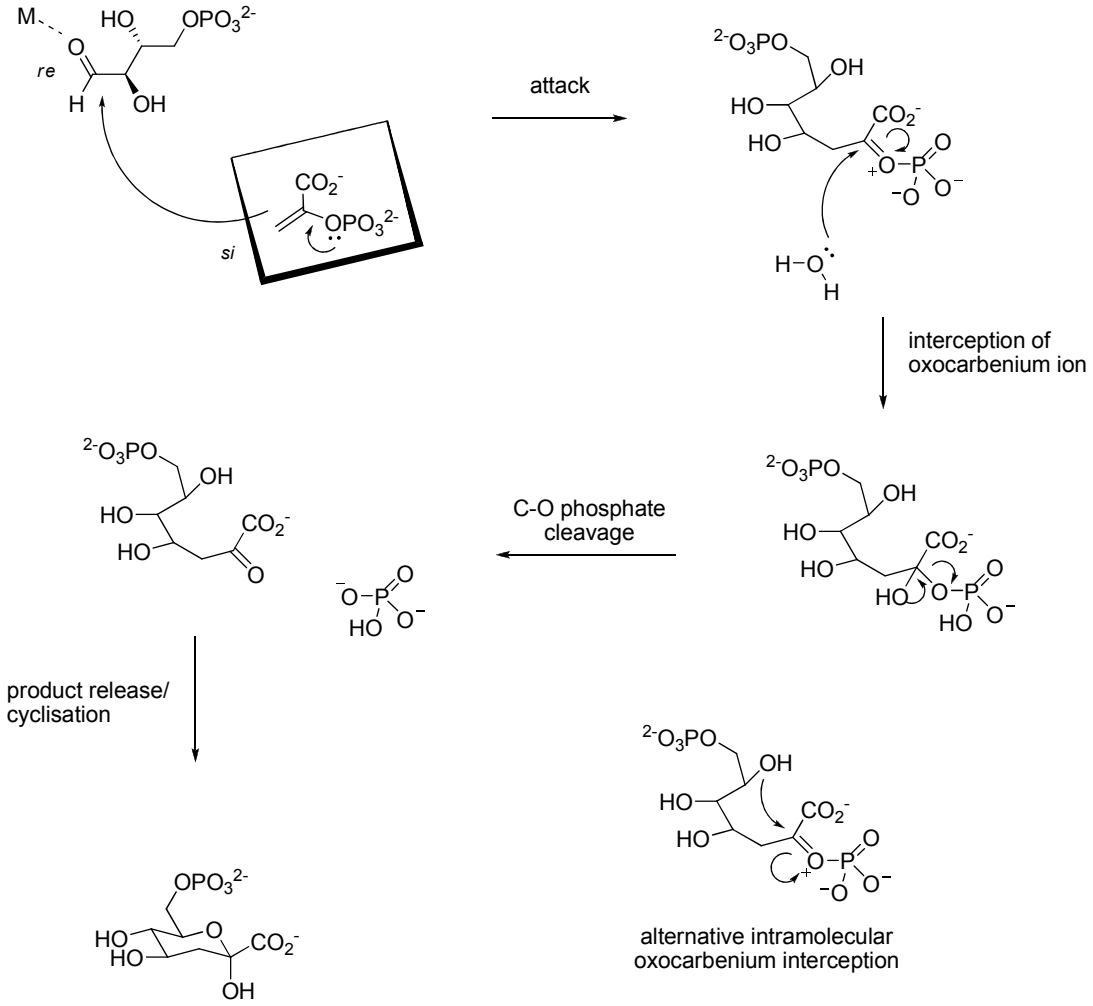

Figure 1.7: Key points of the favoured mechanism for DAH7P synthase

In the mechanism (Figure 1.7), the electron rich enol alkene of PEP attacks the carbonyl group of E4P, which has been activated by coordination of the carbonyl to the metal ion. The resulting oxocarbenium ion is attacked by water, giving rise to a labile phosphate hemiketal intermediate. This intermediate can undergo loss of phosphate, forming the C2 carbonyl of DAH7P and giving the required C-O phosphate bond cleavage. Product release, followed by spontaneous cyclisation in solution gives rise to cyclic DAH7P.

Other variants of this mechanism have been proposed at various times. One possibility has been instead of the oxocarbenium ion being intercepted by water, it is intercepted intramolecularly by the C3 hydroxyl of E4P, giving a cyclic phosphate hemiketal. Explusion of phosphate and interception of the oxonium ion by water would then give the cyclic form of DAH7P, which would be released into solution. This mechanism has been discredited by a number of observations. The compound 3-deoxyE4P is a substrate for the reaction, so if this mechanism does operate, it is not the exclusive mechanism of DAH7P formation.[24] In addition, the study of the structures of DAH7P synthase from a number of species by X-ray crystallography has shown that in every case the DAH7P synthase active site forms a long linear pocket, in which there is insufficient space for such an intramolecular cyclisation.[17, 25-29]

The exact role of the metal ion in DAH7P synthase and related enzymes has been the subject of some debate, and two competing views are held (Figure 1.8). In one view (the Lewis acid mechanism), the metal encourages attack of PEP on E4P by withdrawing electron density from the E4P carbonyl as presented earlier. In the other view (the carbanion mechanism), the coordination of a water molecule by the metal creates a metal-generated hydroxide ion, which can attack PEP at the C2 position. The electrons of the PEP alkene then attack the aldehyde of E4P, either through the intermediacy of a free carbanion[30] (path b) or through a concerted mechanism [31] (path a).

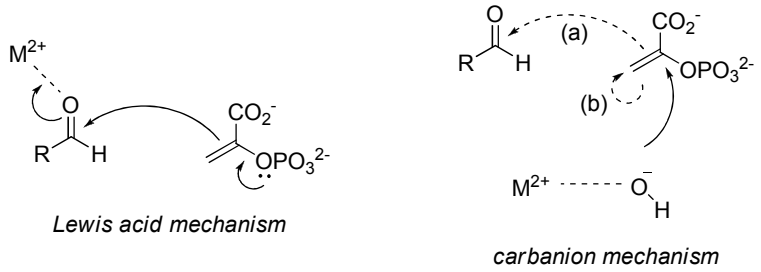

Figure 1.8: The two competing roles for the metal ion in DAH7P synthase

There are a number of problems with the proposed carbanion mechanism. It requires PEP to have an otherwise unprecedented electrophilic character at C2, in order for the attack of hydroxide to occur. In addition, in the free carbanion variant it requires the existence of a resonance unstabilised carbanion, with a likely pK_a of >30, inside an

enzyme active site populated by carbon-hydrogen bonds of greater acidity; in addition to water molecules, carboxylic acids and ammonium ions. Thus it is likely that anything other than the most transient of carbanions would immediately be quenched by hydrogen abstraction from another active site species. The need to propose such an unprecedented mechanism becomes even further lessened when one considers the number of known abiotic Lewis acid promoted alkene-carbonyl reactions; such as the Mukaiyama aldol reaction[32] and Evans asymmetric copper-catalysed ene reaction (Figure 1.9).[33]

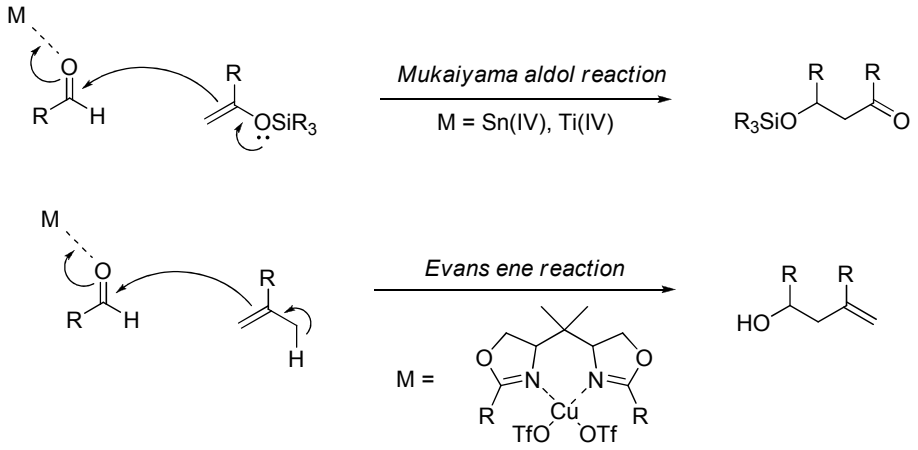

Figure 1.9: Examples of abiotic alkene-carbonyl reactivity promoted by Lewis acids

Furthermore, studies of model compounds has shown the necessary Lewis acid promoted reaction can occur, provided the reaction is intramolecular[34] (Figure 1.10). The reaction occurs rapidly under anhydrous conditions (tin tetrachloride in cold dichloromethane), with an excess of Lewis acid, and gives a single configuration at the former aldehyde centre (C4). The initially formed strained dioxabicyclo[2.2.1]heptane is unstable to the reaction conditions, and undergoes Lewis acid catalysed ring opening. Subsequent reaction of the mixture with acidic methanol returned the monocylic compound in excellent yield.

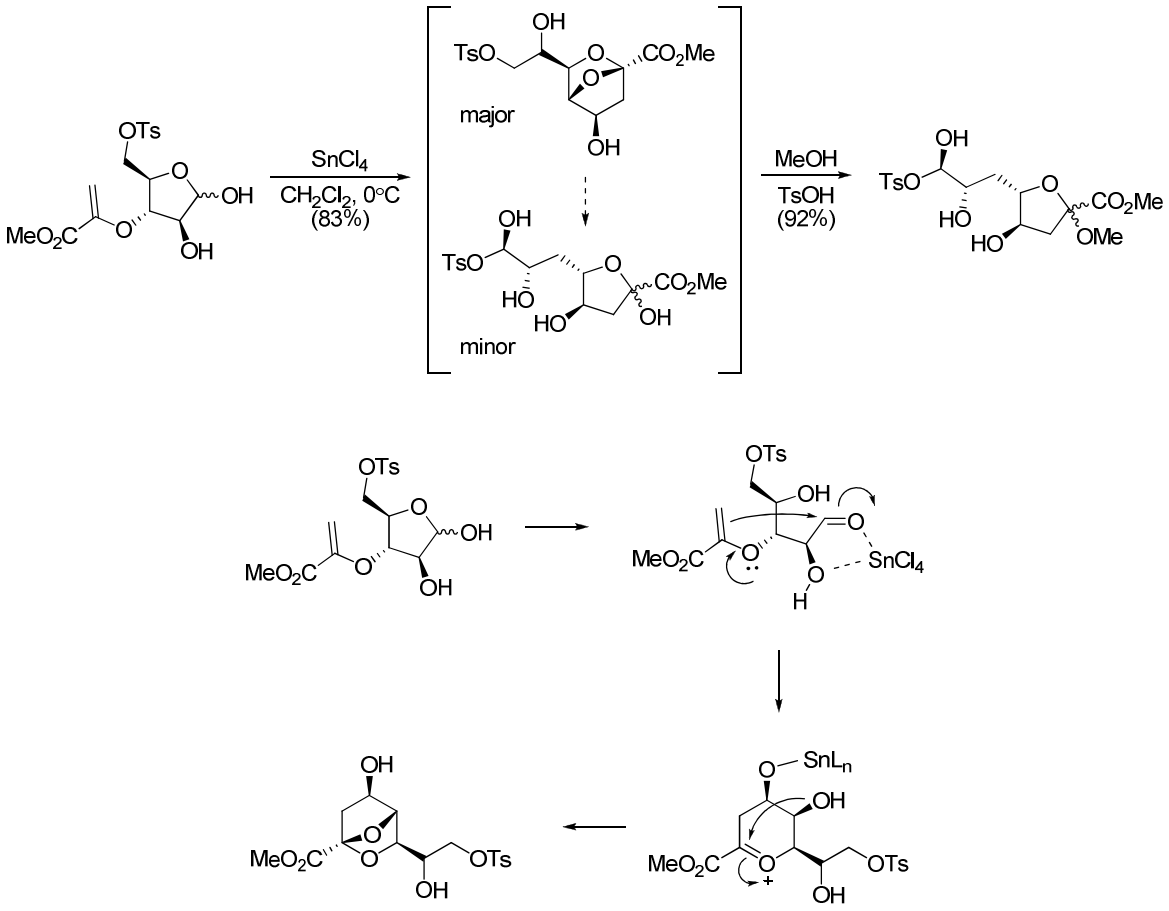

Figure 1.10: A model system for the Lewis acid mechanism

The reaction also occurs under aqueous conditions with a related substrate, utilising mildly acidic conditions (pH 5) and zinc(II) chloride as a promoter, leading directly to the product as a single epimer at C4 (Figure 1.11). Omitting the Lewis acid but reacting at the same pH gives slowed consumption of the enol ether ($t_{1/2}$ ~ 22 hr). In addition, rather than exclusive formation of a single product with D-*manno* stereochemistry, the 4-*epi* D-*gluco* diastereomer is also formed in a 55:45 D-*manno*: D-*gluco* ratio (68% yield based on consumed enol ether), along with breakdown products (32% yield from consumed enol ether). These precedents demonstrate that the reaction can occur under Lewis acid promoted conditions, and in the presence and absence of water. This casts additional doubt on the proposed carbanionic mechanism.

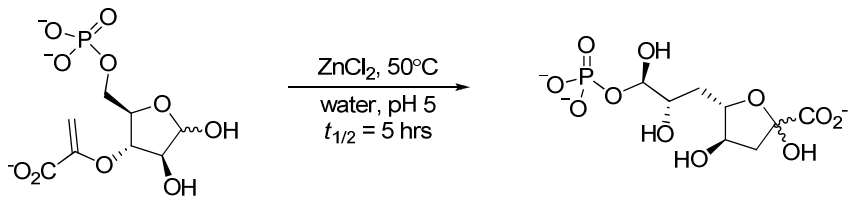

Figure 1.11: An aqueous model system Lewis acid promoted reaction

1.2.2 Enzyme structure

The family of DAH7P synthases have been broadly divided into two groups based on sequence similarities; type I and type II DAH7P synthases[35] (Figure 1.12). Sequence similarities between the two families is ~10%, below the level of significance for such a measurement. Type II DAH7P synthases are distinct in sequence and size (typically ~50 kDa) from type I DAH7P synthases. While originally identified in plants, a large number of bacterial DAH7P synthases (such as those from *M. tuberculosis*, *Helicobacter pylori* and *Campylobacter jejuni*) have recently been identified as belonging to this group.

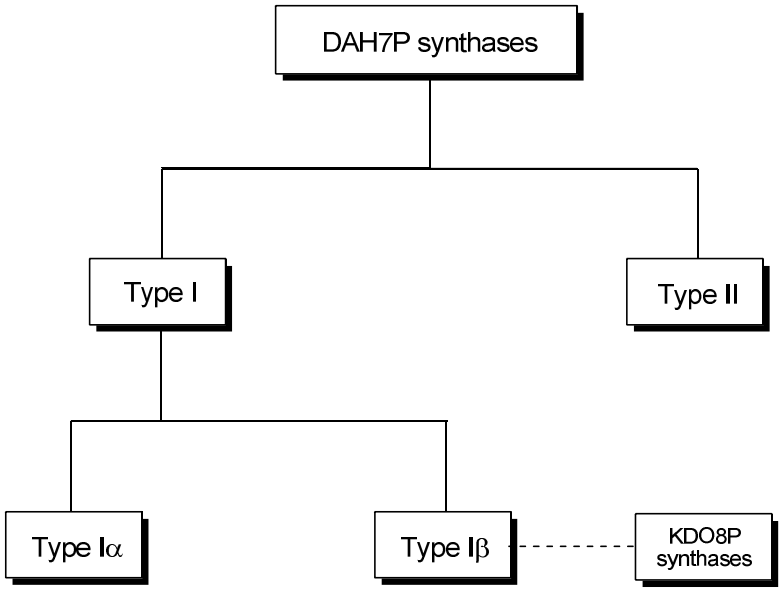

Figure 1.12: The families of DAH7P synthases based on sequence similarity

Type I DAH7P synthases have masses of less than 40 kDa; and represent the most well characterised family of DAH7P synthases. The family is further subdivided on sequence into two subfamilies, Iα and Iβ. The Iβ family is considered ancestral to all

DAH7P and KDO8P synthases; and contains species of comparatively ancient lineages such as *Pyrococcus furiosus* and *Thermotoga maritima.*[36]

The most well characterised examples of DAH7P synthase activity are those from *Escherichia coli*. The three enzymes from *E. coli* are Type Iα, all approximately 38 kDa in size, and are closely related in sequence. The structures of these enzymes have been investigated by X-ray crystallography. The tertiary structures of the *E. coli* enzymes are $(\beta/\alpha)_8$ TIM barrel folds[27], with the active site located near the C-terminal end of the barrel, as is typical with enzymes of this fold.[37]

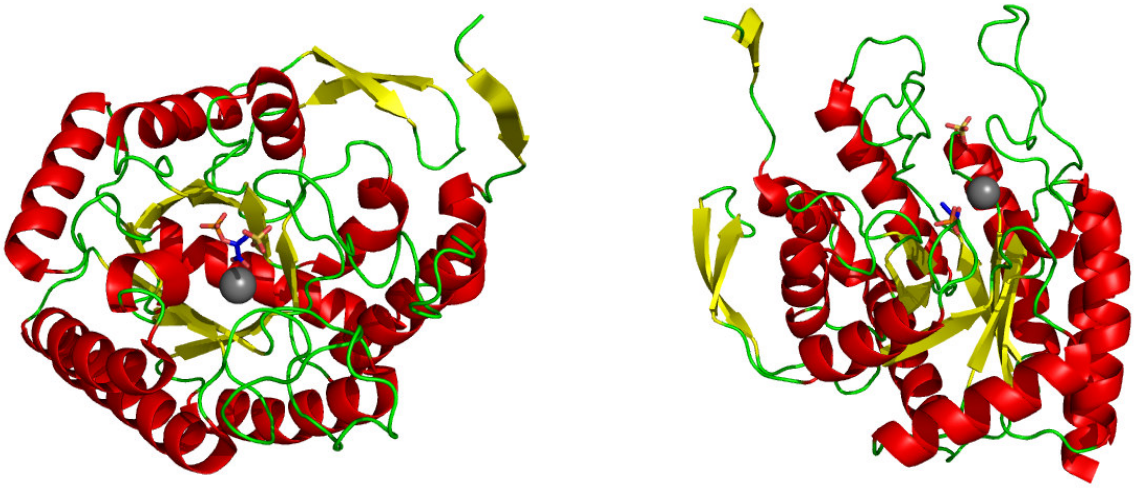

Figure 1.13: Top (left) and side (right) views of a monomeric enzyme unit from *E.coli* DAH7P synthase(phe), with helical (red), sheet (yellow) and loop (green) regions indicated. PEP (C/O/P blue/red/orange respectively), manganese (grey sphere) and a sulfate ion (S/O gold/red respectively) are indicated; the sulfate ion can be taken as an estimate of the position of the phosphate group of E4P in the ternary enzyme-PEP-E4P complex. The side view is taken from the twelve-o-clock position relative to the top view. Drawn from 1n8f, chain A.[38]

Amazingly, despite the large variations in sequence and size across the DAH7P synthase family, Type Iα[27], Iβ[29], and Type II[17] DAH7P synthases all share the general $(\beta/\alpha)_8$ TIM barrel fold; additions of various domains such as regulatory modules comprising the major structural differences between species and classes. Furthermore, despite the low overall sequence similarity; the identity and positions of several key active site residues are absolutely conserved over all classes of DAH7P synthases (Figure 1.15).

These conserved residues are crucial to the operation of the enzyme, and are presumably so important that evolutionary change has not been permitted. The roles of these residues will be illustrated with examples from the structure of the *E. coli* Phe-repressible enzyme.

The metal coordination site is strongly conserved with no natural variations in the four residues responsible for metal coordination across all classes of DAH7P synthase. In *E. coli* DAH7P synthase the metal atom is held in a distorted trigonal bipyrimidal geometry (Figure 1.14), coordinated to the enzyme via histidine, cysteine, asparate and glutamate residues (*E. coli* numbering: H268, C61, D326 and E302 respectively).

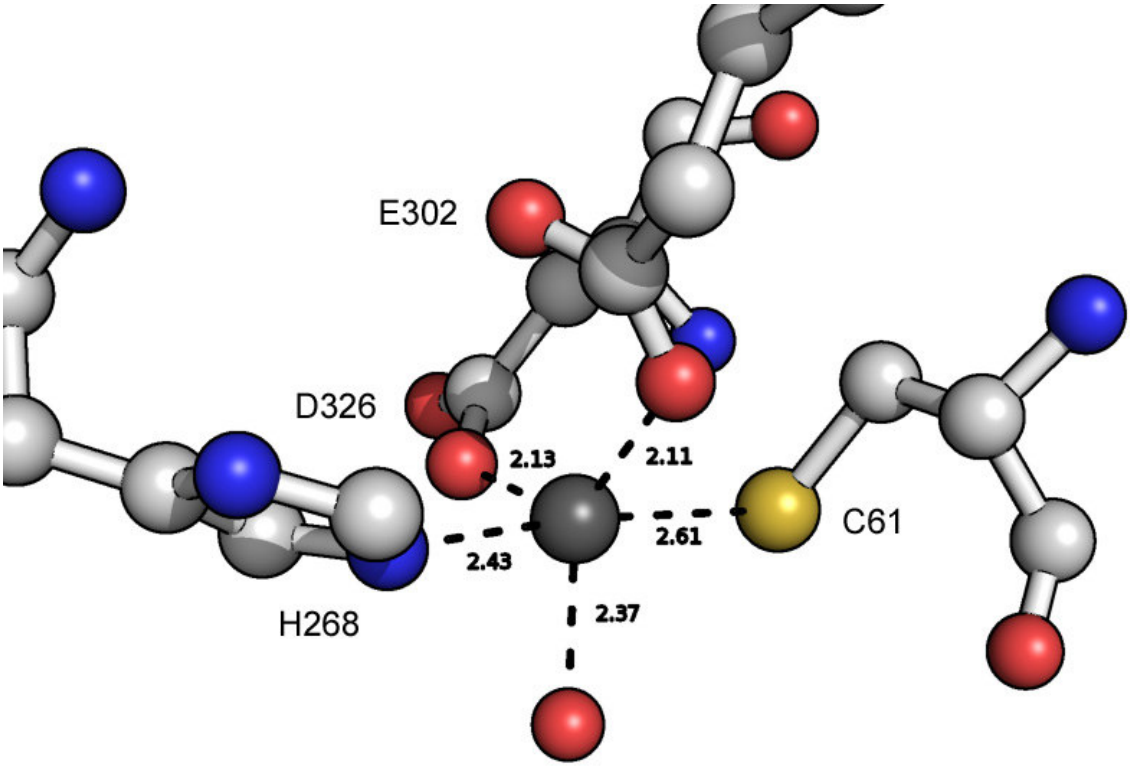

Figure 1.14: Metal coordination environment in *E. coli* DAH7P synthase. The metal (in this case manganese(II)) is held to the enzyme via interactions with absolutely conserved cysteine, histidine, aspartate and glutamate residues. The fifth ligand is a water molecule, located in the E4P site. Bond distances are in angstroms, figure drawn from 1n8f.[27]

Figure 1.15: Structure-based sequence alignment of DAH7P synthases from a variety of classes. Shown are enzymes from *E. coli* (Eco, Iα), *M. tuberculosis* (Mtu, II), *Saccharomyces cerevisiae* (Sce, Iα), *P. furiosus* (Pfu, IβD) and *T. maritima* (Tma, IβD). Roles of key residues discussed in the text are indicated. Alignment generated with Expresso, www.tcoffee.org.

In addition to these interactions, a water molecule is typically found as the fifth ligand, located in the E4P binding site. A comparatively long range (3.13 Å) interaction also exists with one carboxylate oxygen of PEP (not shown).

Interestingly, despite a common metal binding site scaffold, relative metal preferences differ across species. For example, while the Type Iα *E. coli* DAH7P synthase has the relative activities[16] of $Mn^{2+} > Cd^{2+}$, $Fe^{2+} > Co^{2+}$, for Type II *M. tuberculosis* DAH7P synthase the same metals have a different order of activity; namely $Co^{2+} > Mn^{2+}$, $Cd^{2+} >> Fe^{2+}$; with iron(II) being reportedly inactive.[17] The reasons for differing metal activities across species remain to be determined.

The water ligand of the metal centre could be replaced by the carbonyl oxygen of E4P in the enzyme-PEP-E4P ternary complex, activating the carbonyl group to attack. This interaction is yet to be observed by any experimental technique, however has been modelled into *P. furiosus* DAH7P synthase[39]; based on the structure a *P. furiosus* DAH7P synthase-PEP complex[29], and of an inert *S. cerevisiae* DAH7P synthase-PEP-glycerol 3-phosphate complex[40] (Figure 1.16).

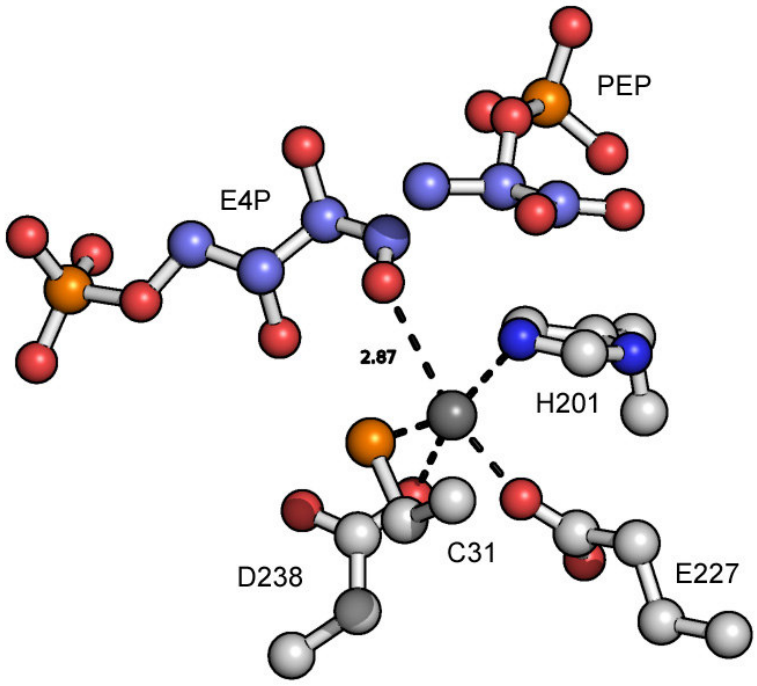

Figure 1.16: E4P (pale blue/red/gold) modelled into *P. furiosus* DAH7P synthase-PEP complex, showing the metal coordination environment postulated to exist in the enzyme-PEP-E4P complex. The carbonyl oxygen-metal distance is indicated in angstroms. Residues interacting with PEP and E4P have been removed for clarity. Generated from the previously published model.[39]

By simply adding an additional carbon to glycerol 3-phosphate (giving E4P), it can be seen that without any distortion of the conformation of the enzyme or the glycerol 3-phosphate the carbonyl group passes within 2.9 Å of the metal ion, giving a distorted trigonal bipyrimidal geometry as observed before. This conformation presents the correct (*re*) face of the aldehyde to the *si* face of PEP, in accordance with the known stereochemical outcome of the DAH7P synthase reaction. PEP C3 sits close to E4P C1 (2.1 Å), and approaches at an angle compressed (74.4°) from the ideal Bürgi-Dunitz trajectory for attack on a carbonyl (105±5°).[41] This compression may reflect the increased polarisation of the carbonyl bond in the metal-carbonyl complex, or the likely differences between the model and the actual transition state geometry of the complex.

In addition to conservation of the metal binding site, many other residues are conserved in the PEP binding site.

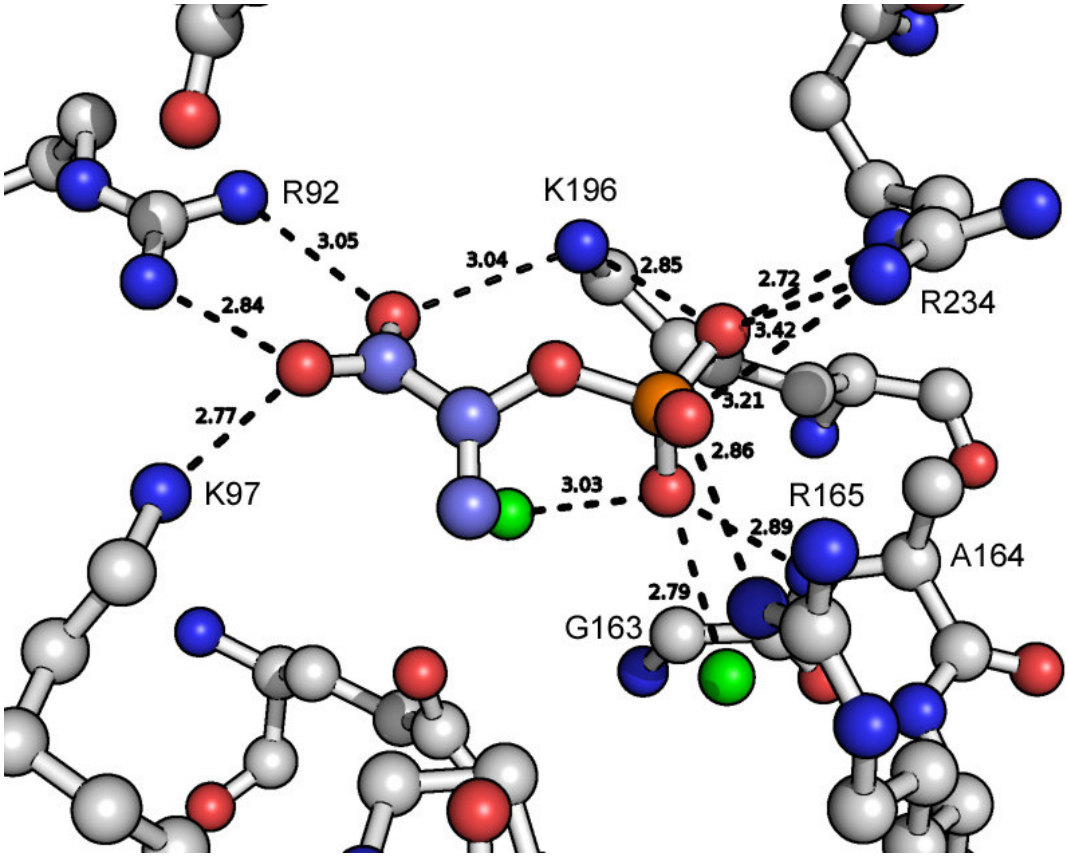

Figure 1.17: The PEP site in *E. coli* DAH7P synthase. Shown is the *si* face of PEP (pale blue/red/orange), surrounding residues (grey/ blue/ red) and close water molecules (green). The metal and metal binding histidine have been deleted for clarity; the metal would positioned in the foreground, between the 8 and 9-o'clock position in this diagram. Distances to neighbouring polar atoms are indicated in angstroms. Drawn from 1n8f.pdb.[27]

As can be seen in Figure 1.17, PEP is recognised by a finely tuned network of non-covalent interactions, mostly with the side chains of amino acids such as lysine and arginine, although a close approach (2.9 Å) with a main chain amide between glycine and alanine exists (*E. coli* numbering: G163, A164). In addition, some contact of the PEP phosphate group with the enzyme is mediated through water molecules. The positively charged residues mediating these interactions are conserved absolutely across all classes of DAH7P synthases (R165, K196, K97, R92 and R234; all marked in Figure 1.17). In addition G163 is absolutely conserved, for presumably steric reasons, while A164 is conserved across the Type I family of DAH7P synthases; in the Type II *M. tuberculosis* and *H. pylori* DAH7P synthases, the corresponding residue is glutamate.[17, 18]

An interesting mechanistic point is illustrated by Figure 1.17. The combination of a R92 and K97 (and potentially the metal ion) interacting with the PEP carboxylate group, pulls the carboxyl group out of the plane of the PEP alkene, increasing the carboxylate-alkene dihedral angle. This phenomenon has been observed in a number of high resolution X-ray crystal structures of DAH7P synthase[27, 28, 40], and the related enzyme KDO8P synthase[42] (Section 1.3). It has been calculated that introducing this twist into the C1-C2 bond of PEP lowers the delocalisation across the α,β-unsaturated carboxylate system; localising the alkene electrons to the C2-C3 bond and increasing the nucleophilicity of the PEP C3.[43]

In addition to these metal and PEP binding residues, several other residues are also conserved. On the *re* face of PEP, between PEP and the wall of the active site lies a hydrogen-bonded network of three water molecules, held in place by interactions amongst themselves, and with both PEP and the enzyme (Figure 1.18).

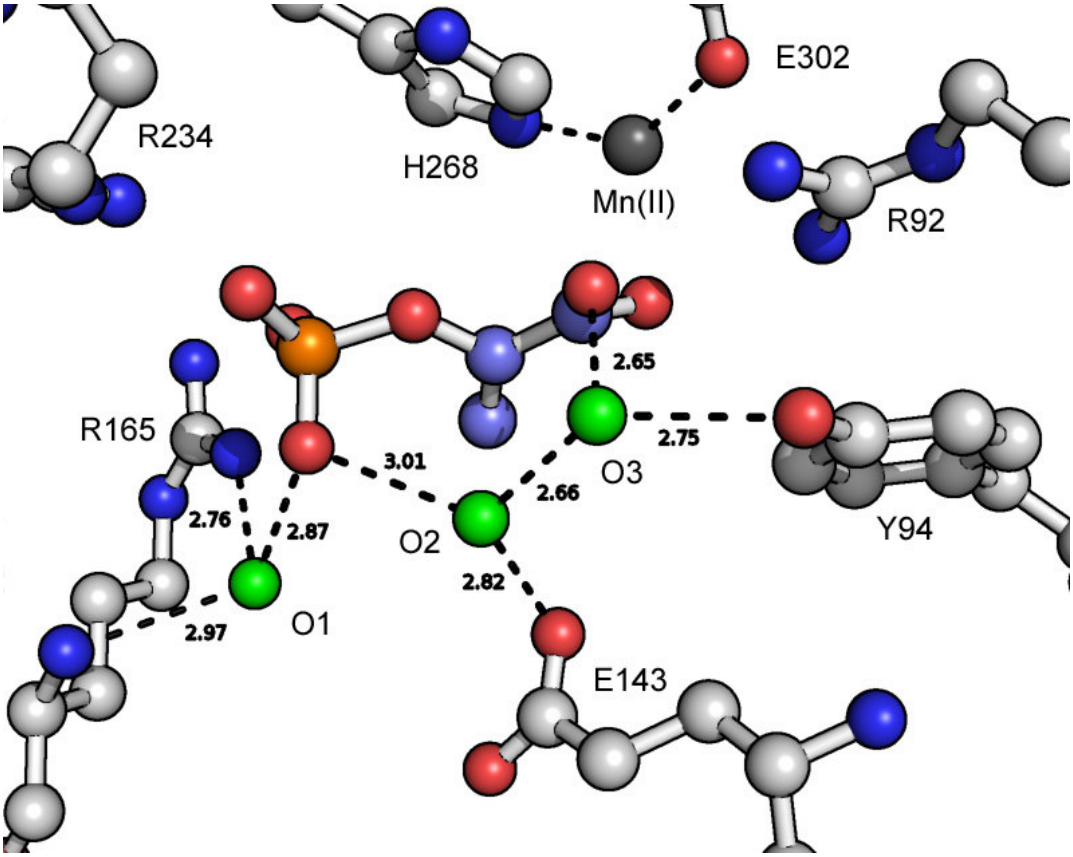

Figure 1.18: The hydrogen-bond network on the *re* face of PEP in *E. coli* DAH7P synthase. Shown are the water molecules (green, O1-O3), PEP (light blue/orange/red), and key residues. Visible in the background are H268, E302 and the manganese(II) atom, in the midground are the PEP-recognising residues R92 and R234.

The glutamate residue holding in place the water O2, E143, is absolutely conserved in all classes of DAH7P synthase. Since the side chain of E143 does not make direct contact with either of the substrates, the metal cofactor or any enzyme residue, it follows that it has been preserved during evolution due to the necessity of having the water O2 on the *re* face of PEP during the reaction. This is supported by X-ray crystallography; the water at position O2 has been observed in a number of high resolution structures.

This suggests that O2 may be one of the substrates of the reaction, and O2 could be conceivably used to quench the oxocarbenium ion intermediate of the reaction, and generate the hemiketal phosphate intermediate. The phosphate group of PEP could be used as a base to sequentially remove hydrogen atoms from O2, resulting in the protonation of phosphate during the final elimination, and the resulting elimination of

dianionic phosphate, which can be reasonably assumed to be more favourable than the elimination of trianionic phosphate (Figure 1.19).

The water on the *re* face is well placed to attack the oxocarbenium ion, although admittedly the angle of attack toward the oxocarbenium ion is compressed relative to the ideal Bürgi-Dunitz trajectory for attack on a carbonyl (84.1° across the O2-PEP C2- enol O unit, compared to the Burgi-Dunitz angle of 105±5°).[41] Although this may reflect the obvious electronic differences between a carbonyl group and the oxocarbenium ion. It is also of note that the *re* face water and the aldehyde of E4P are arranged in an *anti* manner across the PEP double bond.

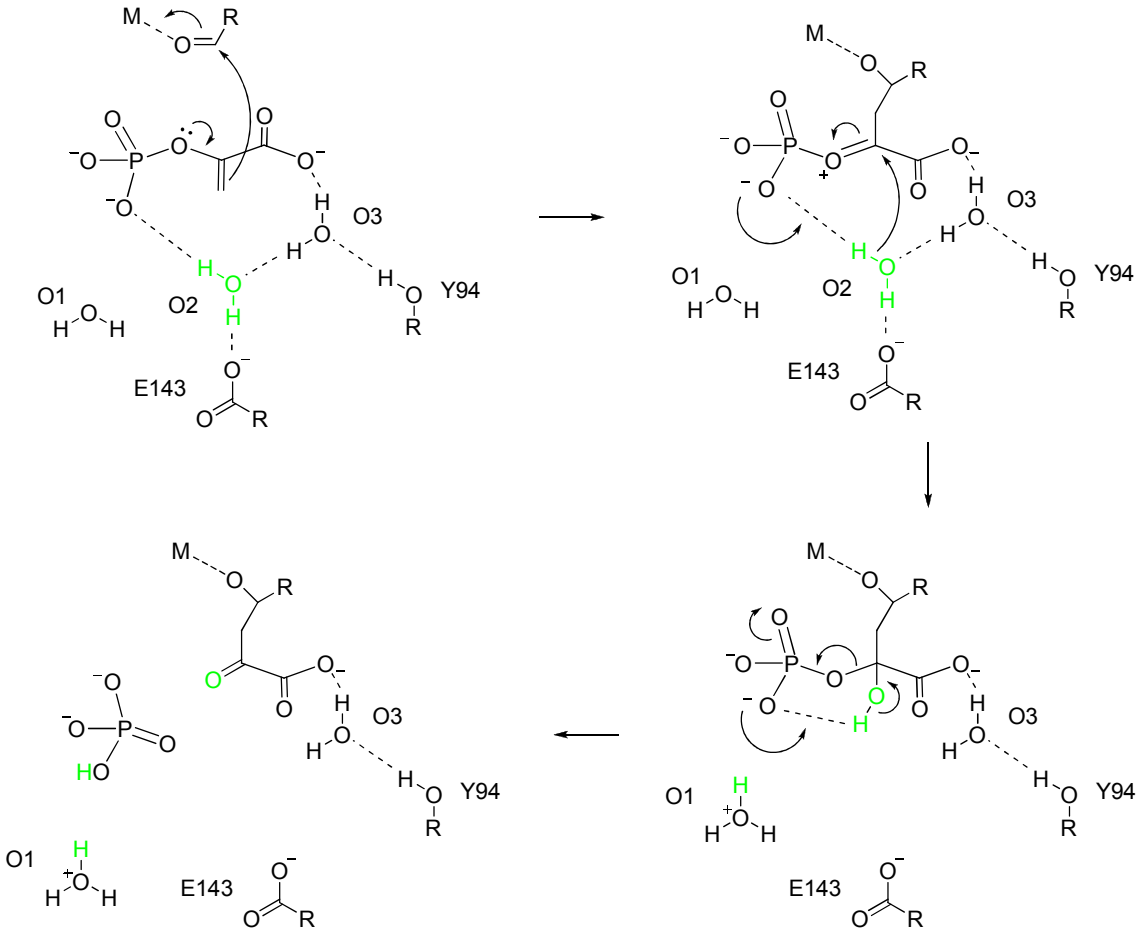

Figure 1.19: A possible role for the conserved water-E143 system on the *re* face of PEP. The relative order of phosphate elimination and alkoxide protonation is not intended to be implied by this diagram.

It is possible that O3 plays a role in the mechanism too, although it should be noted that tyrosine Y94 is not conserved in all DAH7P synthases, whereas it is conserved

across Iα DAH7P synthases in some Type Iβ and Type II DAH7P synthases (such as *P. furiosus* and *M. tuberculosis* DAH7P synthases) Y94 is replaced by a phenylalanine residue.

The final group of absolutely conserved residues lie sequentially in the primary structure of the protein, forming an absolutely conserved KPRT(S) motif (*E. coli* numbering K97, P98, R99, T100) across all DAH7P synthases. From analysis of the X-ray crystal structure it is clear that this motif forms a binding pocket for the enzyme's second substrate E4P (Figure 1.20).

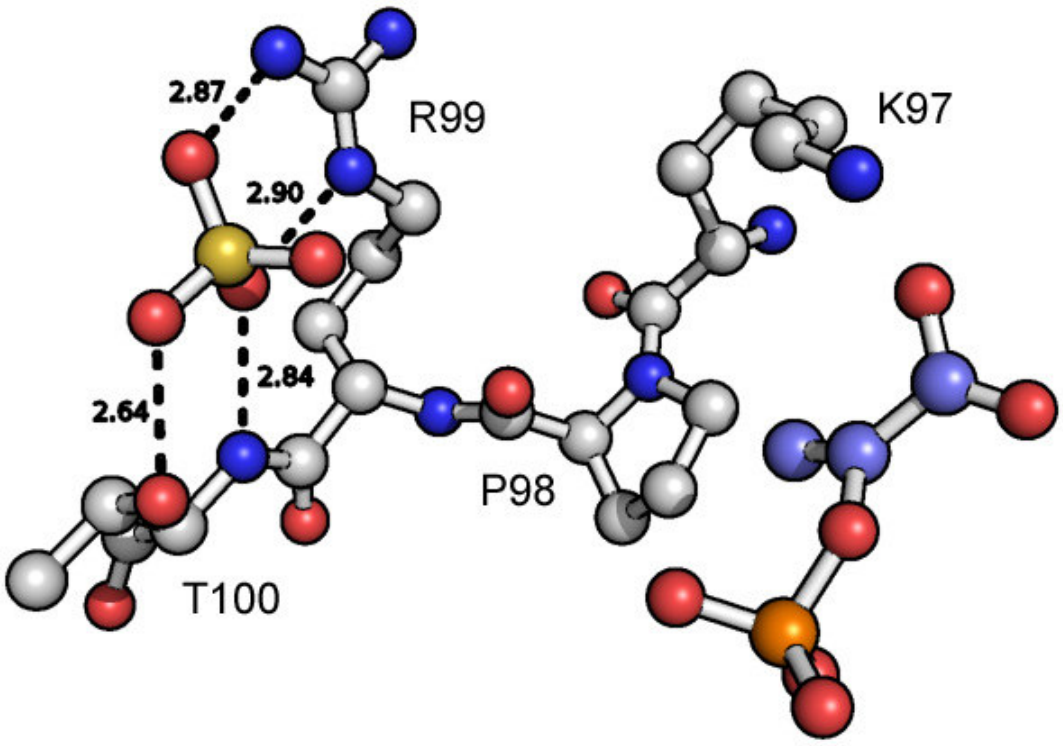

Figure 1.20: The conserved KPRT(S) motif as seen in *E. coli* DAH7P synthase structure 1n8f.pdb[27]. Shown are PEP (pale blue/red/orange) the *E. coli* KPRT motif and an adventitious sulfate ion from the crystallisation conditions (gold/red). This sulfate can be considered a model for the terminal phosphate of E4P. Distances are given in angstroms.

The lysine residue K97 interacts with PEP, as previously mentioned. The proline residue P98 folds the protein backbone toward a new direction. In addition, the ring carbons of P98 have a hydrophobic interaction with C3 of PEP, which may help orientate PEP in the binding site. This could explain why substitution of proline for another residue with flexible backbone torsion angles such as glycine is not seen in

DAH7P synthase sequences. The remaining arginine R99 and threonine T100 (or serine in other sequences) form a binding pocket for the phosphate group of E4P. This interaction can be seen from the adventitious sulfate ion present in Figure 1.20. The guanidinium group of R99 forms a salt bridge with two oxygen atoms of the phosphate, while the backbone amide nitrogen and hydroxyl group of threonine T100 also each form a hydrogen bond. It is of note that unlike the PEP phosphate binding pocket, the E4P phosphate pocket only has an overall charge of +1 (from the arginine guanidinium group), which may suggest the phosphate group of E4P binds in its monoanionic form.

In addition to the phosphate group, E4P possesses two secondary hydroxyl groups which could be used to bind E4P to the enzyme, and orientate it in the active site. These interactions are of considerable importance to the enzyme, as alternative substrate studies have shown removal of both hydroxyl groups of E4P leads to no activity (Figure 1.21).[44]

D-E4P
K_m (*E. coli*): 39±4 μM
k_{cat} (*E. coli*): 26±3 s^{-1}
k_{cat} / K_m: 0.7±0.1 s^{-1} μM^{-1}

dideoxyE4P

not a substrate

Figure 1.21: A comparison of native substrate E4P[39] and dideoxyE4P[44], illustrating the importance of the secondary hydroxyl groups in catalysis

While no structures exist of ternary enzyme-PEP-E4P complexes, the structure of a *S. cerevisiae* DAH7P synthase has been determined to high resolution containing bound cobalt(II), PEP and D-glycerol 3-phosphate (GO3P).[40] The position of GO3P in this structure can be used to infer information about the binding of E4P.

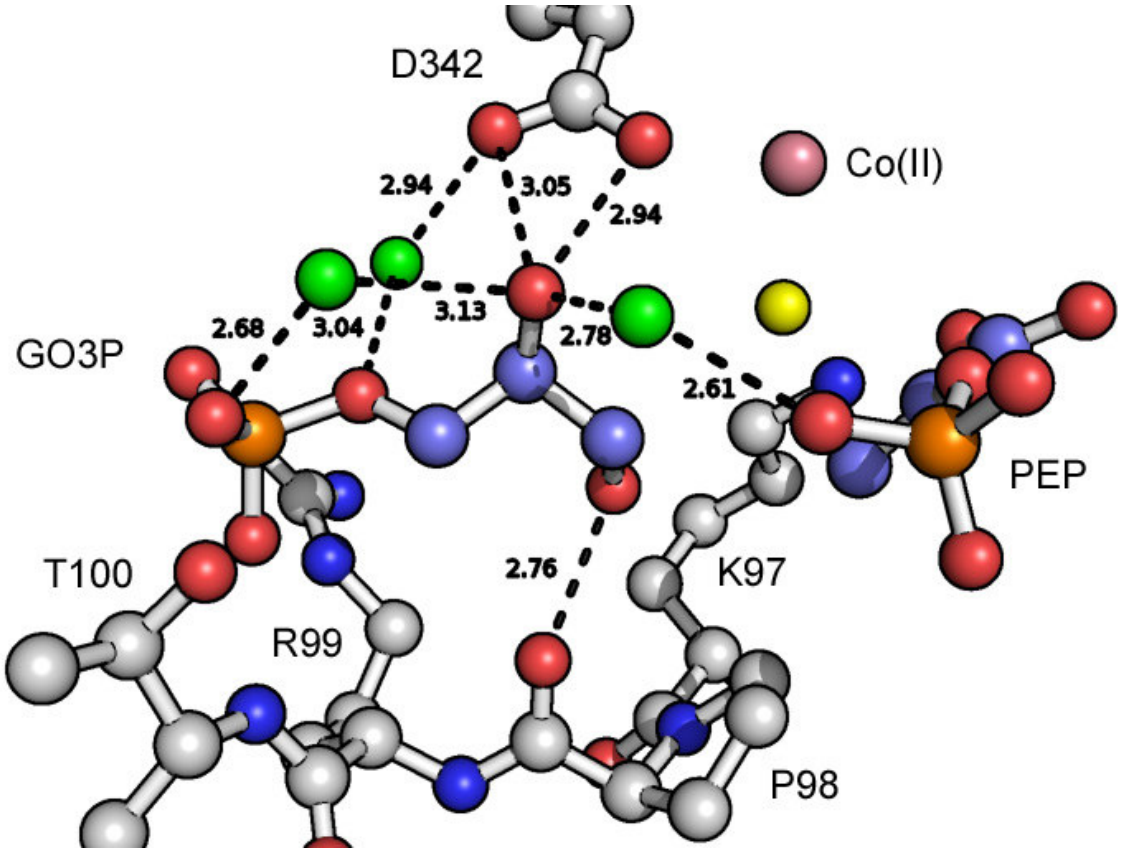

Figure 1.22: The binding of the secondary hydroxyl groups of GO3P in the *S. cerevisiae* DAH7P synthase Co-PEP-GO3P co-complex (PDB: 1of8). Shown in the diagram are PEP and GO3P in pale blue/orange/red (C/O/P respectively), the absolutely conserved KPRT motif and the strongly conserved aspartate D342. Key water molecules mediating interactions with GO3P are in green; the metal coordinated water molecule (equivalent to the E4P carbonyl oxygen) is in yellow. Residues are numbered with the corresponding *E. coli* residue numbers for continuity. Distances are indicated in angstroms.

In addition to the R99-T100 E4P phosphate binding pocket seen earlier (Figure 1.20), the hydroxyl groups of GO3P form contacts both with the enzyme and with several water molecules (Figure 1.22). The C1 hydroxyl group of GO3P (equivalent to the C2 hydroxyl group of E4P) forms a hydrogen bond to the backbone amide oxygen of the conserved proline P100. While this solitary interaction does help E4P bind, it is dispensable; as demonstrated by alternative substrate studies utilising 2-deoxyE4P and D-threose 4-phosphate (T4P).[39, 45] These substrates lack the C2 hydroxyl group or have it in an inverted configuration so it points away from proline P98. In each case, the compounds are still processed as substrates (Figure 1.23).

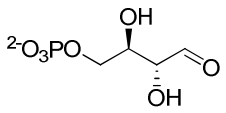

D-E4P
K_m (*E. coli*): 39±4 μM
k_{cat} (*E. coli*): 26±3 s^{-1}
k_{cat} / K_m: 0.7±0.1 s^{-1} μM^{-1}

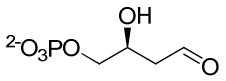

2-deoxyE4P
K_m (*E. coli*): 410±40 μM
k_{cat} (*E. coli*): 25±3 s^{-1}
k_{cat} / K_m: 0.06±0.01 s^{-1} μM^{-1}

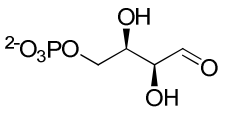

D-T4P
K_m (*E. coli*): 390±13 μM
k_{cat} (*E. coli*): 2.5±0.2 s^{-1}
k_{cat} / K_m: 0.006±0.001 s^{-1} μM^{-1}

Figure 1.23: Kinetic parameters for E4P[39], 2-deoxyE4P[45] and threose 4-phosphate[39] with *E. coli* DAH7P synthase .

Both 2-deoxyE4P and T4P bind to the *E. coli* enzyme with about 10% the affinity of E4P, as indicated by the Michaelis constant K_m, confirming the 2-hydroxyl group does have a role in the E4P-enzyme interaction. Both E4P and 2-deoxyE4P are processed at similar rates as shown by the catalytic constant k_{cat}, indicating that E4P can adopt the conformation required for reaction without the guidance of the C2-hydroxyl group. The reduced k_{cat} for T4P reflects the deleterious effect of the 2-hydroxy-P98 interaction altering the aldehyde orientation. However, both 2-deoxyE4P and T4P are comparitively good substrates for *P. furiosus* DAH7P synthase, indicating that the precise mechanisms of substrate recognition vary across the classes of DAH7P synthase.[39]

The C2-hydroxyl group of GO3P (equivalent to the C3-hydroxyl group of E4P) is positioned to form a number of interactions. It interacts directly with the enzyme through hydrogen bonding with the absolutely conserved metal coordinating aspartate residue D342 (*S. cerevisiae* numbering; equivalent to *E. coli* D326). In addition to interacting with D342, the C2-hydroxyl group of GO3P interacts with a number of water molecules. One water molecule bridges between the hydroxyl group and the phosphate group of PEP, held in place by hydrogen bonds with both groups. It is tempting to speculate that this interaction, and its corresponding effects on the conformations of E4P and PEP, may form part of a signal that initiates the reaction upon E4P binding, by orientating the PEP phosphate group into position that it deprotonates the water O2. A similar interaction between an arabinose 5-phosphate (A5P) hydroxyl and the PEP phosphate group exists in KDO8P synthase, a related enzyme (Section 1.3). [42]

Additionally, the C2-hydroxyl group of GO3P interacts with another water molecule, which in turn interacts with the GO3P phosphate group. The phosphate ester oxygen also hydrogen-bonds to a water molecule held in place by the absolutely conserved metal binding aspartate residue D342. Alternative substrate studies have shown that 3-deoxyE4P is a substrate of Type Iα, Type Iβ and Type II DAH7P synthases, although it binds the *E. coli* enzyme comparatively poorly (K_m 2.7 mM) and is processed slowly (k_{cat} 4.5 ± 0.1 s^{-1}) (Figure 1.24).[24] This suggests that while the 3-hydroxyl is clearly important to high levels of DAH7P synthase activity, it is ultimately disposable if the 2-hydroxyl is present.

D-E4P
K_m (*E. coli*): 39±4 μM
k_{cat} (*E. coli*): 26±3 s^{-1}
k_{cat} / K_m: 0.7±0.1 s^{-1} μM^{-1}

3-deoxyE4P
K_m (*E. coli*): 2700 μM
k_{cat} (*E. coli*): 4.5±0.1 s^{-1}
k_{cat} / K_m: 0.002 s^{-1} μM^{-1}

Figure 1.24: A comparison of E4P[39] and 3-deoxyE4P[24] as DAH7P synthase substrates.

1.3 Related Enzymes

Only a few enzymes share the unusual C-O cleavage of the PEP phosphate bond catalysed by DAH7P synthase: EPSP synthase[46], MurA[47], *N*-acetyl neuraminic acid 9-(phosphate) (NeuNAc(P)) synthases and 3-deoxy-D-*manno*-octulosonate 8-phosphate (KDO8P) synthase.[48] These enzymes can be broadly divided into two categories, enolpyruvyl transferases and PEP aldolases. The enolpyruvyl transferases catalyse the transfer of an enolpyruvyl moiety from PEP to an acceptor alcohol via an addition-elimination mechanism, whereas the PEP aldolases catalyse an aldol-like addition of PEP to an aldehyde (Figure 1.25).

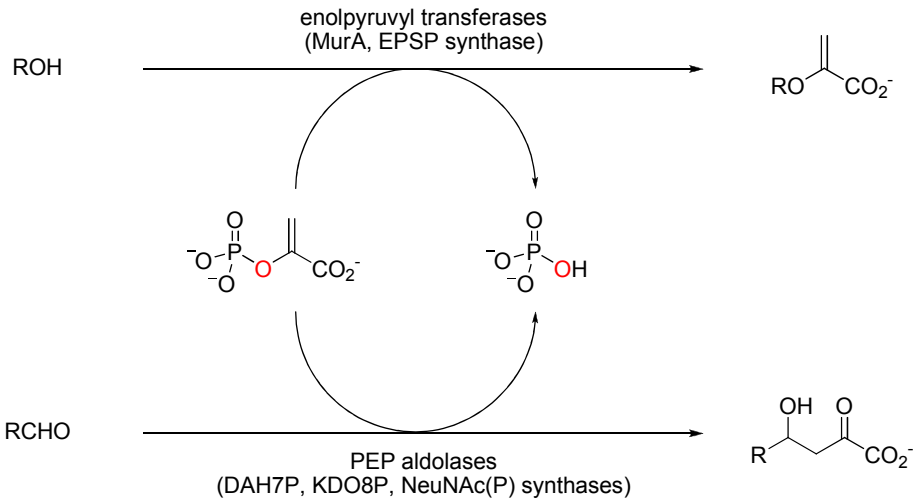

Figure 1.25: Enzymes sharing the unusual C-O cleaving behaviour of DAH7P synthase

While originally thought to be unrelated due to low overall sequence similarity, the aldolases are now thought to be closely related, and it is believed they share a similar mechanism.[36, 49] KDO8P synthases catalyse the addition of PEP to D-arabinose 5-phosphate, to form 3-deoxy-D-*manno*-octulosonate 8-phosphate, an 8-carbon analogue of DAH7P, while NeuNAc synthases catalyse the formation of *N*-acetyl neuraminic acid or *N*-acetyl neuraminic acid 9-phosphate from PEP and *N*-acetyl mannosamine or *N*-acetyl mannosamine 6-phosphate.

The relationship between these enzymes is summarised in the phylogenetic tree in Figure 1.26. This tree summarises the degree of difference between DNA sequences of KDO8P, NeuNAc(P) and two classes of DAH7P synthases in a variety of organisms.[50] In this tree, the line junctions indicate a common ancestor sequence, and the length of the line indicates the degree of relation between the sequences, with shorter lines being more similar to the branch point sequence than longer lines. This tree predicts that all the PEP aldolases are derived from a common ancestor sequence, which is more similar to Type Iβ DAH7P synthases than to any of the other PEP aldolase enzymes.

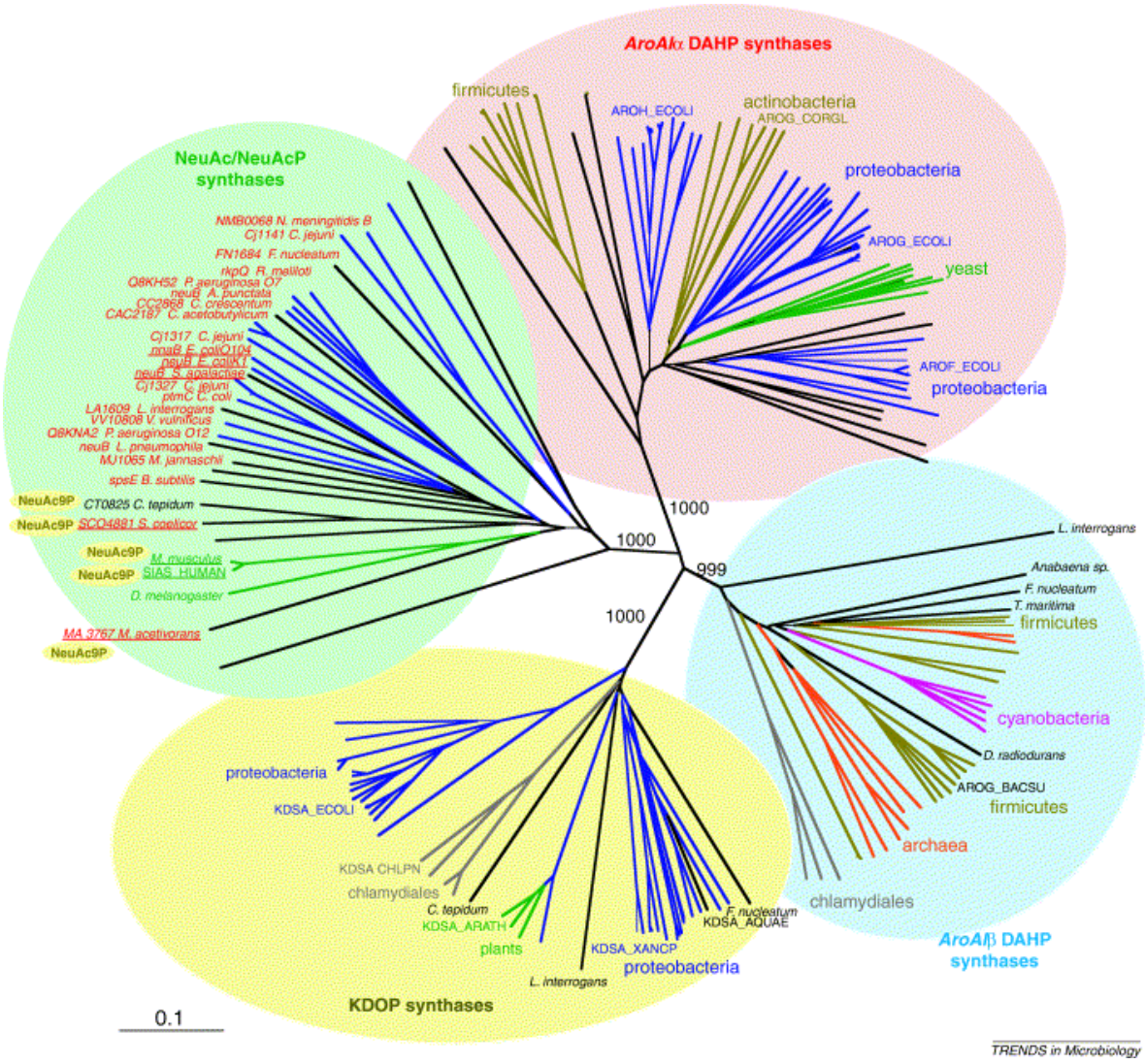

Figure 1.26: Phylogenetic tree of PEP aldolase enzymes. Taken from Bravo *et al.*[50]

The detailed characterisation of NeuNAc(P) synthases is comparatively incomplete, and little work has been published. However, it appears that at least *Campylobacter jejuni* NeuNAc synthase shares the same stereochemical preference as DAH7P synthase (*si* face attack of PEP on the *re* face of an aldehyde).[49] However, the structure of *Neisseria meningitidis* NeuNAc synthase has recently been published, and it is clear despite the level of homology predicted from DNA sequences the structure of the NeuNAc active site is very different to that of DAH7P synthase.[51]

In comparison, KDO8P synthase has been well characterised, and the extensive studies of this enzyme can be used to infer information about DAH7P synthase. The major variation between DAH7P synthases and KDO8P synthases is their difference

in metal dependency. All known DAH7P synthases require a metal ion for activity, and while some KDO8P synthases are metal dependent, others are not[52]. The metal dependent KDO8P synthases are very similar in sequence and structure to metal-independent KDO8P synthases, and several recent studies[53-55] have shown that metal-dependent KDO8P synthases from a variety of species can be converted into metal-independent KDO8P synthases by simply mutating one residue, from a metal-binding cysteine to asparagine.[53-55] This asparagine residue is present and absolutely conserved in metal-independent KDO8P synthases; likewise the cysteine residue is similarly conserved in all metal-dependent KDO8P synthases and all DAH7P synthases. The reverse mutation in metal-independent KDO8P synthases likewise restores metal dependency to metal independent *E. coli* KDO8P synthase.[54, 55] However, the corresponding mutation in the metal-binding site of *P. furiosus* DAH7P synthase (C31N) gives inactive enzyme.[39]

The metal-dependent KDO8P synthases differ from DAH7P synthases in conserved sequences; they all have an absolutely conserved phenylalanine residue in the PEP phosphate-binding pocket, which replaces a correspondingly conserved arginine residue in DAH7P synthases.[39] This phenylalanine is also present in metal-independent KDO8P synthases, and at least one (*N. meningitidis*) NeuNAc synthase.[51] All KDO8P synthases have an additional asparagine-alanine mutation in the active site, which is absent in DAH7P synthases, changing the absolutely conserved KPRT(S) motif in DAH7P synthases (Section 1.2); to a KANRS motif in KDO8P synthases.[39] It is notable that both the hydrophobic recognition of PEP C3 and hydrogen binding to the monosaccharide hydroxyl groups by the KPRT(S) proline is preserved in the KANRS motif.

While these differences may be small, they provide evidence that the underlying mechanisms of KDO8P synthases and DAH7P synthases may be more different than has been previously assumed. A mechanism has been proposed that accounts for these conserved changes in KDO8P synthases (Figure 1.28).[39]

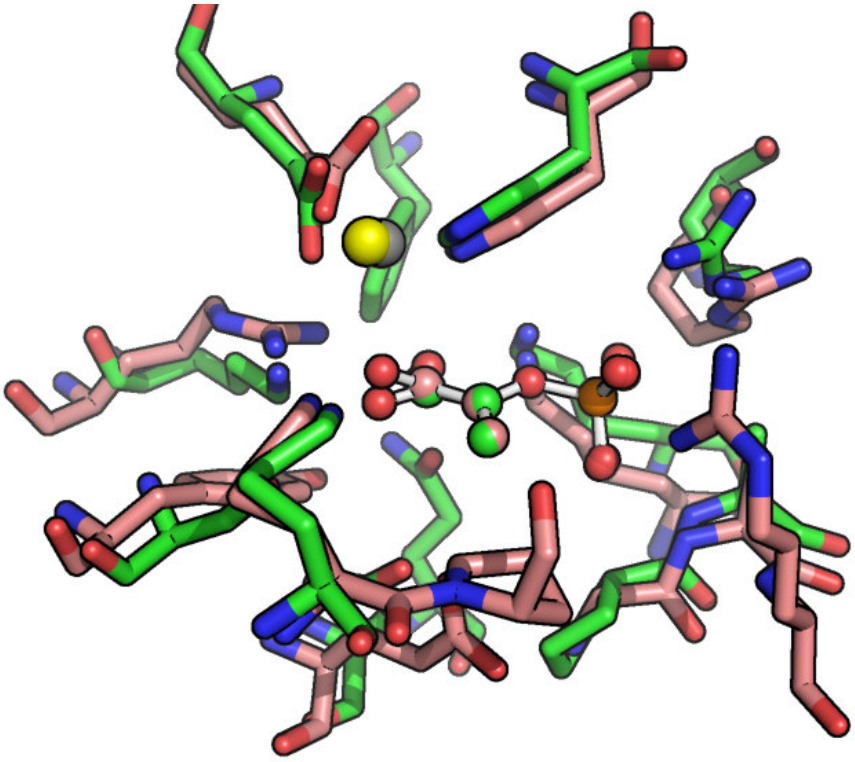

Figure 1.27: Overlay of the active site of *E. coli* DAH7P synthase (salmon) and *A. aeolicus* KDO8P synthase (green), as defined by residues within 4Å of PEP. Structures are from 1n8f.pdb[27] and 1fws.pdb[56] respectively; the three carbon atoms enol oxygen and phosphorus atom of PEP have been overlaid by 3-dimensional least-squares superposition; the RMS-difference between the five atoms is 0.049. The manganese atom in the DAH7P synthase structure is shown in grey, the cadmium atom in KDO8P synthase structure in yellow.

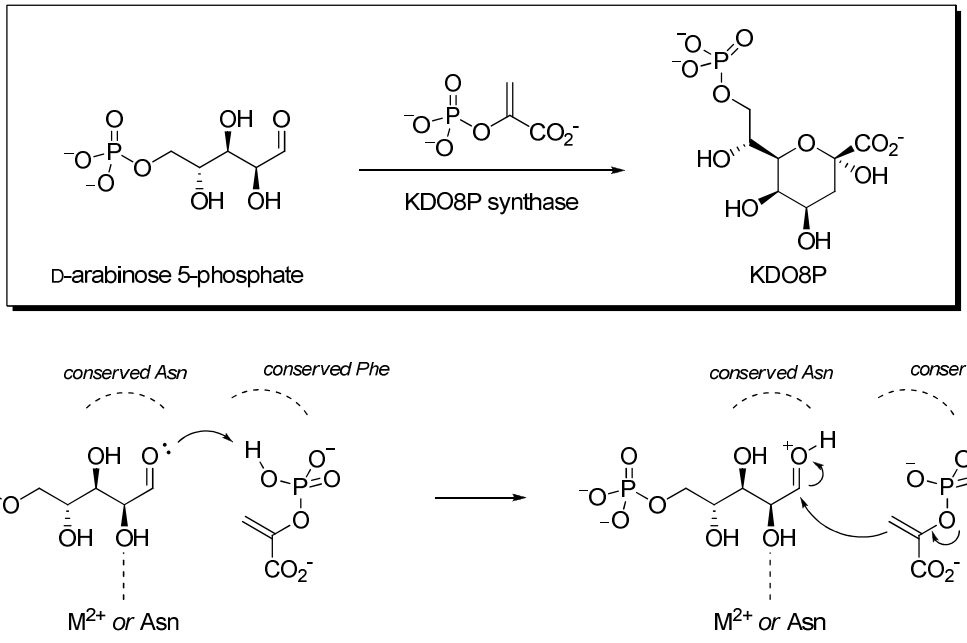

Figure 1.28: The reaction catalysed by KDO8P synthases; and a proposed partial mechanism to account for the conserved sequence differences between KDO8P synthases and DAH7P synthases.[39]

The conserved phenylalanine may ensure that PEP binds as its dianion form, and the weaker phosphate second ionisation may be used to protonate the carbonyl oxygen of A5P, as a protic acid substitute for the metal-based Lewis acid catalysis. The dianionic phosphate can then deprotonate a water molecule to produce a hydroxide ion to intercept the carbocation intermediate, analogous to DAH7P synthase (*vide supra*; Section 1.2, Figure 1.19). Note in this mechanism the metal (in metal dependent enzymes) or the asparagine (replacing cysteine in metal independent enzymes) is in the same location as the metal in DAH7P synthase, and consequently binds the C2-hydroxyl of A5P, rather than A5Ps C1 carbonyl.[39] This proposal explains the observed substrate specificity of KDO8P synthases, where substrates such as ribose 5-phosphate (R5P) and 2-deoxyA5P (which either have the incorrect C2 hydroxyl configuration, or lack the C2 hydroxyl altogether) are not substrates for either metal dependent[30] or independent[57] KDO8P synthases, whereas the corresponding 2-deoxyE4P and T4P are still substrates for DAH7P synthase[39] (*vide supra*). This highlights the role of the C2 hydroxyl-enzyme interaction in orientating the carbonyl group for reaction in KDO8P synthases, whereas in DAH7P synthases the carbonyl is orientated by its interaction with the metal atom.

Despite this proposed difference in carbonyl activation, there are still important similarities in the enzymes. Both enzymes catalyse the addition of the *si* face of PEP to the *re* face of the carbonyl of a sugar phosphate, both bind their substrates in an ordered sequential manner[57], with PEP first and the sugar phosphate second. Both have similar active site architecture, and appear to bind both the PEP and sugar phosphates in similar locations, despite the differing length of their substrates.

The KDO8P synthase reaction has been studied by time-resolved ESI-TOF mass spectrometry, an emerging technique which can be thought of as the mass-spectrometry equivalent of stopped-flow spectrophotometry.[58] This technique allows the detection of enzyme-intermediate complexes with lifetimes of less than 10 ms, and was able to demonstrate the existence of the hemiketal phosphate KDO8P synthase enzyme intermediate (Figure 1.29), providing the first direct support for the proposed mechanism for KDO8P synthase, and consequently supporting the proposed mechanism for DAHP synthase. Both acidic and basic rapid chemical quench techniques had previously failed to detect this intermediate, presumably due to its

lability.[59] The detection of this intermediate is remarkable, given the KDO8P synthase reaction has a half-life of around 7 ms, and clearly demonstrates the promise of this emerging technique.

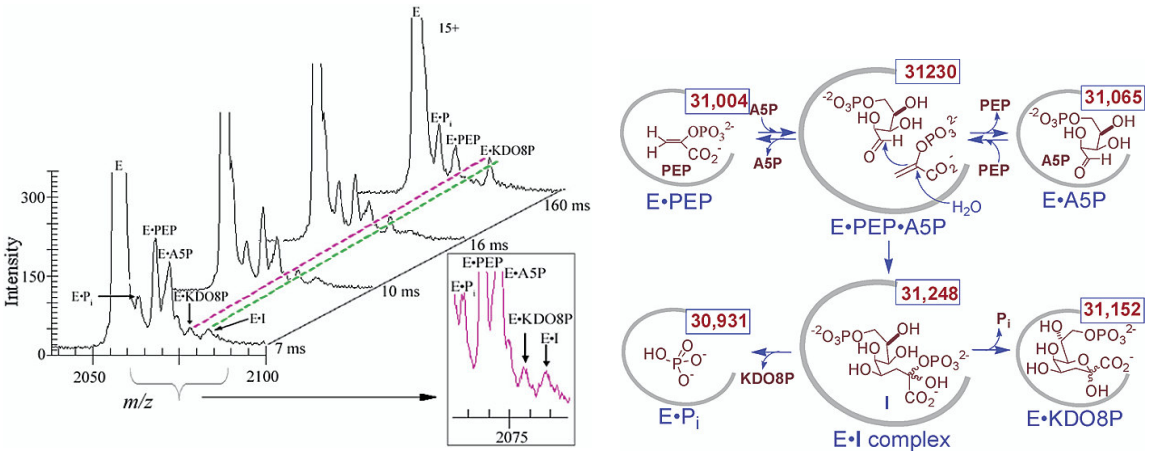

Figure 1.29: Time resolved ESI-TOF mass spectra for the KDO8P synthase reaction, and mechanistic analysis of the mass peaks. Taken from Anderson *et al.*[58]

Utilising the same mass spectroscopy technique, detailed rate data was able to be collected for the KDO8P synthase reaction (Figure 1.30).[60] The formation of the hemiketal phosphate intermediate was found to be rate-limiting (k = 95 s^{-1}), with the rate of intermediate breakdown considerably faster (k = 500 s^{-1}). This agrees well with the overall kinetic constant, determined by more traditional pre-steady state burst kinetics (k = 100 s^{-1}). Whether this data is holds true for the reaction of DAH7P synthase remains to be determined.

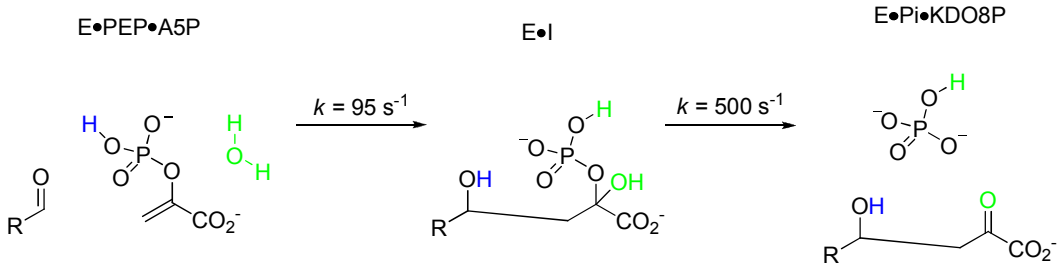

Figure 1.30: Rate constants for the KDO8P synthase reaction

A recent paper containing several high resolution structures of mutant *A. aeolicus* KDO8P synthases claims to have observed directly the hemiketal phosphate intermediate of the reaction (Figure 1.31) in two structures.[42] The authors claim the

intermediate bears the (*R*)-configuration at the ketal carbon, which implicates the PEP *si*-face water as the nucleophile, either by the carbanion mechanism or by quenching the oxocarbenium ion formed in the protic acid activation mechanism.

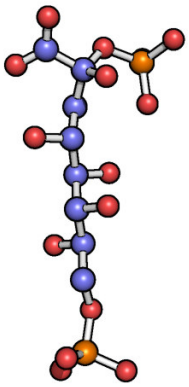

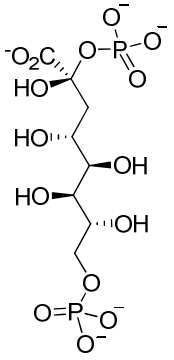

Figure 1.31: The crystallographically observed intermediate as reported by Gatti *et al*; in crystallographic and skeletal representations.[42]

However, this finding should not be taken as certain. The observed intermediate has been previously determined to be highly unstable, and the rate constants for the formation and breakdown of the intermediate have been measured to be 95 s^{-1} and 500 s^{-1} respectively for the *E. coli* enzyme (*vide supra*). The proposed intermediate in one structure is observed in a large unit cell, containing twelve crystallographically independent triple-mutant (C11N/S235P/Q237A) enzyme monomers. In eleven of the twelve active sites; a ternary enzyme-PEP-A5P complex is observed, and the trigonal planar geometry of PEP is evident in most of the active sites. The remaining PEP molecules have some bent character at C2, which is also observed in crystal structures of this enzyme lacking A5P, and in some DAH7P synthases. This bent character has been assigned as degradation of PEP due to Michael addition of water at C3.

In their paper, the authors show a $|F_o\text{-}F_c|$ σA map of the modelled enzyme without the intermediate included; overlaid with the proposed model of the intermediate (Figure 1.32). In this map, the amplitudes of the experimentally observed structure factors (F_o) are compared after subtraction of the structure factors that would be observed for the proposed model (F_c); the mean structure factor amplitude is denoted σ. Ideally, in such a diagram one would expect to see a large unexplained area of electron density, arising from the difference between the observed data (which contains the ligand) and the calculated data (which does not contain the ligand). The heavy atoms of the ligand

(atomic weights of 12 and above) should all appear inside this area, showing they are correctly placed. This should occur at a significant level of signal; such that the amplitudes shown are much greater than the average amplitude. In practice, this level is typically near 3σ (ie. three times the average density). This map (also known as an omit map) constitutes a simple method for assessing whether a ligand in an enzyme structure is a real ligand, rather than an artifact of the cycles of observation and model refinement utilised in macromolecular crystallography. The diagram presented in the paper, contoured at 3σ, clearly shows that the new oxygen atom (the only heavy atom distingushing the intermediate structure from that of the substrates) lies outside the density, giving some doubt to the claimed observation of the intermediate.

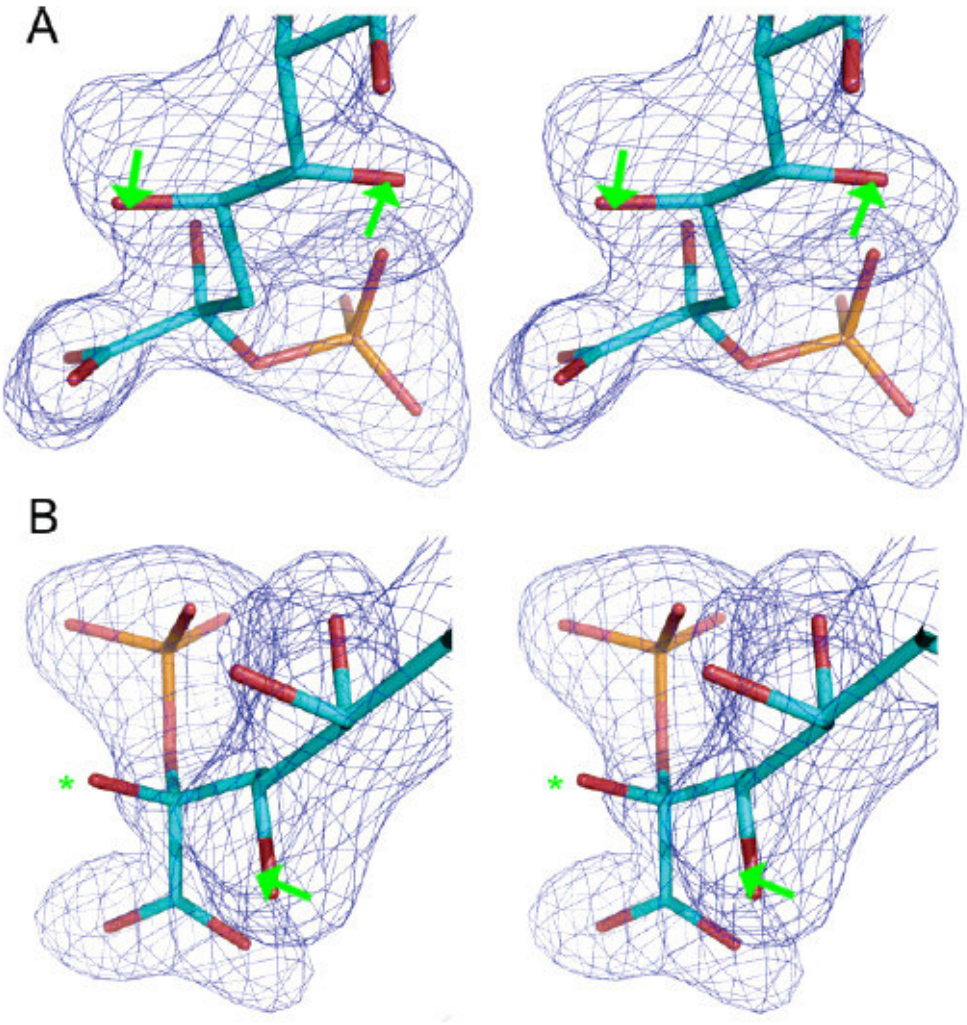

Figure 1.32: Stereo diagram of the $|F_o\text{-}F_c|$ σA (omit) map contoured at 3σ; with the modelled intermediate overlaid. A and B show different representations of the same electron density; the protrusion of the modelled oxygen atom from density has been marked. Deformations of the "intermediate" C4, C5 hydroxyls from areas of peak density are shown on the right (green arrows). Diagram is taken from Gatti *et al*[42], the green elements have been added.

In addition, the C4 and C5 atoms of the intermediate (corresponding to C1 and C2 of A5P) appear to be deformed away from the peak electron density. This could occur if the intermediate had been modelled incorrectly over density derived from two separate molecules, since the observed density is from molecules separated by a larger distance than that across than the covalent C3-C4 bond in the model.

Based on these arguments, the possibility remains that the proposed intermediate is simply an artifact, and partial tetrahedral character introduced by the breakdown of PEP by Michael addition has been misinterpreted during model building. Further work will be required to substantiate the existence of the proposed intermediate and its configuration.

1.4 The project

The intention of this project was to design and synthesise inhibitors for the DAH7P synthase reaction. These inhibitors could help provide information about the enzyme mechanism, and help provide a basis for future drug design work.

There has been little previous published work in this area, and prior to this work only three inhibitors were known (Figure 1.33), and a distinct lack of any designed inhibitors.

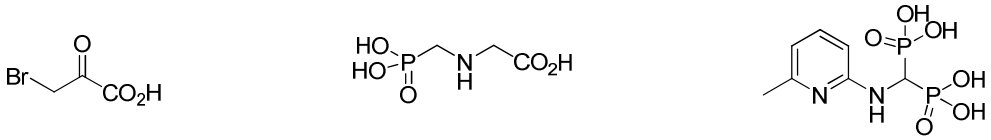

Figure 1.33: Previously reported DAH7P synthase inhibitor

3-Bromopyruvate is an irreversible inhibitor of *E. coli* DAH7P synthase, causing inactivation by covalent modification.[61] The inactivation is competitive with respect to PEP, and the presence of metal ions protects the enzyme from inactivation, suggesting a nucleophilic metal binding ligand such as cysteine is being modified.

Glyphosate (Figure 1.33, centre) has been reported to inhibit plant DAH7P synthases during the search for mechanism of the herbicidal activity of glyphosate.[62] Plant cells

treated with glyphosate have a deficiency of aromatic amino acids, which suggested inhibition of the shikimate pathway. DAH7P synthase was found to be inhibited by glyphosate, but it is now known EPSP synthase is the target of glyphosate.[11] Later work found that there are two plant isozymes of DAH7P synthase, and only one isozyme of DAH7P synthase is inhibited by glyphosate, and only when cobalt(II) is the metal co-factor.[63]

A family of compounds known as methylene bisphosphonates display herbicidal properties when injected into whole plants, in particular the pyridyl bisphosphonate shown on the right in Figure 1.33. Some early work had identified DAH7P synthase as the target of this inhibition, however the reported inhibition constants are modest (0.62 mM against E4P, 0.43 mM against PEP).[64] A more recent paper disputes the author's conclusions, and shows that the target of the methylene bisphosphonates is likely to be farnesyl pyrophosphate synthase, based on potent inhibition by the same pyridyl methylene bisphosphonate (IC_{50}: 23 nM).[65]

In the course of this work a paper was published which claimed to describe a mechanism-based inhibitor of a DAH7P synthase (Figure 1.34).[66] However, the authors have not conducted any enzyme assays to prove this assumption, and their only characterisation consisted of testing growth retardation of whole cells, for which they provide no data, and only state the retardation was "comparatively poor". While the molecule does bear similarity to a proposed enzyme intermediate, it remains to be demonstrated whether it is a DAH7P synthase inhibitor.

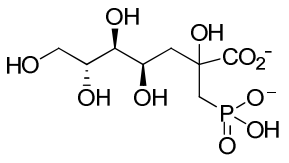

Figure 1.34: The proposed inhibitor of Grison *et al*

While there has been little work on DAH7P synthase inhibition, because of the close relationship between DAH7P synthase and KDO8P synthase the pool of work on KDO8P synthase can be used to provide a basis for the design of DAH7P synthase

inhibitors. There have been four designed inhibitors of KDO8P synthase synthesised and characterised kinetically (Figure 1.35).

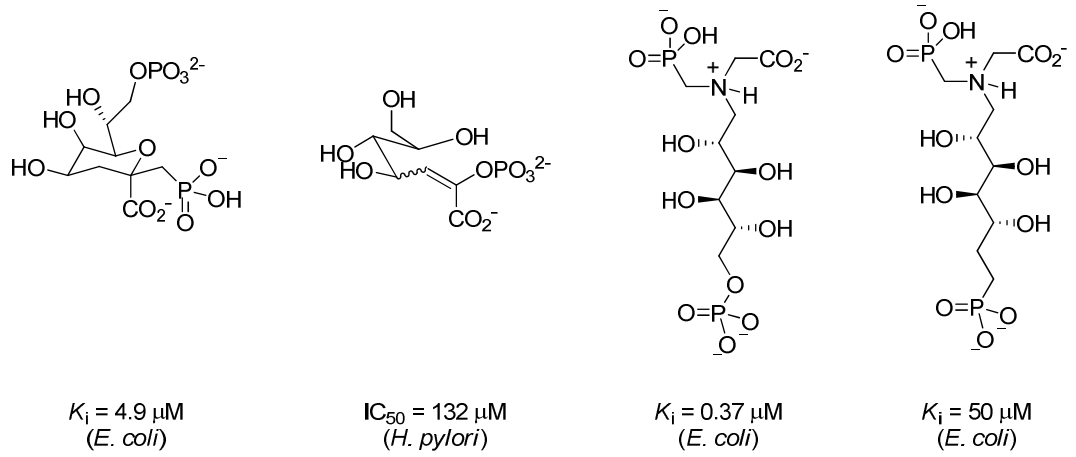

Figure 1.35: Previously designed KDO8P synthase inhibitors

The first pyran molecule (Figure 1.35, left) was designed as an inhibitor of a proposed cyclic intermediate of the KDO8P synthase reaction.[67] The K_i (4.9 μM) against *E. coli* KDO8P synthase is remarkable, given that it is now accepted that KDO8P synthase has a linear mechanism.

It has recently been shown that under some conditions ribose 5-phosphate, which is not a substrate for KDO8P synthase, can bind to the enzyme A5P site in its furanose form.[42] This may explain the ability of the pyran to inhibit KDO8P synthase.

The enol phosphate inhibitor (Figure 1.35, centre left) was designed to mimic the planar nature of the PEP enol phosphate. Despite being the D-*gluco* configuration, and lacking a terminal phosphate group, this compound inhibited *H. pylori* KDO8P synthase in a complex manner, but the molecule did not become incorporated into the active site of *A. aeolicus* KDO8P synthase (as detected by X-ray crystallography) at concentrations up to 4.4 mM.[68] The tertiary amine (Figure 1.35, centre right) was designed to mimic the oxocarbenium ion proposed in the KDO8P synthase mechanism, and has been shown to inhibit KDO8P synthases from a variety of species, with a K_i of 0.37 μM against *E. coli* KDO8P synthase.[69] The analogous phosphonate tertiary amine (Figure 1.35, right) was created in an attempt to improve the antibacterial properties of the earlier amine inhibitor by interfering with a

proposed dephosphorylation, it was found to be a less effective inhibitor, with a K_i of 50 μM against *E. coli* KDO8P synthase.[70]

The structures of the most potent inhibitor in complex with a variety of KDO8P synthase enzymes have been determined by X-ray crystallography.[30, 68, 71] These structures have shown that the inhibitor binds to the enzyme, mimicking the position of PEP and A5P, utilising the same phosphate and carboxylate binding pockets (Figure 1.36).

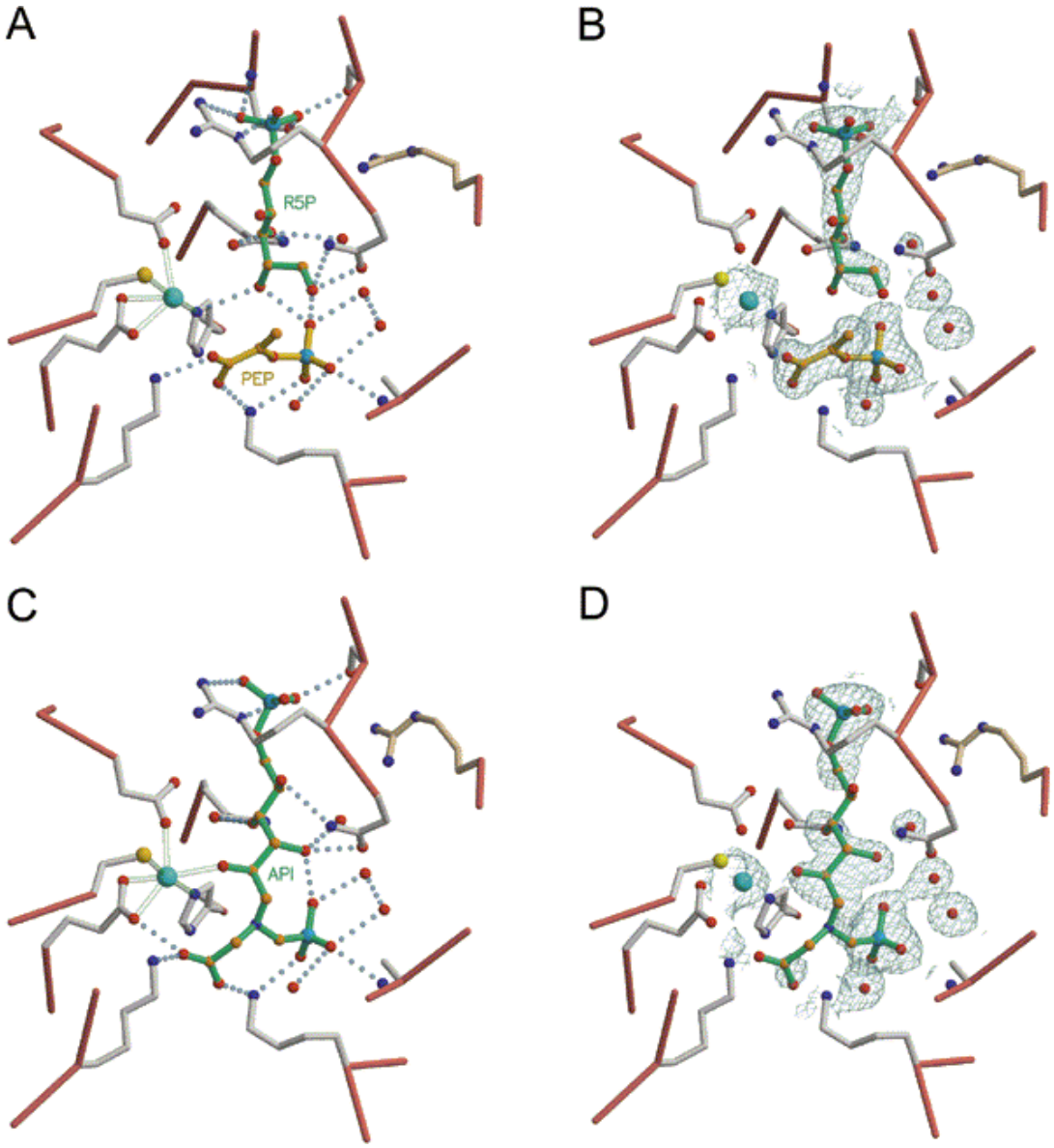

Figure 1.36: A comparison of an inhibitor and substrates bound to *A aeolicus* KDO8P synthase, a metal-dependent KDO8P synthase, and an enzyme•PEP•R5P ternary complex. (A) shows R5P and PEP modelled into the active site,. (B) is a SigmaA weighted omit map, contoured at 0.9σ, of the enzyme•PEP•R5P ternary complex. (C) and (D) show the analogous diagrams for the enzyme•inhibitor complex. Taken from Gatti *et al.*[30]

By comparison of (b) and (d) in Figure 1.36, it can be seen that the inhibitor phosphonate and phosphate groups occupy the PEP and R5P phosphonate binding pockets respectively. It is also of note that the R5P C2 hydroxyl in (A) is not a metal ligand, leading to considerable conformational flexibility in C1 and C2 of R5P, as revealed by the low electron density in these regions. The fact that the equivalent hydroxyl group is a metal ligand in the inhibitor (which has the opposite stereochemistry at the equivalent hydroxyl), leading to the corresponding carbon chain being well defined in the omit map lends weight to the earlier argument (Section 1.3) that the metal is vital for orientating the A5P carbonyl via a metal-C2 hydroxyl interaction.[39] This would also suggest that the inhibitor binding strength is dependent on the hydroxyl orientation at this position, something that is being investigated in our laboratory. The inhibitor carboxylate group is poorly defined in the omit map (d), indicating that it is not strongly bound. This has been tested experimentally[68], with a second-generation inhibitor lacking the carboxymethyl substituent on the amine (Figure 1.37).[68] This compound inhibits *E. coli* KDO8P synthase with a comparable inhibition constant to the original inhibitor, highlighting the low contribution of this group to the enzyme-inhibitor interaction. The finding that removal of the phosphonomethyl moiety leads to no inhibition reinforces the importance of the phosphonate-enzyme interaction.[68]

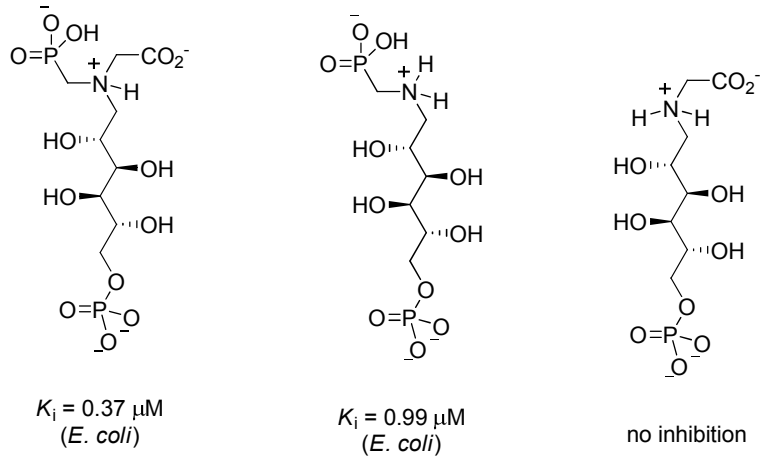

Figure 1.37: Limited SAR of amine KDO8P synthase inhibitors.[68]

Given the success of these compounds against KDO8P synthase, and the similarity in active site architecture between KDO8P synthase and DAH7P synthase, we decided to start our investigations of the inhibition of DAH7P synthase with the analogous

inhibitor reconfigured to mimic the DAH7P synthase oxocarbenium ion. This work is described in Chapter Two. Following this work, studies to design and synthesise other inhibitors of DAH7P synthase are described in Chapters Three and Four.

Chapter Two: Early Approaches to Designed Inhibition of DAH7P synthase

2.1 Inhibitor Design

When this work was commenced there was little known about inhibition of DAH7P synthase. However, work had been carried by other groups on the related enzyme KDO8P synthase; which had resulted in the potent inhibitor 2.1.[69] This molecule was designed as a mimic of the putative oxocarbenium intermediate 2.2 (Figure 2.1), and strongly inhibits *E. coli* KDO8P synthase.

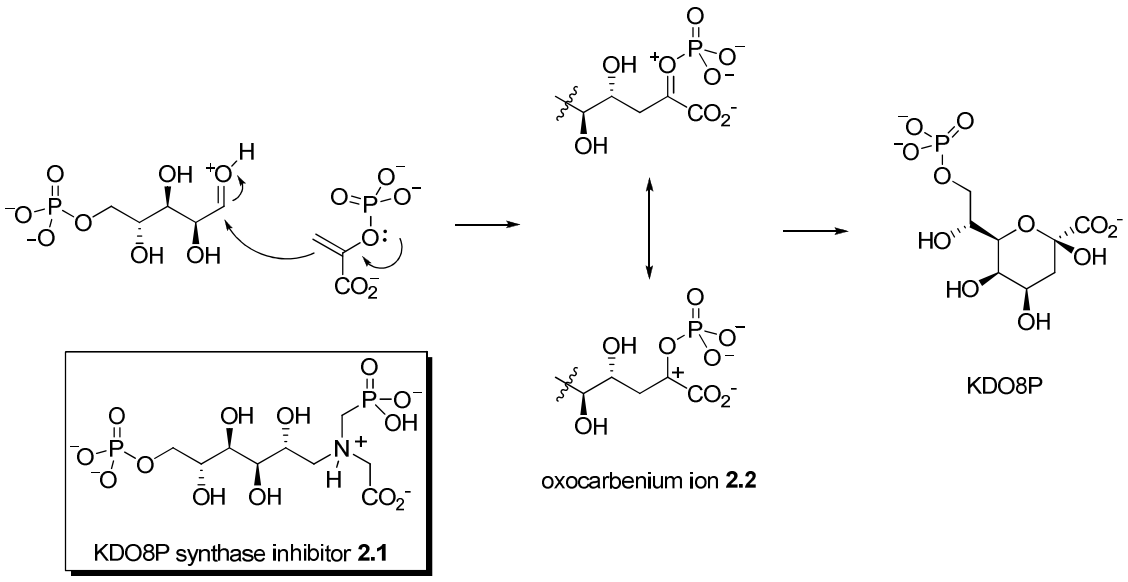

Figure 2.1: KDO8P synthase mechanism and known inhibitor 2.1

Since there are strong mechanistic similarities between the reactions of KDO8P synthase and DAH7P synthase, we proposed that it should also be possible to inhibit DAH7P synthase by mimicking the oxocarbenium ion intermediate involved in the DAH7P synthase reaction.

Designing inhibitors to mimic transition states or intermediates, rather than substrates, can lead to very high potencies.[72] Enzymes achieve catalysis through locating functional groups in such a way as to stabilise a given transition state or intermediate,

in turn lowering the activation energy for the process concerned relative to the spontaneous reaction. Consequently, the best ligand for an enzyme is in fact the transition state for a reaction, rather than the substrate or products. Molecules which mimic this transition states or intermediates can achieve much higher potencies than those which mimic substrates. With this in mind, initial efforts were set toward synthesising proposed inhibitor 2.3.

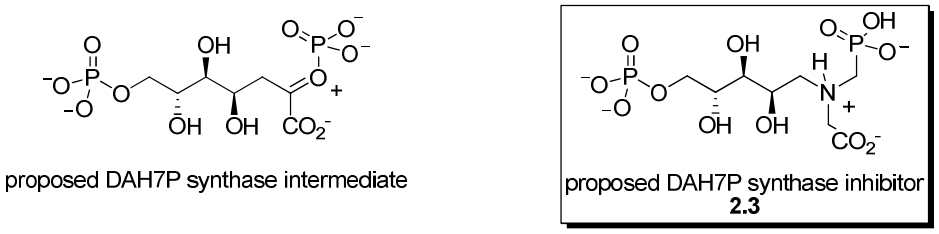

Figure 2. 2: Proposed DAH7P synthase intermediate, and the proposed DAH7P synthase inhibitor 2.3

In earlier work, the synthesis of 2.3 was attempted by directly coupling glyphosate onto a sugar phosphate backbone by reductive amination (Figure 2.3). Due to the high cost of preparative quantities of D-arabinose 5-phosphate, the reaction was modelled by substituting ribose 5-phosphate.

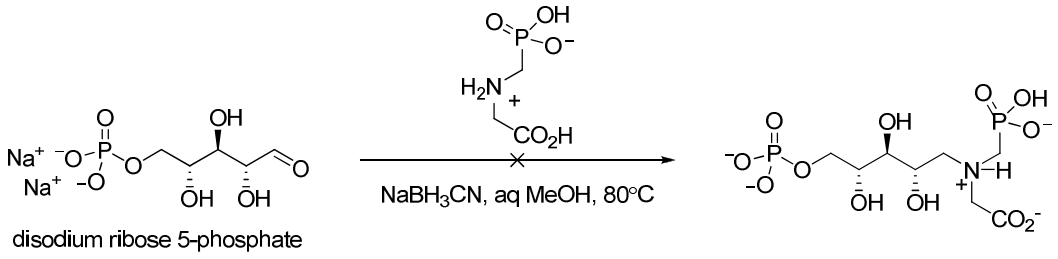

Figure 2.3: Attempted direct approach similar compounds to the desired inhibitor

This approach was unsuccessful, despite the analogous reaction with D-mannose 6-phosphate being successful in both our hands and others. After several attempts at this coupling had failed, a new approach was sought.

Another possible method to construct 2.3 is to build the amino moiety in a stepwise fashion onto a suitable aldehyde bearing the required D-*arabino* stereochemistry (Figure 2.4).

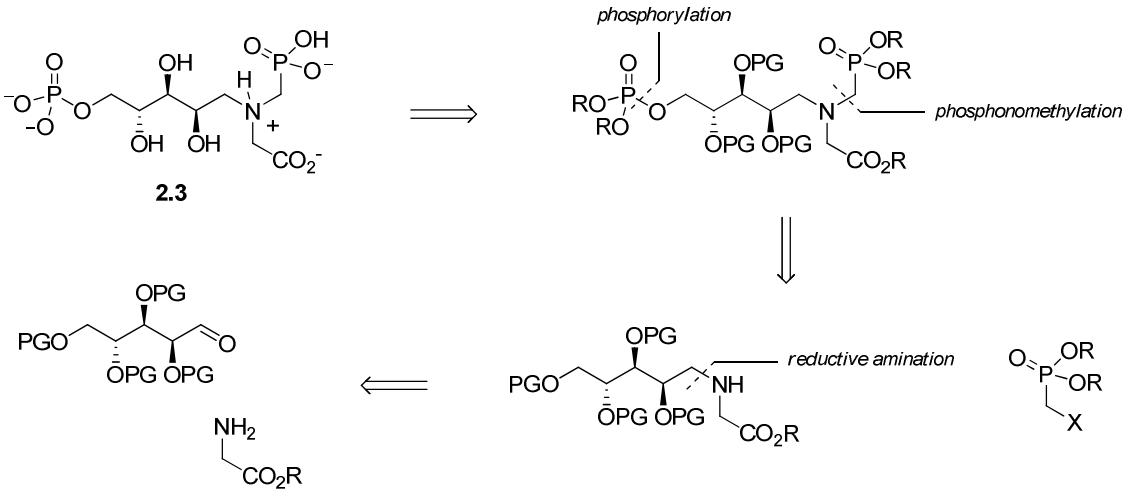

Figure 2.4: Retrosynthesis of proposed inhibitor 2.3

While many methods are available in modern synthesis to construct chiral alcohol and polyol systems, we decided to harvest the chirality in aldehyde 2.4 from the chiral pool, in the form of the relatively cheap and abundant carbohydrate D-arabinose.

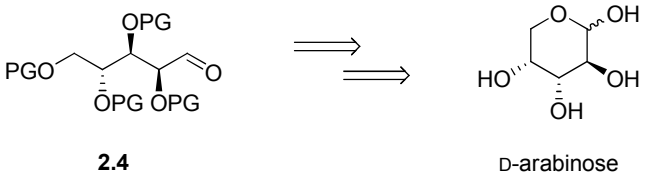

Figure 2. 5: The ultimate source of chirality for 2.4; the carbohydrate D-arabinose

2.2: Synthesis of proposed inhibitor

In order to access all of the chiral hydroxyl groups in D-arabinose, a suitable group has to be introduced to stop the intramolecular cyclisation to the furanose and pyranose forms of the carbohydrate. Due to their success in our earlier work involving D-arabinose, we chose the dithioacetal group to achieve this. Treatment of D-arabinose with aqueous ethanethiol by a modifed literature procedure gave excellent yields of crystalline dithioacetal 2.5 (Figure 2.6).[73]

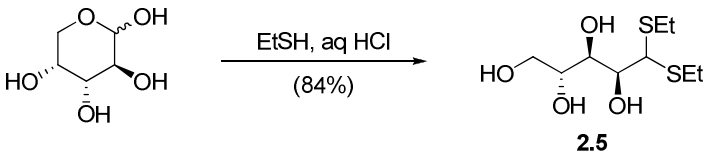

Figure 2.6: Dithioacetal formation reaction

With the hydroxyl groups liberated, suitable protecting groups need to be introduced to the hydroxyl groups to allow regeneration of aldehyde at C1 without problems from competing cyclisation. For reasons of simplicity, we chose to use isopropylidene acetal groups to block the hydroxyl groups. They are cheap and relatively atom economic protecting groups, and are stable to a wide variety of powerful bases, nucleophiles and reducing agents, yet are readily removed by dilute acid. Several possible acetals are possible in a tetraol such as 2.5; but by drawing on the results of a systematic study by Koelln *et al*[74] into the factors affecting product distributions in such systems, an excellent yield of the desired 2,3:4,5 diacetal 2.6 was produced utilising kinetic conditions (Figure 2. 7).

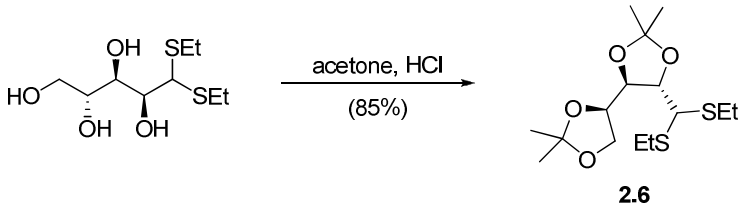

Figure 2. 7: Production of the kinetic 2,3:4,5 diacetonide 2.6

With the hydroxyl groups of 2.5 protected, the C1 aldehyde could be unmasked. Many conditions have been reported to cleave dithioacetals[75]; a possible corollary of this is that no conditions are sufficiently general for widespread adoption.

A wide set of conditions were screened for the deprotection of 2.6; and the removal of this group proved difficult (Figure 2.8). Treatment of 2.6 and related compounds under a variety of conditions[76] failed to produce the required aldehyde, generally giving a lack of reaction. Although in the case of iodine in methanol, decomposition of the starting material was also observed.

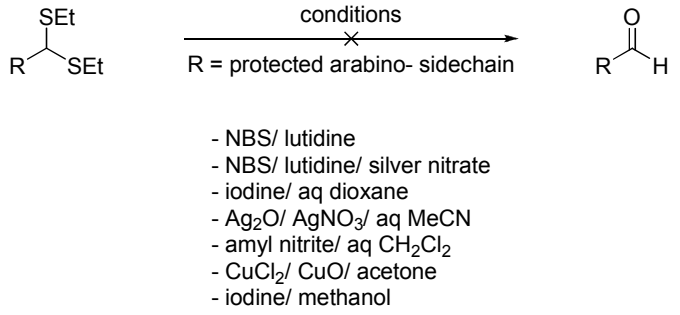

Figure 2.8: Attempted dithioacetal cleavages

In classical synthesis thioacetals have been known to be cleaved readily by exploiting the relatively specific interaction between mercury(II) and sulfur. Due to modern concerns about the toxicity of mercury compounds this method is no longer the technique of first resort;[75] however in our case treatment of 2.6 with mercuric chloride and mercuric oxide in acetone gave an excellent yield of aldehyde 2.7 (Figure 2.9). An attempt to limit the amount of mercury compounds used by substituting calcium carbonate for mercuric oxide was unsuccessful.

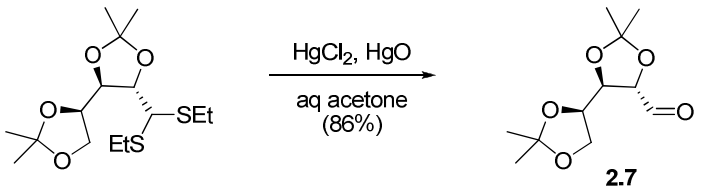

Figure 2.9: Mercury(II) induced deprotection of thioacetal 2.6

With the aldehyde liberated, introduction of the amino group could begin. Initial attempts to introduce the amino group by the method used in the synthesis of the KDO8P synthase inhibitor 2.1[69] (namely direct reductive amination with ethyl glycine hydrochloride and sodium cyanoborohydride) meet with little success, and only small amounts of product were observed. However, by including sodium acetate to allow generation of equilibrium levels of the otherwise unstable ethyl glycine free base, and molecular sieves to drive the imine formation equilibrium by selective absorption of water, good yields of amine 2.8 could be obtained from unpurified aldehyde 2.7 (Figure 2.10).

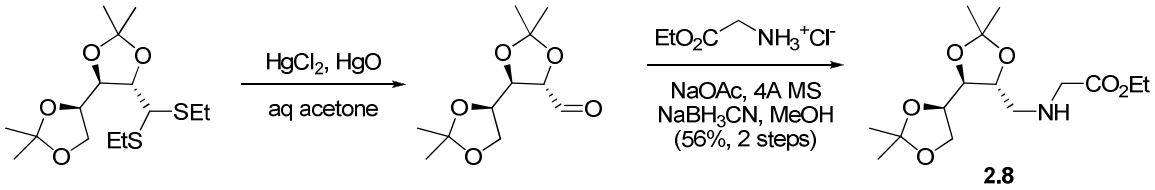

Figure 2.10: Deprotection and reductive amination to give amine 2.8

Further optimisation of the reactions of thioacetal 2.6 with iodine led to conditions where the thioacetal group could be removed in the presence of the sensitive acetonide groups, without resort to mercury compounds. The crude product from this reaction could also be used to generate amine 2.8, albeit in lower overall yield (Figure 2.11).

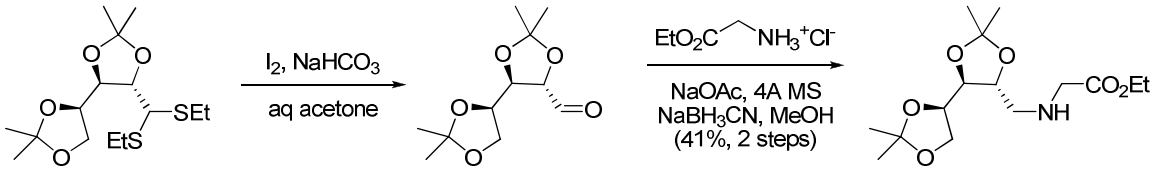

Figure 2.11: Iodine mediated cleavage of thioacetal 2.6; and subsequent reductive amination

With the required amine in hand, a method was required to introduce the phosphonomethyl substitutent. The use of phosphonomethyl sulfonates seemed to be an attractive approach; they can be generated from the corresponding hydroxymethyl phosphonates, which are themselves available from dialkyl phosphites and aldehydes. We elected to use the ethyl protected phosphonates, they are stable as protecting groups, and their use in the synthesis of KDO8P synthase inhibitor 2.1 showed that they could be removed under conditions compatible with our other functionality.

The required hydroxymethyl phosphonate 2.9 could be generated by the reaction between diethyl phosphite and monomeric formaldehyde, produced by thermally cracking paraformaldehyde *in situ*. The reaction performed similarly using either alumina[77] or triethylamine[78] as a basic catalyst (Figure 2.12), but the triethylamine method was operationally simpler, and could be readily run on large scale (28 g of phosphite).

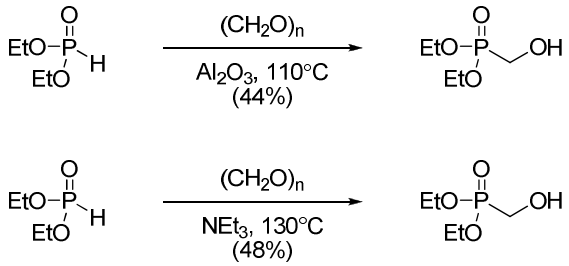

Figure 2.12: Synthesis of diethyl hydroxymethyl phosphonate 2.9

The hydroxymethyl phosphonate 2.9 underwent some decomposition during attempted vacuum distillation; and in practice it was easier to purify the product by solvent extraction; the material produced was of sufficient quality to be used in the following steps.

Treatment of the phosphonate at low temperature with triflic anhydride[79] produced crude triflate 2.10 (Figure 2.13) of approximately 80% purity; due to concerns about the stability of this reagent it was not purified or stored further, but immediately used in the phosphonomethylation reaction after isolation.

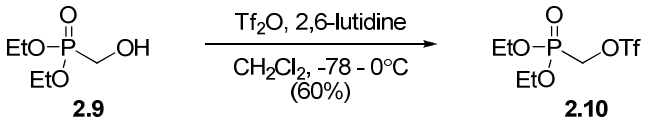

Figure 2.13: Triflation of alcohol 2.9 to give phosphonomethylating reagent 2.10

With a phosphonomethylating reagent in hand, work could begin on installing the phosphonomethyl moiety onto amine 2.8.

In their synthesis of the KDO8P synthase inhibitor 2.1, Du *et al* used a phase transfer method to introduce the phosphonomethyl group (Figure 2.14). However this method required an excess of triflate 2.10, delivered in portions to counter the hydrolysis of the reagent under the aqueous conditions.

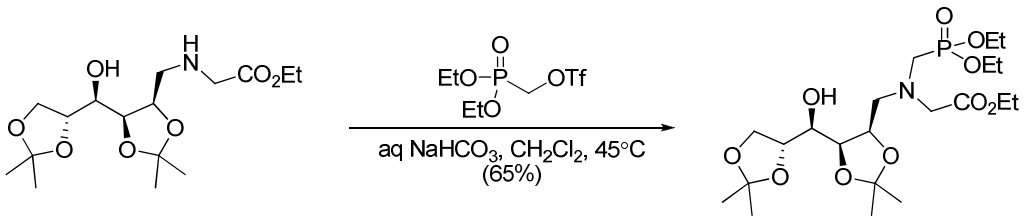

Figure 2.14: The aqueous phase transfer method of Du *et al* for introduction of the phosphonomethyl group[69]

In order to ease acess to proposed inhibitor 2.3, attempts were made to devise an improved method for the phosphonomethylation reaction. The treatment of the potassium amides of secondary amines in dimethoxyethane with alkyl halides has been reported to give good yields of the tertiary amine.[80] However in our case this produced a complex mixture of products that was not further investigated.

With this failure we decided to trial simpler conditions for this reaction. It was reasoned that by utilising a more polar solvent than dichloromethane the rate of the reaction should be increased, and by using an insoluble base as an acid absorbent the reaction should proceed without excessive hydrolysis of triflate 2.10.

Gratifyingly, treatment of amine 2.8 with fresh triflate 2.10 in a heterogenous mixture of acetonitrile and anhydrous potassium carbonate gave good yields of the required aminophosphonate 2.11. This reaction was even effective in cases where triflate 2.11 was the limiting reagent (Figure 2.15), highlighting the low rate of non-productive triflate hydrolysis under these conditions.

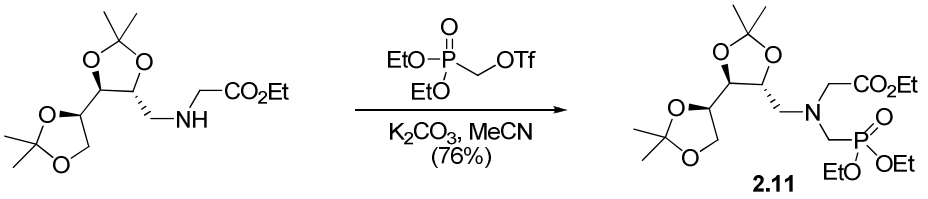

Figure 2.15: Phosphonomethylation of amine 2.8 to aminophosphonate 2.11

With the aminophosphonate portion of the molecule assembled, the distal phosphate needed to be introduced. In order for this to occur, the terminal 4,5-isopropylidene acetal needed to be removed in the presence of both the 2,3-isopropylidene acetal and the aminophosphonate. A comment in the paper describing the synthesis of KDO8P

synthase inhibitor 2.1 suggested that this transformation may not be straightforward,[69] and with this in mind conditions were trialled which were known to show selectivity in deprotection of one isopropylidene acetal over another.

Treatment of aminophosphonate 2.11 with iron(III) chloride hexahydrate adsorbed on silica gel[81] failed, leading only to recovery of starting material. Presumably the traces of acid produced in this system are rapidly neutralised by the basic nitrogen atom in 2.11. Likewise treatment of aminophosphonate 2.11 with zinc(II) nitrate hexahydrate in refluxing acetonitrile failed to give the desired product.[82]

One condition which has been reported to selectively cleave a 4,5-isopropylidene acetal in a 2,3:4,5 di(isopropylidene acetal) is cerium(III) chloride heptahydrate in acetonitrile, containing a trace of oxalic acid.[83] These conditions appeared successful in producing diol 2.12 (Figure 2.16), although the reaction time was considerably longer than the reported time (52 hours for our substrate, versus 0.5 – 2 hours for the substrates in the original paper).

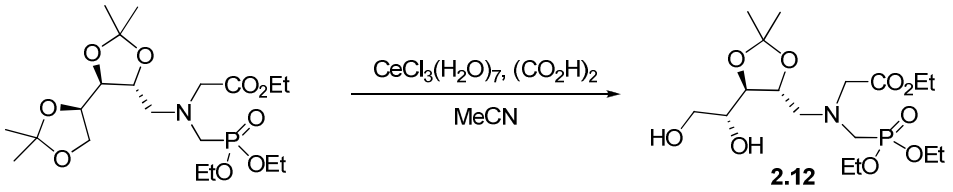

Figure 2.16: Selective cleavage of the terminal acetonide of 2.11 with cerium(III) chloride

The crude product produced by this route was difficult to characterise by NMR spectroscopy, presumably due to traces of paramagnetic cerium(III) in the crude product. It was also too polar for purification by silica flash chromatography. Crude diol 2.12 was directly treated with diethyl chlorophosphate to introduce the terminal phosphate group. Disappointingly, phosphorylation appeared to be only partly selective for the 5-position, and the corresponding polar mixture of compounds were unable to be separated by flash chromatography.

Preliminary investigations showed the mixture was able to separated by costly and time consuming preparative HPLC, however it was felt that a better use of time might be to rework the initial steps of the synthesis to incorporate orthogonal protecting

groups on C5 and the other hydroxyl groups. This would allow selective liberation of the 5-hydroxyl group, and thus sidestep the chemo- and regioselectivity problems encountered in the 4,5-acetonide deprotection and the 5-phosphorylation.

A *tert*-butyldiphenylsilyl (TBDPS) group should fulfill this requirement; it is known to be stable to a variety of conditions yet can be readily cleaved utilising fluoride ions, conditions which leave many other groups unaffected. Furthermore, from earlier work with dithioacetal 2.5, we knew that the group could be regioselectivity introduced at the 5-position in dichloromethane, without problems with further reaction. Accordingly, treatment of thioacetal 2.5 with *tert*-butyldiphenylsilyl chloride gave triol 2.13, bearing the silyl group at the 5-position (Figure 2.17).

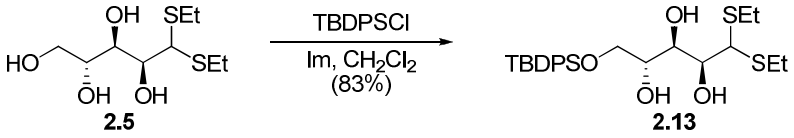

Figure 2.17: Silylation of thioacetal 2.5 to triol 2.13

Attempts to introduce benzyl groups to the 2,- 3- and 4-hydroxyls of triol 2.13 under standard conditions[76] (BnBr, NaH, TBAI) gave a complex mixture of partially benzylated prodcuts, and no improvement was noted using benzyl trichloroacetimidate and catalytic triflic acid (Figure 2.18).[84]

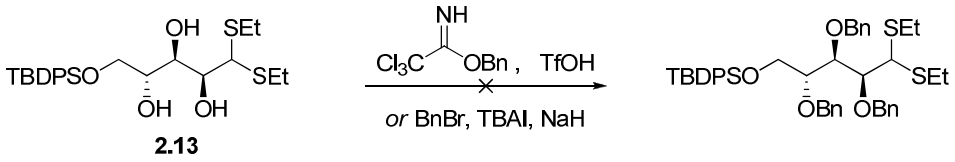

Figure 2.18: Attempted benzylation of triol 2.13

The difficulty in perbenzylating 2.13 is probably due to increasing steric hindrance to reaction as each successive hydroxyl group is benzylated. With this in mind, we attempted to introduce the smaller acetyl group onto triol 2.13, and complete reaction could be achieved under forcing conditions (Figure 2.19). The conditions required to completely acetylate 2.13 are consistent with protection of the triol unit being sterically disfavoured.

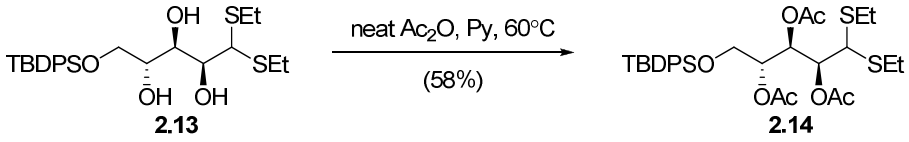

Figure 2.19: Acetylation of triol 2.13 to triacetate 2.14

Deprotection of triacetate 2.14 under our previously developed mercury(II) chloride/ mercury(II) oxide conditions cleanly afforded the corresponding aldehyde 2.15 (Figure 2.20).

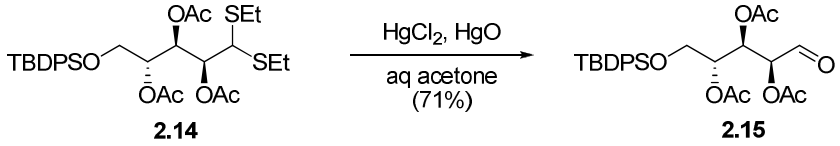

Figure 2.20: Deprotection of the thioacetal of triacetate 2.14 to aldehyde 2.15

Attempts to introduce the amine unit onto aldehyde 2.15 under our previously developed reductive amination conditions returned a complex mixture of products, for reasons which remain unclear. It is possible the electron withdrawing nature of the acetate protecting groups was interfering, or that the acetate groups were sensitive to the reaction conditions.

Based on this, it was decided to utilise a hybrid protecting group scheme, where the 2, 3-hydroxyls are masked as an isopropylidene acetal, the 4-hydroxyl as an acetate, and the 5-hydroxyl as a TBDPS group. Acetal 2.6 was treated with dilute hydrochloric acid in warm aqueous methanol to selectively remove the 4,5-isopropylidene acetal and give diol 2.16 in good yield (Figure 2.21).

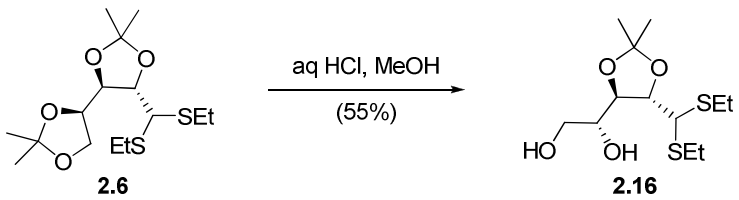

Figure 2.21: Selective removal of the 4,5-acetonide from 2.6 to give diol 2.16

Treatment of diol 2.16 with TBDPSCl, followed by treatment with acetic anhydride and pyridine and catalytic DMAP gave the required protecting group regime in good yield in a convenient one-pot operation (Figure 2.22).

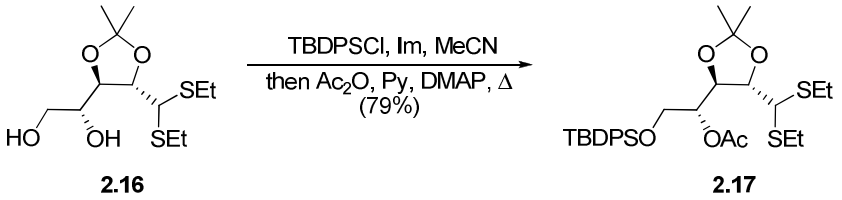

Figure 2.22: One-pot silylation/acetylation to give fully protected thioacetal 2.17

Deprotection of thioacetal 2.17 under our mercury-mediated conditions gave the required aldehyde cleanly, and subsequent reductive amination gave the required amine 2.18 (Figure 2.23).

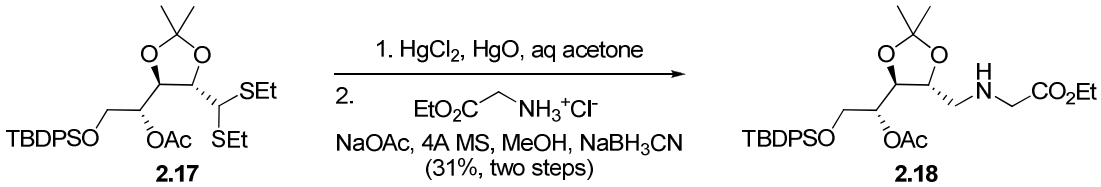

Figure 2.23: Deprotection and reductive amination to give amine 2.18

While the yield of the reductive amination was not as high as that achieved as that with the isopropylidene acetal 2.6, it was adequate for our purposes, and had the advantage of giving an orthogonally protected amine.

Treatment of the amine 2.18 with fresh phosphonomethyl triflate 2.10 under the previously developed heterogeneous conditions gave aminophosphonate 2.19 in fair yield.

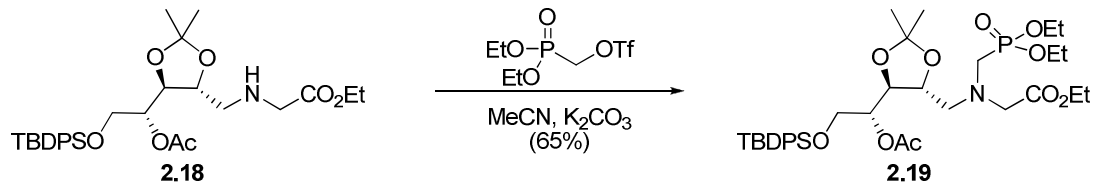

Figure 2.24: Phosphonomethylation of amine 2.18 to aminophosphonate 2.19

With the aminophosphonate 2.19 constructed, the 5-hydroxyl could now be released and phosphorylated. Treatment of aminophosphonate 2.19 with tetrabutylammonium fluoride (TBAF) gave the required alcohol 2.20 cleanly (Figure 2.25). Unlike the diol produced from diactonide 2.8, alcohol 2.20 was readily purified and characterised.

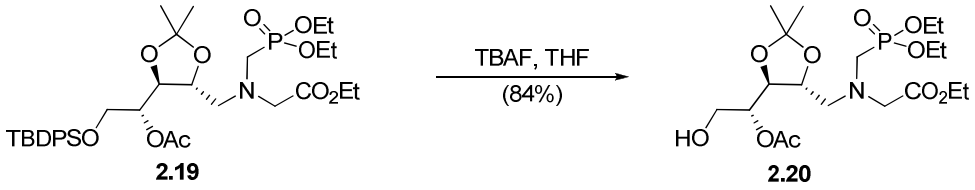

Figure 2.25: Desilylation of 2.19 with TBAF to give alcohol 2.20

Treatment of alcohol 2.20 with freshly prepared diethyl iodophosphate gave a fair yield of terminal phosphate 2.21 (Figure 2.26). The yield of 2.21 is perhaps indicative of the difficulties of working with small quantities of highly polar compounds such as 2.21, rather than the formation of side products.

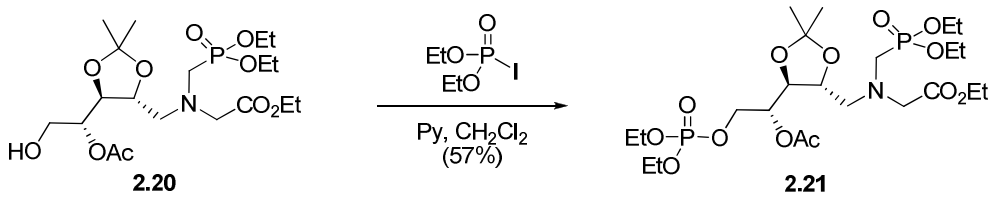

Figure 2.26: Phosphorylation of alcohol 2.20 to give phosphate 2.21

With the final protected compound 2.21 in hand, deprotection could begin. This was achieved by essentially the method used by Du *et al* in the synthesis of the KDO8P synthase inhibitor 2.1; but modified to include simultaneous deprotection of the ethyl phosphate and phosphonate groups in 2.21.

Treatment of 2.21 with trimethylsilyl bromide, in the presence of excess triethylamine to protect the nitrogen atom of 2.21 from alkylation, removed the ethyl groups from the phosphate and phosphonate of 2.21. Treatment with water cleaved the resulting silyl esters, and heating the aqueous mixture to 75°C gave autocleavage of the isopropylidene acetal protecting group, catalysed by the acidic phosphate and phosphonate groups. Treatment with aqueous potassium hydroxide gave cleavage of carboxy ester groups (Figure 2.27).

The resulting mixture of products could be separated by preparative anion exchange chromatography on SourceQ® resin, eluting with a gradient of ammonium bicarbonate. The desired product eluted between at approximately 125 mM ammonium bicarbonate. Detection of the product provided an interesting challenge; detection by standard methods such as ultraviolet absorbance is complicated by the only useful chromophore in 2.3 having an absorbance at around 214 nm, which unfortunately is also a wavelength at which the bicarbonate ion absorbs.

The problem was solved by utilising the Lanzetta assay[85], a colourimetric assay for inorganic phosphate.[85] Treatment of fractions suspected to contain product with calf alkaline phosphatase to cleave the terminal phosphate ester, followed by incubation with the Lanzetta reagent allowed detection of the product.

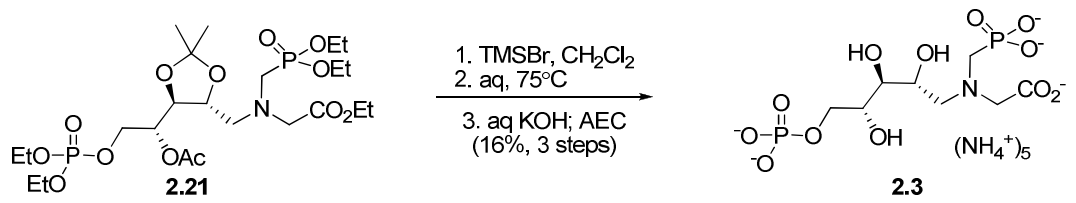

Figure 2.27: Deprotection of precursor 2.21 to target 2.3

Section 2.3: Characterisation of the enzymatic properties of proposed inhibitor 2.3

With the synthesis of our desired target 2.3, investigation of its behaviour with *E. coli* DAH7P synthase could begin. Gratifyingly, qualitative investigations showed 2.3 was indeed an inhibitor of *E. coli* DAH7P synthase; as designed. However, it quickly became apparent that the measurement of a traditional inhibitory constant, K_i, for this compound was complicated by a number of factors.

The binding of 2.3 to *E. coli* DAH7P synthase was complicated by severe time dependence, as 2.3 was incubated with DAH7P synthase for varying lengths of time the apparent inhibition became greater (Figure 2.28). This behaviour indicates that the rate of formation of the enzyme-inhibitor complex is comparatively slow. Close inspection of the progress curves in Figure 2.28 shows that after the initial dilution of the preincubated enzyme-inhibitor solution into the assay cuvette, the maximum rate

is not obtained initially, but only after a lag period. This indicates two things, that the binding of 2.3 to DAH7P synthase is in fact reversible (since irreversibly inactivated enzyme cannot be reactivated, and thus would have a maximum rate at the beginning of the assay); and furthermore that the dissociation rate of the enzyme-inhibitor complex is also slow.

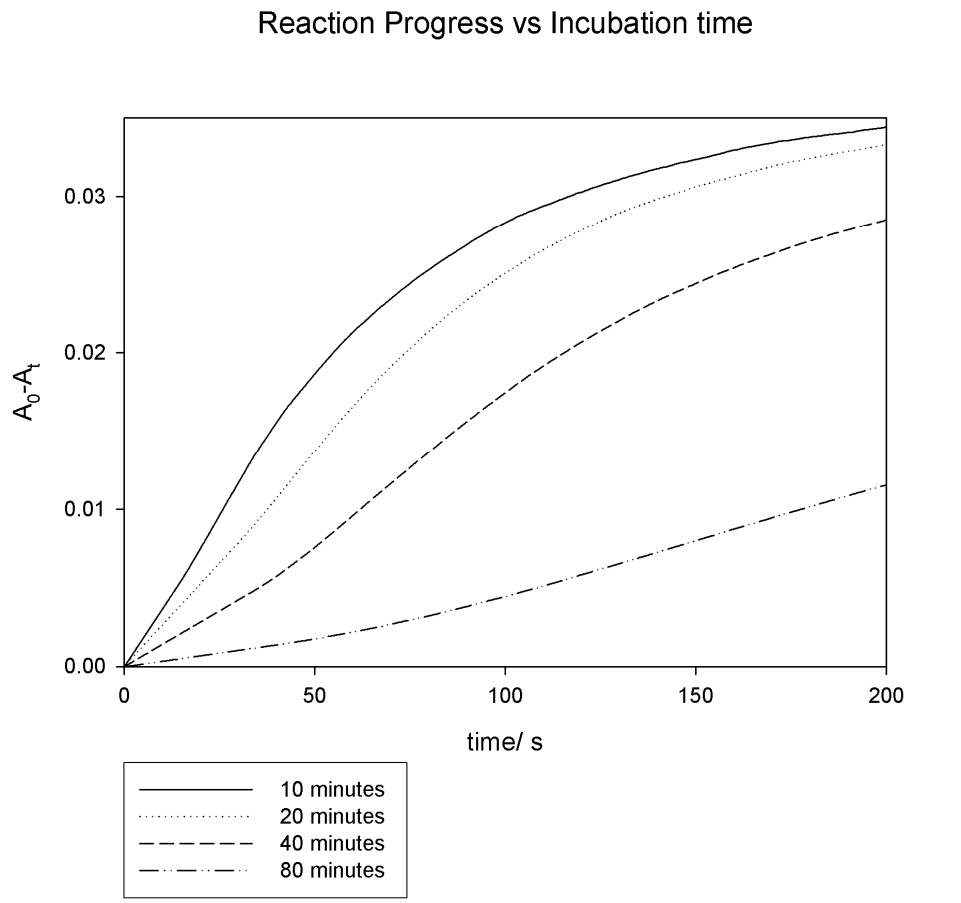

Figure 2.28: Progress curves for enzyme preincubated with inhibitor 2.3 for varying lengths of time. A solution of enzyme (120 µg) and inhibitor 2.3 (900 µM) in BTP buffer (20 µL) was incubated, and at the specified time period an aliquot (2 µL) was removed an used to initiate a substrate cuvette, and the loss of absorbance monitored at 232 nm. Substrate cuvettes contained PEP (25 µM), manganese(II) sulfate (200 µM), E4P (13 µM) in 50 mM pH 6.8 BTP buffer (1 mL).

The slow association and dissociation rates are characteristic of a particular type of enzyme inhibition kinetics, known as slow-tight inhibition.[86] Relevant equilibria for a simple hypothetical example are shown in Figure 2.29.

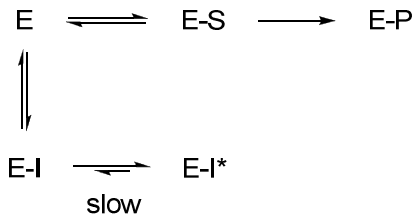

Figure 2.29: Equilibria for slow-tight inhibition

In slow-tight inhibition, the formation of the normal enzyme-substrate complex E-S is hampered by the reversible formation an enzyme-inhibitor complex, E-I, as in simple competitive inhibition. However, in slow-tight inhibition the initial relatively weakly bound E-I complex can undergo a slow isomerisation to a tightly held complex, E-I*, where the equilibrium favours the tightly held complex. This results in a slow sequestering of enzyme as the tight complex E-I*, and a consequent time dependent drop in enzyme concentration (and hence reaction rate).[86]

This behaviour is typically observed in transition state inhibition, and indeed it was observed with the related KDO8P synthase inhibitor 2.1.[69] It arises as a consequence of enzyme mechanism; whereas enzymes achieve catalysis by binding to a transition state or intermediate, this form of the enzyme is not necessarily the optimum for binding the substrates. Consequently enzymes typically exist in several conformers (Figure 2.30); the ground state conformation is one which recognises the enzymes substrate (blue); upon substrate binding a conformational change occurs which rearranges the active site to a form which favours the transition state. The subsequent distortion of the substrate molecule leads to catalysis; the product (red) is released and the enzyme relaxes to its substrate binding state.

If the inhibitor molecule resembles the transition state, it will likely have some affinity for the substrate binding form of the enzyme; and the subsequent isomerisation of the enzyme to the transition state binding form will the tight enzyme inhibitor complex E-I*.

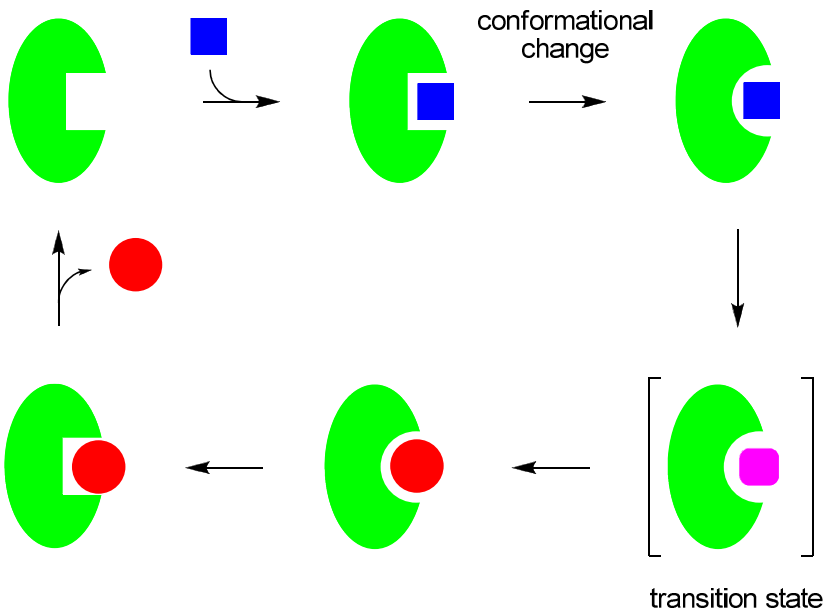

Figure 2.30: Induced-fit enzyme catalysis

Another problem that was present in assays with inhibitor 2.3 was its interaction with other assay components. The parent aminophosphonate of 2.3, glyphosate, is known to form 1:1 and 1:2 metal:ligand coordination complexes with a number of transition metal ions, including manganese(II) [87, 88]. Based on the strong structural similarities between glyphosate and inhibitor 2.3, we were concerned that this might also be a factor in our assay mixtures.

Mixing an aqueous solution of inhibitor 2.3 with aqueous manganese(II) results in a visible yellow colouration. This colouration also occurs with a mixture of glyphosate and manganese(II); and spectrophotometric analysis of the mixture shows the appearance of a broad absorption across the 200-400 nm region, which is much stronger than that expected from a simple additive effect. This absorption is consistent with a charge-transfer transition, which is known to occur in the UV-visible spectra of glyphosate-metal complexes.[88] Furthermore, the presence of manganese(II) in mixtures of preincubated enzyme and inhibitor 2.3 gives a protective effect (Figure 2.31), presumably by the formation of manganese-inhibitor complexes sequestering the inhibitor 2.3.

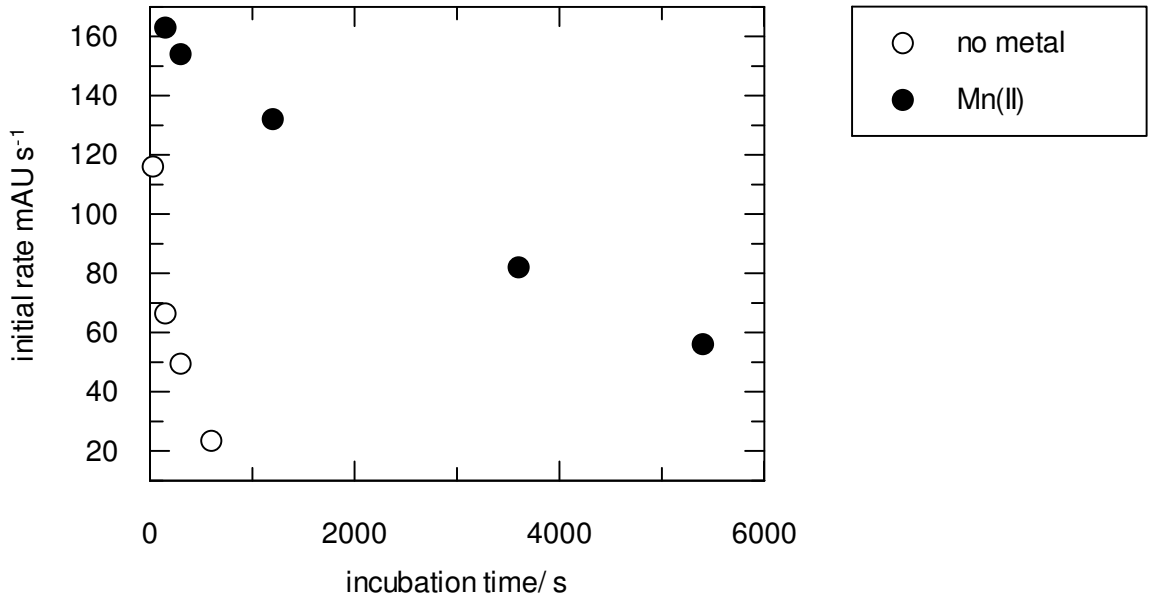

Figure 2.31: Protective effect of manganese(II) on preincubation of inhibitor 2.3 with *E. coli* DAH7P synthase. For the mangenese-free experiment, a series of cuvettes were prepared, containing 80 µM PEP, 200 µM manganese(II) sulfate, 440 µM E4P in a total volume of 940 µL 50mM BTP, pH 6.8, containing 10 µM EDTA. A sample of enzyme (120 µg) and inhibitor 2.3 (3 mM) in 110 µL 50mM BTP, pH 6.8 was incubated, and 20 µL samples added to the cuvettes at time intervals. The loss of PEP was followed spectrophotometrically at 232 nm; the initial rates were determined from linear least-squares regression. The experiment in the presence of mangenese was conducted in the same way, except with 860 µM manganese(II) sulfate present in the incubation solution.

It is worth noting that the inhibition constants of KDO8P synthase inhibitor 2.1 have only been reported for non-metalloenzyme KDO8P synthases such as the enzyme from *E. coli*. Despite the fact that structures of inhibitor 2.1-metalloenzyme complexes (such as *A. aeolicus* KDO8P synthase[30]) have been determined and published; the corresponding inhibition data has not been reported. This may indicate others have encountered similar difficulties.

Based on the dose-response data in Figure 2.32, we estimate that the concentration of inhibitor 2.3 required the reduce the enzyme activity by 50% (IC_{50}) is approximately 6 µM. However, it should be noted like all IC_{50} values, this value is strongly dependent on the assay conditions, and its utility is limited.

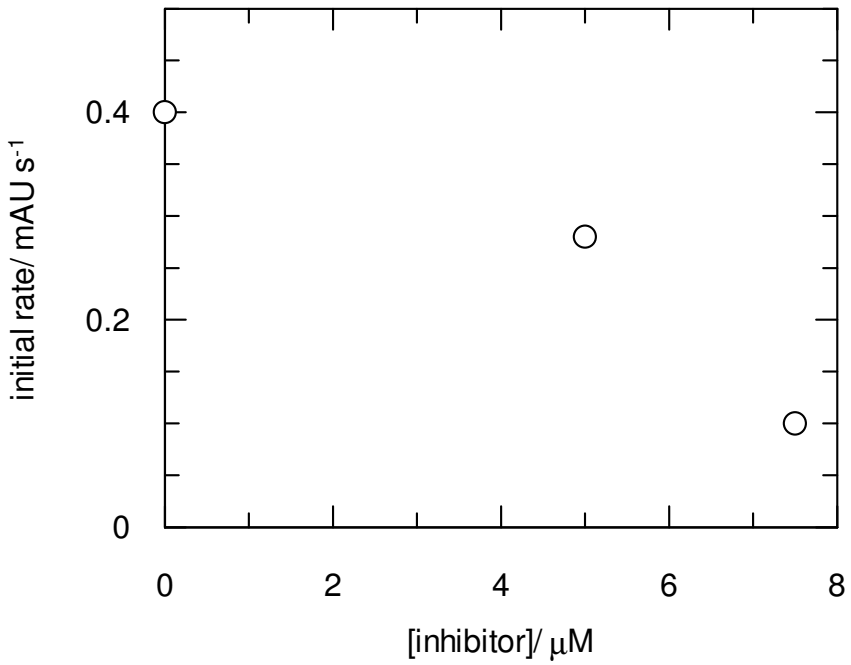

Figure 2.32: Concentration dependent inhibition of *E. coli* DAH7P synthase by increasing concentrations of 2.3. Assay cuvettes contained PEP (25 μM), E4P (15 μM), $MnSO_4$ (45 μM) and were initiated with 2 μL of enzyme-inhibitor solution preincubated for 40 minutes at varying inhibitor concentrations (0 - 3.75 mM). The loss of PEP was followed spectrophotometrically at 232 nm; the initial rates were determined from linear least-squares regression. Inhibitor concentrations shown are the final concentrations in the assay cuvette.

The inhibition of DAH7P synthase by 2.3 was more complex than was hoped, and the availability of the final compound limited detailed analysis. However, our enzyme studies did show that our hypothesis was correct; that it is possible to adapt inhibitors for KDO8P synthase into potent DAH7P synthase inhibitors.

2.4: Summary

In summary, the first designed inhibitor of a DAH7P synthase was synthesised in twelve steps from D-arabinose. This molecular was a very slow onset inhibitor of *E. coli* DAH7P synthase, and detailed analysis was hampered by a number of factors including possible formation of metal-inhibitor complexes *in situ*. Despite these difficulties, the behaviour of the molecule validated the design approach, and demonstrated that the rational design of DAH7P synthase inhibitors was possible.

Chapter Three: Single-Site Inhibitors of DAH7P synthase

3.1: Analysis of aminophosphonates

With the successful synthesis of inhibitor 2.3, a new direction of investigation was required. Due to the lack of previous work on the inhibition of DAH7P synthase, little guidance was available from the literature on what types of molecules would bind to DAH7P synthase. Initial investigations centred around molecules similar to the PEP-mimicking portion of 2.3. Accordingly, the commercially obtained aminophosphonates 3.1 and 3.2 (Figure 3.1) were screened for inhibitory activity. Surprisingly, both molecules failed to inhibit *E. coli* DAH7P synthase well. The rate of enzyme reaction in the presence and absence of each molecule was measured; racemic phosphonoalanine 3.2 failed to inhibit the reaction at concentrations up to 5.5 mM; and only a slight effect of glyphosate 3.1 was observed at a concentration of 1 mM.

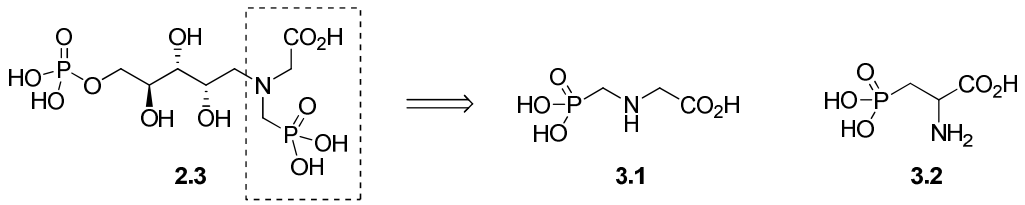

Figure 3.1: Commercially available aminophosphonates 3.1 and 3.2 screened for DAH7P synthase inhibition. The synthesis of 2.3 is described in Chapter Two.

The failure of glyphosate 3.1 to strongly inhibit DAH7P synthase was especially surprising, especially given the inhibitory power of the inhibitor 2.3, where the glyphosate portion was designed to fit to the PEP site. However, this finding suggested a new design method to achieve potent DAH7P synthase inhibition. By discovering molecules that acted as inhibitors of DAH7P synthase by competing against PEP binding, this would give a series of structures known to bind to the enzyme's PEP subsite. By elaborating these molecules to make further contacts with the enzyme, potent DAH7P synthase inhibitors should result.

Due to a paucity of molecules known to bind to the DAH7P synthase PEP-subsite, we decided to prepare and test a variety of potential mimics of PEP. This chapter focuses on the results in this area. The elaboration of these molecules into DAH7P synthase inhibitors designed to display increased potency is described in Chapter Four.

3.2: PEP-mimicking molecules

3.2.1: Changes in geometry at C2

As seen in Chapter One, the enol phosphate moiety of PEP is a crucial part of the DAH7P synthase mechanism. Consequently altering this moiety should interrupt the enzyme's activity, whilst retaining most of the contacts the enzyme uses to bind and recognise PEP. In addition to providing a basis for future inhibitor design, comparisons between these molecules may be able to provide information about the enzyme mechanism of DAH7P synthase.

In order to achieve this three molecules were prepared with a change in geometry from trigonal to tetrahedral at the equivalent of PEP C2; (*R*)- and (*S*)-phospholactates 3.3 and 3.4, and achiral cyclopropane 3.5 (Figure 3.2).

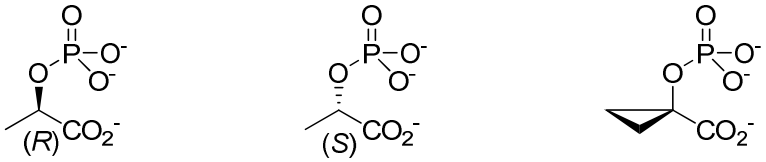

3.3 **3.4** **3.5**

Figure 3.2: PEP-mimicking molecules with changes at the equivalent to C2

Phospholactates 3.3 and 3.4 have been previously prepared in the study of other PEP-utilising enzymes;[89] they have been found to be moderately effective inhibitors of PEP carboxykinase, pyruvate kinase and enolase but have no effect on PEP synthetase. However, their interaction with any C-O cleaving PEP aldolase has not been reported.

Accordingly phospholactates 3.3 and 3.4 were prepared by the phosphorylation of the corresponding methyl lactates with freshly prepared diethyl iodophosphate. Deprotection with trimethylsilyl bromide and aqueous potassium hydroxide, followed by acidification and neutralisation with cyclohexylamine gave the corresponding tris(cyclohexylammonium) phospholactates 3.3 and 3.4 (Figure 3.3).

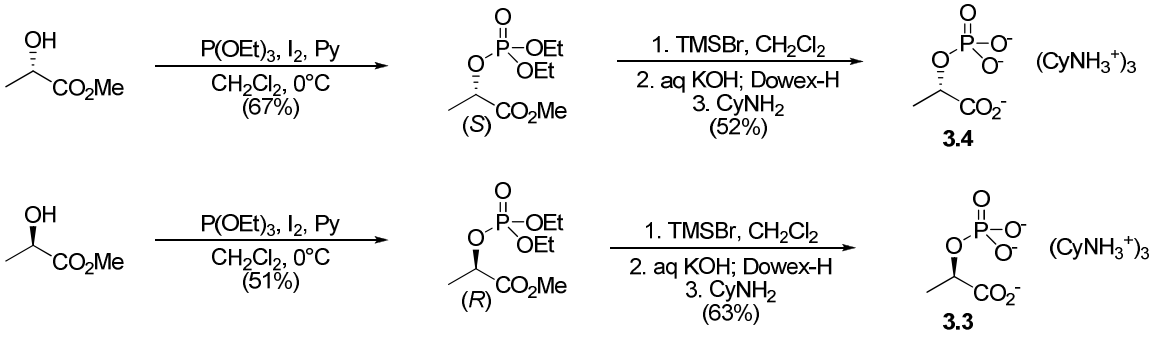

Figure 3.3: Synthesis of phospholactates (*R*)-3.3 and (*S*)-3.4

(*S*)-Phospholactate 3.4 was evaluated as an inhibitor of *E. coli* DAH7P synthase by kinetic assay. Analysis of the initial rate data by a Lineweaver-Burk analysis[90] showed that (*S*)-phospholactate 3.4 is a competitive inhibitor with respect to PEP; fitting of the Michaelis-Menten equation modified for competitive inhibition revealed that (*S*)-phospholactate binds to *E. coli* DAH7P synthase with an inhibition constant K_i of 670 ± 120 μM (Figure 3.4).

In a similar fashion, the interaction of (*R*)-phospholactate 3.3 with *E. coli* DAH7P synthase was measured (Figure 3.5). (*R*)-Phospholactate was a competitive inhibitor with respect to PEP, however the inhibition constant was greater than an order of magnitude stronger than the (*S*)-isomer, with a K_i of 49 ± 8 μM.

The vast difference in affinity between (*R*)- and (*S*)-phospholactate is intriguing, and the causes and implications of this finding for the mechanism of DAH7P synthase are discussed in Chapter Five.

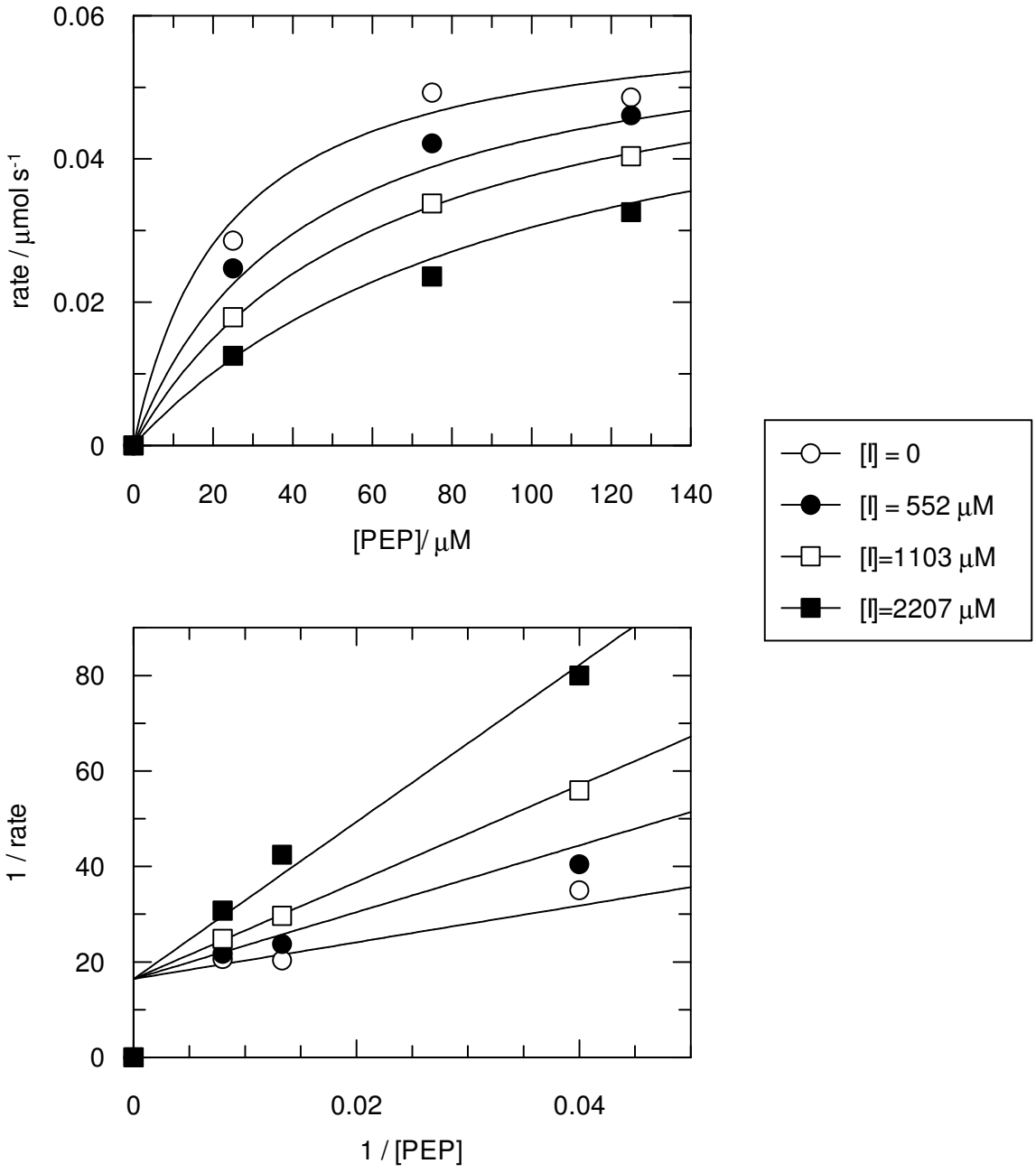

Figure 3.4: Inhibition measurements for (*S*)-phospholactate 3.4 against *E. coli* DAH7P synthase; as Michaelis (top) and Lineweaver-Burk (bottom) plots. Solutions of PEP (20-120 µM), manganese(II) sulfate (100 µM), E4P (200 µM) and (*S*)-phospholactate (0-2207 µM) in 1 mL of BTP buffer (50 mM, pH 6.8) were initiated by the addition of *E. coli* DAH7P synthase (2 µg), and the loss of PEP followed spectrophotometrically at 232 nm. Initial rates were obtained by linear least squares regression of the absorbance data, and converted to progress rates.

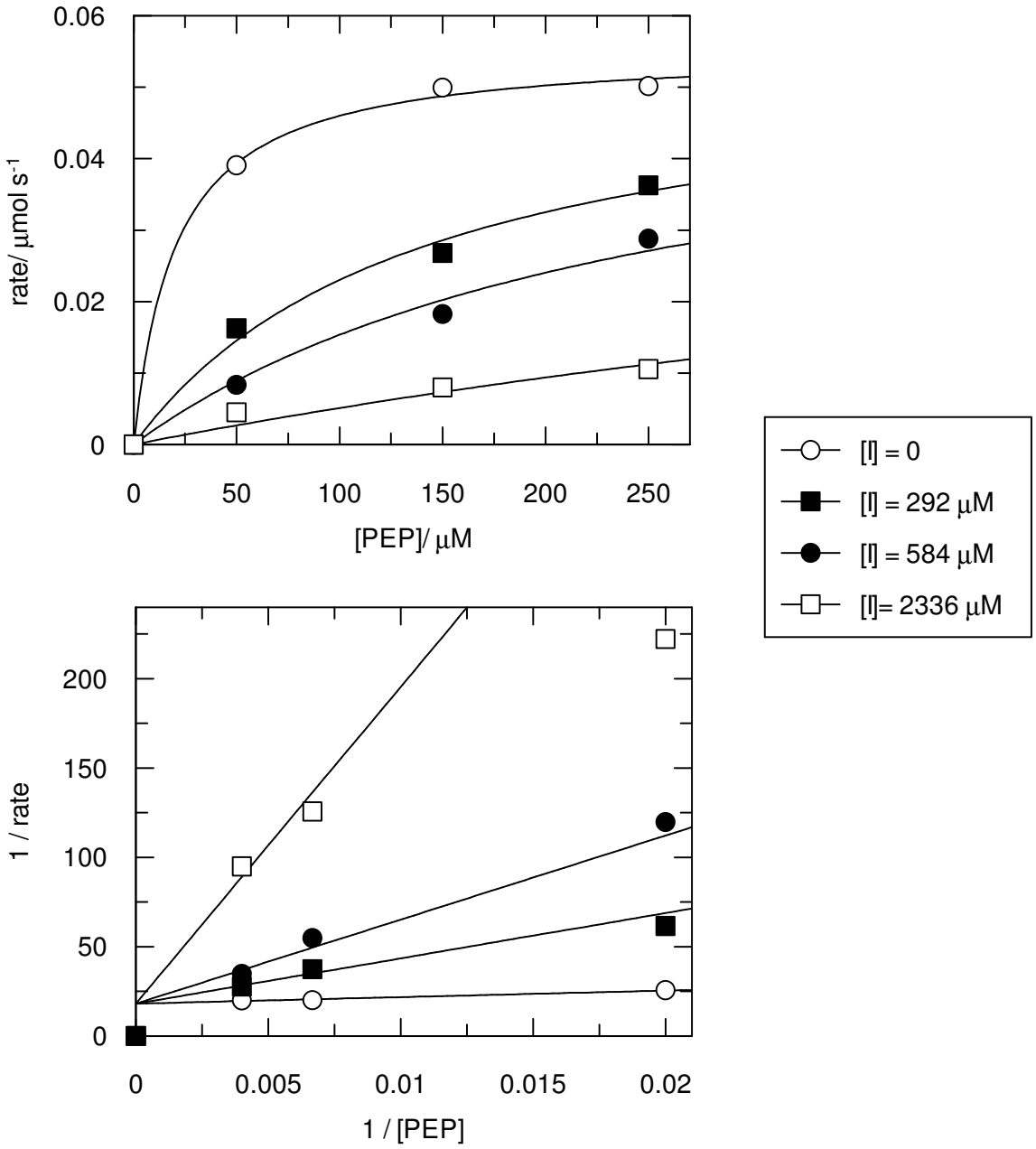

Figure 3.5: Michaelis (top) and Lineweaver Burk (bottom) plots for inhibition of *E. coli* DAH7P synthase by (*R*)-phospholactate 3.3. Solutions of PEP (50-250 µM), manganese(II) sulfate (100 µM), E4P (200 µM) and (*R*)-phospholactate (0-2336 µM) in 1 mL of BTP buffer (50 mM, pH 6.8) were initiated by the addition of *E. coli* DAH7P synthase (2 µg), and the loss of PEP followed spectrophotometrically at 232 nm. Initial rates were obtained by linear least squares regression of the absorbance data, and converted to progress rates.

Cyclopropane 3.5 has previously been reported as an inhibitor of various PEP-utilising enzymes.[91] Cyclopropane 3.5 is generally a more potent inhibitor of these enzymes than either enantiomer of phospholactate, a fact which is attributed to the steric and electronic similarities between cyclopropyl rings and alkenes.[91] However this compound has never been tested against any C-O bond cleaving PEP aldolase.

Treatment of commercially available carboxylic acid 3.6 with freshly prepared diazomethane gave the methyl ester 3.7 which was immediately treated with diethyl chlorophosphate to give phosphoryl ester 3.8 (Figure 3.6).

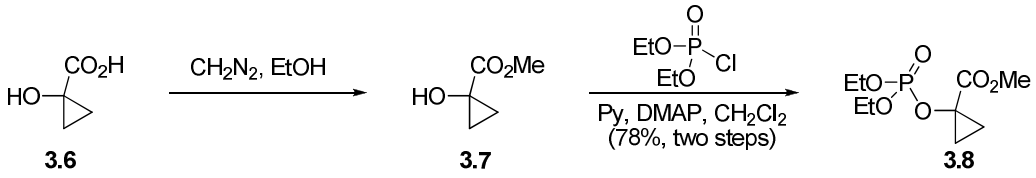

Figure 3.6: Esterification and phosphorylation to give phosphoryl ester 3.8

Treatment of the precursor 3.8 with trimethylsilyl bromide followed by aqueous potassium hydroxide workup gave a white solid. Analysis of this solid by ^{1}H NMR spectroscopy revealed that the major product was in fact α-ketobutyrate 3.9, with only a small quantity of the required cyclopropane 3.5 being present. The ring opened product is presumably produced by neighbouring group assisted hydrolysis of the phosphoryl group; accompanied by ring opening of cyclopropyl group. Hydrolysis of the acyl phosphate produced would then lead to α-ketobutyrate 3.9. The ring opening of cyclopropyl alcohols under basic conditions is a well precedented reaction, with considerable application in organic synthesis.[92]

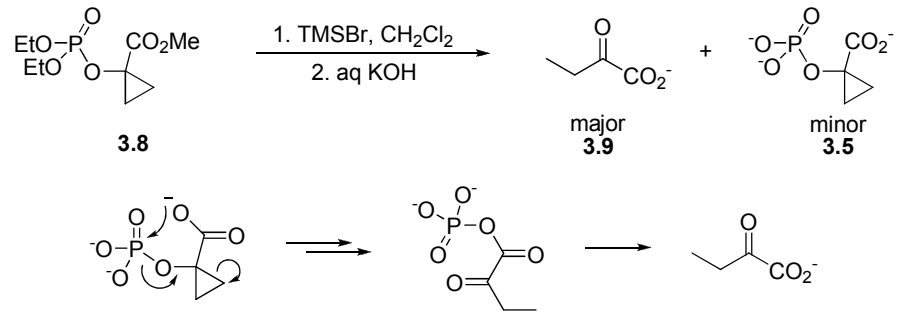

Figure 3. 7: Ring opening reaction of cyclopropane 3.8 during deprotection

However, despite this difficulty, small amounts of crude cyclopropane 3.5 were able to be isolated. Recrystallisation of the crude cyclohexylamine salt from methanol/acetone removed the ring opened product 3.9, and separation of the resulting mixture was achieved by preparative anion exchange chromatography (Figure 3.8).

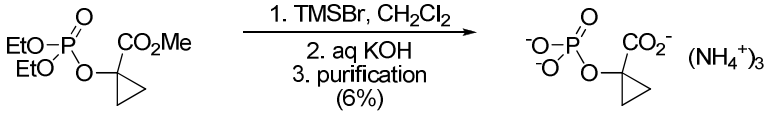

Figure 3.8: Overall purified yield of deprotected cyclopropane 3.5

Analysis of cyclopropane 3.5 as a competitive inhibitor of *E. coli* DAH7P synthase showed that it was a competitive inhibitor with respect to PEP, with a K_i of $\leq 190 \pm 20$ μM (Figure 3.10).

This inhibition constant is less than that determined for (*S*)-phospholactate, and more than that determined for (*R*)-phospholactate. Given that cyclopropane effectively shares the stereochemistry of both stereoisomers of phospholactate, it is also considerably less than the mean value for the phospholactates (360 μM). This may be due to the greater electronic similarities between the cyclopropyl ring system and the PEP alkene than the more strictly sp^3 phospholactate motif.

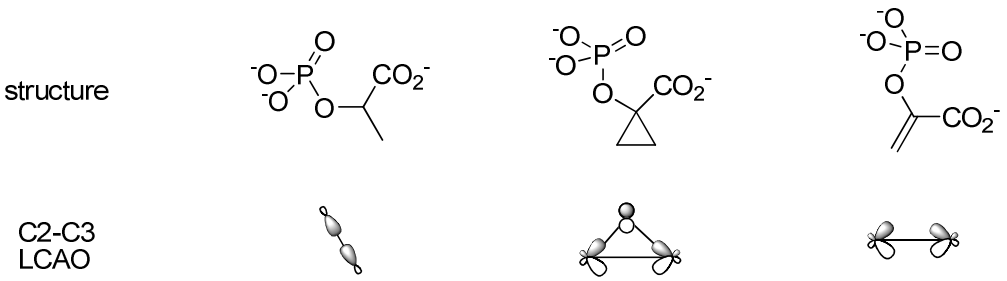

Figure 3.9: Comparison between the structure of phospholactate, cyclopropane 3.5 and PEP; and the linear combination of atomic orbitals (LCAO) contributing to the C2-C3 bond in each

As can be seen in Figure 3.9, the combination of atomic orbitals leading to the C2-C3 σ bond in phospholactate lies in the plane of the bond, whereas in PEP the equivalent bond is formed by overlap above and below the plane of the bond. The bonding in cyclopropanes has been described in a similar manner[93], with the electron density in

the centre of the ring, rather than along the direction of the bonds. This model has been used to explain why cyclopropane rings undergo reactions more similar to alkenes than to other cycloalkanes.[93]

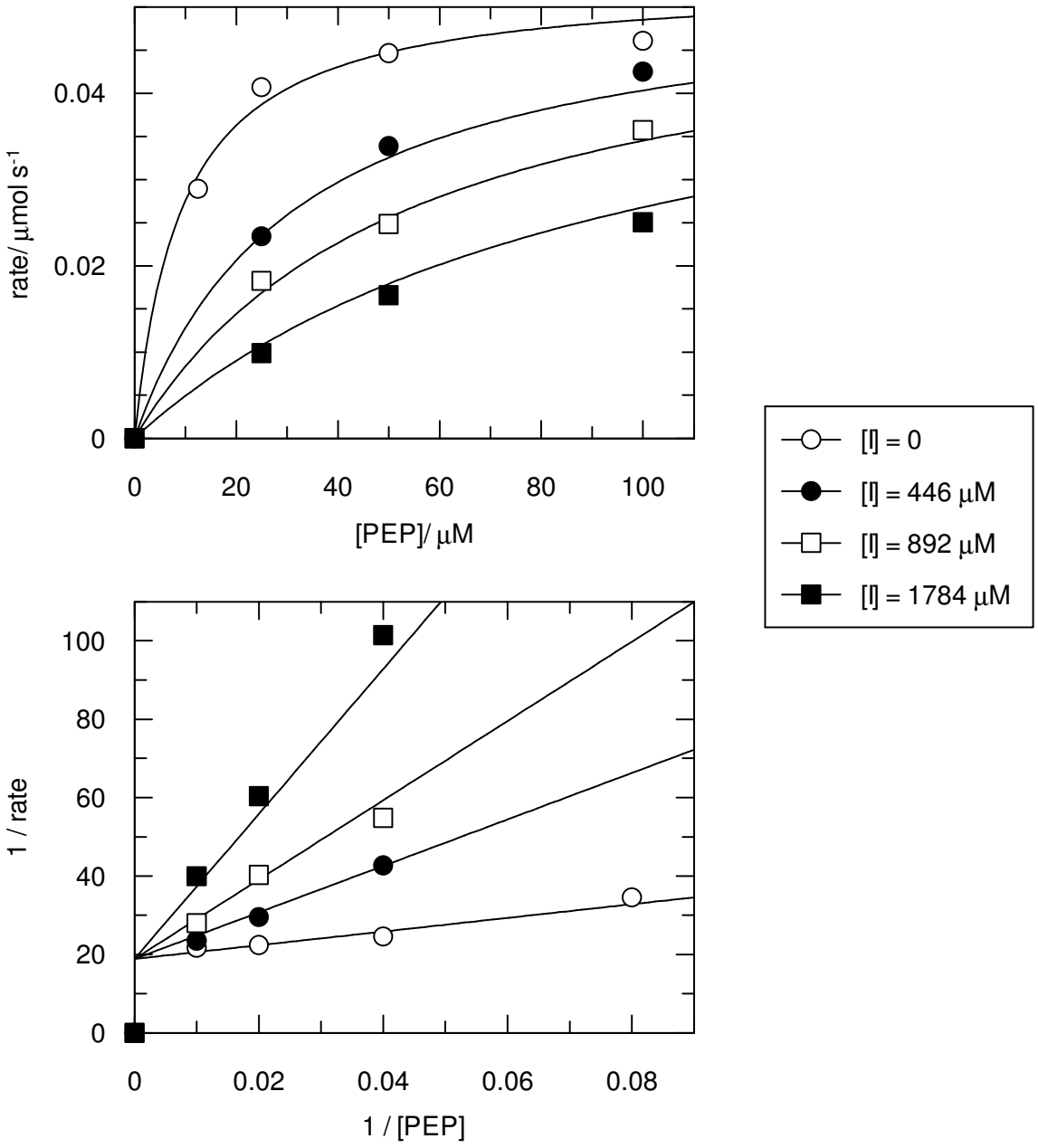

Figure 3.10: Inhibition of *E. coli* DAH7P synthase by cyclopropane 3.5. Solutions of PEP (10-100 µM), manganese(II) sulfate (100 µM), E4P (200 µM) and cyclopropane 3.5 (0-1784 µM) in 1 mL of BTP buffer (50 mM, pH 6.8) were initiated by the addition of *E. coli* DAH7P synthase (2 µg), and the loss of PEP followed spectrophotometrically at 232 nm. Initial rates were obtained by linear least squares regression of the absorbance data, and converted to progress rates.

3.2.2: Removal of the enol oxygen of PEP

The enol oxygen of PEP is a crucial part of the DAH7P synthase mechanism; providing the electron-donating substituent required for nucleophilic attack by the alkene of PEP. The necessity of this oxygen was known at the outset of this work, and both phosphonate[94] 3.10 and difluorophosphonate[95] 3.11 (Figure 3.11) have been found by others to not be substrates for the enzyme reaction, but instead act as inhibitors.

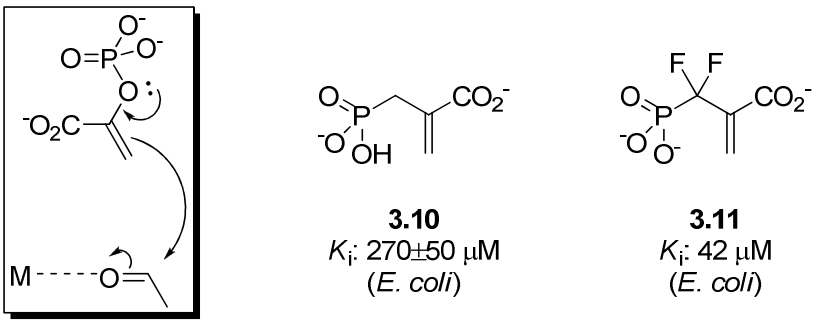

Figure 3.11: The role of the enol oxygen in the enzyme mechanism; and two previously discovered DAH7P synthase inhibitors

With this in mind, a new inhibitor lacking the crucial enol oxygen was designed. In this compound, the alkene has been moved from between C2-C3 of PEP, and instead occupies a position equivalent to the C2-O2 bond of PEP. This compound was designed to mimic the enzyme bound conformation of PEP, which has been observed in a number of enzyme structures (determined by X-ray diffraction) to have a *syn* relationship between the phosphorus atom and C3 of PEP (Figure 3.12). By having a (*E*)-vinyl phosphonate, the *syn* relationship is preformed and locked in position. This would be expected to give the binding of vinyl phosphonate 3.12 an entropic advantage over the binding of allylic phosphonate 3.10, as the entropic cost of restricting the conformation of the phosphonate has been paid during the formation of the vinyl phosphonate alkene, rather than during the inhibitor-enzyme association. This lower loss of entropy should lead to a larger Gibbs free energy of association, and hence a lower inhibition constant.

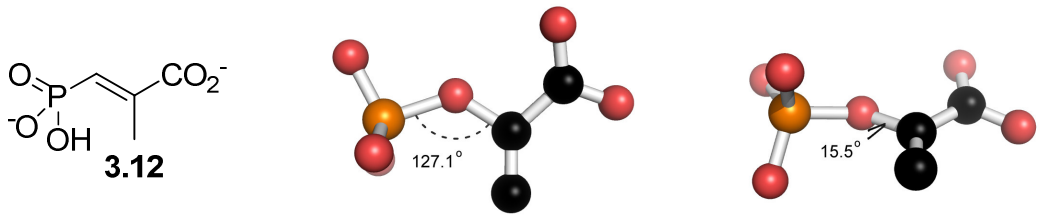

Figure 3.12: Relationship between proposed inhibitor 3.12 and PEP active site geometry (PEP as found in the structure of *S cerevisiae* DAH7P synthase; PDB accession number: 1of8.pdb).[40]

The Horner-Wadsworth-Emmons (HWE) reaction was chosen to construct the vinyl phosphonate, utilising tetraethyl methylene bisphosphonate.

The presence of different alkali metal cations in Wittig and HWE reactions has been shown to influence the stereochemical outcome of these reactions[96]. However, there has been little work on HWE reactions with bisphosphonates or α-ketoesters as reaction partners. The stereoselectivity of the required HWE reaction was investigated utilising lithium diisopropylamide, lithium chloride/ 1,7-diazabicyclo-[5.4.0]-undec-7-ene (DBU),[97] sodium bis(trimethylsilylamide) and potassium *tert*-butoxide as bases. The reactions were carried out on a small scale, and after aqueous workup the stereoselectivity was determined on the crude mixtures by NMR spectroscopy (Figure 3.13).

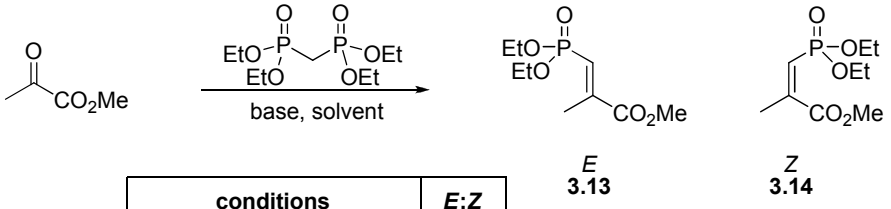

conditions	*E*:*Z*
tBuOK, THF, -78°C	20:80
NaHMDS, DME, THF, 0°C	50:50
LiCl, DBU, MeCN, RT*	70:30
LDA, THF, -78°C	85:15

* low conversion after 48 hours

Figure 3.13: Investigation of the stereochemical outcome of the HWE reaction

The stereoselectivity was dependent on the alkali metal ion used, with the reaction selective toward the (*E*)-isomer with the small lithium cation, but (*Z*)-selective with

the larger potassium anion. Lithium chloride and DBU, previously reported as a mild system for HWE reactions gave only low conversion, with mostly starting materials present after 48 hours at room temperature.[97] However, preforming the lithium anion at -78°C with LDA gave improved conversion, and slightly improved stereoselectivity. A model to explain the stereochemical outcome of similar HWE reactions has not been reported in the literature; however a model has been proposed to explain the outcome of this and related reactions, which is presented in Chapter Four (Section 4.6).

In order to access both the (*E*)- and (*Z*)-isomers for further study, the reaction was carried out utilising sodium (bistrimethylsilyl)amide, giving a moderate overall yield of vinyl phosphonates (Figure 3.14).

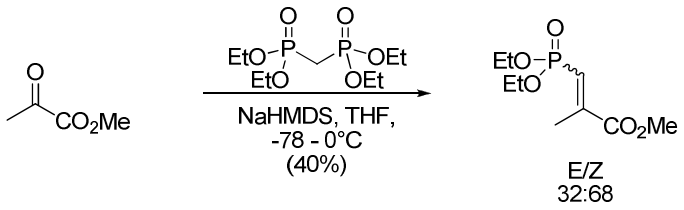

Figure 3.14: Preparative scale HWE reaction

The stereochemistry of the vinyl phosphonates was assigned by ^{1}H NMR spectroscopy, utilising a 1D transient nuclear Overhauser enhancement spectroscopy (NOESY) experiment. In the NOESY experiment, a selected resonance is irradiated, and the through-bond magnetisation transfer is eliminated, leaving the much weaker through-space transfer of magnetisation between nuclei. This transfer decreases with the sixth root of the distance between the nuclei;[98] so intramolecular distances can be readily judged by the strength of the resulting nuclear Overhauser enhancement (NOE). The NOESY spectra for the two isomeric vinyl phosphonates are shown in Figure 3.15. In the undesired (*Z*)-isomer 3.14, the allylic methyl protons are on the same face as the vinyl proton, and a typical NOE is observed between them (blue box). No such signal is present in the spectrum of the (*E*)-isomer 3.13, where the corresponding protons are on opposite faces.

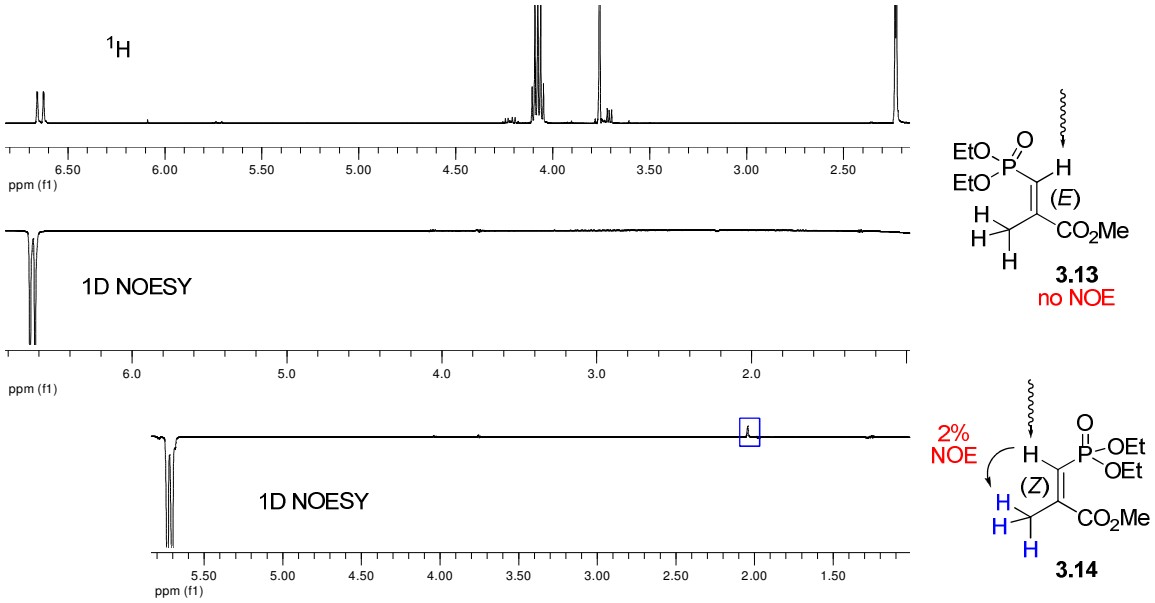

Figure 3.15: ^{1}H and 1D-NOESY spectra of (*E*)-vinyl phosphonate 3.13, and NOESY for (*Z*)-vinyl phosphonate 3.14, showing the diagnostic NOESY signal

Interestingly, the (*Z*)-isomer 3.14 was unstable during purification, and despite clean separation of the two isomers during chromatography, the (*Z*)-isomer was obtained as a mixture containing ~10-15% (*E*)-product 3.13 on every occasion. A photochemical process involving the electron-deficient double bond may be responsible for this, namely a photochemical $\pi \rightarrow \pi^*$ transition allowing momentary rotation of the former double bond, followed by relaxation $\pi^* \rightarrow \pi$ giving some product with the (*E*)-configuration.

Treatment of the purified (*E*)-vinyl phosphonate 3.13 with trimethylsilyl bromide, followed by aqueous potassium hydroxide, gave the desired phosphonate 3.12 as its tris(cyclohexylammonium) salt.

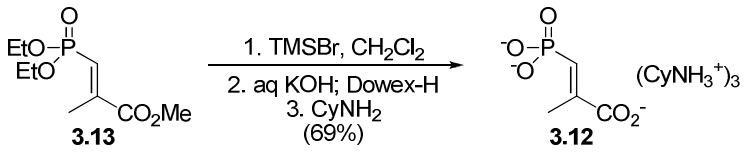

Figure 3.16: Deprotection of 3.13 to vinyl phosphonate 3.12

Attempts to deprotect the isolated (*Z*)-isomer under the same conditions led to further decomposition. Enzyme assay of the mixture of compounds obtained showed vastly

decreased inhibition when compared the same concentration of (*E*)-isomer, and further pursuit of the (*Z*)-isomer was abandoned.

The (*E*)-vinyl phosphonate 3.12 was assayed as an inhibitor against *E. coli* DAH7P synthase (Figure 3. 17). Gratifyingly, (*E*)-vinyl phosphonate 3.12 proved to be a potent inhibitor of DAH7P synthase, competitive with respect to PEP, with a K_i of 4.7 ± 0.7 μM.

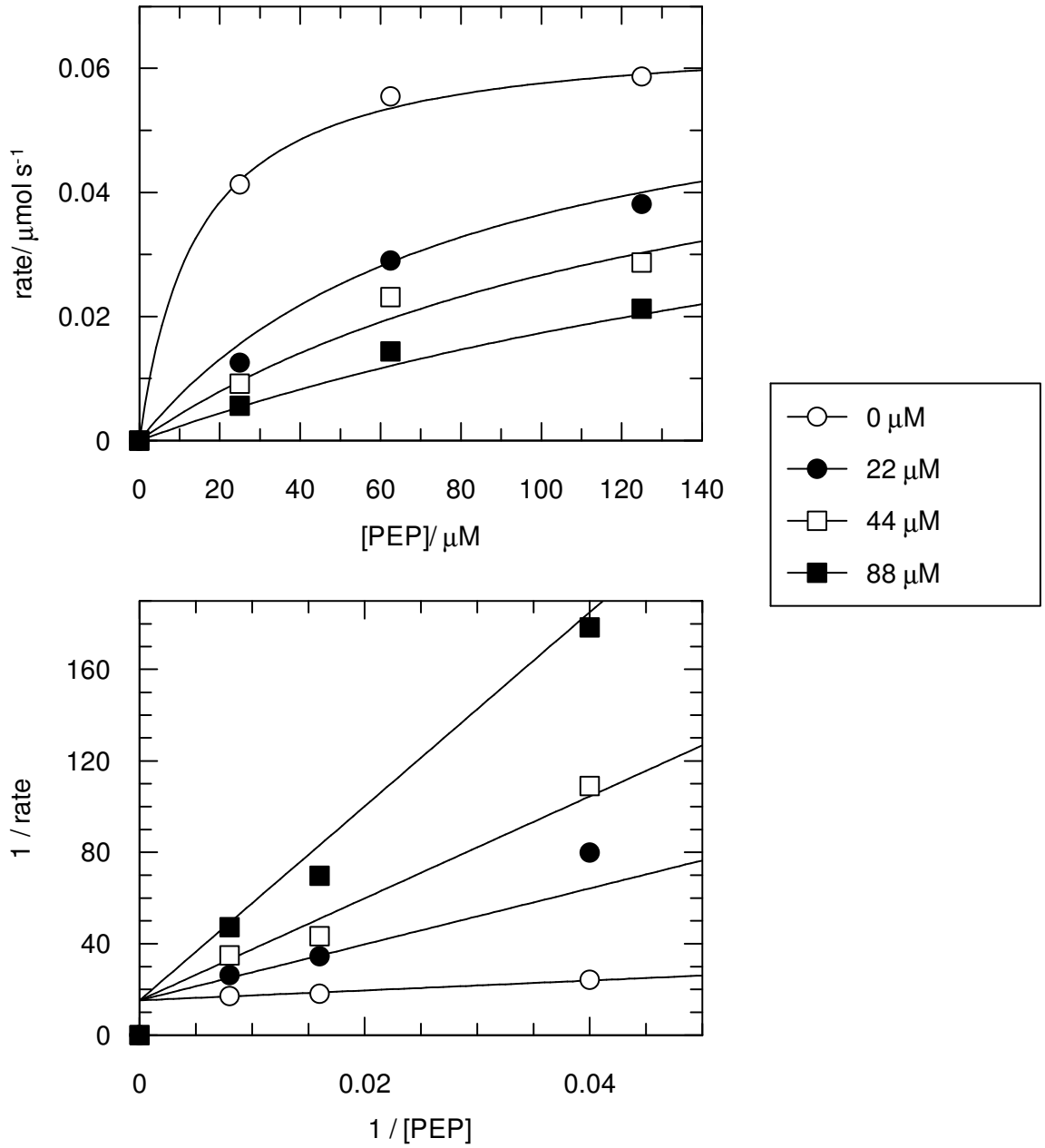

Figure 3. 17: Inhibition of DAH7P synthase with vinyl phosphonate 3.12. Solutions of PEP (20-120 μM), manganese(II) sulfate (100 μM), E4P (200 μM) and vinyl phosphonate 3.12 (0-88 μM) in 1 mL of BTP buffer (50 mM, pH 6.8) were initiated by the addition of *E. coli* DAH7P synthase (2 μg), and the loss of PEP followed spectrophotometrically at 232 nm. Initial rates were obtained by linear least squares regression of the absorbance data, and converted to progress rates.

Although vinyl phosphonate 3.12 was a potent inhibitor, its affinity might be improved by increasing its ability to mimic PEP. Phosphonates have decreased acidity compared to phosphates, due to the decreased electron withdrawing properties of oxygen relative to carbon. The acidity of phosphonates can be increased by mimicking the electron-withdrawing properties of oxygen by adding one or two fluorine atoms to the phosphonate carbon (Figure 3.18).[99]

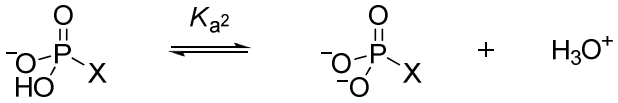

-X-	pK_{a2}
O	6.4
CH_2	7.6
CHF	6.5
CF_2	5.4

Figure 3.18: Acidities of phosphates, phosphonates, monofluoro- and difluorophosphonates. Acidity data taken from Romanenko *et al.*[99]

With this in mind, we designed fluorinated compound 3.15. While the fluorine atoms are not on the phosphonate carbon, they are vinylogous to it, and so may still have the desired effect.

Treatment of methyl 2,2,2-trifluoropyruvate under the LDA HWE conditions described above, gave a moderate yield of trifluorinated vinyl phosphonate 3.16 (Figure 3.19). A single isomer was obtained under these conditions.

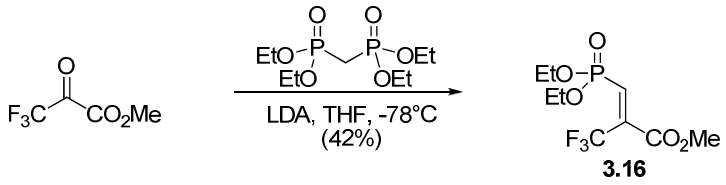

Figure 3.19: Synthesis of trifluorinated vinyl phosphonate 3.16

Due to the lack of the necessary nuclei for a NOESY experiment, the configuration of this compound was provisionally assigned as (*Z*). This was based on the similar shift of the vinyl proton ^{1}H signal between (*E*)- vinyl phosphonate 3.13 and 3.16, as well as

the single product observed under lithium HWE conditions. It should be noted that though (*E*)-3.12 and (*Z*)-3.16 share the same configuration, they differ in assignment due to the relative substituent priorities under the Cahn-Ingold-Prelog system of nomenclature.

Treatment of ester 3.16 under our standard trimethylsilyl bromide deprotection conditions gave the desired phosphonate 3.15 as its tris(cyclohexylammonium) salt (Figure 3.20).

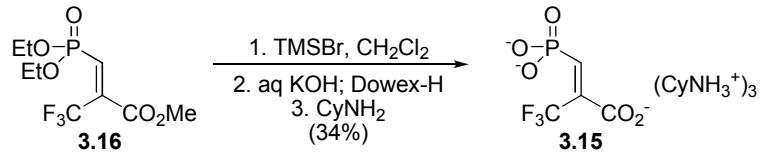

Figure 3.20: Deprotection of fluorinated phosphonate 3.16

Fluorinated phosphonate 3.15 was tested as an inhibitor of *E. coli* DAH7P synthase (Figure 3.21). Phosphonate 3.15 proved to be an effective inhibitor of DAH7P synthase, competitive with respect to PEP, with a K_i of 8.8 ± 2.5 μM.

Unfortunately fluorinated phosphonate 3.15 was not significantly more potent than its non-fluorinated equivalent 3.12. This could be due to a number of factors; one possible explanation is the size of the trifluoromethyl substituent is slightly greater than the methyl group it replaces.[100] The methylene group of PEP sits in close proximity to a conserved active site proline residue (Figure 3.22), so any gain in binding from improving pK_{a2} in 3.15 may be balanced in steric clashes between the fluorine atoms and the proline residue, disfavouring binding.

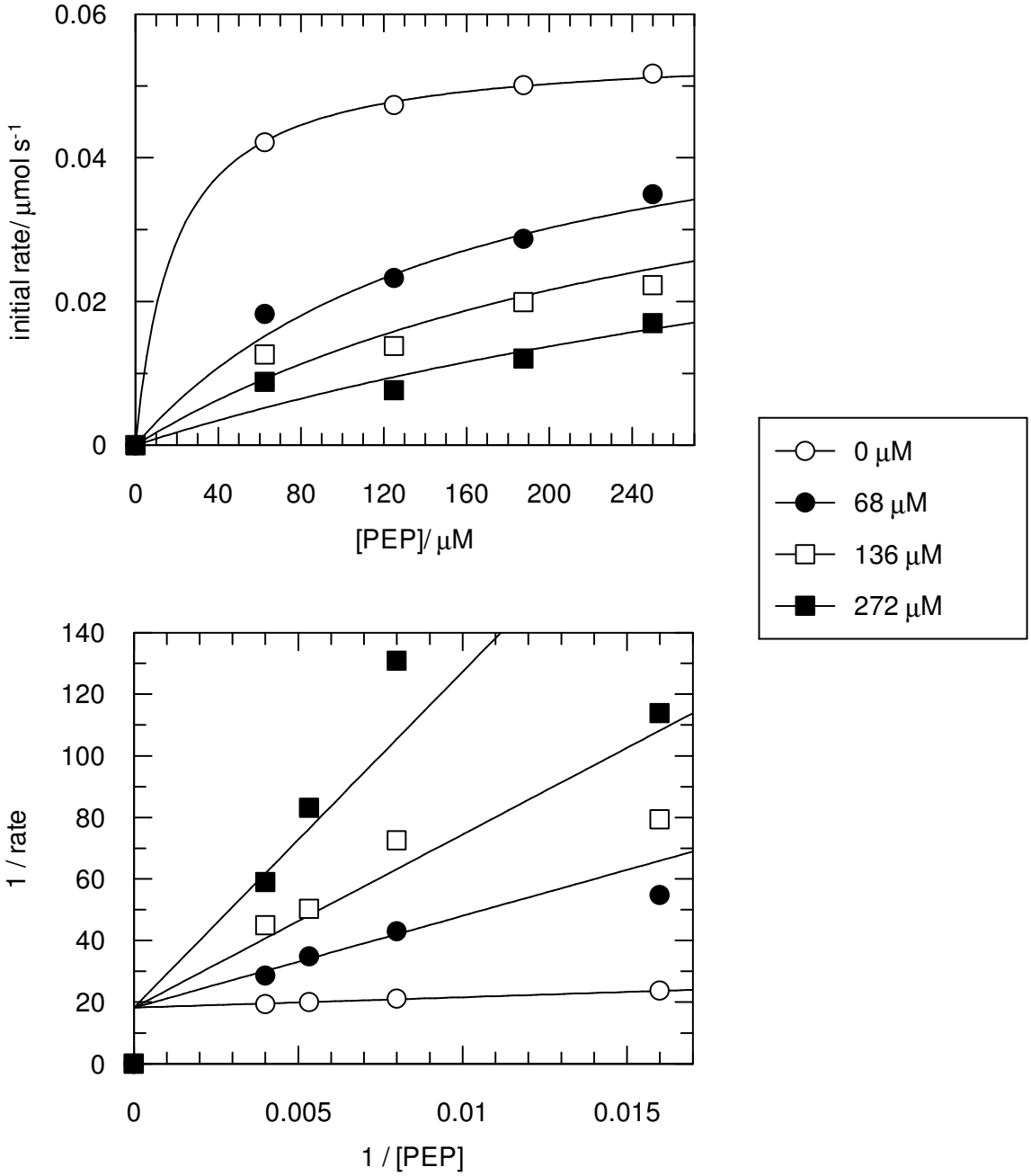

Figure 3.21: Inhibition data for trifluorinated vinyl phosphonate 3.15. Solutions of PEP (50-250 µM), manganese(II) sulfate (100 µM), E4P (200 µM) and trifluorinated vinyl phosphonate 3.15 (0-272 µM) in 1 mL of BTP buffer (50 mM, pH 6.8) were initiated by the addition of *E. coli* DAH7P synthase (2 µg), and the loss of PEP followed spectrophotometrically at 232 nm. Initial rates were obtained by linear least squares regression of the absorbance data, and converted to progress rates

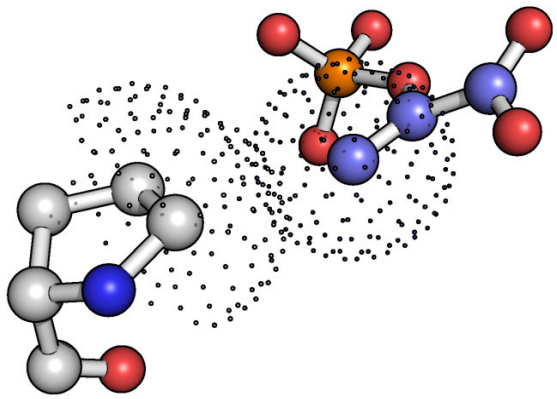

Figure 3.22: Close contacts between PEP and the conserved active site proline (P133) in *S. cerevisiae* DAH7P synthase (PDB: 1of8).[40] The dots are drawn at the Van der Waals contact radii for the carbon atoms in each structure; the centre to centre distances between the proline ring carbons Cγ and Cδ and PEP C3 are 3.8 and 4.0 Å, respectively.

3.2.3: Compounds retaining the enol substructure

The enol phosphate substructure of PEP is a crucial component of the enzyme mechanism. As was seen in Section 3.2.2, the enol oxygen also has an effect on substrate binding, by decreasing the pK_{a2} of the neighbouring phosphoryl group. These favourable effects could be incorporated into an inhibitor, if some way was found to stop the enzyme processing the enol phosphate as a substrate.

Considering the Lewis-acid mechanism of DAH7P synthase activity, for the enol alkene to act as a nucleophile, activation of the aldehyde electrophile is required. In DAH7P synthase this is proposed to be achieved by coordination of the aldehyde carbonyl to the metal centre, so in principle disrupting this interaction should stop the enzyme reaction.

One method to achieve this aim would be to incorporate a strong coordinating group into a PEP-like compound. Once the compound binds to the enzyme, the coordinating group should become a metal ligand, and block coordination of the aldehyde carbonyl, rendering the PEP-like compound inert to the enzyme reaction.

Cyanophosphate 3.17 (Figure 3.23) has previously been reported as an inhibitor of the PEP-metalloenzymes pyruvate kinase and PEP carboxylase,[101] and its inhibition

constant was found to be dependent on the metal cofactor used, with inhibition of the manganese(II)-enzyme complex more than 10-fold greater than that for the magnesium(II)-enzyme complex in each case. Interestingly, the compound is also a weak substrate of pyruvate kinase.[101]

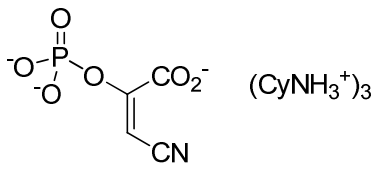

Figure 3.23: CyanoPEP 3.17

This compound seemed ideal, so efforts were made to prepare it by the known preparation. Treatment of diethyl oxalate with the potassium anion of acetonitrile, generated *in situ* from acetonitrile and potassium ethoxide, gave a good yield of a pale yellow solid identified as potassium enolate 3.18 (Figure 3.24).

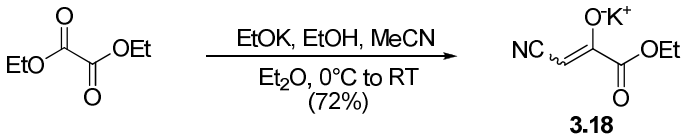

Figure 3. 24: Generation of potassium enolate 3.18

Attempts to phosphorylate this compound by a slight modification of the literature method, substituting commercially available and comparatively stable diethyl chlorophosphate for its dimethyl equivalent, led only to small quantities of the desired product. Attempts to create a more naked anion by adding 10 mol% 18-crown-6 also failed to give clean reaction.[102] In each case the reaction mixture rapidly became deep brown-black upon addition of the phosphorylating reagent. In addition, it was suspected the enol phosphate was unstable toward chromatography, so we required a method to maximise the production of the desired compound and minimise the production of byproducts. To more closely investigate this reaction, a time course ^{31}P NMR experiment was conducted (Figure 3.25).

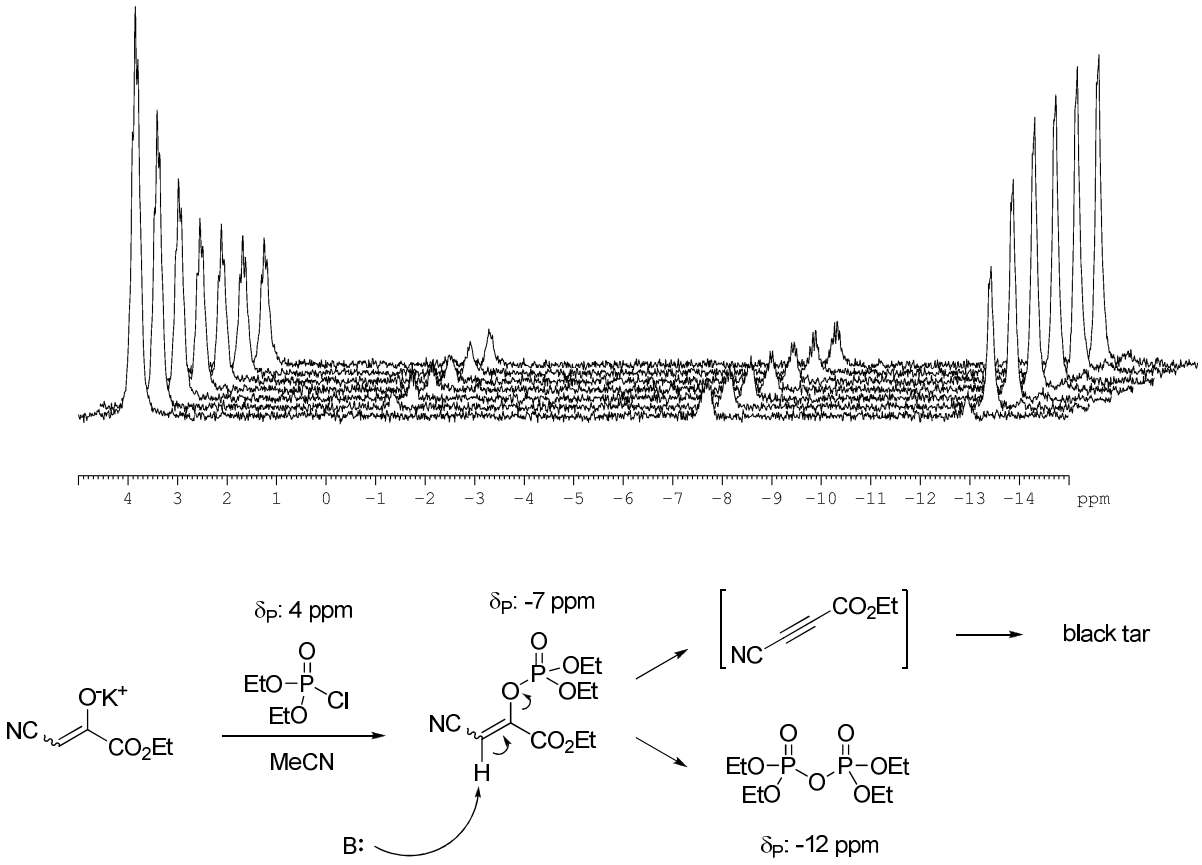

Figure 3.25: ^{31}P NMR spectroscopy of a timecourse experiment of the enolate phosphorylation reaction, time between each spectrum is 150 minutes

Analysis of the spectrum shows the slow disappearance of a signal at around 4 ppm, which corresponds with a slow increase in another peak at -13 ppm. These signals correspond to diethyl chlorophosphate and tetraethyl pyrophosphate respectively. The small signal at -7 ppm is assigned as the desired product, based on a correlation between the vinylic proton and this phosphorus signal in a ^{31}P-^{1}H HMBC experiment.

What is clear from the above spectra is that a steady population of the desired product is formed quickly, and no increase in this product is observed with increased reaction time. However, the diethyl chlorophosphate continues to be consumed for several more hours, being slowly converted to tetraethyl pyrophosphate. Based on this evidence it is proposed that the desired product is being destroyed in the reaction mixture at a similar rate to its formation; presumably by elimination of phosphate across the enolate ester system promoted by the remaining alkoxide ion.[103] The potassium diethyl phosphate produced rapidly reacts with the remaining diethyl

chlorophosphate, forming tetraethyl pyrophosphate. Once the entire alkoxide ion is consumed the elimination ceases, and no more tetraethyl pyrophosphate is produced, nor diethyl chlorophosphate consumed. The dark colouration of the reaction mixture can be explained by formation of polymeric side products from the highly electron-deficient alkyne side product produced.

Based on this analysis, it should be possible to rapidly quench the reaction and still obtain a similar yield of the desired product, and minimise the production of difficultly separated tetraethyl pyrophosphate. Gratifyingly, conducting the reaction for only ten minutes returned a good yield of crude product (Figure 3.26), of greater purity than attained by previous methods.

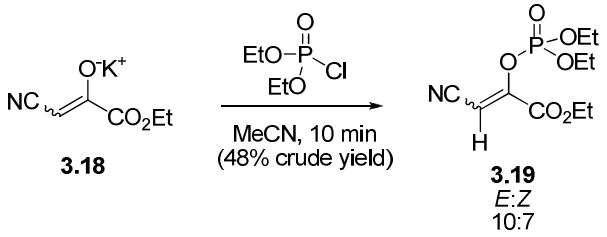

Figure 3.26: Rapid phosphorylation of enolate 3.18

Deprotection of the product with trimethylsilyl bromide, isolation as its cyclohexylammonium salt and recrystallisation from methanol/ether gave a solid containing (*E*)-cyanophosphoenolpyruvate 3.17 (Figure 3.27), the (*Z*)-isomer presumably being unstable to the deprotection conditions as described in the original publication.[101]

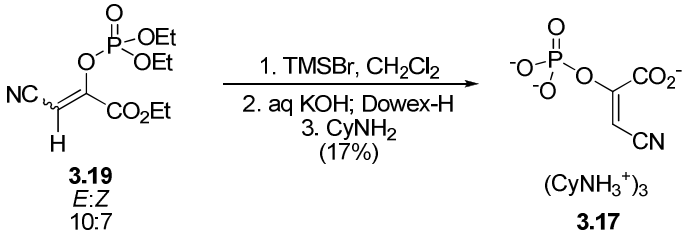

Figure 3.27: Deprotection and isolation of (*E*)-cyanophosphoenolpyruvate 3.17

With the small quantity of impure 3.17 produced by this route it was possible to briefly study its interaction with *E. coli* DAH7P synthase. (*E*)-

Cyanophosphoenolpyruvate 3.17 undergoes a slow hydrolysis under the assay conditions, as revealed by a slow decrease in absorbance at 232 nm. This hydrolysis is enzyme concentration dependent, but independent of E4P concentration. Based on this, it was presumed the enzyme was catalysing dephosphorylation of 3-cyanoPEP to 3-cyanopyruvate. A spectrophotometric coupled assay utilising *E. coli* DAH7P synthase, rabbit lactate dehydrogenase and NADH showed oxidation of NADH was occurring, which supports this theory. Similar behaviour has been noted during studies of 3-halophosphoenolpyruvates[95]. Based on the consumption of NADH in the coupled assay system, this hydrolysis proceeds at a slow rate (~20 pmol min^{-1}) under typical assay conditions.

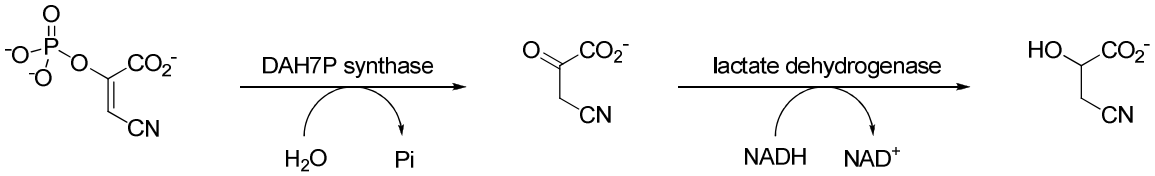

Figure 3.28: Enzymatic hydrolysis to cyanopyruvate, and *in situ* enzymatic reduction.

Attempts to accurately quantify the amount of (*E*)-cyanophosphoenolpyruvate 3.17 present by dephosphorylating the compound with pyruvate kinase, reducing the 3-cyanopyruvate to 3-cyanolactate with lactate dehydrogenase, and quantitating the amount of NAD^+ produced (Figure 3.28) spectrophotometrically was unsuccessful, with readings significantly higher than that plausible by weight per volume measurements. The concentration of (*E*)-cyanophosphoenolpyruvate in solution was estimated based on the weight of solid used, assuming it was pure (*E*)-cyanophosphoenolpyruvate 3.17. (*E*)-Cyanophosphoenolpyruvate 3.17 proved to be an inhibitor of *E. coli* DAH7P synthase, competitive with respect to PEP, with an inhibition constant $K_i \leq 75 \pm 25$ μM. The results of these studies are shown in Figure 3.29.

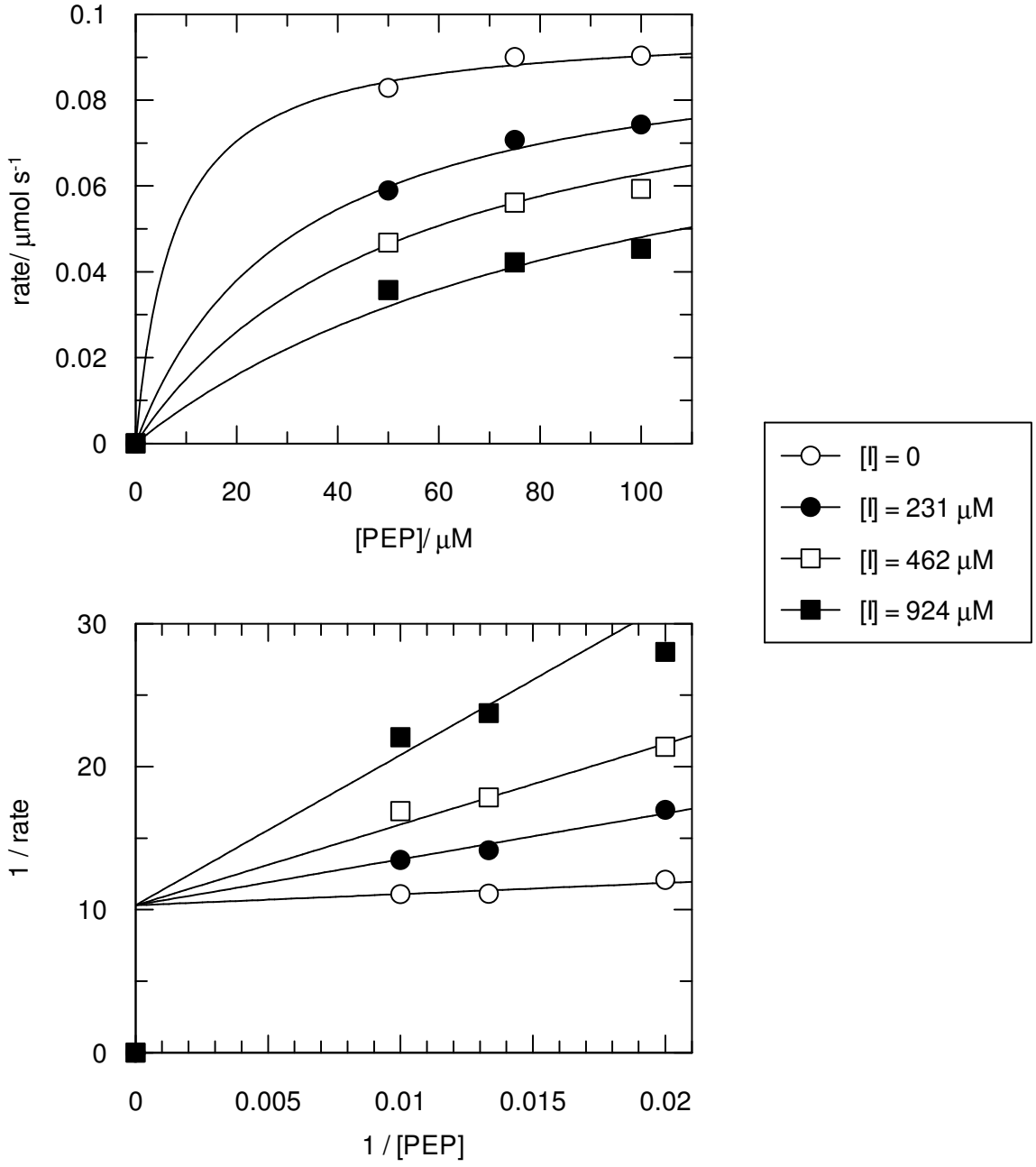

Figure 3.29: Inhibition properties of (*E*)-cyanophosphoenolpyruvate 3.17. Solutions of PEP (50-100 µM), manganese(II) sulfate (100 µM), E4P (200 µM) and (*E*)-cyanophosphoenolpyruvate 3.17 (0-924 µM) in 1 mL of BTP buffer (50 mM, pH 6.8) were initiated by the addition of *E. coli* DAH7P synthase (2 µg), and the loss of PEP followed spectrophotometrically at 232 nm. Initial rates were obtained by linear least squares regression of the absorbance data, and converted to progress rates

Another possible way to disrupt the enzyme would be to substitute the phosphoryl group for a similar group, whilst retaining the enol substructure. A compound with these features is the enol sulfate 3.20 (Figure 3.30).

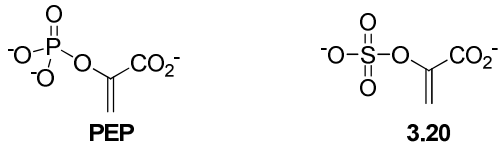

Figure 3.30: Comparision between enol phosphate PEP and enol sulfate 3.20

The effect of heteroatom enol esters other than the natural phosphate of PEP on the reactivity of DAH7P synthase has not been reported, so it was possible that the sulfate 3.20 may even be a substrate for DAH7P synthase. Adventitous sulfate ions has been observed in DAH7P synthase crystal structures, occupying the E4P phosphate pocket when E4P or an analogue is not present.[26] With this in mind, sulfate 3.20 was prepared by a modified literature route.[104] Treatment of ethyl bromopyruvate with sodium cyanoborohydride under mildly acidic conditions gave bromolactate 3.21 in an acceptable yield (Figure 3.31), given the possibility of side reactions such as ester reduction and bromide displacement.

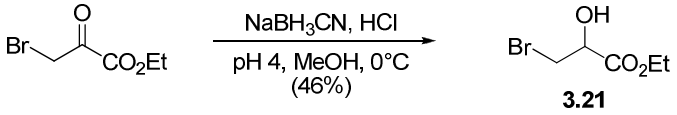

Figure 3.31: Reduction of bromopyruvate to lactate 3.21

Treatment of lactate 3.21 with pyridine-sulfur trioxide complex gave the pyridinium sulfate 3.22 in good yield as a viscous oil (Figure 3.32).

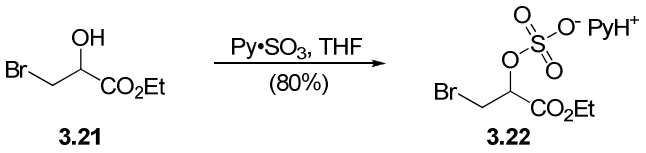

Figure 3.32: Sulfation of lactate 3.21 with pyridine-sulfur trioxide complex to sulfate 3.22

Treatment of unstable pyridinium sulfate 3.22 with an excess of aqueous potassium hydroxide, added slowly in portions, gave elimination and ester hydrolysis in the one pot, to give a solution of sulfoenolpyruvate (SEP) 3.20 (Figure 3. 33).

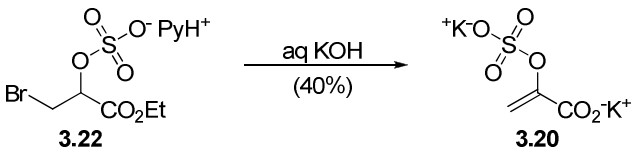

3.22 **3.20**

Figure 3. 33: One-pot elimination and saponification to give sulfoenolpyruvate 3.20

After quenching the excess base, SEP was isolated as its barium salt, which was purified by selective precipation. Treatment of this salt with Dowex-50X8 K^+-form returned the dipotassium salt of SEP in acceptable overall yield.

Analysis of the behaviour of SEP toward *E. coli* DAH7P synthase was then carried out. Initial studies showed SEP was not an inhibitor of DAH7P synthase under normal conditions, with no significant inhibition observed up to a 10 mM level of SEP. Based on this lack of inhibition, it was thought SEP may be processed by the enzyme under the reaction conditions, however no loss of SEP was observed spectrophotometrically; with enzyme-manganese(II), enzyme-copper(II), enzyme-zinc(II) or enzyme-cobalt(II) as catalysts. Since KDO8P synthase is thought to bind and utilise the dianionic form of PEP, rather than the trianionic form like DAH7P synthase, reactivity with KDO8P synthase was also investigated. Treatment with metal-independent *Neisseria meningitidis* KDO8P synthase, or metal dependent *Acidithiobacillus ferreoxidins* KDO8P synthase also failed to show any consumption of SEP. This apparent lack of binding or reactivity with either DAH7P synthase or KDO8P synthase was perplexing, and in order to ensure that the spectrophotometric results were accurate we carried out an NMR time-course experiment, where SEP was incubated overnight with E4P, manganese(II) sulfate and *E. coli* DAH7P synthase (Figure 3.34).

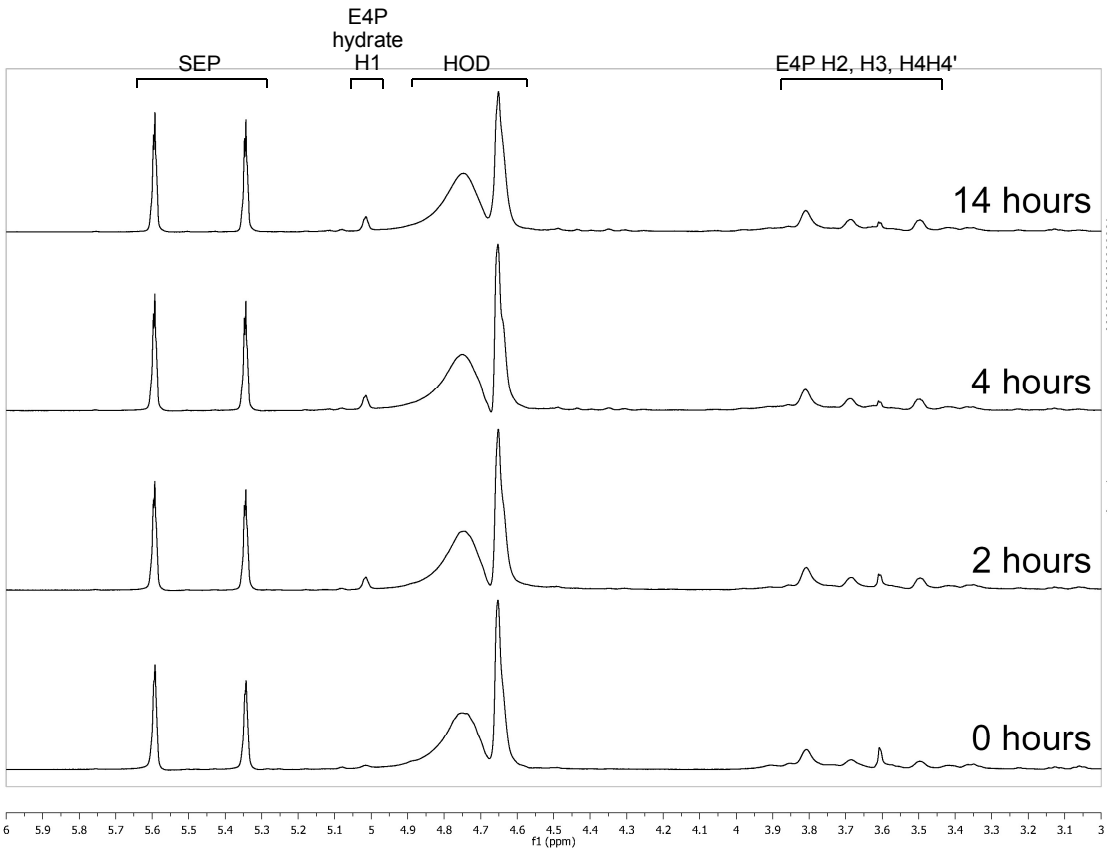

Figure 3.34: ^{1}H NMR spectroscopy study of SEP with E4P in the presence of *E. coli* DAH7P synthase. A solution of SEP (41 mM), E4P (18 mM), and manganese(II) sulfate (42 µM) in 20% D_2O/H_2O (600 µL) was adjusted to pH 6.8 with a small quantity of 1 M sodium hydroxide. *E. coli* DAH7P synthase (400 µg) was added, and the mixture monitored overnight at room temperature by NMR spectroscopy, utilising a ^{1}H presaturation pulse sequence.

Analysis of the spectra showed that no DAH7P-like product had been formed, and that no SEP had been consumed through non-productive hydrolysis. This confirmed the stability of SEP toward DAH7P synthase.

The intensity of one unknown peak at around δ 5 ppm had changed significantly. This peak was further analysed by a selective total correlation spectroscopy (selTOCSY) NMR experiment. In a selTOCSY experiment a resonance of choice is irradiated, and after a suitable delay, t_{mix}, the spectrum is collected. The signals that appear are those belonging to protons that can be excited by magnetisation transfer during $t_{mix;}$ which are those protons within the same spin system as the irradiated proton. The selTOCSY experiment (Figure 3.35) showed that this peak was likely to be E4P hydrate, formed

by slow equilibration between the oligomeric and monomeric forms of E4P during the overnight run.

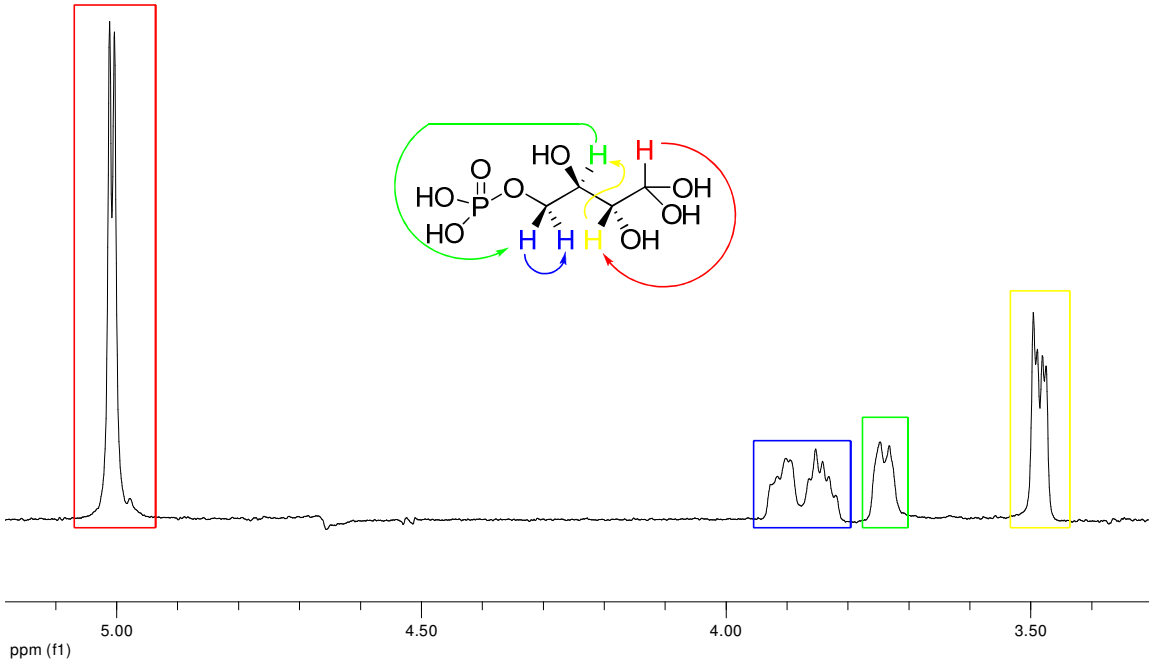

Figure 3.35: selTOCSY analysis of the changed δ 5 ppm peak, t_{mix} = 150 ms.

Addition of an aliquot of the NMR reaction mixture after overnight incubation to a mixture of PEP, E4P and manganese(II) showed that enzyme was still catalytically competent, ruling out any irreversible covalent enzyme modification as the cause of the non-reactivity of SEP.

The failure of SEP 3.20 to be processed by or inhibit DAH7P synthase was surprising. Since its stability to the reaction conditions has been verified, the failure of SEP to inhibit DAH7P synthase (even when present in a two hundred fold molar excess with relation to PEP) can be taken as indication that it is failing to bind to the enzyme PEP binding site. However, in the absence of PEP; E4P is known to rapidly covalently inactivate DAH7P synthase, by imine formation between the presumably Lewis acid activated aldehyde of E4P with an active site lysine in the PEP pocket.[105] This inactivation quickly renders DAH7P synthase inactive under typical assay concentrations of E4P (~ 200 μM) in the absence of PEP. However, no such inactivation occurred in the NMR experiment despite a very high E4P concentration (18 000 μM), indicating a protective effect of SEP. This suggests that in the absence of PEP, a weak enzyme-SEP complex can form, and obscure the lysine from imine

formation. However it is clear that this complex is unable to be continue the normal reaction pathway to DAH7P, perhaps indicating a role of the PEP phosphate group in initiating the enzyme reaction.

The vast difference in affinity between PEP and SEP is surprising, since the single atom change from PEP to SEP can be considered a conservative change. Semi-empirical calculations (AM1 level) show little difference in overall minimised geometry and key bond lengths between the gas phase structures of PEP and SEP, and with the exception of the P-O bond length these calculations agree well with the PEP geometry found by X-ray crystallographic analysis of *S. cerevisiae* DAH7P synthase-PEP-G3P complex.[40]

The one obvious difference between SEP and PEP is the charge state. The phosphate of PEP is capable of being either mono- or dianionic; the sulfate of SEP is only capable of being a monoanion. The failure of SEP to inhibit DAH7P synthase might suggest that the enzyme exclusively binds the trianionic form of PEP, with exceptional selectivity. This finding is hard to reconcile with the fact that simple phosphonates, whose dominant form at the assay pH would be dianionic, are capable of competing with PEP for DAH7P synthase very effectively (*vide supra*). It may be possible that the enzyme PEP phosphate binding pocket has evolved a suitable method for discriminating between phosphate and sulfate groups, in order to avoid inhibition by free sulfate ions in the cell. The mechanism of this discrimination is unclear, and not obvious in nature. Efforts to understand this discrimination utilising computational methods are described in Chapter Five.

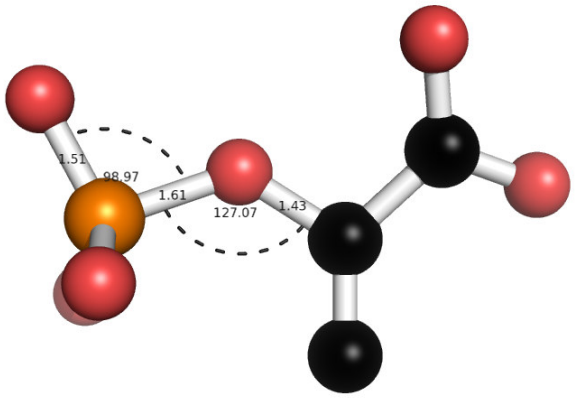

Figure 3.36: Crystallographically determined PEP geometry, from 10f8.pdb[40]

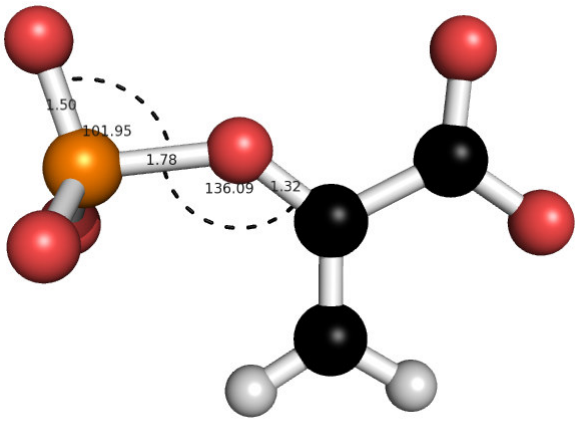

Figure 3. 37: Calculated (AM1) PEP geometry

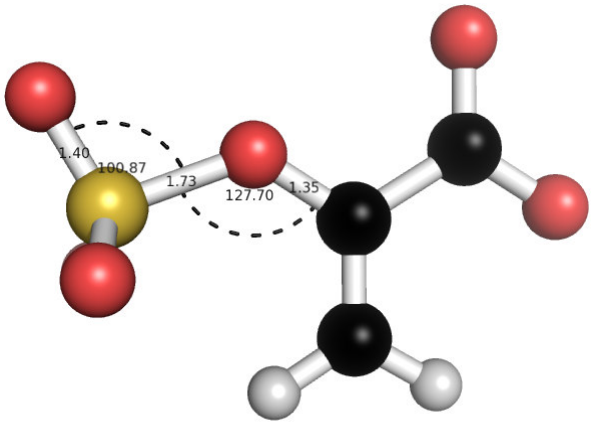

Figure 3. 38: Calculated (AM1) SEP geometry

3.2.4: Compounds bearing other functional groups

In addition to the designed molecules characterised above, the interaction of DAH7P synthase with small compounds containing more diverse functional groups was also measured.

Fosfomycin 3.23 is produced by cultures of certain *Streptomyces* species, and is now a clinically important antibiotic. Its molecular target is MurA (UDP-*N*-acetylglucosamine-enolpyruvate transferase), a member of the enolpyruvyl transferase family of enzymes. These enzymes catalyse the transformation of an alcohol and PEP to an enolpyruvyl ether and phosphate, via phosphate C-O bond cleavage. Fosfomycin inhibits MurA by covalent modification of a nucleophilic cysteine residue.[106]

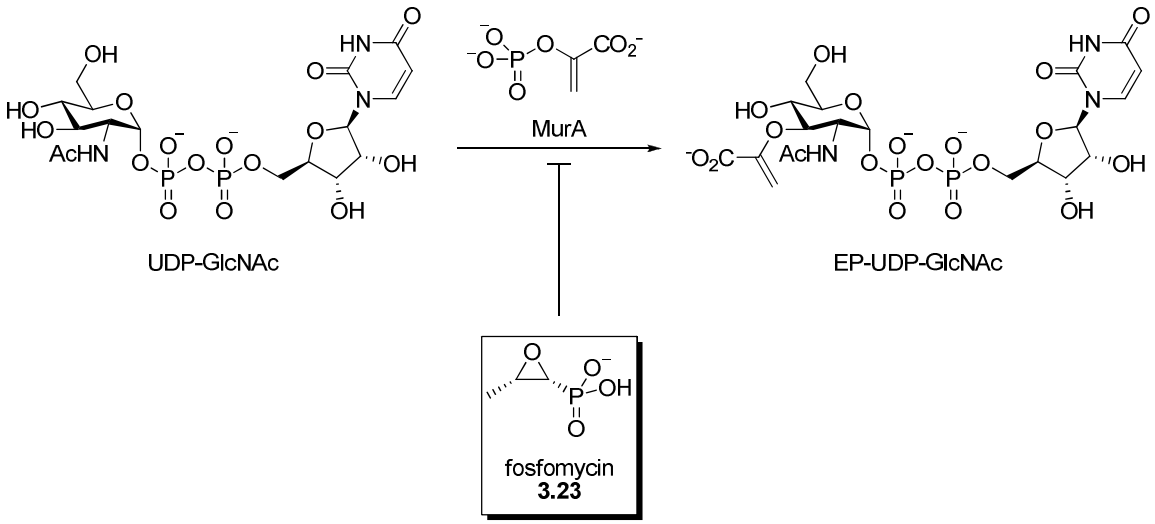

Figure 3.39: The reaction of UDP-*N*-acetylglucosamine-enolpyruvate transferase; and its inhibitor fosfomycin 3.23.

Since DAH7P synthase also possesses an active site cysteine, fosfomycin was investigated both as a reversible competitive inhibitor and as a time-dependent irreversible inhibitor of *E. coli* DAH7P synthase. No inhibitory activity of either type was observed. This finding indicates the importance of both the carboxyl group and the phosphoryl group in targeting molecules to the PEP binding site.

With the discovery of routes to β-substituted β-halo-α-ketoesters, PEP mimicking compounds that could be prepared from these compounds became of interest. Heterocyclic compounds have many properties that make them favourable as enzyme inhibitors and medicines; they offer a readily functionalised scaffold for the attachment of functionality, and often have favourable metabolic stability.[107] In addition, many families of heterocycles can be prepared from α-haloketones, making them potentially accessible as branches from the synthetic routes in Chapter 4, and thus of interest as DAH7P synthase inhibitors.

In order to investigate the use of heterocyclic compounds in the inhibition of DAH7P synthase, aminothiazole 3.24 was prepared as a representative member. It bears a carboxyl group to orientate it in the enzyme active site; and the multiple heteroatoms allow the possibility of favourable hydrogen bonding contacts in the PEP phosphate binding pocket. Aminothiazole 3.24 was readily prepared by treatment of bromopyruvic acid with thiourea; followed by treatment with sodium acetate (Figure 3.40).

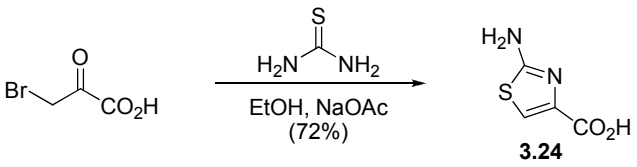

Figure 3.40: Synthesis of thiazole 3.24

The sodium salt of aminothiazole 3.24 was assayed as an inhibitor of *E. coli* DAH7P synthase, no inhibition was seen under standard conditions up to 0.4 mM, and its intense UV absorbance made assay at high concentrations impractical. The failure of this compound to inhibit DAH7P synthase again reinforced the necessity of both carboxyl and phosphoryl groups in potential inhibitors.

The antibiotic fosmidomycin 3.25 was isolated as an antibacterial agent from cultures of *Streptomyces lavendulae*, further studies determined it is active against some Gram-positive and most Gram-negative bacteria[108, 109]. The biological target of 3.25 remained a mystery for several years, until the discovery of the non-mevalonate pathway in the mid- 1990s.[110, 111] The non-mevalonate pathway provides some organisms with an alternative method to synthesise the isoprenoid precursors

isopentenyl diphosphate (IPP) and dimethallyl diphosphate (DMAPP); themselves used to synthesise a number of primary and secondary metabolites. Further studies determined fosmidomycin was a potent inhibitor of 1-deoxy-D-xylulose 5-phosphate reductoisomerase (DXR), which catalyses the conversion of 1-deoxy-D-xylulose 5-phosphate (DXP) to 2-*C*-methyl-D-erythritol 4-phosphate (MEP); the second step of the non-mevalonate pathway (Figure 3.41).[112]

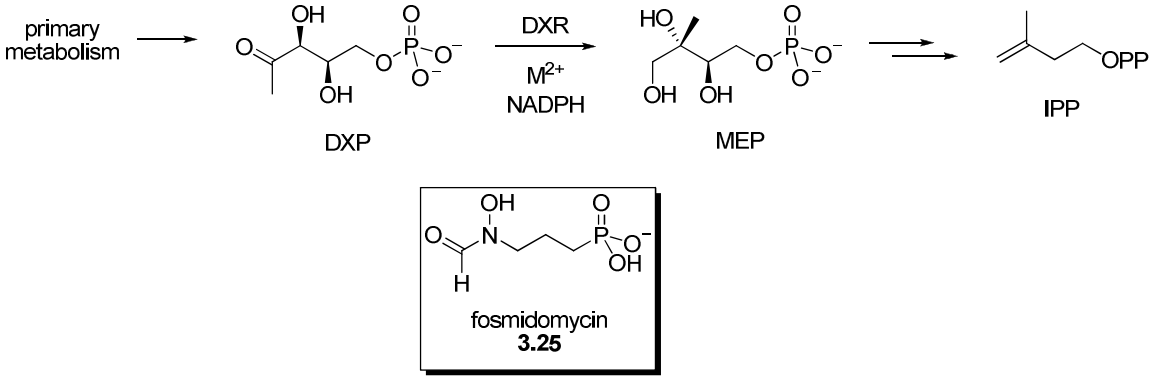

Figure 3.41: Fosmidomycin 3.25 and DXR

The mechanism of inhibition of DXR by fosmidomycin has been studied by detailed enzyme kinetics and X-ray crystallography; fosmidomycin binds as a slow-tight inhibitor of DXR, competitive with DXP with an initial inhibition constant K_i of 215 nM, and a tight inhibition constant K_i* of 21 nM[113] (Figure 3. 42).

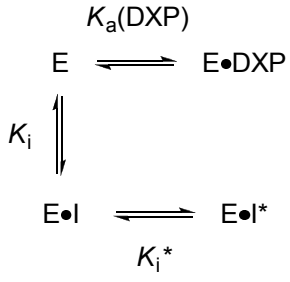

Figure 3. 42: Relevant equilibria for slow-tight inhibition of DXR by fosmidomycin

Crystallographically, fosmidomycin binds its phosphonate group at the DXR phosphate binding pocket, and the formylhydroxamate portion forms bidentate ligand for the metal cofactor, in this case magnesium(II).[114]

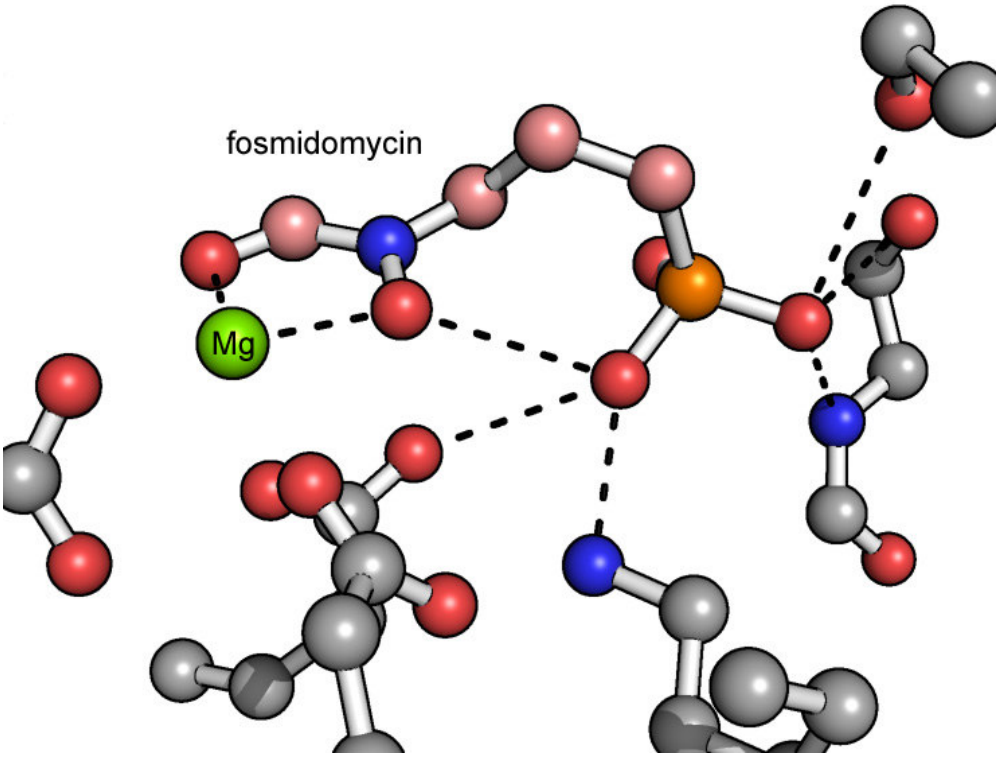

Figure 3. 43: Binding of fosmidomycin (salmon/red/blue/orange C/O/N/P respectively) to *E. coli* DXR-magnesium complex (PDB accession code: 2EGH).[114]

Despite a lack of sequence, structural or mechanistic homology; the structure and behavior of DXR bears obvious parallels with the binding of E4P to DAH7P synthase. Both enzymes bind their substrates through a phosphate distant from the site of reactivity, and both enzymes exploit a divalent metal ion for catalysis. Both *E. coli* enzymes have maximum activity with manganese(II).[16, 113] DXR catalyses a retro-aldol reaction as part of its mechanism,[115] a known side reaction of DAH7P synthase under some conditions.[105]. DAH7P synthase substrate E4P is a known poor alternative substrate of DXR,[113] and compounds bearing the *threo* stereochemistry of DXP are alternative substrates of DAH7P synthase.[39] Based on these parallels we postulated if fosmidomycin is capable of inhibiting DXR; then it should, by extension, be capable of inhibiting DAH7P synthase (Figure 3.44).

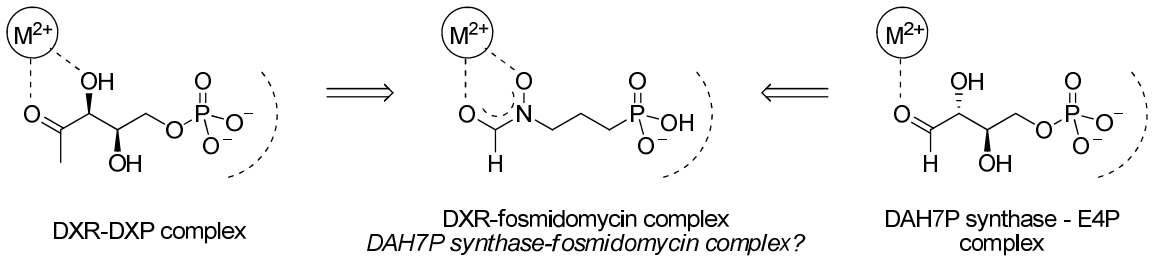

Figure 3.44: A comparison of DXR-DXP, DAH7P synthase-E4P and metalloenzyme-fosmidomycin complexes

Based on this a commercial sample of fosmidomycin was obtained, and a preliminary study showed gratifyingly it is an effective inhibitor of DAH7P synthase. However, detailed studies to determine the inhibition mechanism led to a surprising discovery. Fosmidomycin is not a competitive inhibitor with respect to E4P; it is uncompetitive, as signaled by the parallel lines on a Lineweaver-Burk plot (Figure 3.46). If fosmidomycin bound as we had postulated, competitive behaviour with respect to E4P would be expected (Figure 3.45).

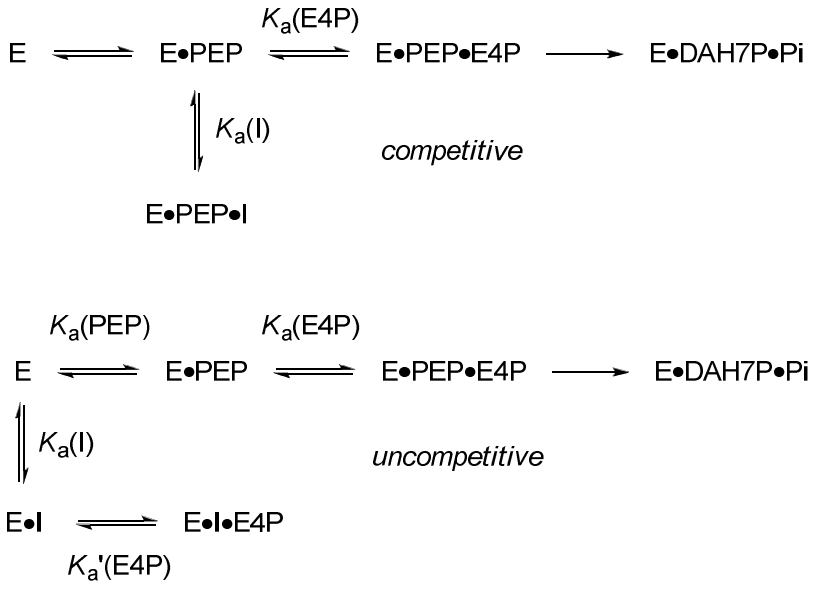

Figure 3.45: Relevant equilibria for competitive and uncompetitive behaviour with respect to E4P. In the competitive model, both E4P and fosmidomycin (I) compete for the same intermediate, in the uncompetitive model E4P and I are not in direct competition for the same species. For simplicity, the metal association equilibrium prior to substrate binding has been omitted, as have the product release equilibria.

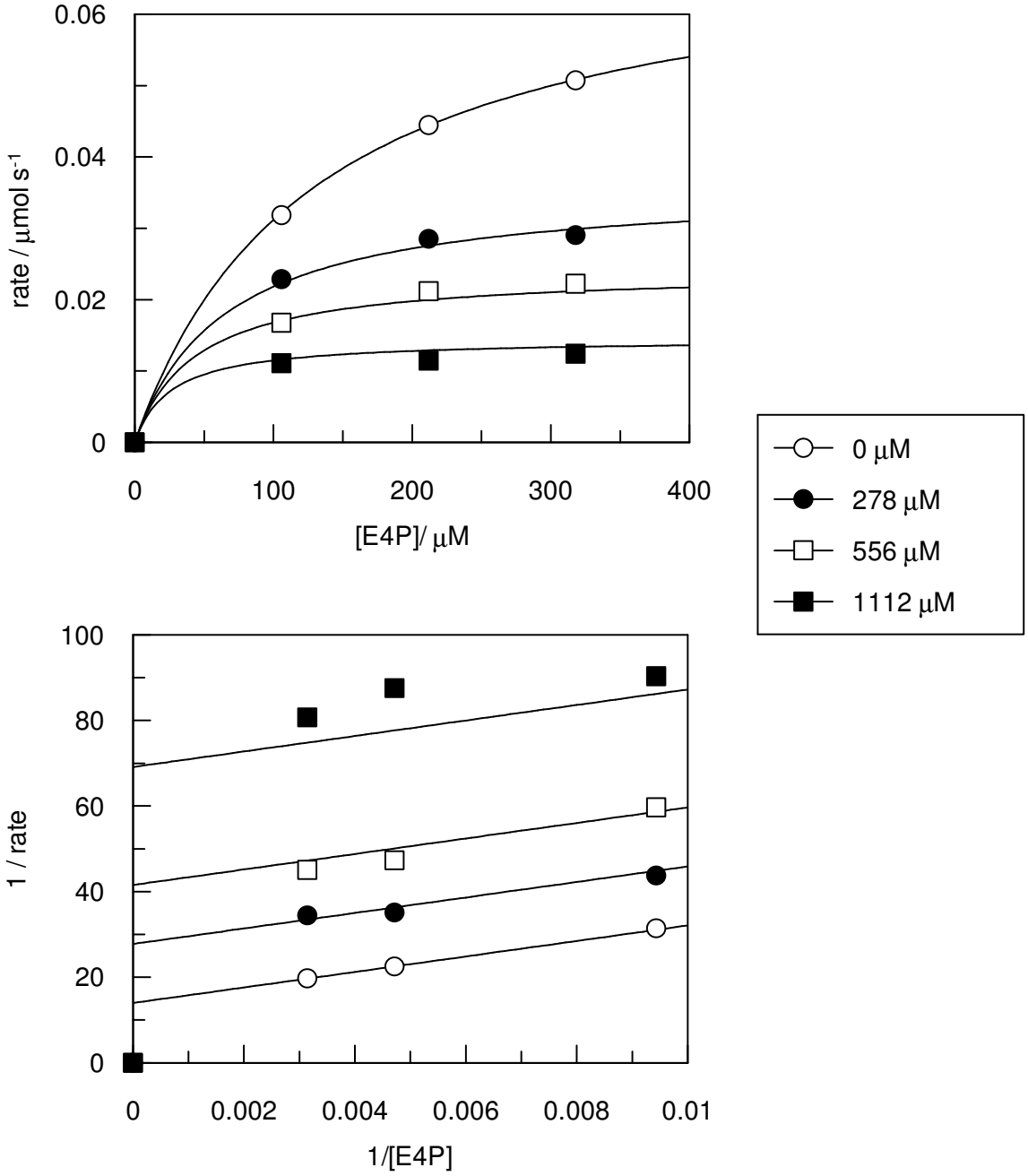

Figure 3.46: Inhibition of DAH7P synthase with fosmidomycin with relation to E4P; in both Michaelis-Menten and Lineweaver-Burk representations. Solutions of PEP (100 µM), manganese(II) sulfate (100 µM), E4P (100-300 µM) and fosmidomycin (0-1112 µM) in 1 mL of BTP buffer (50 mM, pH 6.8) were initiated by the addition of *E. coli* DAH7P synthase (2 µg), and the loss of PEP followed spectrophotometrically at 232 nm. Initial rates were obtained by linear least squares regression of the absorbance data, and converted to progress rates

In the competitive model (Figure 3.45), both E4P and fosmidomycin compete for the same intermediate enzyme-PEP complex. Consequently, the rate of the reaction in the

presence of fosmidomycin is primarily a function of the concentrations and association equilibrium constants for both fosmidomycin and E4P.

In the uncompetitive model, E4P and fosmidomycin bind at distinct sites, and are not in competition for the same position on the enzyme. Assuming fosmidomycin binds at the PEP site, the rate is then primarily a function of the concentrations and association equilibrium constants for fosfomycin and PEP. The concentration of E4P will still be expected to have a slight effect in this scenario, since it exerts an effect on the relative concentrations of the enzyme-PEP and enzyme-fosmidomycin complexes through the ratio of its association constant with each species.

Assuming the uncompetitive model in Figure 3.45 is correct, it would be expected that fosmidomycin would be a competitive inhibitor with relation to PEP, since fosmidomycin and PEP compete for the same position on the enzyme. Further experiments showed that this is indeed the case; fosmidomycin competitively inhibits *E. coli* DAH7P synthase with respect to PEP (Figure 3.47), with a surprisingly potent inhibition constant of 35 ± 4 μM.

This result was initially surprising; since we had already demonstrated with several diverse scaffolds (*vide supra*) that for a compound to inhibit DAH7P synthase competitively with respect to PEP it required both phosphoryl and carboxyl groups. Fosmidomycin only has a phosphonate group, so does not obey this finding. However, once the phosphonate has bound to the enzyme phosphate pocket, the carbon chain of fosmidomycin could then adopt a conformation that allowed the formylhydroxamate access to the metal ion. The corresponding chelate complex would then constitute an additional contact with the enzyme, which would strengthen the inhibitor-enzyme interaction.

If this is the case, one might expect slow kinetics for the binding of fosmidomycin to the enzyme: an initial low affinity phosphonate-phosphate pocket interaction, followed by metal-hydroxamate complexation, giving a higher affinity enzyme-inhibitor complex. This would manifest itself as a time dependency in the inhibition of DAH7P synthase with fosmidoycin, a behaviour which is in fact observed (Figure 3.48).

In addition, one would expect the inhibition of DAH7P synthase by fosmidomycin might vary depending on the particular metalloenzyme complex used, since the stability of the resulting hydroxamate complex can be expected to be dependent on the characteristics of the *d*-orbitals at the metal centre, which themselves are dependent on both metal type and ligand environment. This behaviour is also observed, while both enzyme-manganese(II) and enzyme-iron(II) complexes are affected to the same extent by 280 μM fosmidomycin, the corresponding enzyme-cobalt(II) complex is affected to a much lesser extent (Figure 3.48). A detailed analysis of these results is confounded by a number of factors; however the difference does indicate a role for the metal ion in inhibition of DAH7P synthase with fosmidomycin.

The behaviour of fosmidomycin towards DAH7P synthase raises interesting questions about the mechanism of fosmidomycin antibacterial activity. While it is clear that DXR is the primary target of fosmidomycin activity (with a K_i three orders of magnitude smaller than that against DAH7P synthase), the role of DAH7P synthase should not be overlooked. At least one of the outward signs of fosmidomycin action (reduced levels of vitamin K synthesis) can be also explained by DAH7P synthase inhibition, since while the isoprene side chain of vitamin K is non-mevolonate pathway derived, the quinone portion is shikimate pathway derived. In addition, fosmidomycin has recently been found to possess activity toward malarial parasites[116] such *P. falciparum*, which as well as possessing a non-mevalonate pathway is one of the few classes of eukaryotes to possess a shikimate pathway.[117] At very least, given the potency of unelaborated fosmidomycin as a lead structure against DAH7P synthase, and the known whole organism properties of fosmidomycin, fosmidomycin should serve as a useful starting point for the design of antibiotics targeting DAH7P synthase. Possible future directions for this research, along with computational investigations of the fosmidomycin-enzyme complex are discussed in Chapter Five.

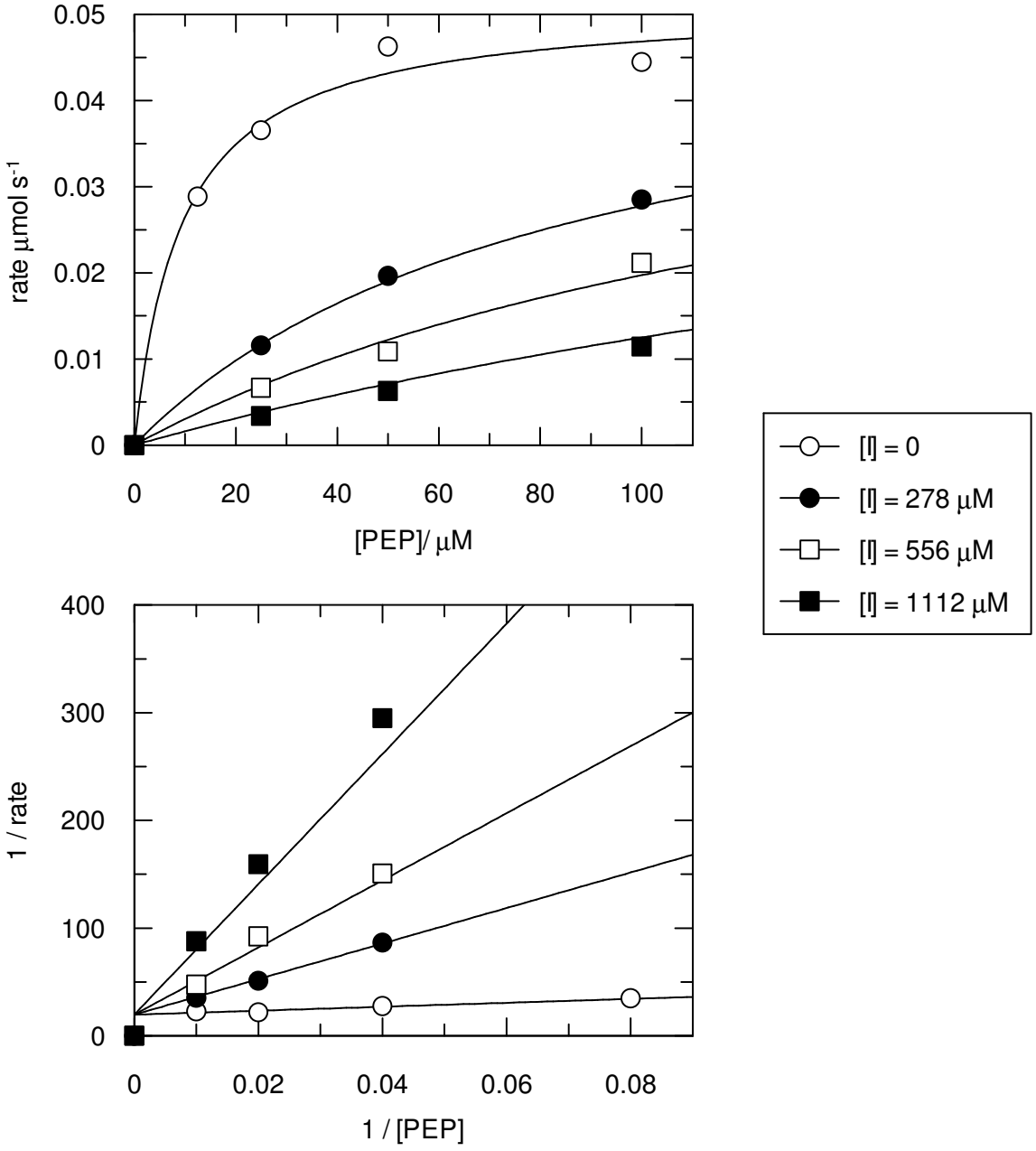

Figure 3.47: Inhibition of *E. coli* DAH7P synthase by fosmidomycin, with relation to PEP; in both Michaelis-Menten (top) and Lineweaver-Burk (bottom) representations. Solutions of PEP (20-100 µM), manganese(II) sulfate (100 µM), E4P (200 µM) and fosmidomycin (0-1112 µM) in 1 mL of BTP buffer (50 mM, pH 6.8) were initiated by the addition of *E. coli* DAH7P synthase (2 µg), and the loss of PEP followed spectrophotometrically at 232 nm. Initial rates were obtained by linear least squares regression of the absorbance data, and converted to progress rates

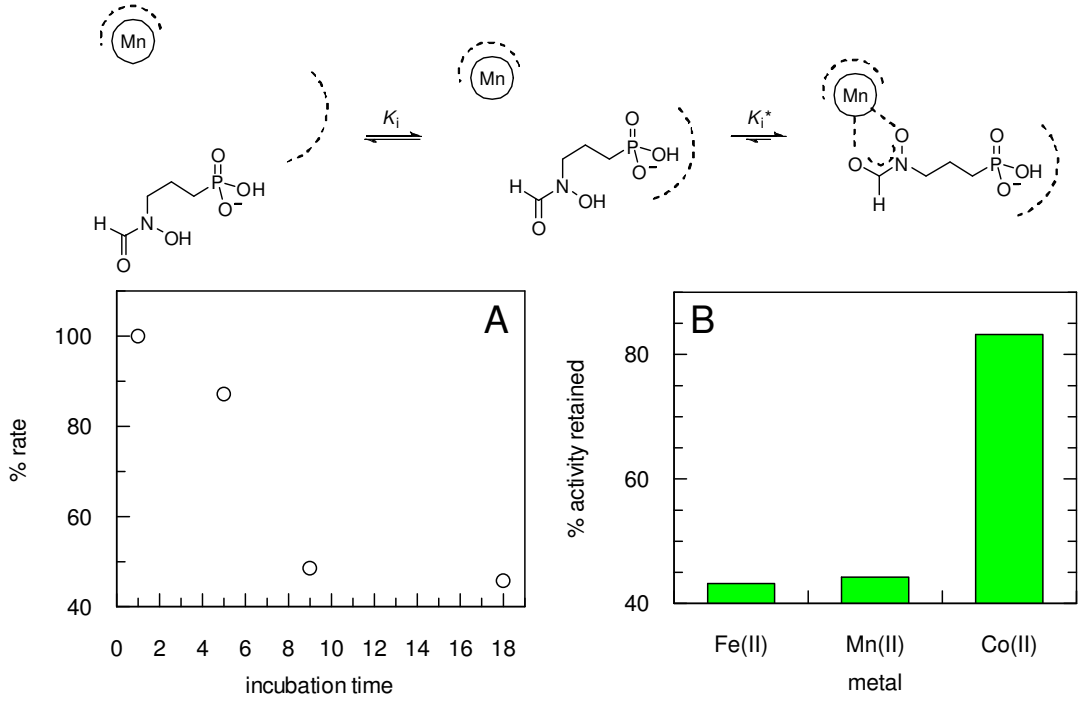

Figure 3.48: A possible slow-tight binding mechanism of fosmidomycin inhibition, and time (left) and metal (right) dependency of fosfomycin inhibition.

A. Time dependence: Fosmidomycin (280 µmol) and *E. coli* DAH7P synthase (20 µg) were incubated at 0°C in 50 mM BTP, pH 6.8 (30 µL) , and at the time indicated a portion (2 µL) was removed and used to initiate a cuvette of PEP (50 µM), E4P (200 µM) and manganese(II) sulfate (100 µM) in 1mL BTP buffer (50 mM, pH 6.8), and the initial rates taken.

B. Metal dependence: Cuvettes of PEP (50 µM), E4P (200 µM) and the appropriate metal salt ($FeSO_4$, $MnSO_4$, $CoCl_2$; 100 µM) in 50 mM BTP, pH 6.8 were initiated with *E. coli* DAH7P synthase (2 µg), and the initial rates taken. The measurement was repeated in the presence of 280 µM fosmidomycin. Reported values are means of duplicate experiments.

3.3: Summary

In summary, a number of small molecule inhibitors were designed and synthesised for DAH7P synthase. It was shown that DAH7P synthase can accept PEP-like molecules with tetrahedral geometries at the equivalent to PEP C2 (Figure 3.49). For chiral tetrahedral molecules such as phospholactate, it was shown the configuration of the C2 stereocentre has a strong influence on the affinity of binding. Even the most potent of the molecules tetrahedral at C2 bound to the enzyme approximately 25-fold weaker than PEP, indicating a preference of the enzyme for the trigonal planar geometry of PEP at C2.

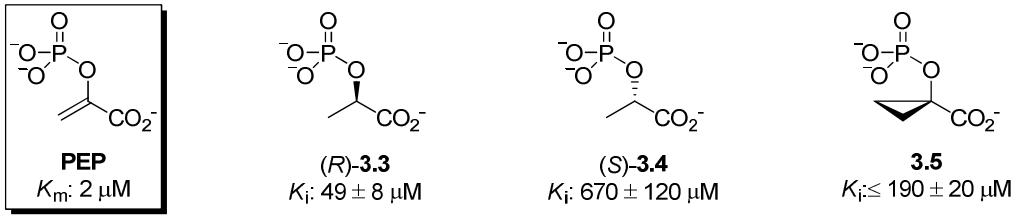

Figure 3.49: C2 tetrahedral inhibitors of DAH7P synthase compared to PEP

The importance of entropic effects in enzyme-inhibitor interactions were highlighted in the interactions of molecules with a trigonal planar geometry at the equivalent position to PEP C2. By simply restricting the conformation of a single rotatable bond; a greater than a 50-fold improvement in inhibitor potency was observed between previously reported allylic phosphonate 3.10 and conformationally restricted vinyl phosphonate 3.12.[94, 95] The binding of the conformationally restricted vinyl phosphonate was unable to be improved by substituting the methyl hydrogen atoms for fluorine atoms, although the binding was not strongly weakened by this modification either (Figure 3.50).

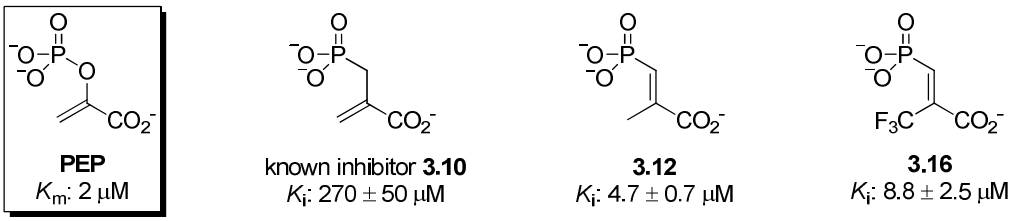

Figure 3.50: The behaviour of molecules with trigonal planar geometries at C2

The necessity of a phosphate or phosphonate group in order to achieve DAH7P synthase inhibition was demonstrated by the failure of thiazole 3.24 and sulfoenolpyruvate 3.20 to inhibit *E. coli* DAH7P synthase. The remarkable failure of sulfoenolpyruvate 3.20 demonstrates a strong specificity of the enzyme for the PEP phosphate group. While necessary for inhibition (as shown by thiazole 3.24), the presence of a phosphate mimicking group is not sufficient for inhibition of DAH7P synthase, as shown by the failure of fosfomycin 3.23 (Figure 3.51).

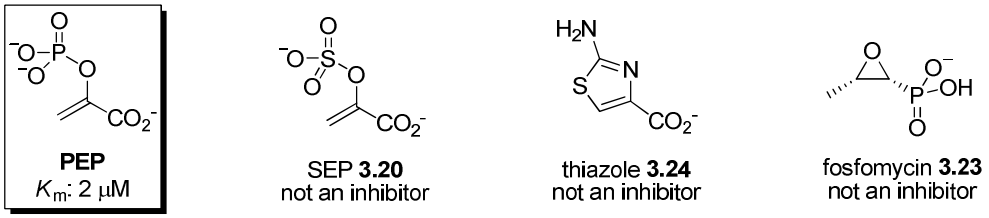

Figure 3.51: PEP and compounds that fail to inhibit DAH7P synthase.

The aminophosphonates 3.1 and 3.2 were also not strong inhibitors of the enzyme, perhaps at least partially due to the destabilising repulsion of the positively charged ammonium group from the highly positively charged PEP binding site (Figure 3.52).

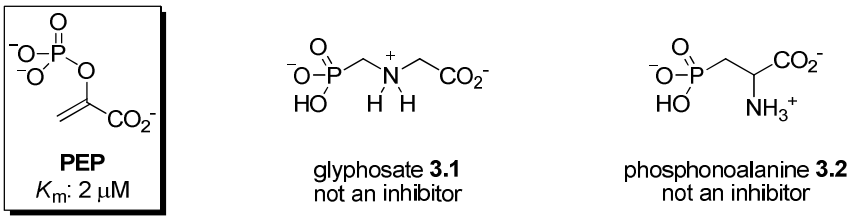

Figure 3.52: PEP and failed aminophosphonate molecules

The utility of exploiting metal-inhibitor interactions in the inhibition of DAH7P synthase was demonstrated (Figure 3.53); by using a PEP analogue bearing a strong metal coordinating group, cyanoPEP 3.17. The interaction of an inhibitor with the DAH7P synthase metal site was also invoked in the inhibition of DAH7P synthase by fosmidomycin 3.25, a clinically important antibiotic. The strong interaction of fosmidomycin with DAH7P synthase highlighted the potential dispensability of groups mimicking the carboxylate group of PEP as long as other contacts with the enzyme are made.

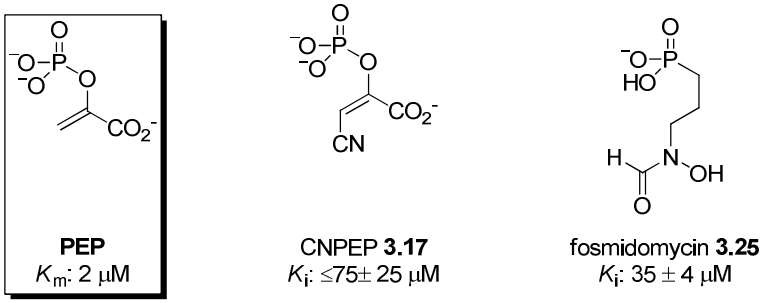

Figure 3.53: PEP compared to inhibitors exploiting inhibitor-metal interaction

Chapter Four: Novel, Dual-Site inhibitors of DAH7P synthase

4.1: Inhibitor design

With the better understanding of the DAH7P synthase PEP binding site gained by the studies in Chapter Three, work could now begin on designing new high affinity inhibitors for DAH7P synthase.

In order to improve the binding of inhibitors to DAH7P synthase, we decided to utilise the principle of multivalency. Multivalency in inhibitor design involves elaborating an existing inhibitor so that it contains additional binding motifs, allowing the molecule to simultaneously interact with multiple sites on the target, and create a more stable enzyme-inhibitor complex by utilising the binding energy associated with both binding sites[118] (Figure 4.1).

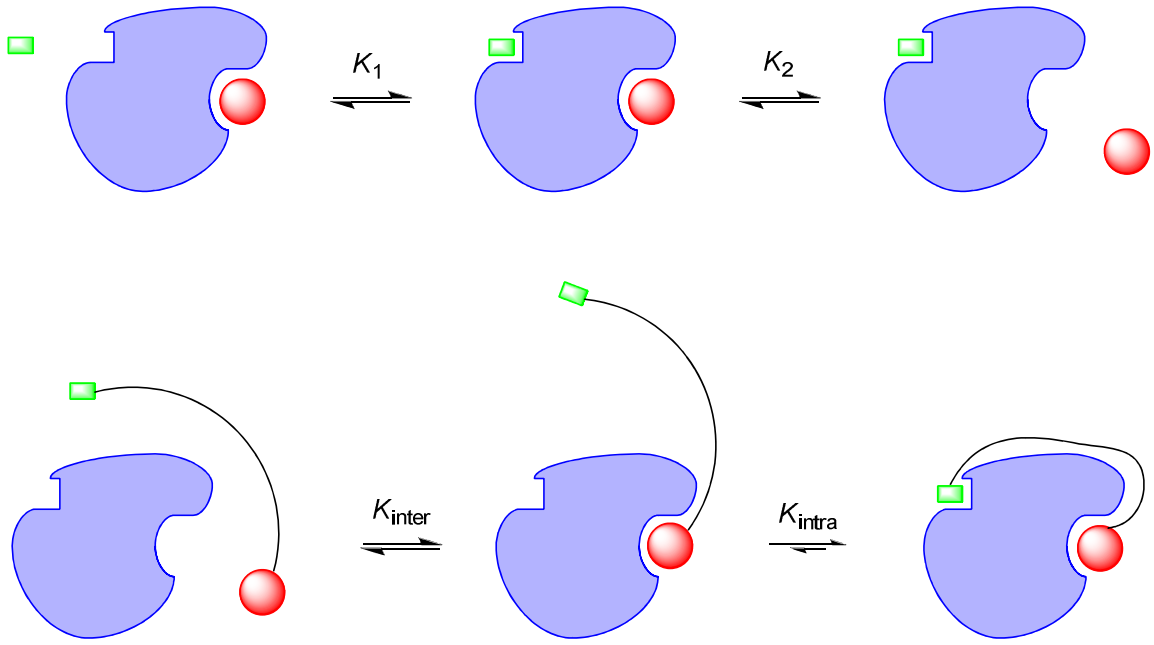

Figure 4.1: Comparison between mono and multivalent binding to an enzyme with two independent sites

This approach also makes the second binding event effectively intramolecular; so while the first binding event is controlled by the dissocation constant K_d and the relative concentrations of enzyme and ligand, the binding at the second site is dependent not on the overall concentration of ligand, but on the effective concentration, C_{eff}.[118] The effective concentration is a function of the probability of the two binding motifs being found at an appropriate distance to allow the second binding event to occur, and for long chains (greater than 15 linker atoms) C_{eff} can be estimated by assuming the linker behaves as a random coil, with suitable adjustments for linker flexibility and space occupied by the protein which cannot be occupied by the linker.[118] The intramolecular binding interaction is stronger than the corresponding intermolecular interaction. This can be explained on entropic grounds, when the enzyme and ligand are free in solution, the each have an associated translational entropy along each axis of their movement. When the two molecules interact to form a complex, there is a corresponding loss in entropy, as the total of six translational degrees of freedom (along *x*, *y* and *z* for each molecule) is reduced to just three (*x*, *y*, and *z* for the whole complex). This decrease in entropy forms a component of the overall Gibbs energy of interaction. However, if the binding event is intramolecular, then the reactants and products each have three degrees of translational entropy, which results in a smaller entropy decrease, and thus a smaller Gibbs energy of interaction (and hence a stronger interaction).[118]

In order to apply this principle to DAH7P synthase inhibitors, we decided to elaborate our known PEP-mimicking inhibitors by adding a distal phosphate, capable of interacting with the E4P phosphate binding pocket. In order to better understand the contribution of the distal phosphate, multivalent inhibitors were designed utilising strong, moderate and weak PEP-mimicking motifs (Figure 4. 2). For the linker we chose a simple tetramethylene carbon chain, it should be more readily constructed than the corresponding triol portion of DAH7P, while still providing the appropriate spacing between the PEP-mimicking end and the distal phosphate. While the absence of alcohol groups on the chain might be expected to provide a large decrease in binding affinity for enthalpic reasons, the interaction of the enzyme with the linker will reduce the conformational flexibility of the linker, resulting in a decreased entropy of interaction. The entropic cost of freezing the rotation of a carbon-carbon bond is approximately 2 kJ mol^{-1}, the values for other single bonds range from

approximately 0.4 – 4 kJ mol^{-1}.[118] In order to form hydrogen bonds from a triol unit in the linker, the positions of multiple ligand atoms and additional receptor atoms must be restricted, and this loss of entropy works against the increased enthalpy of binding.

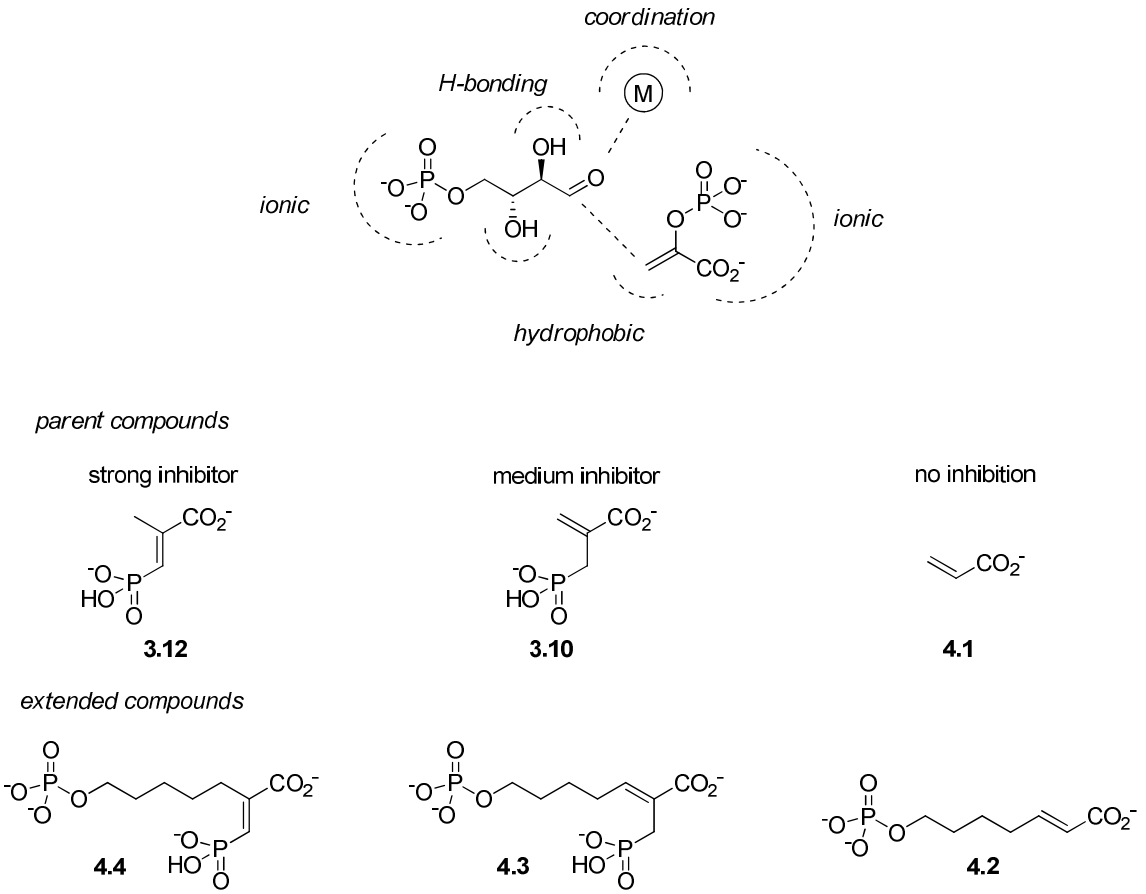

Figure 4. 2: The interaction of substrates and cofactors with DAH7P synthase, and corresponding multivalent inhibitors. Inhibitor 3.10 has been previously reported by other workers[94, 95], as outlined in Chapter Three.

With the appropriate designs in place, focus shifted to constructing the required molecules.

4.2: Synthesis of acrylate 4.2

The proposed inhibitor 4.2 was designed in order to probe the influence of a PEP phosphate mimic on multivalent inhibitors. As shown in Chapter Three, occupying the PEP phosphate binding pocket was required for inhibition of DAH7P synthase for simple PEP mimicking compounds; thus whether the addition of a distal phosphate

could create inhibition from otherwise poor compounds was of interest. Preliminary investigations showed that the parent compound, acrylate 4.1, did not display detectable inhibition of DAH7P synthase.

Synthesis of the weak multivalent inhibitor 4.2 was envisaged to be relatively straightforward; the PEP-mimicking portion could be directly coupled to the linker portion, already containing the distal phosphate in a protected form (Figure 4.3). This convergent approach was designed to minimise protecting group manipulations during the synthesis. In order to construct the C2-C3 bond, alkene cross metathesis was chosen. Whereas ring-closing alkene metathesis has rapidly become an established synthetic tool, alkene cross metathesis is an emerging technique for forming acyclic double bonds.[119] The synthesis of 4.2 should provide an ideal example for this technique; the product double bond is disubstituted and electron-deficient, which should drive the reaction away from the statistical distribution of initially formed dimeric homocoupled alkenes, and toward a single product.[119]

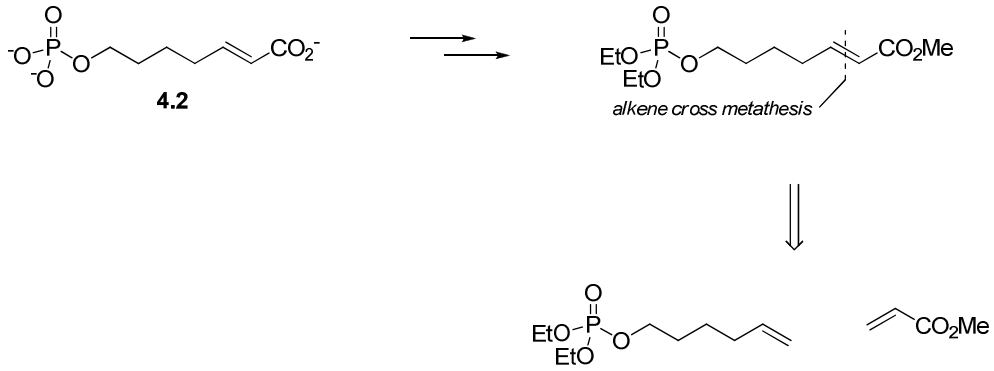

Figure 4.3: Disconnection of weak inhibitor 4.2 via cross-metathesis

The required phosphoalkene was readily prepared from commercially available 5-hexen-1-ol by phosphorylation with diethyl chlorophosphate (Figure 4.4).

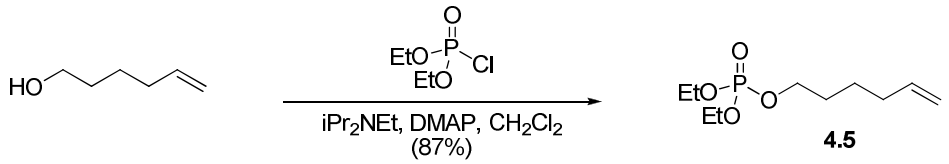

Figure 4.4 Production of phosphoalkene 4.5

Treatment of the phosphoalkene 4.5 with two equivalents of methyl acrylate and a catalytic quantity of the second generation Grubbs catalyst[120] gave an excellent yield of acrylate 4.6 with excellent diastereoselectivity (Figure 4.5). The ruthenium-containing catalyst degradation products tenaciously coordinated the product (presumably mediated by the phosphoryl group), however two rounds of ruthenium ligand exchange with DMSO[121] followed by column chromatography gave near colourless material.

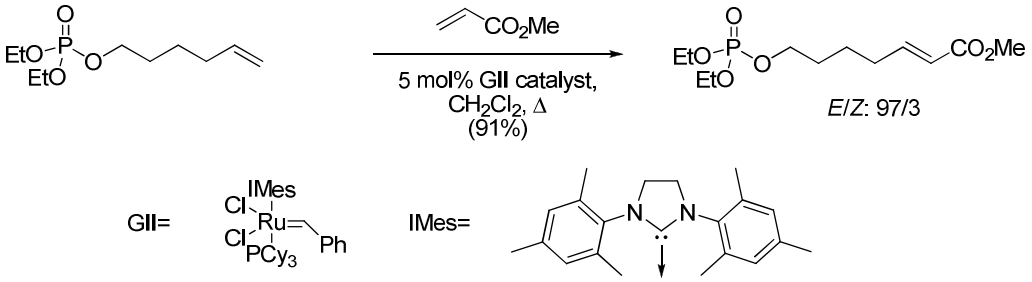

Figure 4.5: Alkene cross metathesis leading to acrylate 4.6

Deprotection of acrylate 4.6 with trimethylsilyl bromide, followed by treatment with aqueous potassium hydroxide, gave a mixture of products which could be separated by preparative anion-exchange chromatography to give the desired inhibitor 4.2 in low yield (Figure 4.6).

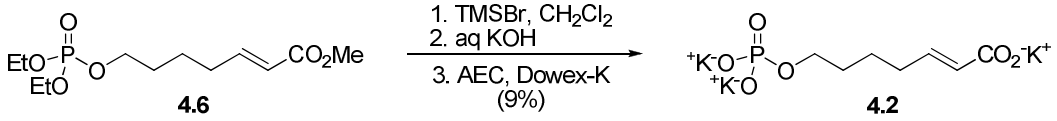

Figure 4.6: Deprotection and purification to give target 4.2

4.3 Inhibition properties of acrylate 4.2

The ability of acrylate 4.2 to inhibit the DAH7P synthase reaction was measured by enzyme inhibition assay against *E. coli* DAH7P synthase. At typical assay concentrations no effect was seen on the rate of the enzyme reaction; and at 1 mM acrylate no significant inhibition was observed even at low PEP concentrations (Figure 4.7). Due to the weak inhibition shown by acrylate 4.2, a more detailed kinetic characterisation was not attempted.

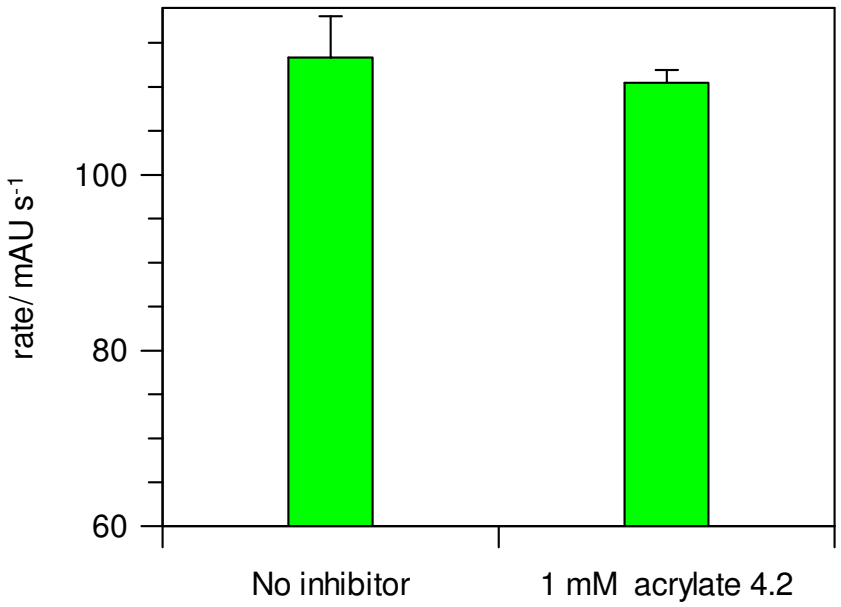

Figure 4.7: The effect of acrylate 4.2 on *E. coli* DAH7P synthase activity. A solution of PEP (50 µM), manganese(II) sulfate (100 µM), E4P (200 µM) and acrylate 4.2 (0 or 1 mM) in 1 mL of BTP buffer (50 mM, pH 6.8) was initiated by the addition of *E. coli* DAH7P synthase (2 µg), and the loss of PEP followed spectrophotometrically at 232 nm. Initial rates were obtained by linear least squares regression of the absorbance data, and converted to progress rates. Values are averages of triplicate experiments, error bars are drawn at one standard deviation.

The inability of extended acrylate 4.2 to strongly inhibit DAH7P synthase is not unexpected, and validates our design approach. Considering that acrylic acid does not inhibit DAH7P synthase, it suggests that simultaneous interaction of the inhibitor with both the PEP and E4P subsites are required in order to achieve inhibition, and as before a mimic of the PEP phosphate group is required for binding to the PEP phosphate site. Further analysis of the binding of 4.2 and other compounds to DAH7P synthase is presented in Chapter Five.

4.4: Synthesis of allyl phosphonate 4.3

4.4.1: Alkene metathesis approaches

Our initial synthetic scheme for the allyl phosphonate 4.3 sought to apply alkene metathesis chemistry, which had performed well in the synthesis of acrylate 4.2. However, alkene cross metathesis chemistry is sensitive to both steric and electronic

effects in the olefin,[119] and the necessary substrate olefin for cross metathesis possesses both steric (1,1-disubstitution) and electronic (electron deficiency) deactivating properties. It was feared that this combination would make the olefin unreactive toward cross-metathesis, and such properties have been previously observed.[122]

Based on the prospect of this difficult coupling, it was decided to perform a ring closing metathesis to form the key bond; transesterification of the product medium-ring lactone 4.8 would give the necessary acyclic alkene 4.7, and the phosphonate and phosphate groups could then be introduced (Figure 4.8).

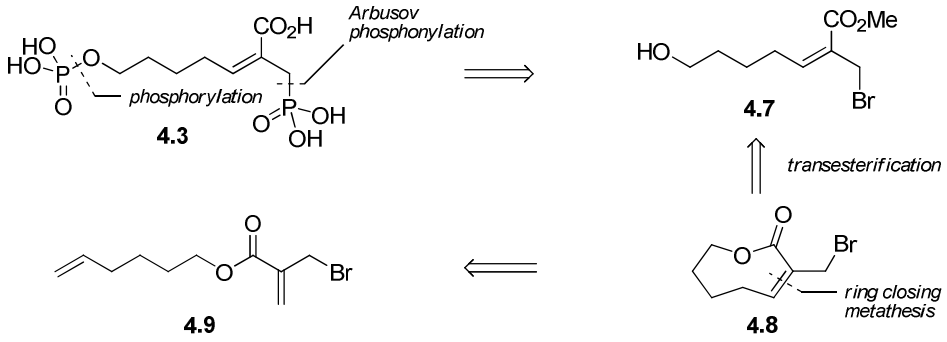

Figure 4.8: Retrosynthesis of allylic phosphonate 4.3

In order to carry out this scheme, access to the bromoacrylate ester 4.9 was required. Reported esterifications of 2-(bromomethyl)acrylic acid are typically limited to simple alkyl esters,[123, 124] formed by Fischer esterification. The yields are generally moderate, due to competing polymerisation processes. Attempted generation of 2-(bromomethyl)acryloyl chloride is reported to lead to extensive exchange of the halide, leading to mainly 2-(chloromethyl)acryloyl chloride.[125]

In order to access the required ester, we decided to explore alternative esterifications. However, the required ester was surprisingly difficult to access. Steglich esterification with dicyclohexylcarbodiimide (DCC) and 4-(dimethylamino) pyridine (DMAP) led to no identifiable product. Steglich esterifications of acrylates are reported to be difficult due to side reactions involving nucleophilic addition to the acrylate alkene, presumably the presence of an allylic bromide makes this addition even more

facile.[126] Attempted esterification with PyBOP/DMAP also gave no product,[127] as did attempts to utilise the acryloyl-trifluoroacetyl mixed anhydride.

Transesterification is a mild method for the formation of esters in sensitive substrates, and can be accomplished under both acid and base catalysis. The variety of conditions available made this method seem like a useful approach, and consequently we required access to methyl (bromomethyl)acrylate 4.10. However given the difficulty in synthesising esters of 2-(bromomethyl)acrylic acid (*vide supra*), we decided to start with the ester bond intact, and add the bromomethyl substituent. Treatment of methyl acrylate under Baylis-Hillman conditions gave a low yield of the required allylic alcohol 4.11 (Figure 4.9).[128]

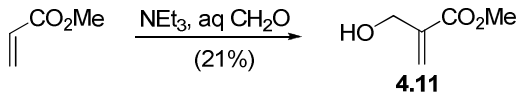

Figure 4.9: Baylis-Hillman reaction of methyl acrylate to give alcohol 4.11

Though the yield of the alcohol was low, the reagents are commodity chemicals, readily available in litre quantities, and the reaction is readily performed on a large (50 g) scale. Treatment of the allyl alcohol 4.11 under conditions reported[128] to give the desired bromide 4.10 instead gave the saturated dibromide 4.12 as the major product, with the desired bromide 4.10 present as a minor product in a chromatographically inseparable mixture. Bromination of the alcohol under other previously reported[129] conditions gave rise to a good yield of crude product, but distillation returned a low yield of the desired bromide, although it was free of contamination by the dibromide (Figure 4.10).

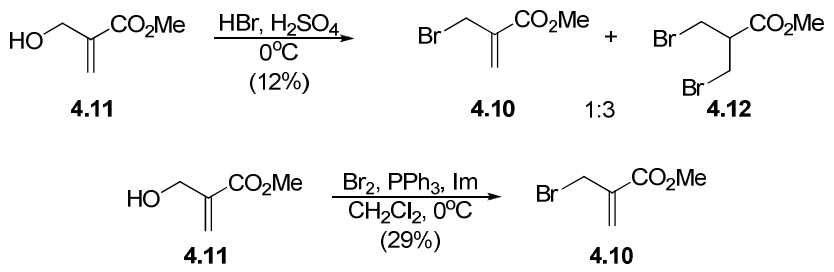

Figure 4.10: Bromination to give (bromomethyl)acryl ester 4.10 by two literature methods[128, 129]

Transesterification of the methyl ester was then attempted. Treatment of 4.10 with 1.5 equivalents of alcohol 4.13 in refluxing toluene, in the presence of catalytic toluenesulfonic acid gave a slow conversion to hexenyl ester 4.9 by TLC. Attempts to improve conversion by sequestering the formed methanol in 4Å or 13X molecular sieves were unsuccessful (Figure 4.11).

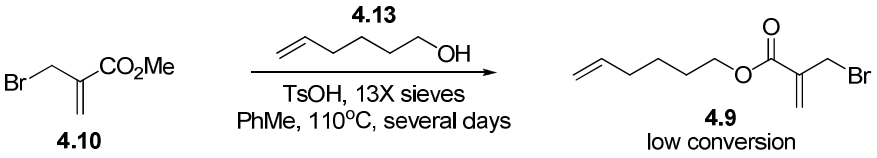

Figure 4.11: Attempted transesterification with toluenesulfonic acid

Otera's distannoxane catalysts have been recommended as transesterification catalysts for difficult cases, the reactions proceed under mild conditions, do not require a large excess of alcohol, and can be carried out with less than 1 mol% of catalyst.[130-132] Treatment of methyl ester 4.10 with alcohol 4.13 in the presence of 1 mol% distannoxane 4.14 gave some conversion to products by TLC, but the reaction was slow. Addition of further alcohol or catalyst did not seem to increase conversion (Figure 4.12). Conducting the reaction in 10% dichloroethane/hexanes under microwave irradiation gave a similar mixture of products after 160 minutes; however no improvement in conversion was seen.

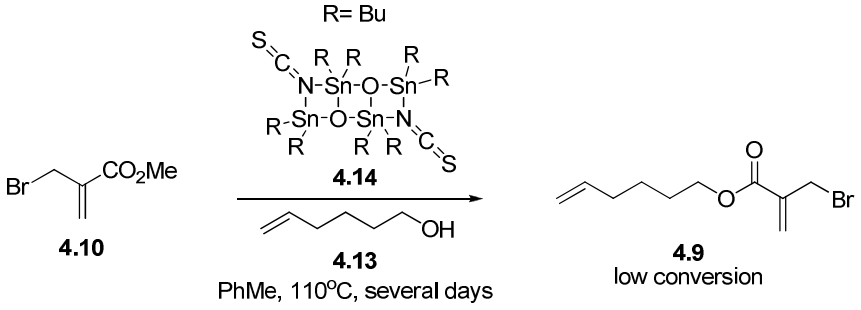

Figure 4.12: Attempted transesterification with Otera catalyst 4.14

With the failure of these simple approaches to esterification, it was thought the Mitsunobu reaction might be a useful method to prepare the ester.[133] The Mitsunobu reaction had been used successfully to form a related ester by Furstner *et al*[134]; and in our case treatment of hexenyl alcohol 4.13 with a slight excess of

(bromomethyl)acrylic acid under Mitsunobu conditions gave a good yield of the corresponding diene ester 4.9 (Figure 4.13).

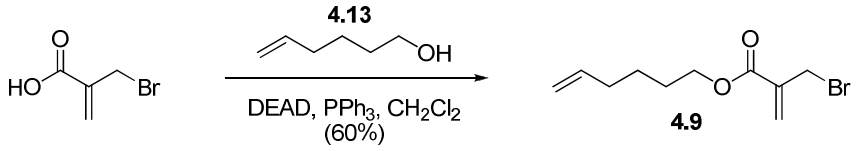

Figure 4.13: Diene ester 4.9 from the Mitsunobu reaction

With the required diene 4.9 in hand, the pivotal ring closing metathesis step was investigated. The production of lactones by ring closing metathesis was an early application of this methodology, and both small ring lactones and macrolactones are now commonly generated via this route. The production of medium rings by this route is considered more challenging, in particular the preparation of eight-membered rings such as the desired lactone 4.8, but examples of eight-membered ring closure are known.[135]

Treatment of a dilute solution of diene 4.9 under microwave irradiation, with two 2 mol% portions of the Grubbs second generation catalyst[120], gave after two ten minute irradiations complete conversion of the starting diene to a single permanganate reactive species by TLC. Isolation of this product showed that instead of the expected lactone 4.8, the linear dimer 4.15 had been formed, as a 9:1 *E*:*Z* mixture (Figure 4.14).

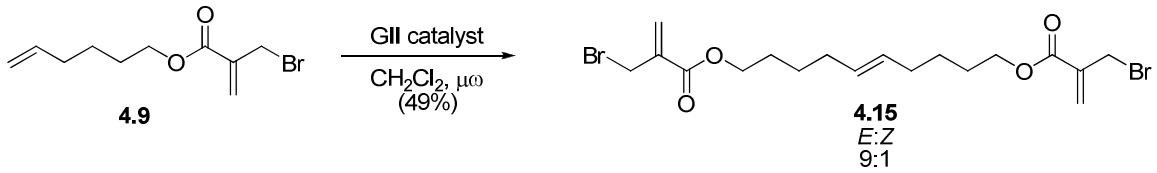

Figure 4.14: Initial microwave metathesis reaction leading to linear dimer 4.15

In order for the linear dimer 4.15 to form, the catalyst must react with the terminal monosubstituted alkene of 4.8, extruding ethylene to form the intermediate metallocarbene 4.16, which instead of undergoing the desired intramolecular ring closing reaction to give the lactone 4.8, undergoes a cross-metathesis reaction with another molecule of 4.9 giving the linear dimer 4.15 (Figure 4.15).

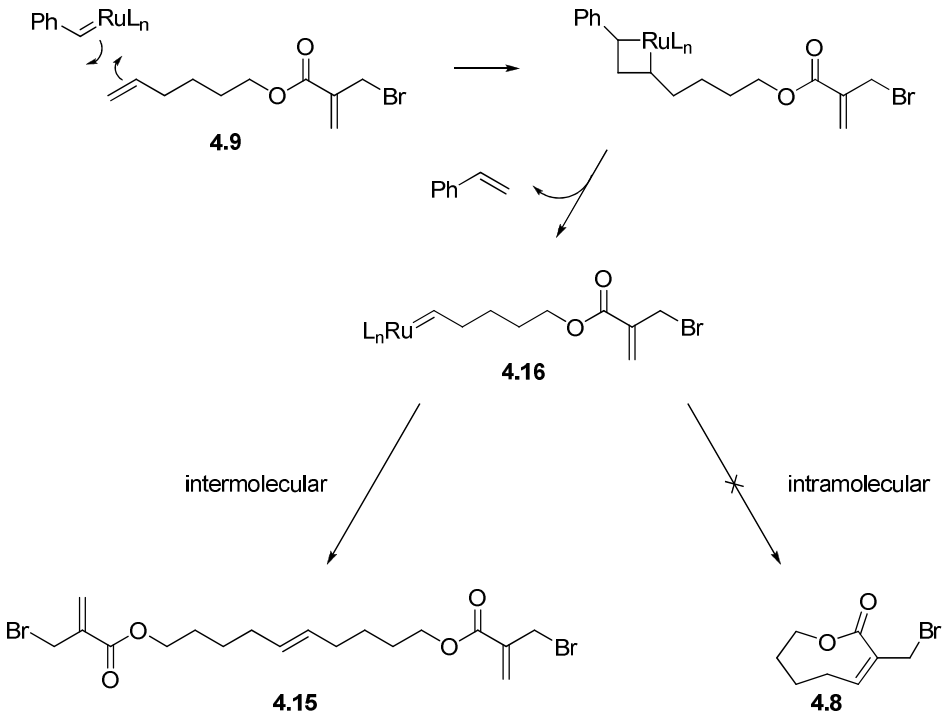

Figure 4.15: Possible fates of metallocarbene 4.16

Given the rapidity of the microwave reaction, it was reasoned that the linear dimer 4.15 obtained may simply be a kinetic product, and that on further reaction may be converted into the desired ring closed product. However, metathesis under conventional heating for longer reaction time showed no formation of the desired lactone, and resubjecting the isolated linear dimer 4.15 to further reaction with Grubbs second generation catalyst in toluene at 80°C showed no conversion of the linear dimer 4.15 to lactone 4.9. This implies that dimer 4.15 is a dead-end product of the metathesis process, and cannot be further processed by the catalyst into the desired lactone.

With this fact in mind, a number of attempts were made to modify the conditions of the metathesis reaction to promote the intramolecular ring closure over the formation of the dead end dimer product 4.15. Reducing the concentration of the diene 4.9 should reduce the likelihood of metallocarbene 4.16 encountering another molecule of diene before it has a chance to ring close to the desired 4.8. Accordingly, higher dilution conditions than those orginally chosen were screeened. Reducing the concentration of diene from 20 mM to 5 mM did not succeed in producing the desired

lactone 4.15, and using ultra-high dilution conditions (diene concentration: 111 μM) in toluene had no effect other than slowing the overall reaction.

Since changing the diene concentration had little effect, other possibilities were explored. The Grubbs second generation catalyst has a broad substrate specificity, but an acknowledged weakness is its decreased reactivity toward sterically or electronically challenging alkenes.[119] A variety of other commerically available catalysts were explored, including the Grubbs first generation catalyst[136], the Hoveyda-Grubbs first generation catalyst,[137] and the Hoveyda-Grubbs second generation catalyst.[138] None of these catalysts succeeded in producing the desired lactone. The phosphine-free Grubbs second generation catalyst[139] was prepared (Figure 4.16), in the hope its greater rate of initiation may prove beneficial, but it too was unsuccessful in producing the lactone 4.8.

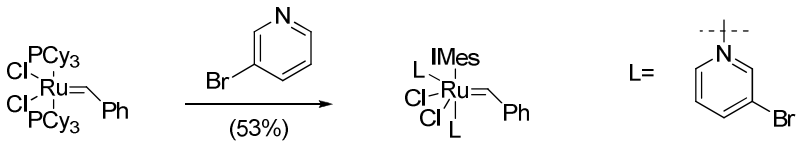

Figure 4.16: Preparation of the second generation phosphine-free Grubbs catalyst[139]

It was possible that acrylate alkene may be forming a dead end complex with the catalyst, converting it into a catalytically inactive chelate complex such as 4.17 (Figure 4.17), a problem that has been reported for other acrylates[140]. The addition of mild Lewis acids such as titanium(IV) isopropoxide has been reported to improve catalyst reactivity in these cases.[140] It has been proposed these co-catalysts work by competing with the ruthenium atom for coordination with the carbonyl oxygen; forming bimetallic complexes such as 4.18 (Figure 4.17),[140] however it has not been addressed whether these reagents simply increase the rate of precatalyst activation by scavenging the free phosphine produced during catalyst activation.

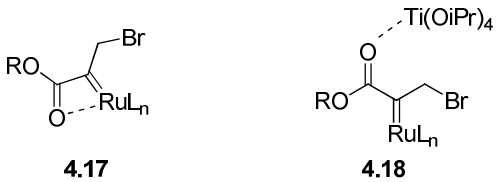

4.17 **4.18**

Figure 4.17: Inactive chelate 4.17, and activated bimetallic complex 4.18

Attempts to overcome this supposed catalyst inactivation by slow addition of fresh catalyst to a refluxing dilute solution of diene over a period of eight hours, or simultaneous slow addition of a solution of diene and a solution of catalyst to refluxing solvent were unsuccessful. Likewise, the addition of catalytic quantities (10-25 mol% with relation to diene 4.9) of titanium(IV) isopropoxide had no effect.

Another method of potentially slowing the undesired dimerisation step would be to utilise the sensitivity of Grubbs second generation catalyst to steric effects, and use a more hindered repalcement for the terminal monosubsituted alkene. This alkene would lead to the same metallocarbene intermediate 4.16, while the additional bulk should slow the undesired intermolecular dimerisation step, and perhaps allow the desired intramolecular ring closure to occur.

Cross metathesis of diene 4.9 with excess (*Z*)-diacetoxybutene in the presence of Grubbs second generation catalyst gave a good yield of hindered diene 4.19 after chromatography, as an inseperable 93:7 *E*/*Z* mixture. Also isolated was a small quantity of the symmetrical dimer 4.15 (Figure 4.18).

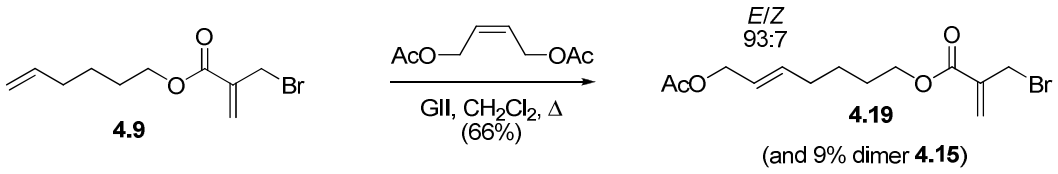

Figure 4.18: Synthesis of the hindered diene 4.19

However, treatment of the hindered diene 4.19 with Grubbs second generation catalyst in the presence of titanium(IV) isopropoxide also failed to give the desired lactone, instead returning unreacted starting material, symmetrical dimer and traces of catalyst-derived styrene products. Presumably the diacetoxybutene produced during the formation of the dimer 4.15 was lost in the aqueous workup used to quench the titanium(IV) isopropoxide.

At this stage it was decided that the source of the problem was perhaps the formation of the medium ring lactone, since no analogous examples to our desired ring closure are known, and the formation of an eight membered ring is known to be a very

difficult ring size to close with ring closing metathesis.[135] In order to test this hypothesis, allyl ester 4.20 was prepared under similar Mitsunobu conditions to those used for hexenyl ester 4.9 (Figure 4.19).

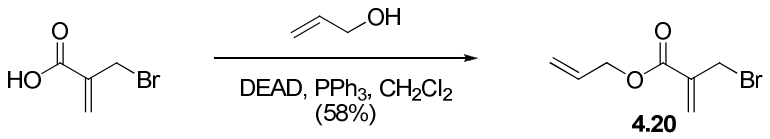

Figure 4.19: Synthesis of allyl ester 4.20

Treatment of allyl ester 4.20 under ring closing metathesis conditions should give rise to a five-membered ring lactone, a more favourable process than closing a medium ring lactone. The most similar example to this ring closure in the literature is one reported by Furstner *et al* in the total synthesis of the marine natural product (*S*,*S*)-(+)-dehydrohomoancepsenolide;[134] slow addition, high dilution and titanium(IV) isopropoxide cocatalysis was required to achieve the ring closure (Figure 4. 20). Notable in this reaction is the chemoselectivity for closure of the 5-membered ring over possible enyne metathesis products containing larger 8-13 membered rings.

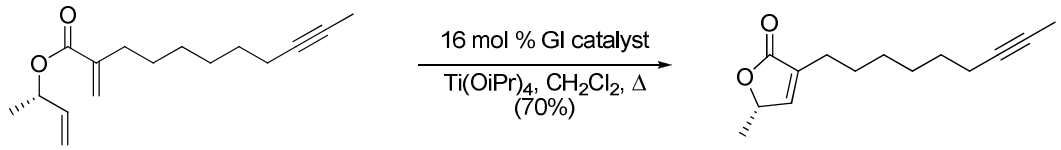

Figure 4. 20: Furstners ring closing metathesis en route to (*S*,*S*)-(+)-dehydrohomoancepsenolide[134]

Attempts to apply the conditions of Furstner to closing the ring of allyl diene 4.20 were unsuccessful; the use of Grubbs second generation catalyst also failed to give the desired lactone product, instead linear dimer 4.21 was isolated (Figure 4.21).

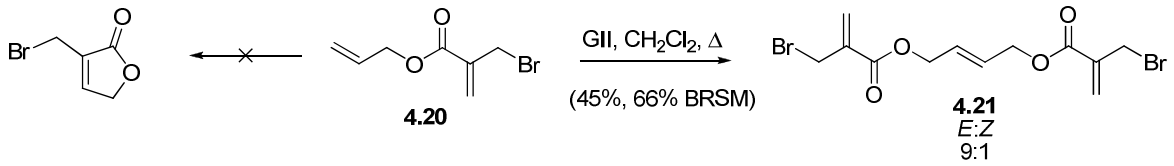

Figure 4.21: Attempted ring closing metathesis of allyl diene 4.20

In summary, despite a thorough investigation of possible metathesis reaction conditions, no conditions were found that gave any cyclised lactones from 2-(bromomethyl)acrylates. Factors that are known to slow metathesis reactivity and exist in 2-(bromomethyl)acrylates include 1,1-disubstitution, large allylic substituents, and an electron withdrawing group directly attached to the alkene.[119] No metathesis reactions of related 2(halomethyl)acrylates are known in the literature; an anomaly in an area of such active research. In addition, a recent systematic study of ring closing metathesis of 2-alkyl acrylates found that while six membered rings are formed in good yield, five and seven membered rings are formed in moderate yield, and attempts to produce eight and nine membered rings led solely to dimerisation of the more reactive terminal alkene as seen here with 2-(bromomethyl)acrylates.[141] Based on the results obtained, and the indications in the literature, a new approach to our desired inhibitor 4.3 was sought.

4.4.2: Allylic rearrangement approaches

With the failure of our earlier metathesis approach, a new method to access to the phosphonate inhibitor 4.3 was required. The addition of a variety of carbon and heteroatom nucleophiles to β'-acetoxy-α,β-unsaturated esters is known to proceed not via a direct substitution at the β' carbon, but via a sequence of initial Micheal addition followed by elimination from the resulting ester enolate to give an overall S_N2' substitution (Figure 4.22).[142]

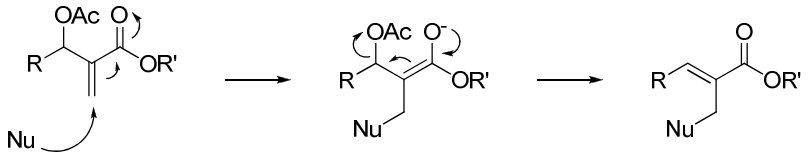

Nu: R_2CuLi; RMgBr; malonates; H^-; RNH_2; RCO_2^-; ROO^- RS^-; N_3^-, Br^-

Figure 4.22: Tandem addition/ transposition reaction of β'-acetoxy-α,β-unsaturated esters[142]

Furthermore, it has been reported that trialkylphosphites behave similarly, giving allylic phosphonium ions, which in turn dealkylate to allylic phosphonates in a manner analogous to the Arbusov reaction (Figure 4.23).[143]

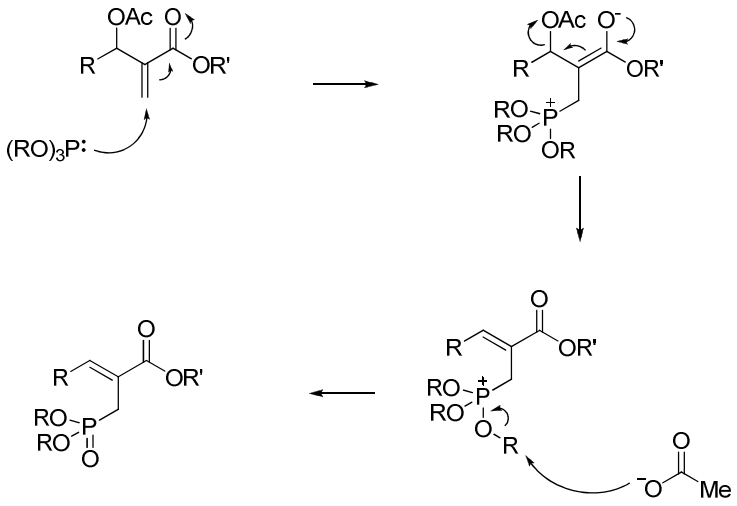

Figure 4.23: Sequential addition/transposition/dealkylation reaction with trialkylphosphites[143]

Based around this new method for creating an allylic phosphonate, a new retrosynthetic scheme was designed around gaining access to allylic alcohol 4.22 (Figure 4.24).

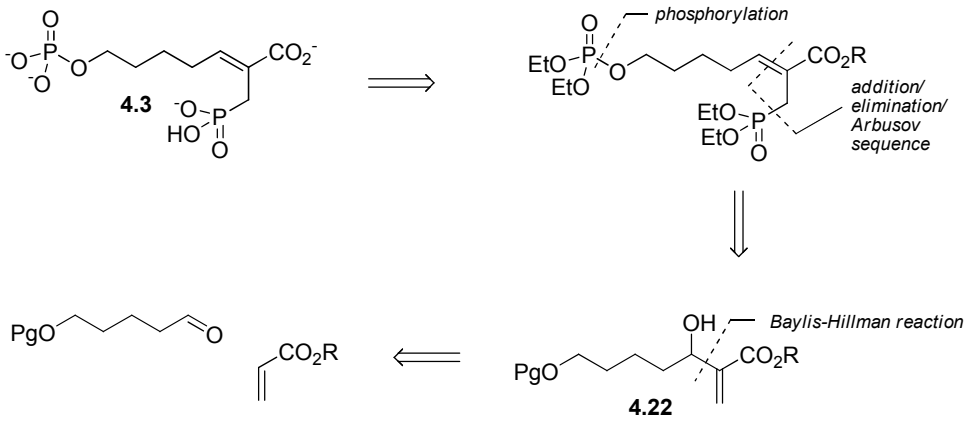

Figure 4.24: Retrosynthesis of allylic phosphonate 4.3 via a Baylis-Hillman reaction

In order to form the key allylic alcohol 4.22, the Baylis-Hillman reaction was explored. The Baylis-Hillman reaction[144] is an organocatalytic carbon-carbon bond formation, in which a nucleophilic species (typically 1,4-diazabicyclo[2.2.2]octane, also known as DABCO) adds reversibly to an electron deficient olefin, and the intermediate zwitterionic enolate formed attacks a carbonyl group. Subsequent elimination of the catalyst reforms the original olefin, giving a net exchange of the vinylic carbon-hydrogen bond for a carbon-carbon bond (Figure 4.25).[144] Virtually

ignored for a decade after its discovery, the reaction has undergone a renaissance in recent years with the rising interest in organocatalysis.[144]

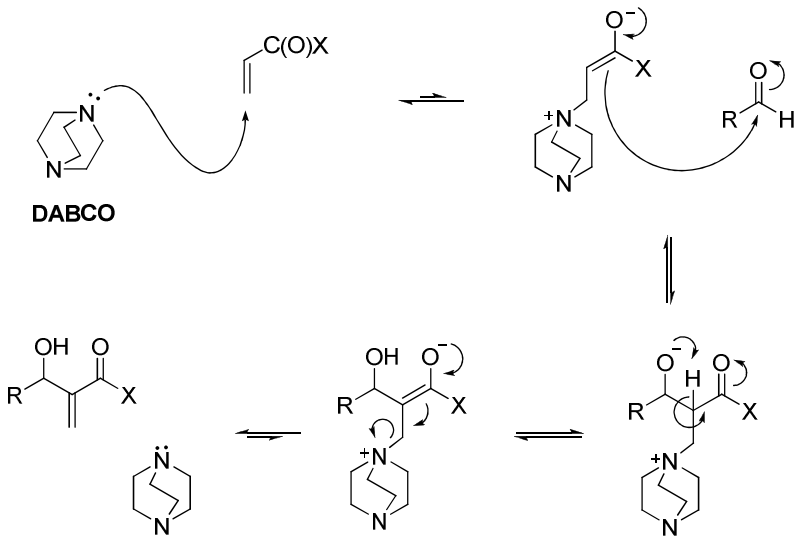

Figure 4.25: The generally accepted mechanism of the Baylis-Hillman reaction[144]

Selective monoprotection of 1,5-pentanediol using a 3:1 ratio of diol to *tert*-butyldimethylsilyl chloride gave the desymmetrised alcohol 4.23 in good yield (Figure 4.26).

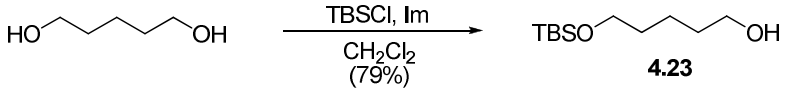

Figure 4.26: Monoprotection of pentanediol to give alcohol 4.23

Oxidation of alcohol 4.23 with the periodinane 2-iodoxybenzoic acid (IBX) gave a good yield of the corresponding aldehyde 4.24 (Figure 4.27).[145]

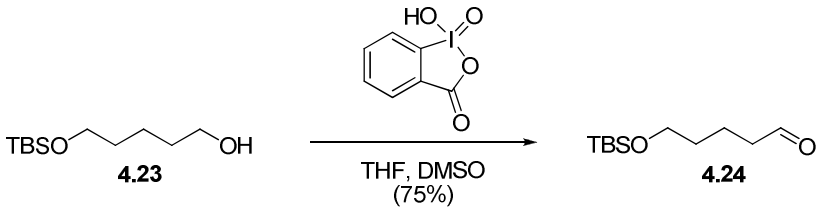

Figure 4.27: Production of aldehyde 4.24 by IBX oxidation

However, treatment of aldehyde with methyl acrylate and DABCO failed to give the required allylic alcohol 4.22. Similar Baylis-Hillman reactions to the desired transformation remain unreported with related aldehydes. Despite the renewed popularity of the Baylis-Hillman reaction, it is reported to work best with comparatively electron deficient aldehydes such as aromatic aldehydes, particularly those with electron withdrawing *para* substituents. Reaction times have been found to stretch into weeks for unfavourable aldehydes, and the product acrylates are prone to further side reactions, such as polymerisation promoted by the reaction conditions.[144] Mindful of the likely difficulty in having a key step with such a long reaction time early in the synthesis, we sought an alternative method for the construction of the C2-C3 bond.

The use of 2-lithio or 2-magnesioacrylates as nucleophiles is largely unreported, presumably due to ease of the metalloacrylate to undergo side reactions such as conjugate addition. This observation is supported by the literature, the only examples of lithio- or magnesio- acrylates involve halogen-metal exchange on 2-haloacrylates disubstituted at the 3-position, conducted at low temperature.

The corresponding vinyl alanes 4.25 however, have been recommmended as a way to overcome the shortcomings of the Baylis-Hillman reaction.[146] These alanes are reported to react readily with aldehydes at room temperature. The vinyl alanes system can be prepared by hydroalumination of propolic esters 4.26, with diisobutylaluminium hydride (DIBAL) in the presence of either highly carcinogenic hexamethylphosphoramaide (HMPA)[147] or the safer *N*-methylmorpholine *N*-oxide (NMO)[146], resulting in the overall transformation as shown in
Figure 4.28.

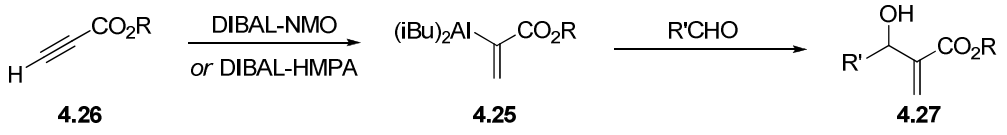

Figure 4.28: Hydroalumination of propiolic esters 4.26 to vinyl alanes 4.25 and subsequent nucleophilic attack on aldehydes to give allyl alcohols 4.27

This methodology seemed like a promising method to construct the allylic alcohol functionality in 4.22. In order to investigate the method, the known model reaction with benzaldehyde was undertaken according to the literature[146], and the corresponding allylic alcohol was indeed formed, albeit in a low yield (
Figure 4.29).

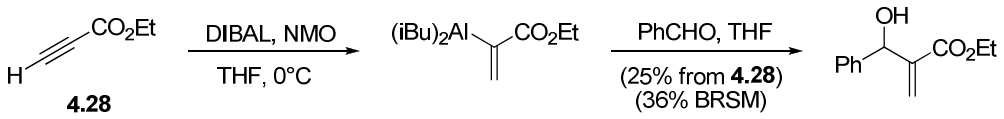

Figure 4.29: Hydroalumination/ nucleophilic attack of benzaldehyde

Application of this reaction to our system was then undertaken. The *tert*-butyldiphenylsilyl (TBDPS) protected aldehyde 4.30 was prepared in two steps from 1,5-pentanediol (Figure 4.30).

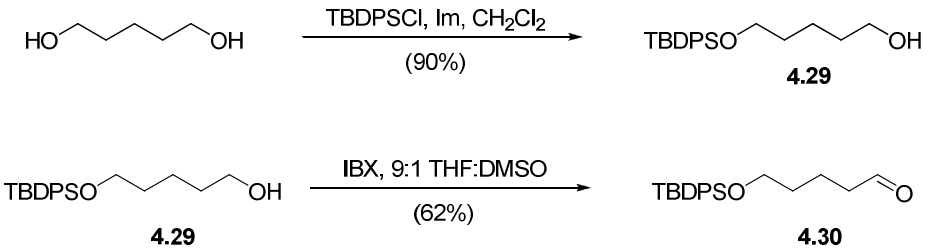

Figure 4.30: Preparation of aldehyde 4.30

Ethyl propiolate was treated with preformed DIBAL-NMO complex at 0°C for thirty minutes, and then aldehyde 4.30 was introduced. After workup, analysis of the reaction mixture by ^{1}H NMR spectroscopy showed only starting material was present, contaminated with traces of the desired product 4.31 (<0.5% based on integration) (
Figure 4.31). Allowing the alane to react with the aldehyde overnight failed to give the desired product, and heating the mixture to 50°C also failed to produce 4.31.

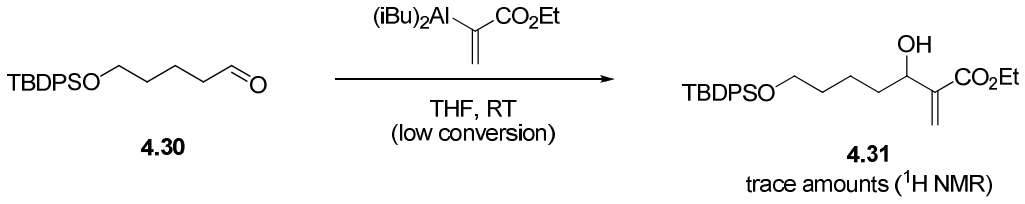

Figure 4.31: Attempted synthesis of allylic alcohol 4.31 by analogy to Figure 4.29

The reason for the failure of these reactions was unclear, but it was thought that it may be due to the lower electrophilicity of the aliphatic aldehyde 4.30 compared with the aromatic aldehyde in benzaldehyde. It was reasoned that if this was the case, it may be possible to circumvent this problem by increasing either the electrophilicity of the aldehyde by Lewis acid activation; or increasing the nucleophilicity of the organometallic reagent by transmetallation. Treatment of a mixture of vinyl alane and aldehyde 4.30 with zinc(II) bromide in order to give transmetallation to the more reactive zinc species failed to give any product. Lewis acid activation of the aldehyde with boron trifluoride etherate managed to give a low yield of the desired allyic alcohol 4.31, however extensive polymerisation was also observed. Rerunning the reaction at -78°C suppressed visible signs of polymerisation, but also failed to give any product (Figure 4.32).

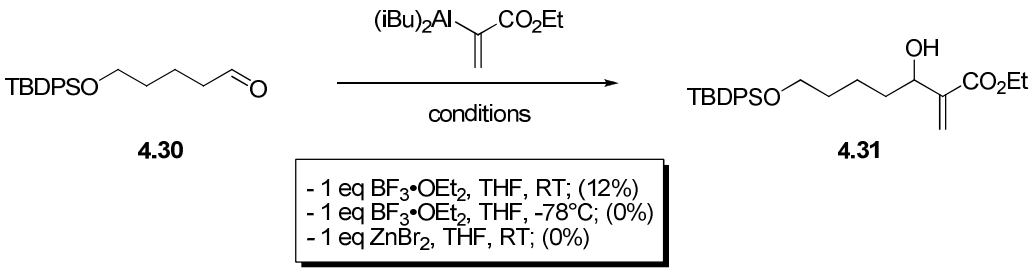

Figure 4.32: A summary of attempts to react a vinyl alane with aldehyde 4.30

The failure of the vinyl alane to react with the aldehyde 4.30 was disappointing, however a recent report supports these findings.[148] The authors observed a complete failure of a vinyl alane to react with their aliphatic aldehyde (Figure 4. 33), yet managed to achieve a good yield of the corresponding product with benzaldehyde.

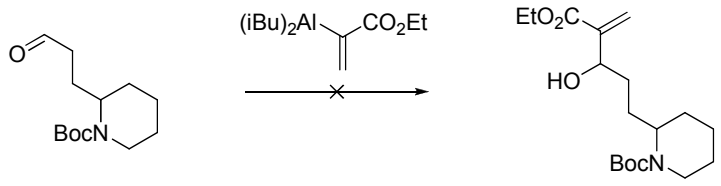

Figure 4. 33: A literature exampleof the failure of a vinyl alane to react with an aliphatic aldehyde[148]

It is tempting to speculate that this unreliability is the reason why, despite the drawbacks of the Baylis-Hillman reaction, the vinyl alane methodology has failed to achieve widespread adoption, although it has been known for almost twenty years.[147]

In order to confirm suspicions that other metalloacrylates were unsuitable as vinyl anion equivalents, we prepared the vinyl bromide 4.32. Although expensive commercially, it can be prepared readily on a 0.25 mol scale from readily available precursors, by a bromine addition/dehydrobromination sequence (Figure 4.34).[149]

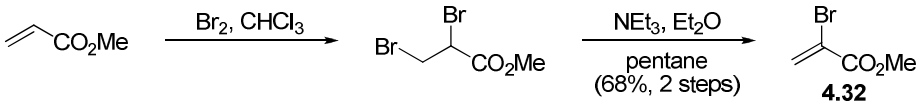

Figure 4.34: Bromination/dehydrobromination sequence delivering bromoacrylate 4.32

Attempts to produce a novel anion equivalent from vinyl bromide 4.32 by radical metallation[150] with titanocene(III) chloride, produced by reduction of titanocene dichloride with elemental zinc or manganese failed. Attempts to prepare the corresponding unreported organozinc reagent with Reike zinc[151] failed, as did the attempted preparation of the corresponding novel organochromium(II) reagent with chromium(III) chloride in the presence of manganese and catalytic nickel(II) chloride[152] (Figure 4.35). It is probable in these reactions that Micheal addition of any organometallic reagent formed to the remaining vinyl bromide 4.32 was occuring, resulting in polymeric materials rather than stable organometallic species.

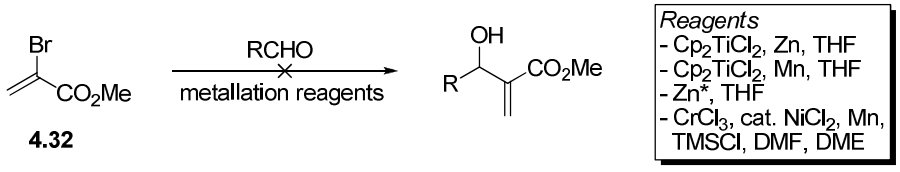

Figure 4.35: Attempts to find a novel vinyl anion equivalent

With the failure over both the Baylis-Hillman reaction and the vinyl alane addition, we still lacked a suitable method for creating the required allylic alcohol. In both of the failed approaches, the readily polymerisable acrylic alkene is conceivably to blame, with its nature placing a limit on the allowable reaction conditions.

One possible method to evade these polymerisation related problems is to form the C2-C3 bond with a reagent containing an alkene masked as another functional group, which can be converted to the alkene when desired under conditions mild enough to limit polymerisation. One approach that has been used is to mask the alkene as a tertiary amine; with subsequent quaternisation and Hoffmann elimination to return the alkene (Figure 4.36).[153]

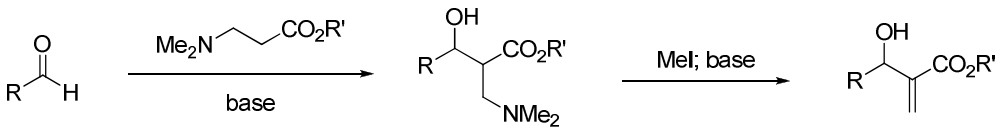

Figure 4.36: A masked alkene approach[153] to acrylates , utilising a Hoffman elimination

With this approach the key bond forming step then becomes an ester enolate addition to an aldehyde.

The required masked acrylate reagent 4.33 was generated by a modified literature procedure; treatment of methyl acrylate with aqueous dimethylamine, followed by distillation from calcium hydride gave amine 4.33 cleanly (Figure 4.37). The use of readily available aqueous dimethylamine avoids the difficulty of handling anhydrous dimethylamine, required in the original preparation.[154]

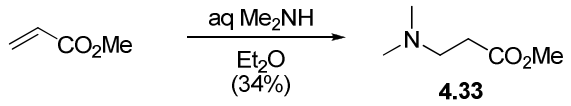

Figure 4.37:Synthesis of masked acrylate reagent 4.33

Because of the base sensitivity of the TBS protecting group, tetrahydropyranyl ether (THP) protected alcohol 4.34 was prepared in excellent yield from 1,5-pentanediol and dihydropyran by treatment with the non-toxic mild acid catalyst bismuth(III) nitrate pentahydrate (Figure 4.38).[155]

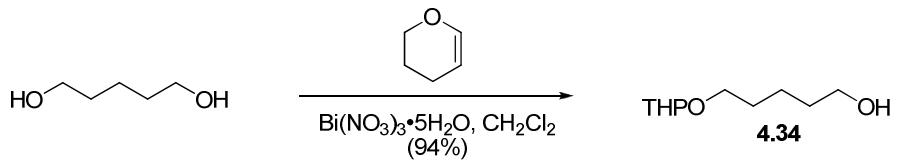

Figure 4.38: Formation of THP ether 4.34

Oxidation of alcohol 4.34 with IBX in refluxing THF gave only a moderate yield of aldehyde 4.35, presumably due to the acidic nature of IBX.[145] Oxidation utilising buffered Dess-Martin periodinane,[156] or under Swern oxidation conditions,[157] delivered the required aldehyde 4.35 in good yield (Figure 4.39).

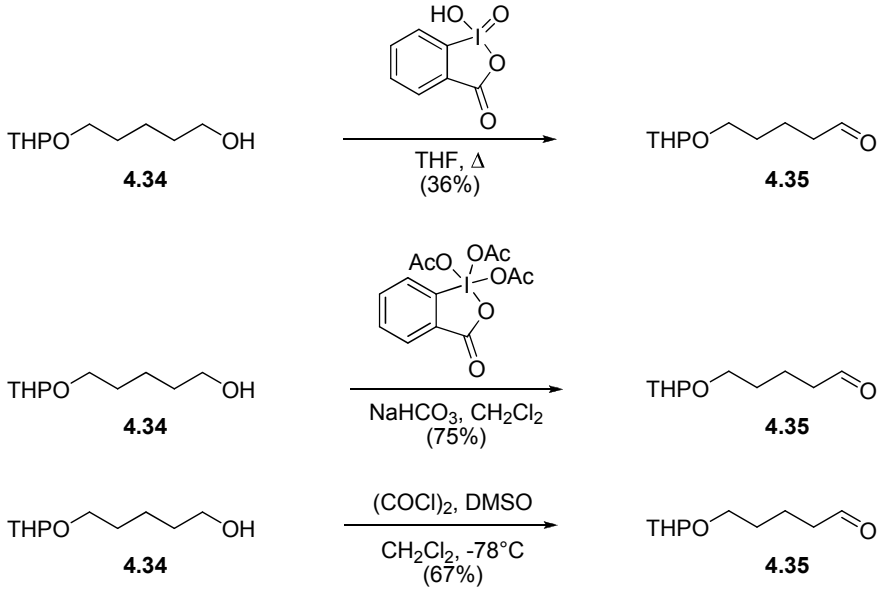

Figure 4.39: Oxidation of alcohol 4.34 to aldehyde 4.35 utilising various reagents

Treatment of aldehyde 4.35 with the lithium enolate of masked acrylate reagent 4.33 gave the aminoalcohol 4.36, which was not purified but immediately treated with excess methyl iodide, and the quaternary amine 4.37 decomposed with sodium bicarbonate to give the acrylate 4.38 (Figure 4.40). Despite this procedure succeeding, the yields were low and erratic, ranging from 17% to 1%. Again it is likely that the reason for this low yield was ready polymerisation of the acrylate under the basic conditions of the elimination, this observation being supported by the large amounts of baseline material observed in TLC analysis of the elimination step, and in the final flash chromatography step.

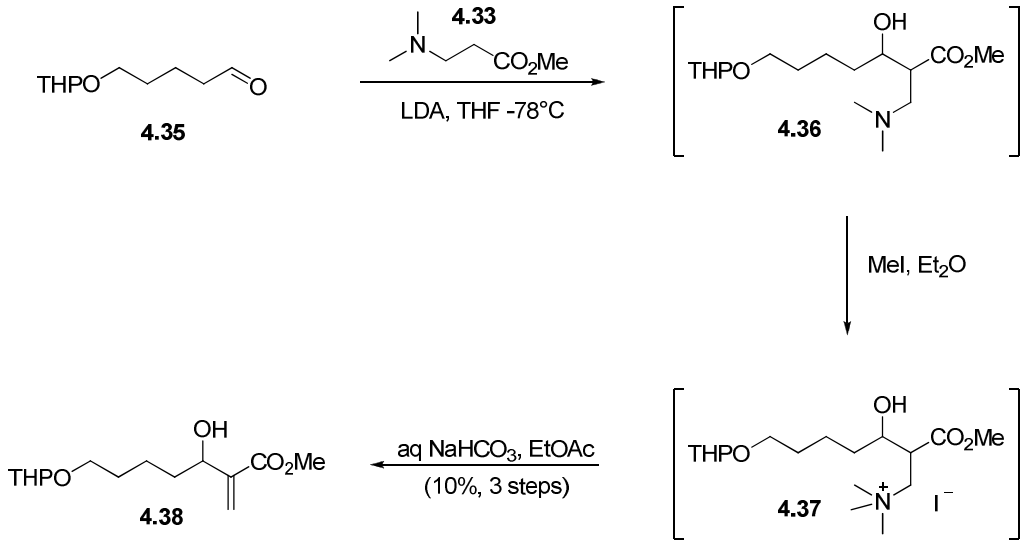

Figure 4.40: Synthesis of acrylate 4.38 using a masked alkene approach

Although the yields of acrylate 4.38 were low, they proved the validity of a masked alkene approach to these compounds, and signalled the need for a masked alkene that could be unmasked under milder conditions.

Sulfoxides undergo thermal elimination to form alkenes at high temperatures, or by treatment with alkoxide bases at lower temperatures.[158] While we felt these conditions would be too aggressive for our sensitive system, they alerted us to the fact that aryl selenoxides also undergo thermal elimination, but under much milder conditions than their sulfur analogues (Figure 4.41).[159] This difference in reactivity has been attributed to the greater basic character of the selenoxide oxygen atom.[159]

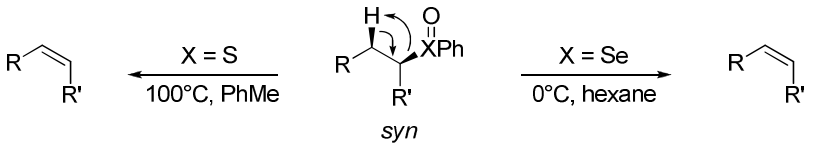

Figure 4.41: The difference in reactivity between sulfoxides and selenoxides, from Jones *et al*[159]

A very recent report has detailed the use of selenoxides to access acrylates substituted at the β-position,[148] and although β-substituted acrylates are less prone to polymerisation than unsubstituted acrylates, we felt a similar method could work for our system.

The required selenium masked acrylate 4.39 was prepared by treatment of racemic ethyl 2-bromopropionate with sodium phenylselenide; itself freshly prepared by reductive cleavage of diphenyl diselenide (Figure 4.42).[160]

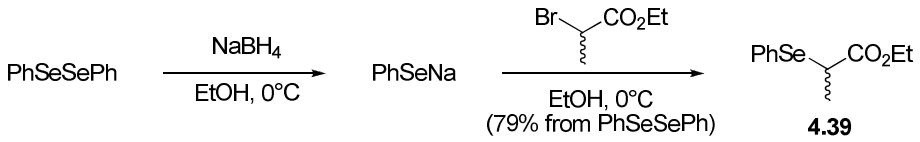

Figure 4.42: Preparation of the selenium masked acrylate 4.39

Treatment of the lithium enolate of selenide 4.39 with aldehyde 4.30 (*vide supra*) gave a good yield of the diasteromeric selenides, as a separable mixture of *syn* and *anti* adducts (Figure 4.43). The assignment of relative stereochemistry of the two centres is based on comparison of the ^{13}C NMR spectra of these compounds with reported spectra of similar compounds with known relative stereochemistry, in the *anti* adduct the shifts of the carboxyl, methyl and alcohol carbons are all shifted downfield relative to the *syn* adduct.[161]

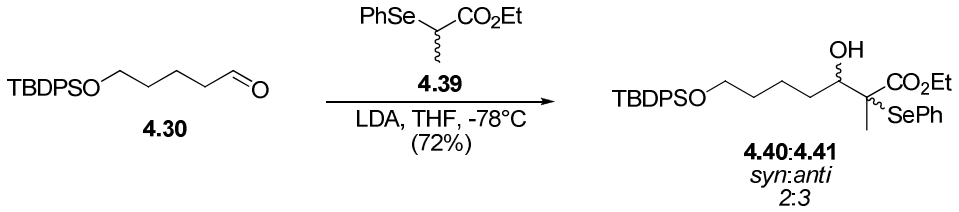

Figure 4.43: Production of the masked acrylates 4.40 and 4.41

The stereochemical outcome of this reaction can be rationalised by considering the stereochemistry of the enolates formed. Using the Ireland model, it can be seen that the transition states leading to both the (*E*) and (*Z*)-enolates experience destabilising 1,3-diaxial interactions, but the transition state leading to the (*E*)-enolate has a larger steric clash between the bulky phenylselenide group and an isopropyl group of LDA (Figure 4.44).[162]

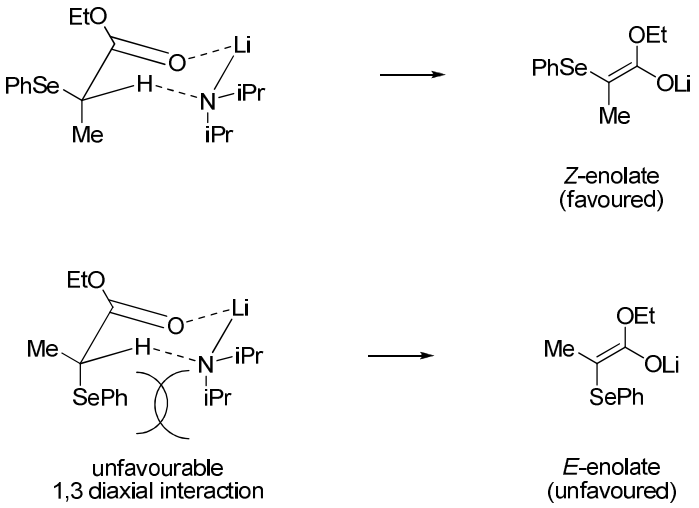

Figure 4.44: Interactions in the transition states leading to the enolates of selenide 4.39

This will result in a larger proportion of the (*Z*)-enolate being formed under the reaction conditions. This difference in enolate proportions is carried through the enolate addition, resulting in a larger proportion of the *anti* adduct (
Figure 4.45).

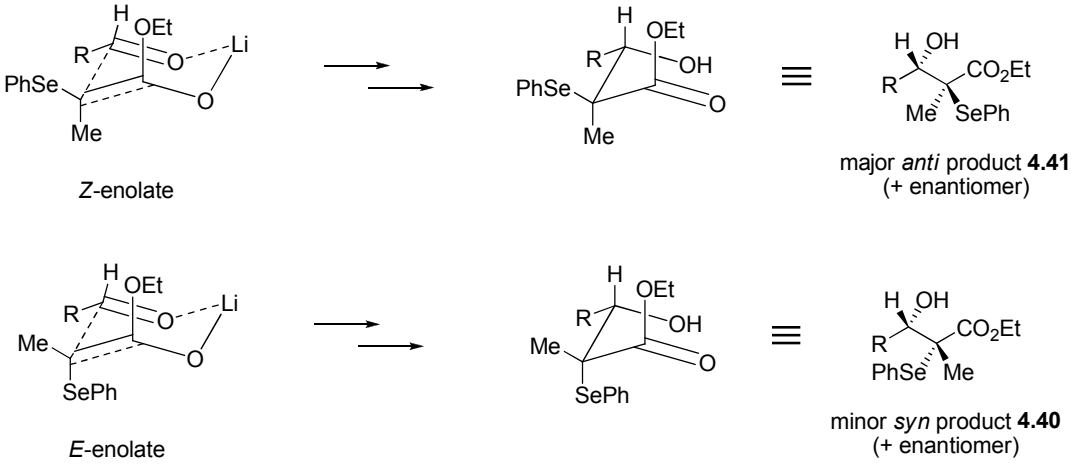

Figure 4.45: The outcome of the enolate addition for (*E*) and (*Z*) enolates of 4.39

Both the *syn* 4.40 and *anti* 4.41 aldol products cleanly underwent elimination to the desired acrylate 4.42 upon oxidation to the corresponding selenoxide with aqueous hydrogen peroxide (Figure 4.46). The mild conditions of this elimination can be attested by the excellent yield of these sensitive compounds. The difference in yield in these reactions is probably attributable to differences in scale rather than differences

in reactivity, in each case a single product was observed after removal of the phenylselenoic acid by aqueous extraction.

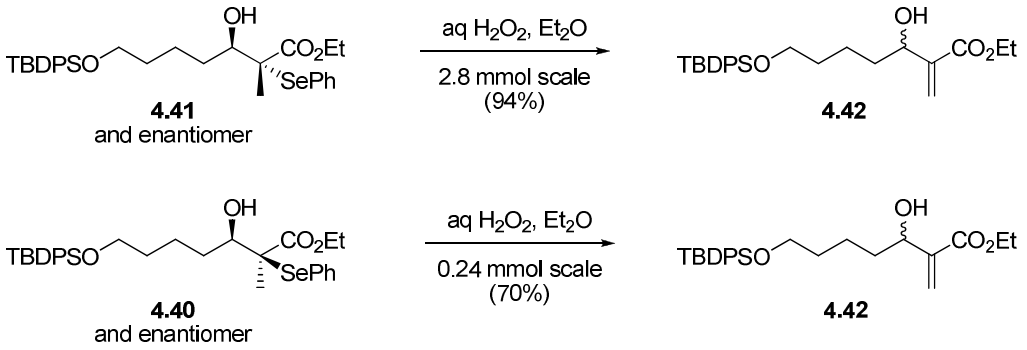

Figure 4.46: One-pot oxidation/elimination of selenides 4.40 and 4.41 to reveal acrylate 4.42

In principle the selenoxide formed by oxidation of 4.40 and 4.41 could eliminate to give the desired acrylate 4.42, or alternatively across the C2-C3 bond, to give the enolate 4.43 (Figure 4.47). The failure to observe any products derived from 4.43 in this reaction can be attributed to a kinetic effect, as the rate of elimination of selenoxides has been shown to be strongly dependent on the pattern of substitution on the β-carbon (Figure 4.47).[163] In our case, the undesired C2-C3 elimination would be slowed both by alkyl substitution and by the presence of an oxygen atom at C3.

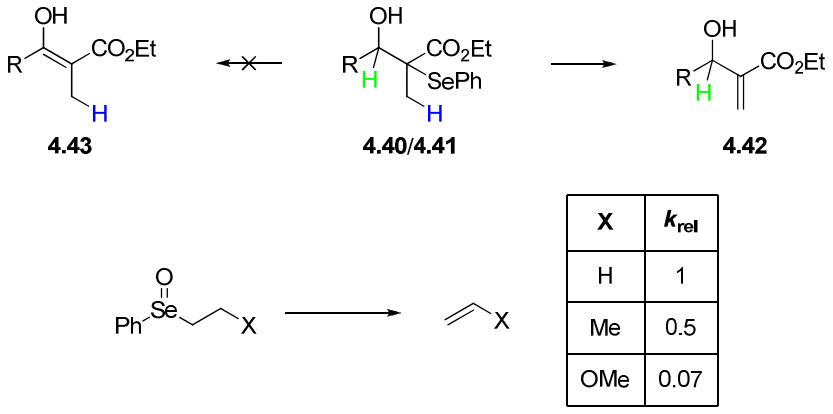

X	k_{rel}
H	1
Me	0.5
OMe	0.07

Figure 4.47: Possible selenoxide elimination routes, and literature rates of selenoxide elimination. Kinetic data from Reich *et al*[163]

With the desired allylic alcohol 4.42 in hand, work could begin on the key addition/elimination sequence. Treatment of alcohol 4.42 with cold acetyl chloride and pyridine gave acetate 4.44 in excellent yield (

Figure 4.48).

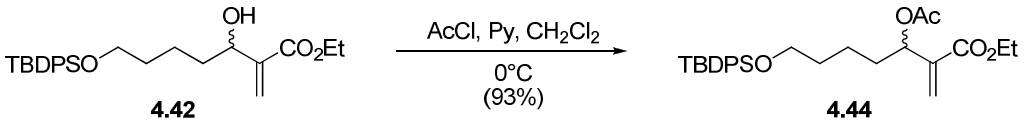

Figure 4.48: Acetylation of alcohol 4.42

Heating the acetate 4.44 in neat triethylphosphite in a Carius tube induced the planned addition/elimination/dealkylation sequence[143], to give the required allylic phosphonate 4.45 in excellent yield (
Figure 4.49).

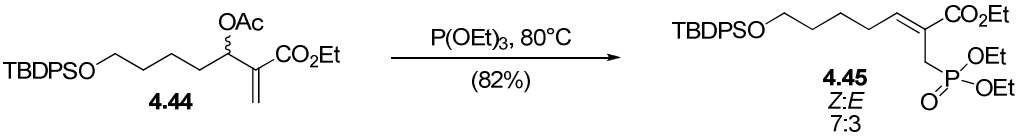

Figure 4.49: Production of allylic phosphonate 4.45

The phosphonate 4.45 was obtained as a chromatographically inseparable mixture of (*Z*) and (*E*) isomers, in a ratio of 7:3 as determined by ^{1}H and ^{31}P NMR spectroscopy. As the optimum geometry of the final product was unknown, the mixture of diastereomers was carried through the remainder of the synthesis.

The stereochemistries of the alkenes in 4.45 were determined by ^{1}H NMR NOESY experiments. Irradiation of the alkene protons in the major and minor products (red and green in Figure 4.50) showed that only the minor product gave a NOE with the methylene phosphonate hydrogens (blue). In addition, irradiation of the methylene phosphonate hydrogens produced only one NOE with the alkene protons, to the alkenyl proton in the minor product. Based on this data, the distance between the methylene phosphonate protons in the minor product must be shorter than that in the major product, hence the assignment of the minor and major isomers of 4.45 as (*E*)- and (*Z*)-alkenes respectively (Figure 4.50).

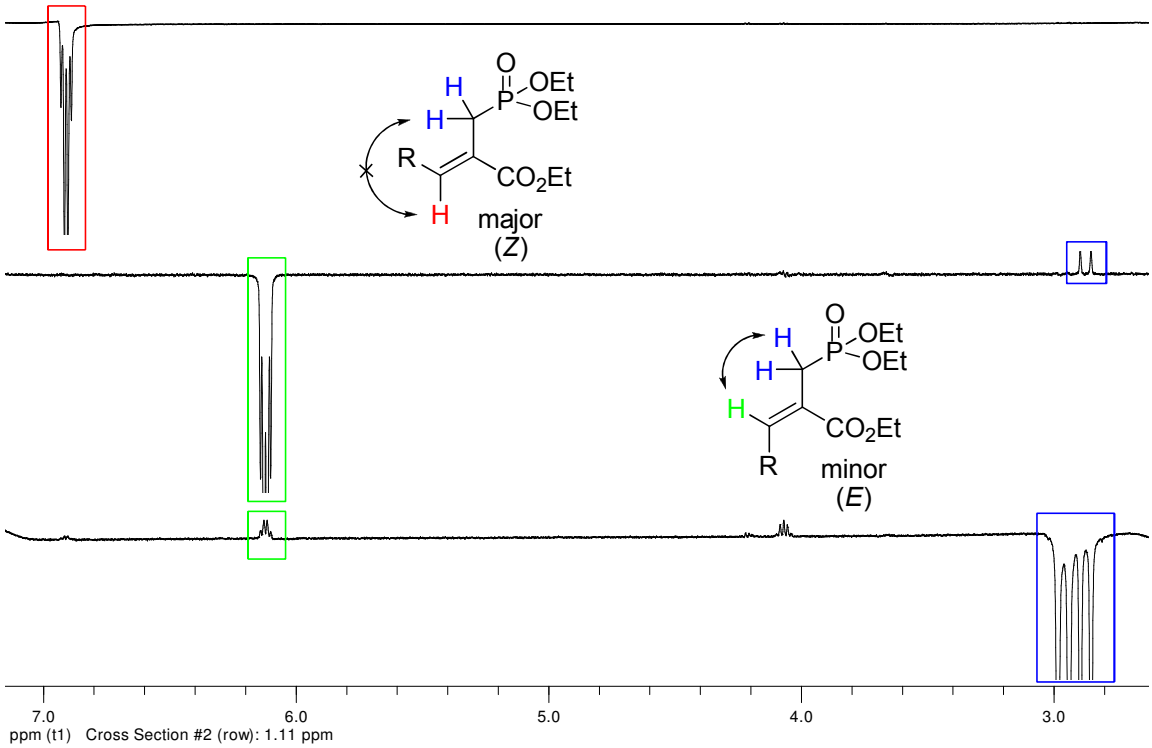

Figure 4.50: 1D NOESY data for allylic phosphonate 4.45

This moderate stereoselectivity of the reaction for the (*Z*)-isomer is in accordance with other observations reported in the literature. While an explanation of the stereoselectivity was not given by the original discoverers of this reaction, the stereoselectivity can be explained by considering the intermediates in the reaction (Figure 4.51).

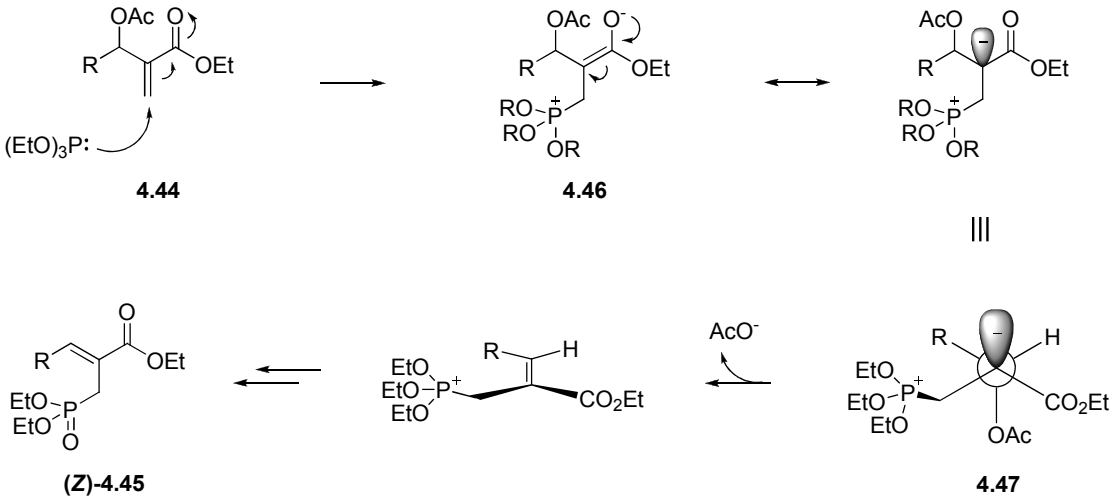

Figure 4.51: Origin of the stereoselectivity in the phosphonate formation reaction

After addition of the phosphite to alkene 4.44 (Figure 4.51), the zwitterionic phosphonium enolate 4.46 is formed, which can be considered to have significant carbanion character at C2. This carbanion is likely to adopt an antiperiplanar conformation with respect to the acetate leaving group during elimination, and could adopt the staggered conformation 4.47. This conformation minimises the steric interaction between the ester group and the alkyl tail R, and subsequent $E1_{cb}$ *anti* elimination and Arbusov-like phosphonium dealkylation gives the major (*Z*)-phosphonate.

The ester carbon in 4.47 is bulkier than the carbon that bears the phosphonium ion, but the distant bulk of the phosphonium group is reflected in the moderate stereoselectivity of the reaction. This model for the observed stereoselectivity is supported by evidence from the original publication of this reaction (Figure 4.52).[143] Replacement of the ester group with a cyano group reverses the stereoselectivity of the reaction, which can be explained by the loss of the ester-R group steric interaction. The use of bulky aryl R groups leads to greater stereoselectivity than simple propyl or hexyl alkyl groups, and the stereoselectivity is only slightly effected by changing the distant aryl *para* substituent from an electron-withdrawing chloride to electron-donating methoxy group; indicating the increased stereoselectivity observed with aryl R groups is primarily steric in origin. No variation in the phosphite or carboxylate ester groups is reported in the paper, however by the model presented here larger carboxylate ester groups combined with smaller phosphite ester groups would be likely to result in increased (*Z*) selectivity.

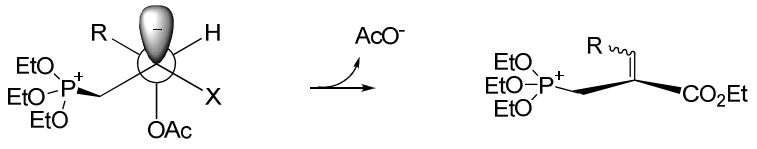

X = CO_2R' (*Z*)-selective
X = CN' (*E*)-selective

for X = CO_2R':

R = 1° alkyl - 7:3 (*Z*)-selectivity
R = aryl - 9:1 (*Z*)-selectivity

Figure 4.52: Literature examples of the phosphonate formation reaction, showing variation in stereochemical outcome with variation of the R and X groups [143]

With the key phosphonate formation complete, the distal phosphate needed to be introduced. Deprotection of the TBDPS group was readily achieved with tetrabutylammonium fluoride (TBAF), giving alcohol 4.48 in excellent yield (Figure 4.53).

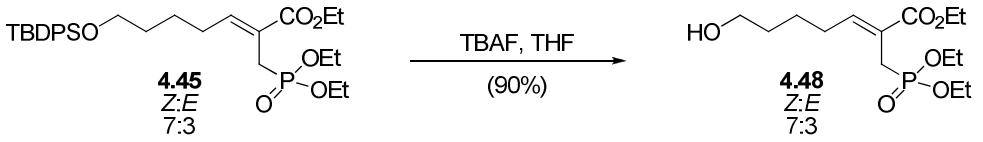

Figure 4.53: Deprotection of silyl ether 4.45 with TBAF

Phosphorylation of this alcohol with diethyl chlorophosphate in the presence of DMAP gave the phosphate ester 4.49 in excellent yield (Figure 4.54).

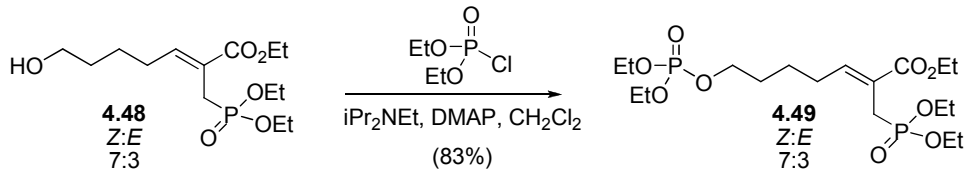

Figure 4.54: Phosphorylation of alcohol 4.48

Treatment of the hexaester 4.48 with trimethylsilyl bromide to remove the phosphate and phosphonate ester groups, followed by treatment with aqueous potassium hydroxide to simultaneously remove the resulting silyl ester groups and the carboxylate ester gave a mixture of products, which after separation by anion exchange chromatography and counter-ion exchange with Dowex-50X8 H^+-form and potassium hydroxide gave the desired target 4.3 in low yield (
Figure 4.55).

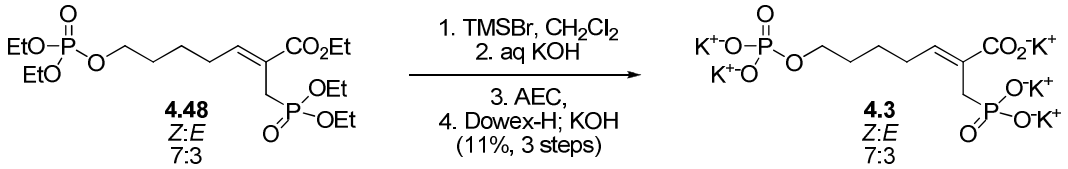

Figure 4.55: Final deprotection to give target 4.3

The yield was low presumably due to poor chemoselectivity in the phosphate deprotection step; however the route was able to provide sufficient quantities of putative inhibitor 4.3 for measurement of its inhibitory properties against DAH7P synthase by enzyme kinetic assay.

4.5 Inhibition properties of allylic phosphonate 4.3

The inhibition properties of allylic phosphonate 4.3 were analysed against *E. coli* DAH7P synthase, by the method described in Chapter Six. Initial results showed that phosphonate 4.3 was an inhibitor of DAH7P synthase. Detailed analysis showed that phosphonate 4.3 is a competitive inhibitor with respect to PEP, as evidenced by a Lineweaver-Burk transformation of the initial rate data. Global non-linear regression fitting of the initial rate data to the Michaelis-Menten equation, modified to include the presence of a competitive inhibitor, showed that allylic phosphonate 4.3 inhibits DAH7P synthase with an inhibition constant K_i of 154 ± 20 μM (Figure 4.57).

This inhibition constant is a considerable improvement over that known for the parent PEP-mimicking portion 3.10, validating and demonstrating the advantages of a multivalent approach to DAH7P synthase inhibition (Figure 4.56).

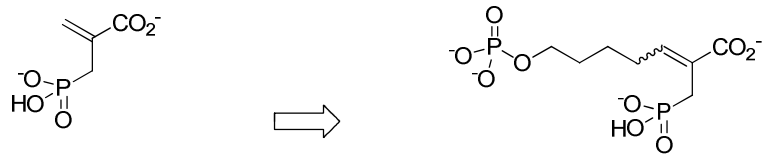

3.10
K_i: 270 ± 50 μM
(*E. coli*)

4.3
K_i: 154 ± 20 μM
(*E. coli*)

Figure 4.56: A comparison of parent compound3.10 and the improved multivalent inhibitor 4.3[94]

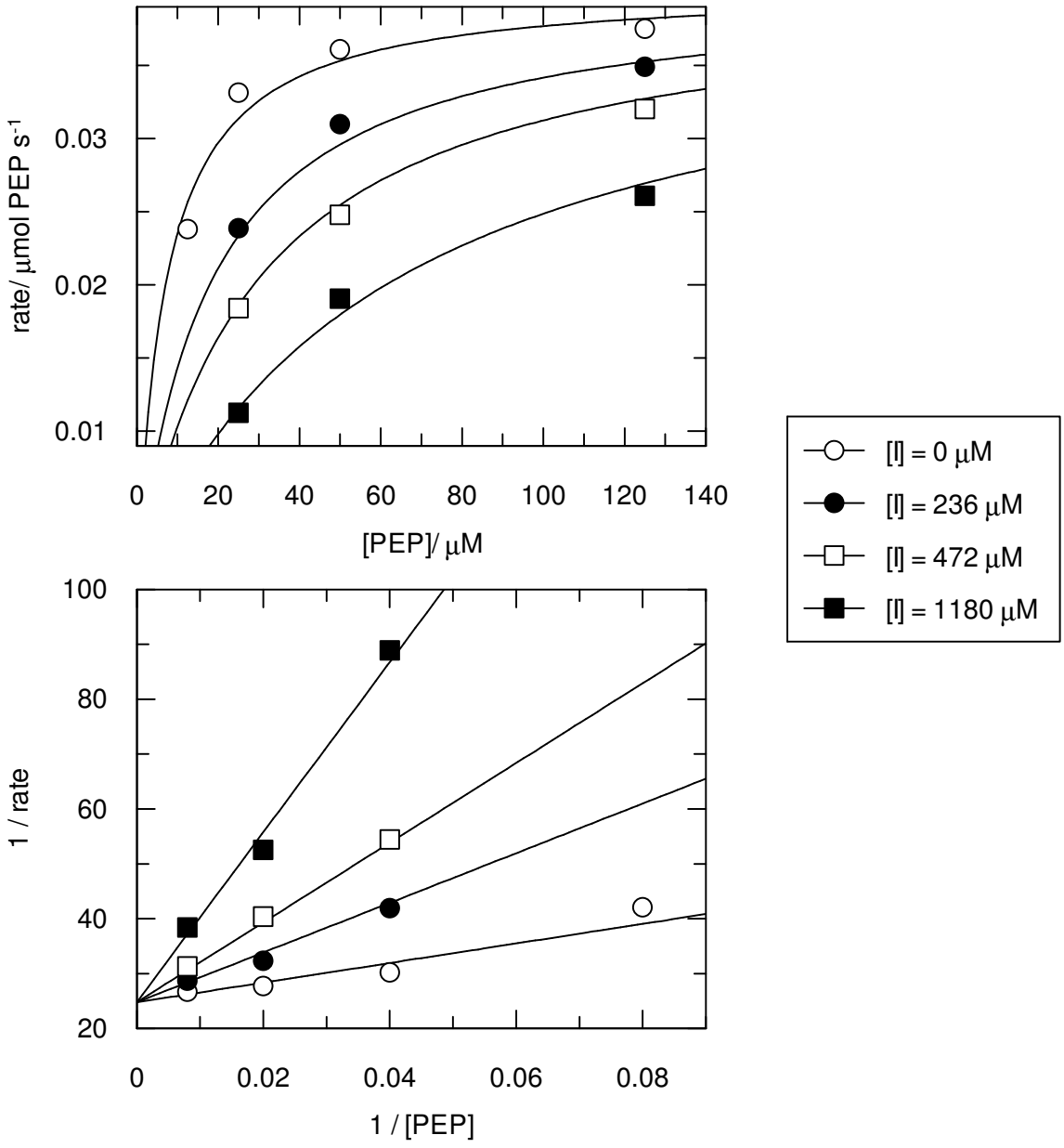

Figure 4.57: Inhibition properties of allylic phosphonate 4.3; presented as both Michaelis-Menten (top) and Lineweaver-Burk (bottom) plots. Solutions of PEP (10-120 µM), manganese(II) sulfate (100 µM), E4P (200 µM) and allylic phosphonate 4.3 (0-1180 µM) in 1 mL of BTP buffer (50 mM, pH 6.8) were initiated by the addition of *E. coli* DAH7P synthase (2 µg), and the loss of PEP followed spectrophotometrically at 232 nm. Initial rates were obtained by linear least squares regression of the absorbance data, and converted to progress rates

4.6: Synthesis of vinyl phosphonate 4.4

In order to access the vinyl phosphonate 4.4 a similar disconnection to that used to prepare the parent PEP mimicking compound 3.12 was envisaged (Figure 4.58). This involved accessing the key vinyl phosphonate functionality through a Horner-Wittig-Emmons reaction of α-ketoester 4.50.

This disconnection required access to α-ketoester 4.50, which we envisaged preparing via the simultaneous alkyne double oxidation/ esterification chemistry of Li *et al.*[164] This chemistry has been used in the syntheses of several carbohydrate α-ketoacids including D-3-deoxy-*arabino*heptulosonate.[165, 166] The required bromoalkyne 4.51 could in turn be prepared by attack of an acetylene anion equivalent on a suitable electrophile, followed by introduction of the bromine atom. The advantage of introducing the alkyne unit as a two-carbon unit by a nucleophilic substitution, as opposed to adding one carbon with a transformation such as the Corey-Fuchs reaction, is that the chemistry should also be applicable to derivatives of D-arabinose, allowing more complex derivatives bearing chiral hydroxyl groups to be prepared at a later stage.

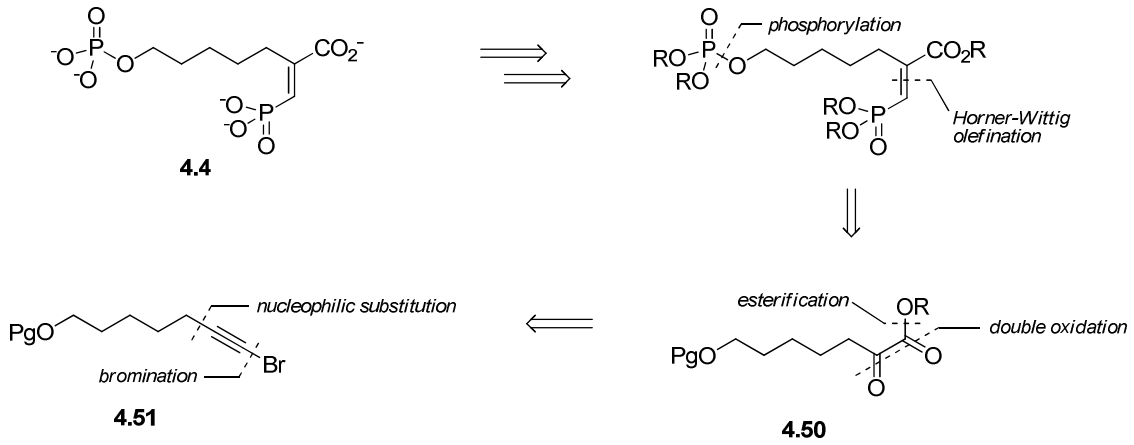

Figure 4.58: Initial retrosynthesis of vinyl phosphonate 4.4

The synthesis began with the preparation of a suitable electrophile for alkynylation; to this end bromide 4.52 was prepared by selective monobromination[167] of 1,5-pentanediol followed by protection of the remaining hydroxyl group as its TBDPS

ether (Figure 4.59). The modest yield of these steps is probably due to the facile ring closure of the intermediate bromoalcohol to volatile tetrahydropyran.

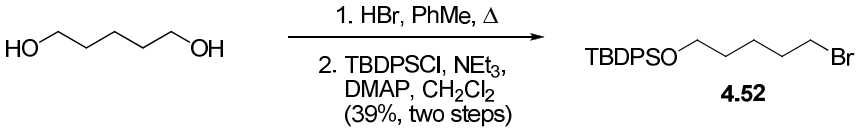

Figure 4.59: Bromination and protection of pentanediol to give bromide 4.52

Treatment of bromide 4.52 with lithium acetylide ethylene diamine complex by the method of Romeril *et al*[168] returned a moderate yield of the desired alkyne 4.53 (Figure 4.60).

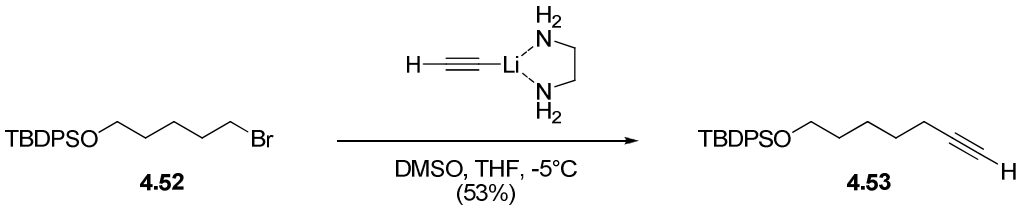

Figure 4.60: Nucleophilic alkynylation to give alkyne 4.53

Treatment of this alkyne with *N*-bromosuccinimide in the dark with catalytic silver(I) acetate gave a high yield of the 1-bromoalkyne 4.54 (Figure 4.61).

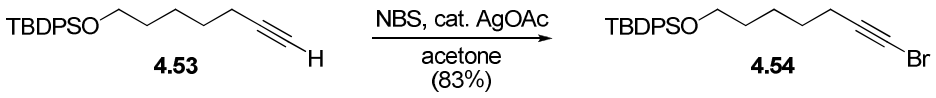

Figure 4.61: Bromination of 4.53 via the corresponding silver acetylide

Treatment of bromoalkyne 4.54 under the double oxidation conditions of Li[164], namely potassium permanganate in buffered aqueous methanol, did not give rise to a significant amount of the expected ketoester. However, a thick film of material was noted on the inside of the reaction flask. It was presumed that this film indicated the solubility of bromoalkyne 4.54 in the reaction media was low. This is consistent with the literature, as the reported examples of this double oxidation involve protected polyol fragments derived from carbohydrates (Figure 4.62). These compounds are likely to have a much larger solubility in the cold aqueous reaction media than a hydrocarbon such as 4.54.

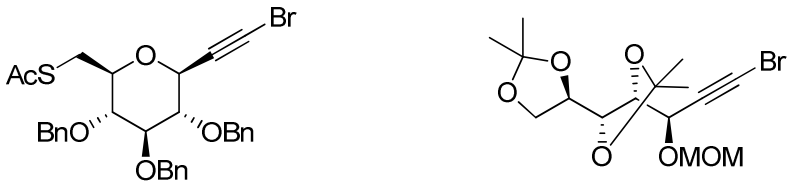

Figure 4.62: Typical known substrates for the double oxidation reaction[169, 170]

Based on these observations, co-solvents were screened to improve the solubility of bromoalkyne 4.54 while maintaining a homogenous reaction mixture. The addition of ethyl acetate to the reaction mixture was successful in producing a low yield of the desired ketoester 4.54 (Figure 4.63).

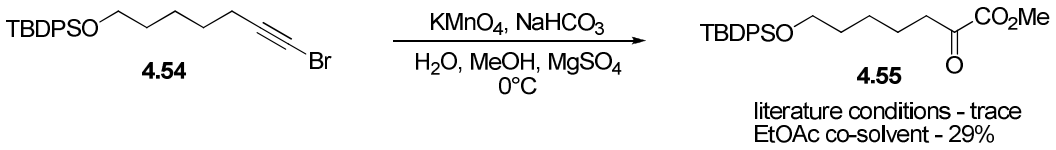

Figure 4.63: Double oxidation of bromoalkyne 4.53 to α-ketoester 4.54

While these conditions were successful in producing small quantities of the desired ester, given the number of possible side reactions (oxidative cleavage of the ketoester, oxidation of methanol, interception of the acyl halide intermediate by water), it was felt that further deviation from the presumably optimised conditions of Li would be a process fraught with difficulty. Given the moderate yields of the steps in this synthesis, other options were investigated.

The selective addition of Grignard reagents to oxalate esters at low temperatures has been reported to give rise to α-ketoesters (Figure 4.64);[171] the intermediate magnesium alkoxide is stabilised by intramolecular coordination at the temperature of the reaction, and slows the double addition typically seen with esters. A model Grignard reagent was prepared; and after a number of attempts to optimise the selective monoaddition a moderate yield of α-ketoester was obtained (Figure 4.64). However these results were unable to be extended to bromide 4.52, as the requisite Grignard reagent 4.56 was unable to be formed from bromide 4.52 by standard techniques. It is of note that despite the general utility of such a Grignard reagent, its preparation remains unreported.

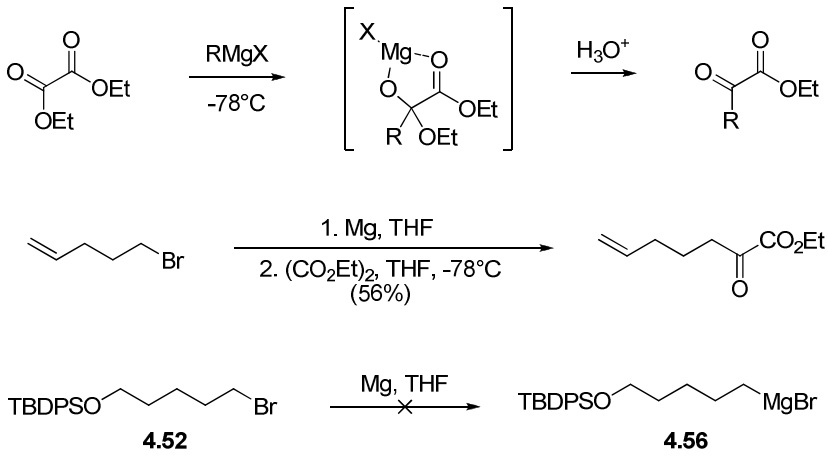

Figure 4.64: Grignard route to α-ketoesters

With the failure of this route, other approaches were investigated. The rearrangement of α-chloroglycidic esters to β-halo-α-ketoesters is another approach reported to provide the α-ketoester framework; and the corresponding β-iodo compounds can be readily reduced back to the α-ketoester.[172] The required α-chloroglycidic esters can be prepared by two carbon elongation of aldehydes, in a modified Darzens condensation.[173]

This approach seemed promising for a number of reasons. The required hydrocarbon aldehydes are not only readily prepared, but the corresponding D-*arabino*polyol aldehyde is accessible via the chemistry developed in Chapter Two. Furthermore, α-chloroglycidic esters are versatile synthetic intermediates, and can be converted directly to other functionality of interest (Figure 4.65) such as enol phosphates and α-hydroxyesters, and many other arrangements are possible by transformation of the derived β-halo-α-ketoesters.[174, 175] This should allow ready adaptation of the synthesis to the production of structurally diverse inhibitors.

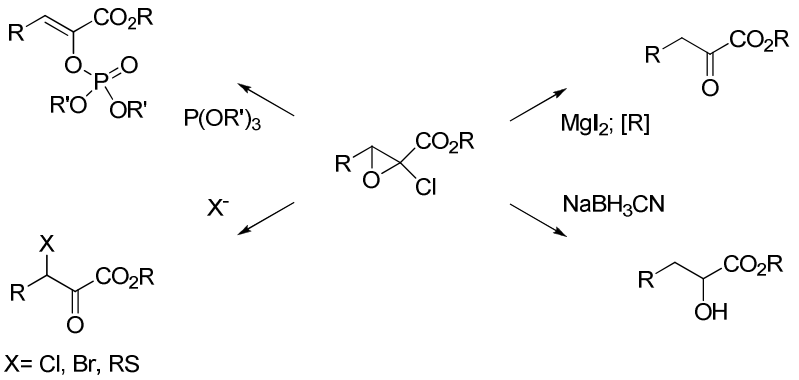

Figure 4.65: Known conversions of α-chloroglycidic esters to enol phosphates,[174] β-halo-α-ketoesters,[173] α-hydroxyesters,[175] and α-ketoesters[172]

The Darzens reaction precursor 4.57 was readily prepared by esterification of dichloroacetic acid, on a large scale. The isopropyl ester was selected due to its success in similar reported applications in the literature[173].

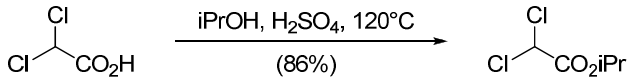

Figure 4. 66: Production of Darzens precursor 4.57

Treatment of a mixture of aldehyde 4.30 (*vide supra*) and dichloroester 4.57 with potassium isopropoxide in ether gave the desired α-chloroglycidic ester 4.58 after aqueous workup. Due to concerns about the stability of α-chloroglycidic ester 4.58, it was not purified further but treated immediately with freshly prepared magnesium iodide at low temperature; a reductive workup with commercial aqueous sodium hydrogen sulfite afforded the desired α-ketoester 4.59 in a low yield after flash chromatography (

Figure 4.67).

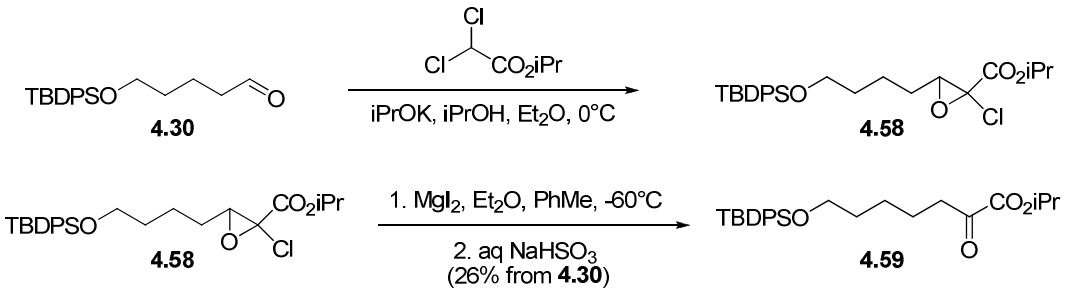

Figure 4.67: Synthesis of α-ketoester 4.59 via a modified Darzens condensation

The low yield of the Darzens sequence was disappointing. However, it should be noted the yield is similar or better than that obtained by our other routes, and this route incorporates the carbon-carbon bond formation and the α-ketoester into the same sequence. The entire transformation from aldehyde 4.30 to α-ketoester 4.59 (including preparation of fresh magnesium iodide) can be carried out in one day.

Interestingly, the α-ketoester 4.59 in chloroform contains ~20% of the corresponding enol tautomer, a comparatively large portion when compared with a typical ketone such as acetone.[158] Similar behaviour for other α-ketoesters has been reported, but no evidence was presented.[173] It is conceivable that in these cases the enol tautomer is stabilised by conjugation of the enol alkene with the ester group.

In our case, the identity of this species as the enolate was initially presumed based on the chemical shift of the vinyl proton; and is supported by its associated ^{13}C shift and phase obtained from a combined heteronuclear single quantum coherence – distortionless enhancement by polarisation transfer (HSQC-DEPT) experiment, as well as in the selective total correlation spectroscopy (selTOCSY) spectrum shown in Figure 4.68.

In this experiment a selected resonance is irradiated, and after a mixing period the spectrum is measured. The resulting spectrum shows only protons which can be excited by magnetisation transfer from the irradiated proton, and transfer is limited to protons within the same spin system. In the selTOCSY spectrum in Figure 4.68, the enol vinyl proton (red) has been irradiated, and strong spin transfer to the neighbouring allylic protons (green) can be seen. In addition, a weak transfer giving a signal at δ 2.8 ppm can be observed. This signal is due to the α-methylene protons (blue) of ketone 4.59, and arises due to equilibration between the keto and enol forms of 4.59 on the NMR timescale, resulting in an apparent intermolecular magnetisation transfer.

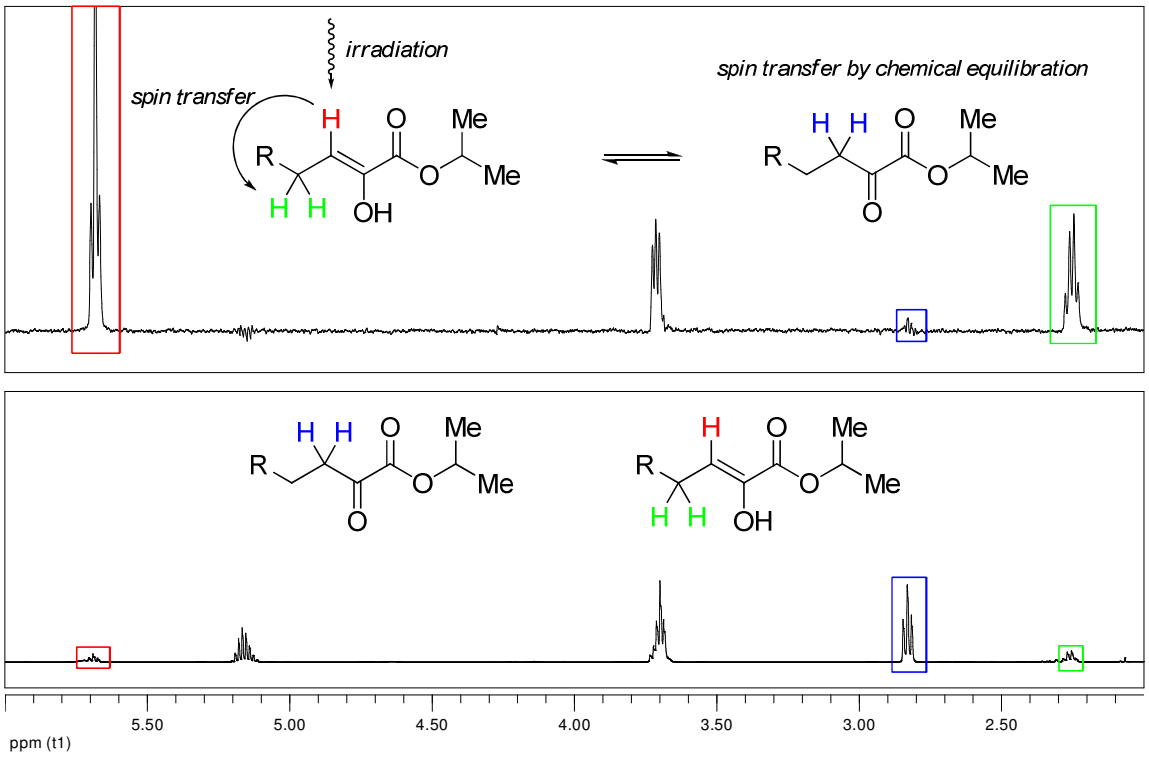

Figure 4.68: selTOCSY (top) and standard ^{1}H (bottom) NMR spectra for purified ketoester 4.59

With the α-ketoester 4.59 in hand, work could begin on the Horner-Wittig-Emmons (HWE) reaction to install the vinyl phosphonate. From the work in Chapter Three, it was apparent that the stereochemical outcome of this reaction was sensitive to the counterion of the stabilised phosphonate carbanion. Investigations with α-ketoester 4.59 showed the same phenomenon (Figure 4.69), lithium counterions tended to promote the formation of the desired (*E*)-isomer 4.60; while the larger sodium counterion gave mixtures enriched in the undesired (*Z*)-isomer 4.61. With LDA as a base, quenching at -78°C gave little product, long reaction times at room temperature gave increased amounts of undesired (*Z*)-isomer 4.61, but a short period at room temperature gave good selectivity. A caveat is an associated decrease in overall yield, although these reactions were conducted on a small scale so changes in yield on a larger scale may be much less than indicated by these results (Figure 4.69). The overall low yields may be due to trapping of the ketone as its enol tautomer, due to previously observed facile tautomerisation of α-ketoester 4.59.

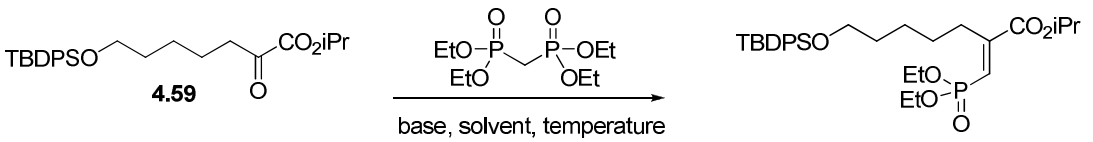

conditions	scale	yield	*E*:*Z*
NaHMDS, THF, DME, 0°C*	2.15 mmol	54%	1:2
LDA, THF, -78°C	0.5 mmol	trace	-
LDA, THF, -78°C - 20°C, o/n	0.25 mmol	41%	1.5:1
LDA, THF, -78°C - 20°C, 2 hr	0.25 mmol	31%	8.2:1

*TBS protected

Figure 4.69: Effect of reaction conditions on the stereochemical course of the HWE reaction

The stereochemistry of the vinyl phosphonates was assigned by 1D transient nuclear Overhauser enhancement spectroscopy (NOESY). The 1D-NOESY spectra for the two seperated isomeric vinyl phosphonates are shown in Figure 4.70.

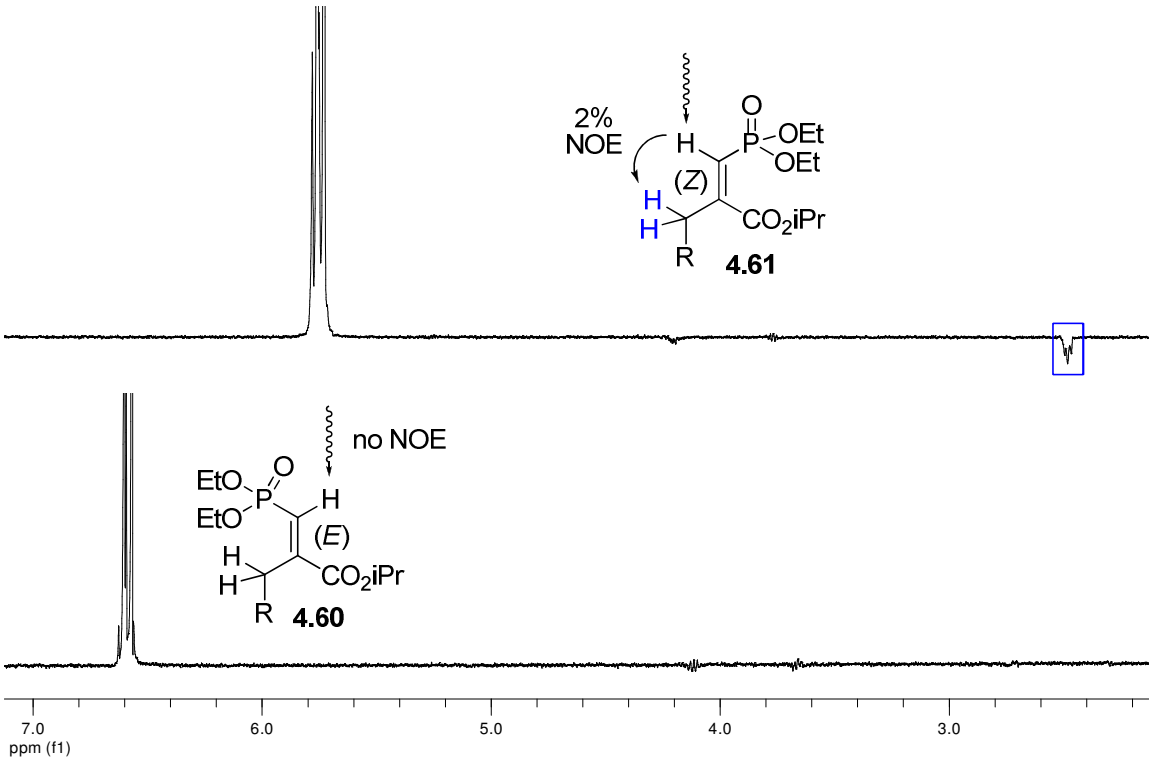

Figure 4.70: NOESY spectra for vinyl phosphonates 4.60 and 4.61

In each case, the vinyl hydrogen has been irradiated, and in the case of the undesired (*Z*)-isomer 4.61, a NOE is observed (blue) between the vinyl hydrogen and the allylic hydrogens, due to their presence on the same face of the double bond. In the desired (*E*)-isomer 4.60, under the same conditions no such NOE occurs, as the vinyl and

allylic hydrogens are fixed further apart. Of note is the shift of the vinyl hydrogen is strongly dependent on double bond geometry, a phenomenon that was also observed in the shorter analogue 3.12 (Chapter Three).

The origin of the stereoselectivity of these reactions has not been studied, however based on the known mechanism and stereoselectivity of the HWE reaction a possible model is shown in Figure 4.71.[96]

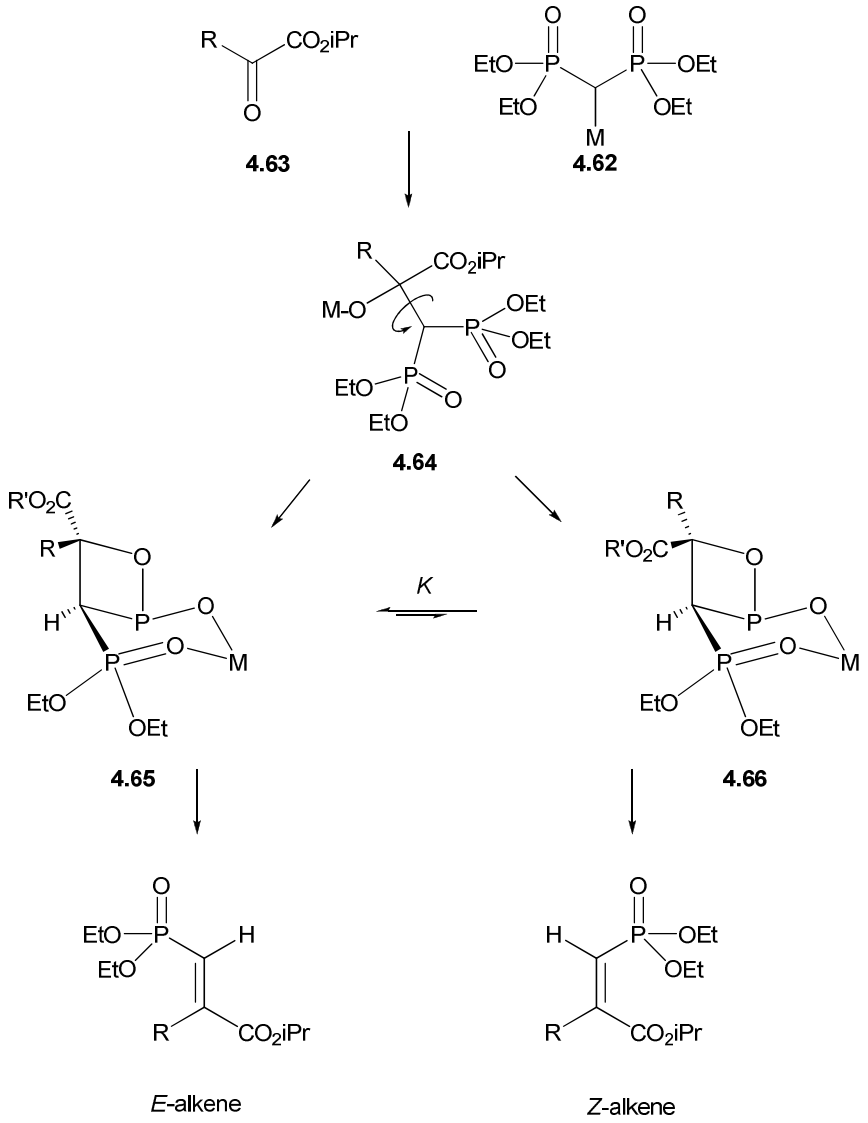

Figure 4.71: A model for the origin of the stereoselectivity in the HWE reaction

Initial attack of the stabilised carbanion 4.62, where M is a lithium or sodium atom, on the α-ketoester 4.63 gives the alkoxide 4.64, which can then undergo intramolecular nucleophilic attack at phosphorus to give rise to two possible

oxaphosphatanes 4.65 and 4.66, which can interconvert (substituents on the rear phosphonate are omitted for clarity). The oxaphosphetanes 4.65 and 4.66 lead to the (*E*)- and (*Z*)-configured product respectively. The oxaphosphetane 4.66 is raised in energy relative to 4.65, due to a steric clash between the isopropyl ester and the ethyl phosphoester groups. A lesser steric clash between the isopropyl ester and first carbon of the hydrocarbon chain exists in 4.65. This explains the observed temperature effect, as more thermal energy is removed from the system, the equilibrium will increasingly favour the lower energy oxephosphetane 4.66; subsequent elimination of diethyl phosphate results in a higher proportion of the (*E*)-configured product.

The differing stereoselectivities with different metal ions is also explained by this model. It is known from extensive studies of the aldol reaction, that the stereoselectivity of an aldol addition is dependent on enolate counterion. The aldol reaction proceeds through a cyclic six-membered transition state similar to that which has been proposed here for the HWE addition, and the origin of the counterion effect in the aldol reaction is attributed to the smaller metals having shorter metal-oxygen bond distances, which tighten the cyclic transition state.[176] In this case, the small ionic radius of lithium may also have this effect, by holding the cyclic intermediate more tightly and exacerbating the difference in energy of the two oxaphosphetane intermediates.

Treatment of the (*E*)-vinyl phosphonate 4.60 with TBAF in THF cleanly removed the TBDPS ether, giving the alcohol 4.67 in good yield (Figure 4.72).

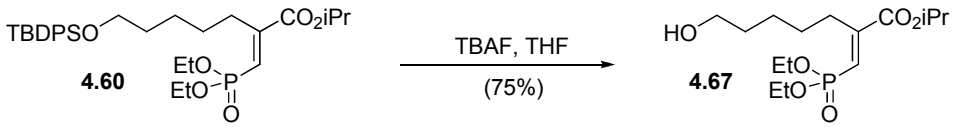

Figure 4.72: Deprotection of 4.60 with TBAF

Treatment of alcohol 4.67 with diethyl chlorophosphate and DMAP gave the phosphate ester 4.68 in excellent yield (
Figure 4.73).

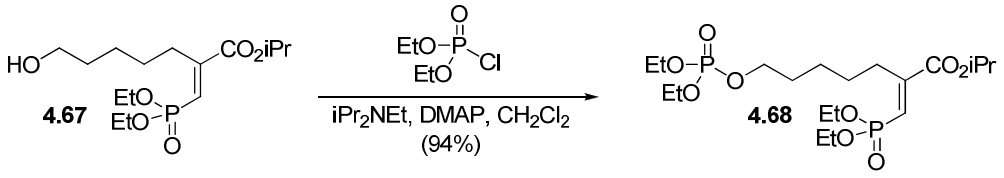

Figure 4.73: Phosphorylation of 4.67

Treatment of the ester 4.68 with trimethylsilyl bromide, followed by aqueous potassium hydroxide, anion-exchange chromatography and lyophilisation gave a small amount of white solid. Analysis of this solid by ^{1}H and ^{31}P NMR spectroscopy showed that it contained several vinyl phosphonate species. Resubjecting this material to careful anion-exchange chromatography gave the desired vinyl phosphonate 4.4, but as a 1:1 mixture of (*E*)- and (*Z*)-isomers (Figure 4.74).

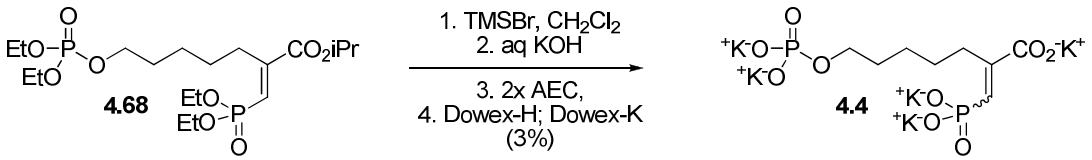

Figure 4.74: Deprotection of 4.68 to give vinyl phosphonate 4.4.

The reason for the isomerisation side reaction is unclear. Similar isomerisation was not observed in the preparation of the parent compound 3.12 (Chapter Three), which suggests that the distal phosphate is in some way responsible for the side reaction. Isolation of the bromide side product 4.69 (Figure 4.75), produced by non-chemoselective phosphate cleavage, showed that it was only in the (*E*)-configuration, which supports this hypothesis. The chemistry of similar compounds is relatively unexplored, and a search for related phenomena in the literature was unsuccessful.

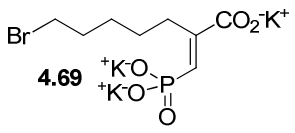

Figure 4.75: Bromide side product 4.69

One possible mechanism for the isomerisation reaction would be a reversible addition of the distal phosphate to the electron-deficient alkene in 4.4, to give phospholactone

4.70. This lactone could then ring open by elimination of phosphate, returning the alkene of 4.4 but as a mixture of stereoisomers (Figure 4. 76).

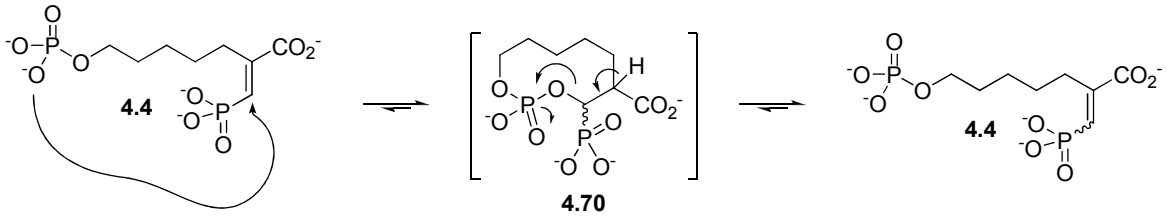

Figure 4. 76: A possible distal phosphate dependent mechanism for the isomerisation of 4.4

While the required medium-ring cyclisation might not normally be considered facile, it should be noted that only traces of phospholactone 4.70 need be formed in the reaction mixture in order for the isomerisation to proceed, as long as equilibration between open-chain 4.4 and phospholactone 4.70 is rapid.

Despite the disappointing yield of target 4.4 and its isomerisation, sufficient material was obtained by this route for characterisation of its inhibition properties against DAH7P synthase.

4.7 Inhibition properties of vinyl phosphonate 4.4 and related compounds

The inhibitory properties of vinyl phosphonate 4.4 were assayed against *E. coli* DAH7P synthase. Based on a Lineweaver-Burk analysis of the initial rate data, the inhibitor was determined to be competitive with respect to PEP (Figure 4.77). At higher concentrations of 4.4 the data deviated from an idealised Lineweaver-Burk plot. The reason for this deviation remains unclear, but may be due to added complications introduced by the bisubstrate nature of vinyl phosphonate 4.4, or by the mixture of (*E*)- and (*Z*)-isomers present. The inhibitor 4.4 was not found to be time-dependent in its action, with no significant difference in inhibition when the inhibitor was preincubated for times ranging from thirty seconds to thirty minutes.

Fitting of the initial rate data to the Michaelis-Menten equation (Figure 4.77) modified for competitive inhibition showed that vinyl phosphonate 4.4 was a potent inhibitor of DAH7P synthase; with an inhibition constant K_i of 5.3 ± 0.6 μM. This result is similar

to the unelaborated compound 3.12, however the unelaborated compound 3.12 consisted solely of the designed (*E*)-isomer, the corresponding (*Z*)-isomer is a much weaker inhibitor of DAH7P synthase.

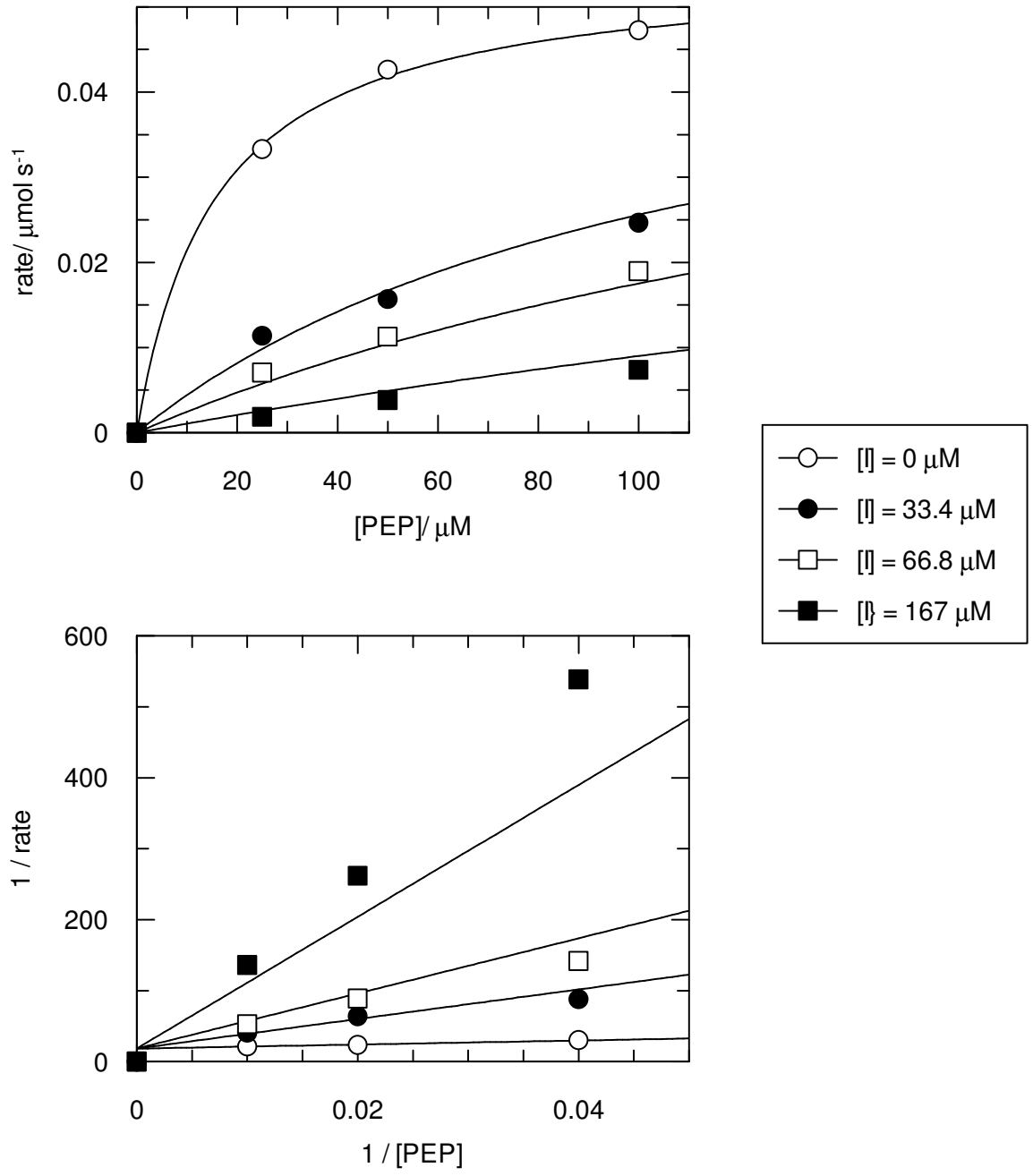

Figure 4.77: Inhibition properties of bisubstrate vinyl phosphonate 4.4 against *E. coli* DAH7P synthase. Solutions of PEP (25-100 µM), manganese(II) sulfate (100 µM), E4P (200 µM) and vinyl phosphonate 4.4 (0-167 µM) in 1 mL of BTP buffer (50 mM, pH 6.8) were initiated by the addition of *E. coli* DAH7P synthase (2 µg), and the loss of PEP followed spectrophotometrically at 232 nm. Initial rates were obtained by linear least squares regression of the absorbance data, and converted to progress rates

The undesired bromide 4.69, produced by non-regioselective dealkylation during the deprotection step was also evaluated as an inhibitor of *E. coli* DAH7P synthase. It too proved to be a potent inhibitor of *E. coli* DAH7P synthase, with a K_i of 3.6 ± 0.4 μM (Figure 4.78).

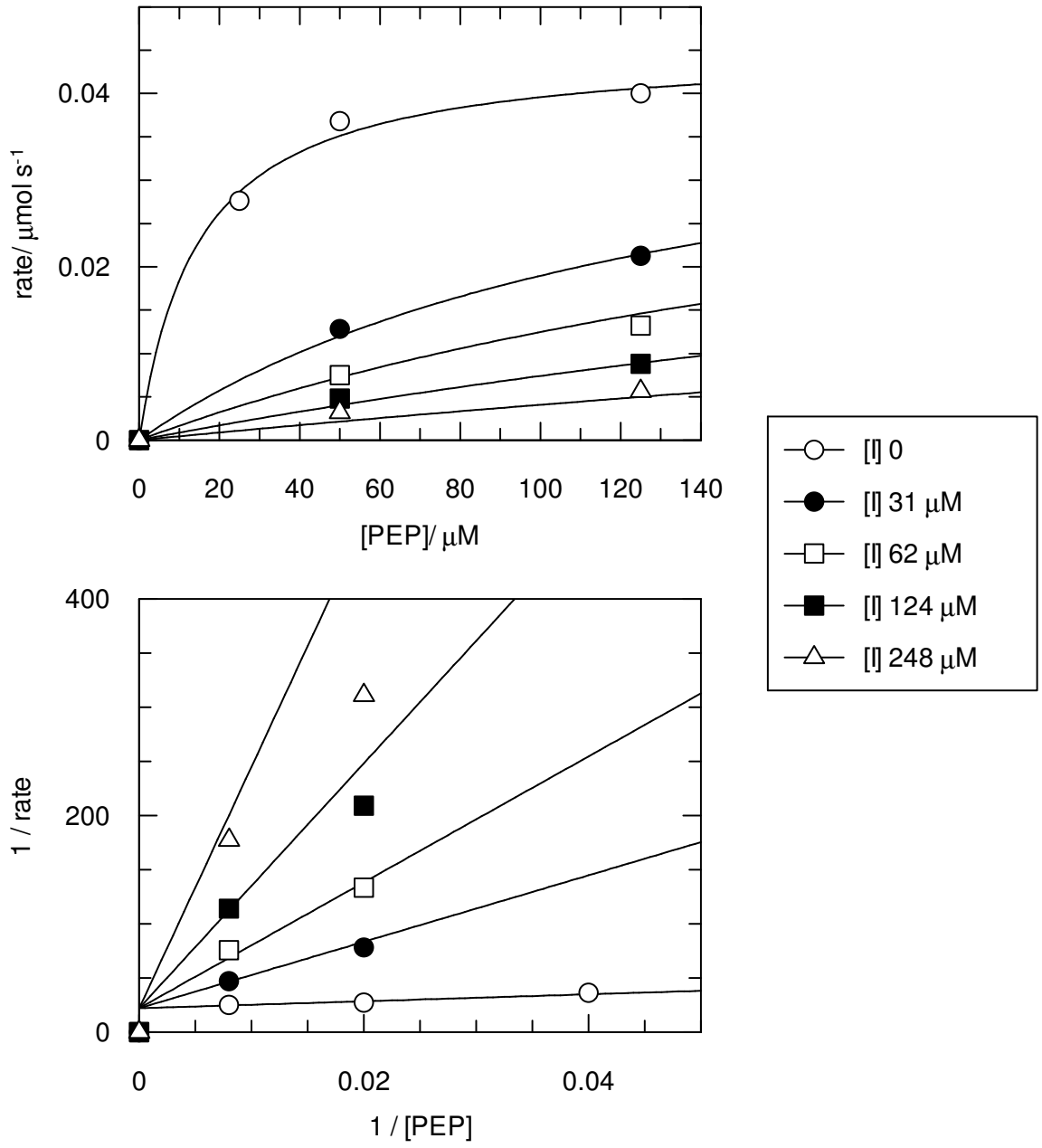

Figure 4.78: Bromide 4.69 as a DAH7P synthase inhibitor. Solutions of PEP (25-100 μM), manganese(II) sulfate (100 μM), E4P (200 μM) and bromide 4.69 (0-248 μM) in 1 mL of BTP buffer (50 mM, pH 6.8) were initiated by the addition of *E. coli* DAH7P synthase (2 μg), and the loss of PEP followed spectrophotometrically at 232 nm. Initial rates were obtained by linear least squares regression of the absorbance data, and converted to progress rates

The potency of bromide 4.69 was initially surprising, since it lacks the terminal phosphate group designed to enhance the binding of these compounds to DAH7P synthase. One possible explanation is the reaction of the bromide with a nucleophilic active site residue could anchor the compound in the active site, in a similar manner to a terminal phosphate.

In order to investigate this possibility, the interaction of bromide 4.69 with *E. coli* DAH7P synthase was investigated by time-course kinetic experiments. No significant time-dependence in the interaction of bromide 4.69 with DAH7P synthase was observed.

Based on these results, it appears the interaction of bromide 4.69 with DAH7P synthase is predominantly non-covalent in nature. In addition, the presence of a distal bromine atom appears to have little positive or negative influence on the binding affinity of bromide 4.69.

4.8 Summary

In this chapter the extension of small PEP-like molecules to larger molecules capable of interacting with both the enzymes PEP site and the E4P phosphate site was investigated. These inhibitors were proposed to be more potent that the isolated PEP-like portion, and indeed for allylic phosphonate 4.3 this hypothesis was found to be correct, with a considerable increase in potency on extension (Figure 4.79).

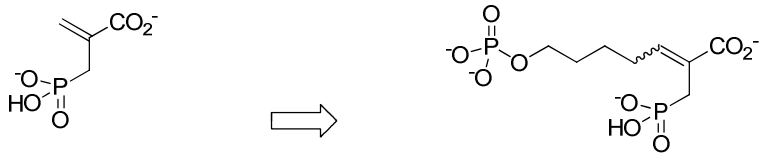

3.10
K_i: 270 ± 50 μM
(*E. coli*)

4.3
K_i: 154 ± 20 μM
(*E. coli*)

Figure 4.79: A comparison of PEP-like fragment 3.10 and bisubstrate inhibitor 4.3[94, 95]

The addition of a distal phosphate group was not sufficient to create strong inhibitors from molecules which do not strongly interact with the enzyme PEP site, as seen for acrylate 4.2 (Figure 4. 80).

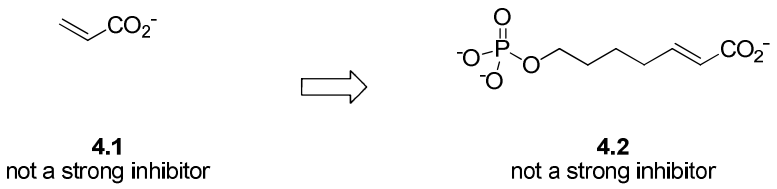

4.1
not a strong inhibitor

4.2
not a strong inhibitor

Figure 4. 80: Influence of the distal phosphate where the PEP end does not strongly bind to the PEP site

This result implies that the PEP-like portion of the molecule is the major contributor to the overall binding affinity of the bisubstrate molecules. This is again illustrated with the bromide 4.69, which has a similar inhibition constant to its parent compound 3.12 (Figure 4.81). This result also suggests that the hydrocarbon linker is not introducing any destabilising steric or hydrophobic effects to the enzyme-inhibitor interaction.

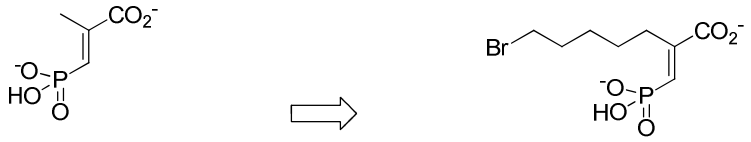

3.12
K_i: 4.7 ± 0.7 μM
(*E. coli*)

4.69
K_i: 3.6 ± 0.4 μM
(*E. coli*)

Figure 4.81: PEP-mimicking compound 3.12 and bromide 4.69

The study of the molecule bearing the most potent PEP-like portion was complicated by a previously unknown terminal phosphate dependent isomerisation. Despite this obstacle, characterisation of a 1:1 mixture of stereoisomers showed a similar inhibition constant to that for the unelaborated PEP-like compound 3.12 (Figure 4.82).

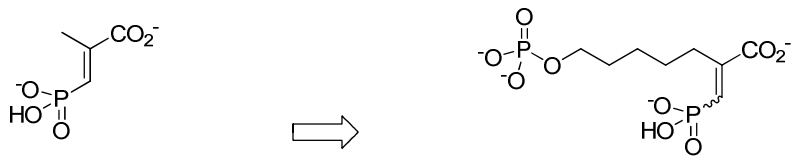

3.12
K_i: 4.7 ± 0.7 μM
(*E. coli*)

4.4
K_i: 5.3 ± 0.6 μM
(*E. coli*)

Figure 4.82: Similar inhibition constants displayed by parent (*E*)-phosphonate 3.12 and mixture 4.4

The behaviour of the isomeric mixture 4.4 indicates that the inhibition constant for the designed compound is likely to be in the low μM range. Assuming no contribution of any kind from the (*Z*)-isomer of 4.4 gives an inhibition constant of ~ 2.5 μM. Intriguingly, this improvement from 3.12 is similar to that observed upon extension of the allylic phosphonate 4.3, where a ~1.75-fold increase in binding is observed from the PEP-mimicking 3.10.

Chapter Five: Discussion, Modelling and Future Directions

5.1: Inhibition Results Summary

The aim of this project was to investigate the inhibition of DAH7P synthase. This aim has been achieved, with a number of new inhibitors of DAH7P synthase designed, synthesised and evaluated during the course of this project (Figure 5.1).

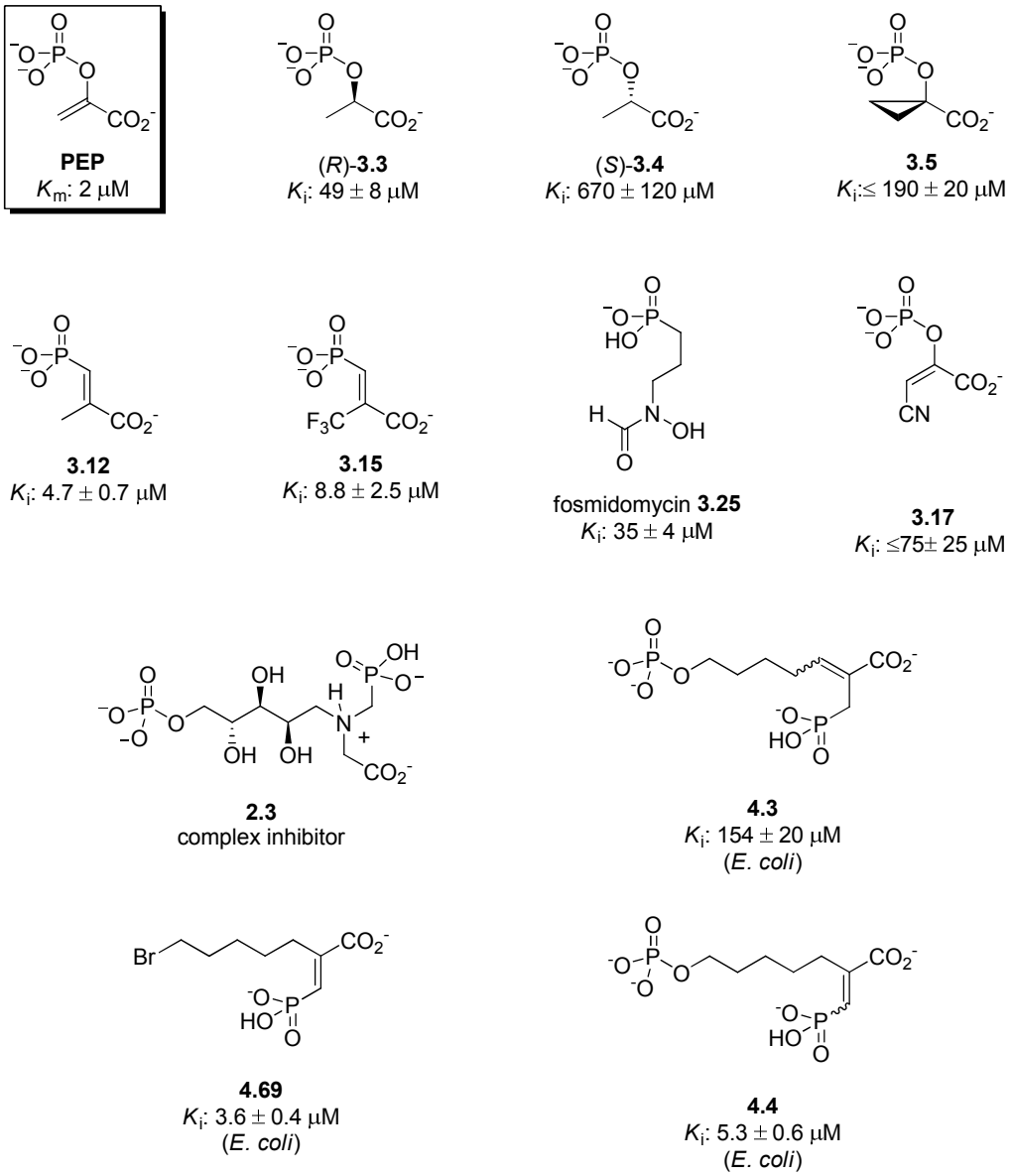

Figure 5.1: A summary of inhibitors of *E. coli* DAH7P synthase discovered during this project, compared to the structure of PEP

In addition to these inhibitors, a number of compounds have been shown that do not inhibit DAH7P synthase (Figure 5.2). These compounds also provide insights into the components necessary for DAH7P synthase inhibition.

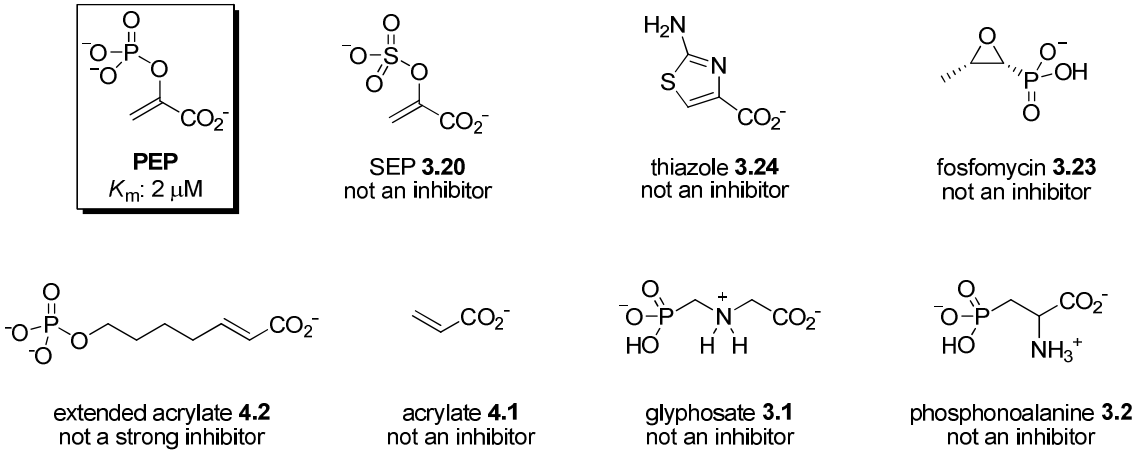

Figure 5.2: Compounds found to not be inhibitors of DAH7P synthase, compared with PEP.

From comparisons between these molecules, new insights into the inhibition of DAH7P synthase can be obtained. In this chapter, interpretations of the binding of these molecules are presented, using in part information gleaned from molecular modeling studies of the putative enzyme-inhibitor complexes. Possible directions for future work are also presented.

5.2: (R) and (S)-phospholactate, and cyclopropane 3.5

As was discovered in Chapter Three, both (*R*)- and (*S*)-configured phospholactate are inhibitors of DAH7P synthase, however despite possessing the same functionality the (*R*)-isomer is a more potent inhibitor by more than an order of magnitude (Figure 5.3).

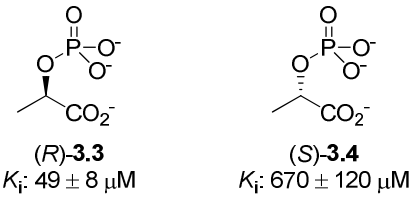

Figure 5.3: (*R*) and (*S*)-phospholactate

The reason for this difference is not immediately obvious. PEP is trigonal planar at C2, so the difference in affinity is presumably not based on differences in substrate mimicking. However, there is a possible mechanistic explanation.

The mechanism of DAH7P synthase requires attack by a water molecule at PEP C2 during some stage of the reaction; with the water oxygen atom ultimately becoming the carbonyl oxygen of linear DAH7P during subsequent phosphate elimination. As was discussed in Chapter One, opinion differs on the exact mechanism by which this takes place, but the most chemically reasonable of the proposed mechanisms is shown in Figure 5.4.

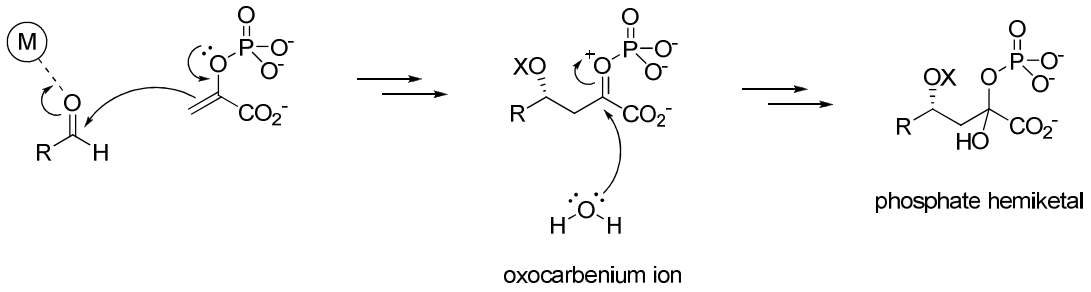

Figure 5.4: The Lewis-acid mechanism of DAH7P synthase activity

From analysis of the structures of DAH7P synthases and KDO8P synthases determined by X-ray diffraction, it is clear that several water molecules are structurally conserved across enzyme, species and family divides. Two such waters fall within close proximity to PEP C2, one in a pocket on the *re* face of PEP and another coordinated to the metal (or held by hydrogen bonding in non-metallo KDO8P synthases) on the *si* face of PEP (Figure 5.5).

Due to their proximity and conservation, these water molecules are candidates to be the nucleophilic water which intercepts the oxocarbenium ion during the enzyme reaction. As discussed in Chapter One, the water on the *re* face is a better candidate for the water nucleophile. The metal coordinated water on the *si* face is probably an artifact of the experimental conditions; it occupies the only accessible coordination site on the metal, which would be required by the E4P carbonyl oxygen atom during the enzyme reaction. The corresponding water in non-metallo *A. aeolicus* KDO8P

synthase mutants has been shown to be replaced by the carbonyl of A5P in high-resolution structures of the enzyme-PEP-A5P ternary complex.[42]

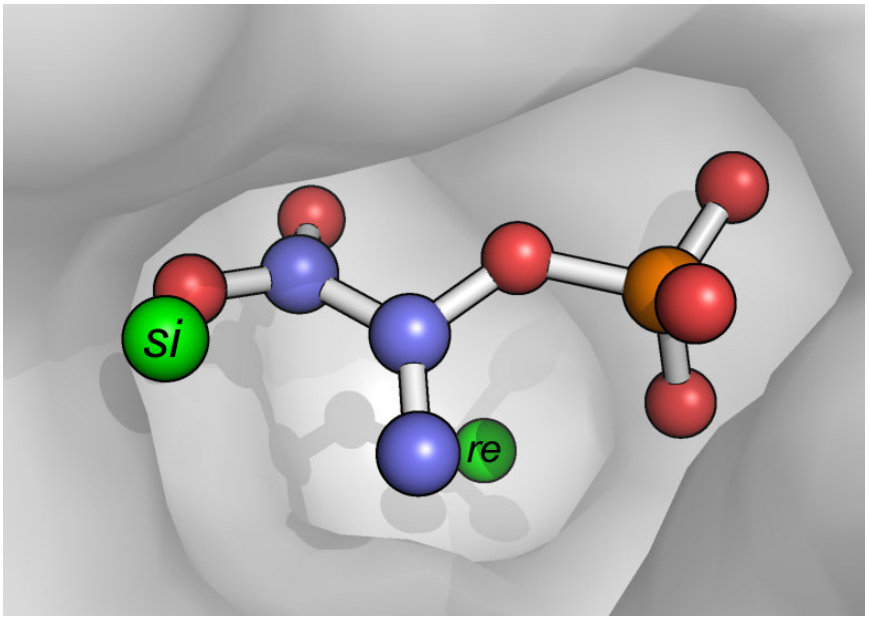

Figure 5.5: Conserved water molecules (green) on the *si* and *re* faces of PEP inside the *S. ceravisae* DAH7P synthase active site (PDB: 1of8)[40]. The view is from the E4P pocket; the surface indicates solvent-accessible active site surface, spheres are drawn at 30% of the relevant atoms Van der Waals contact radius. Hydrogen atoms are omitted. The presence of a pocket for the *re*-face water is clearly visible.

The oxocarbenium ion produced during the enzyme reaction is prochiral, so attack of water from the *re* and *si* faces will result in different diastereomeric hemiketal phosphates; which are epimers at C2. Attack of the *re*-face water would give a (*S*)-configured hemiketal phosphate.

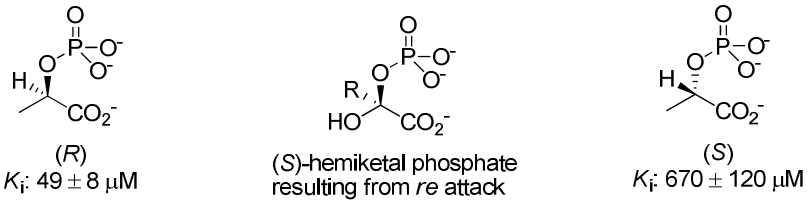

Figure 5.6: Comparison of (*R*), (*S*)-phospholactates and the (*S*)-hemiketal phosphate

The (*S*)-hemiketal phosphate shares the same configuration as the more potent (*R*)-isomer of phospholactate; if the lactate methyl group is considered a mimic of the similarly sized hydroxyl group in the hemiketal phosphate. Thus the (*R*)-isomer may be better recognised by the transition state form of the enzyme, resulting in increased

affinity for the (*R*)-isomer. However, the opposite form of the argument can be composed if the lactate methyl group is considered a mimic of the PEP methylene group.

In order to gain a better insight into the affinity difference between (*R*)- and (*S*)-phospholactate, the possible enzyme-inhibitor complexes were investigated by computational chemistry. The active site architecture of the highest resolution *E. coli* DAH7P synthase structure, 1n8f[27], was isolated, prepared and energy minimised, and both enantiomers of phospholactate docked using Glide[177].

Interestingly, the resulting model enzyme-inhibitor complexes showed the (*R*)-enzyme complex was the slightly more stable, as indicated by a Glide score slightly more than 10% larger than that for the (*S*)-enzyme complex (Figure 5.7). The Glide score reflects both favourable and unfavourable interactions, such as hydrogen bonds and steric clashes. However, the difference in observed Glide score is not large considering the difference in inhibition constant. This may reflect the fact the molecules are being forced to fit the ground state form of the enzyme, which might fail to fully show any affinity increase the (*R*)-isomer has from mimicking the hemiketal phosphate intermediate.

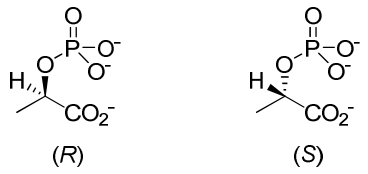

	K_i /μM	glide score
(*R*)	49±8	-5.585
(*S*)	670±120	-5.174

Figure 5.7: Comparison of experimental and theoretical binding strengths of (*R*) and (*S*) phospholactate

A close investigation of the docking results shows that both the phosphate and carboxylate groups of the inhibitors occupy their respective sites in the PEP site, and have their methyl groups pointing on opposite sides to the plane of PEP, with the C2-methine proton occupying the position of the PEP methylene group (Figure 5.8). This result is consistent with the earlier suggestion that (*R*)-phospholactate is more potent due to it mimicking the chirality of the hemiketal phosphate intermediate resulting from attack of the *re* face water.

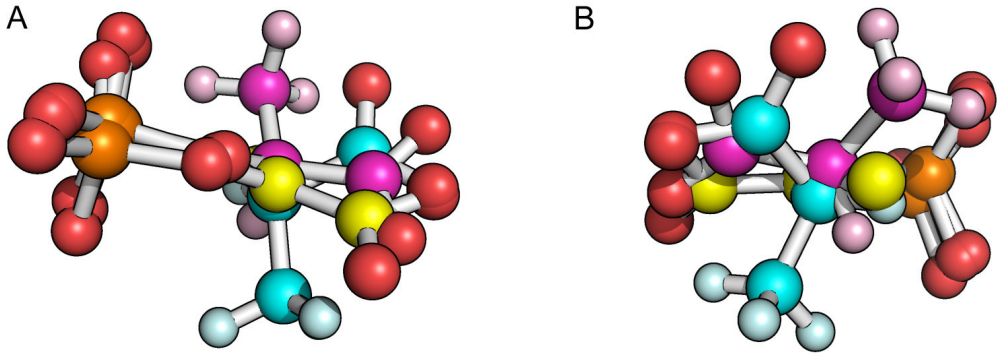

Figure 5.8: Comparison of the calculated positions of (*S*)- (mauve) and (*R*)- (cyan) phospholactates with the crystallographically determined position of PEP (yellow) in the crystal structure of *E. coli* DAH7P synthase (1n8f)[27]. A: view along the PEP C2-C3 bond, in the plane of PEP, highlighting the similar phosphate positions and the dissimilar methyl and methylene positions. B: view down the PEP plane from the carboxyl side, highlighting the similar locations of the PEP methylene and lactate methine hydrogen atoms.

In each case, the phosphate group is very similarly positioned, perhaps indicating it is the main interaction responsible for positioning the molecules. In the model (*R*)-3.3-enzyme complex and the crystallographically determined enzyme-PEP complex, a carboxyl group oxygen occupies a similar position in space. In the corresponding model (*S*)-3.4 complex, both carboxyl oxygens straddle the site without either occupying it. This inability of the carboxyl group of (*S*)-3.4 to bind in the same place as PEP and (*R*)-3.3 seems to be related to the ability of the enzyme site to tolerate the out of plane methyl group. In the model (*S*)-3.4 complex the methyl group points toward the ring carbons of the conserved proline P98 (Chapter One); the docked position putting the methyl hydrogens close (2.86 Å) to the proline methylene hydrogens. This steric interaction prevents further twisting of (*S*)-3.4, in turn preventing optimum fit of the carboxylate to the PEP site.

Based on this analysis, one might expect cyclopropane 3.5 to bind in a fashion similar to (*R*)-phospholactate 3.3, in order to minimise this proposed proline-inhibitor steric interaction. This conclusion could also be reached from comparision of the inhibition constants, rather since cyclopropane 3.5 has significantly smaller inhibition constant than (*S*)-phospholactate (Figure 5.9).

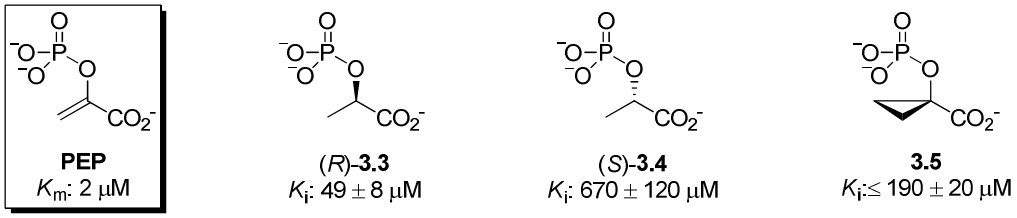

Figure 5.9: Comparison of phospholactates 3.3 and 3.4, cyclopropane 3.5 and PEP

By the model of phospholactate binding presented earlier, this would suggest cyclopropane 3.5 lacks the proposed destabilising methyl-proline interaction in it inhibitor-enzyme complex, which is observed with (*S*)-phospholactate. This possibility was investigated by docking cyclopropane 3.5 in the same manner as (*R*)- and (*S*)-phospholactate. As was suggested by their corresponding inhibition constants, the modelled interaction of cyclopropane 3.5 with the enzyme closely resembles that of (*R*)-phospholactate. In the model, one methylene of the cyclopropane falls into the same position as the methylene of PEP; the remaining methylene of the cyclopropane group is pushed into the *re*-face water pocket (Figure 5.10). This allows the cyclopropyl group to adopt the furtherest possible position from proline P98. This finding reinforces the proposed role of proline P98 in the stereoselectivity of phospholactate binding by *E. coli* DAH7P synthase.

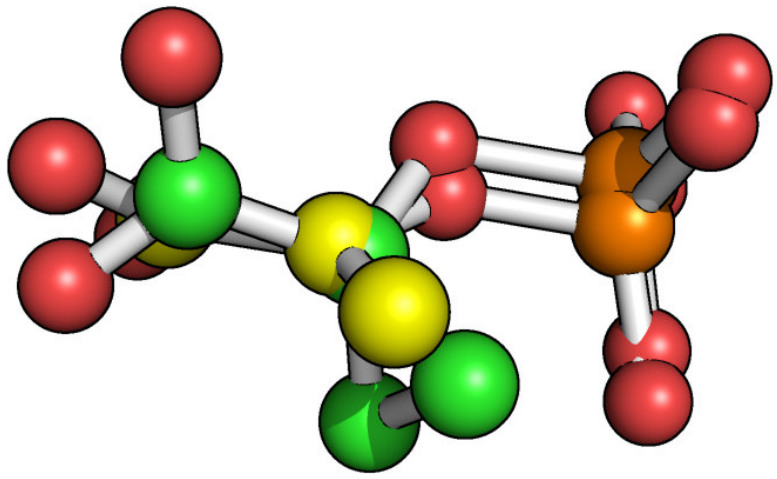

Figure 5.10: A comparison of the crystallographically determined position of PEP in *E. coli* DAH7P synthase structure 1n8f[27] (yellow carbons), and the calculated position of cyclopropane 3.5 (lime green carbons)

The glide score determined for the interaction of cyclopropane 3.5 (-3.69) is larger than that determined for either enantiomer of phospholactate (-5.59 for (*R*), -5.17 for (*S*)), which would suggest that cyclopropane 3.5 interacts more weakly with the enzyme than either enantiomer of phospholactate. Since from kinetic studies it is clear this is not the case, it may simply reflect the shortcomings of current docking methodology.

In the model (*R*)-phospholactate-enzyme complex, the methyl group falls into a pocket in the floor of the active site, which is normally occupied by the *re*-face water (see Figure 5.5 for a diagram of this pocket). The methyl group and *re* face water are closely placed (C-O distance: 2.80 Å), which would prevent simultaneous binding of the *re*-face water and this conformation of (*R*)-3.3. This might suggest the *re*-face water is readily displaced, which potentially highlights its role in the enzyme mechanism, since the water which attacks the oxocarbenium ion is consumed with each turnover. The presence of this pocket allows optimum overlap of the carboxylate of (*R*)-phospholactate with the PEP carboxylate site, presumably increasing its affinity relative to (*S*)-phospholactate.

Displacement of this water may provide an additional increase in the affinity of the enzyme for (*R*)-3.3 in another manner. By releasing a well-ordered water molecule from the active site, the loss of entropy upon binding (*R*)-3.3 is lessened, which may result in an increased affinity. Such a phenomenon has been observed in the design of inhibitors for HIV-1 protease.[178] In principle, a similar phenomenon may occur during the binding of cyclopropane 3.5, since it also utilises the pocket on the *re* face of PEP, which help may explain why it is a more potent inhibitor than (*S*)-phospholactate.

However, entropic contributions to protein-ligand interactions are complex and poorly understood; and contradictory examples of affinity loss on water displacement are known.[179] Water molecules are traditionally treated as displaceable in docking,[180] and the water molecules are typically stripped during preparation of the active site architecture unless they mediate protein-ligand interactions. Furthermore, the force-fields used for docking are poor at predicting water-apolar interactions. A recent systematic study of this problem found that water molecules in partially apolar environments, which make less than three hydrogen bonding contacts with

neighbouring residues, are typically displaceable upon inhibitor binding.[180] Based on this criterion, the *re*-face water might be considered displaceable, as it is only close enough to make one direct hydrogen bond with the active site via glutamate E143; although an additional hydrogen bond mediated via a second water molecule to tyrosine Y94 and a hydrogen bond with the PEP phosphate group are also present (Figure 5.11).

One method to investigate this postulated displacement of the *re*-face water will be to analyse the interaction of (*R*)-phospholactate with DAH7P synthase by X-ray crystallography.

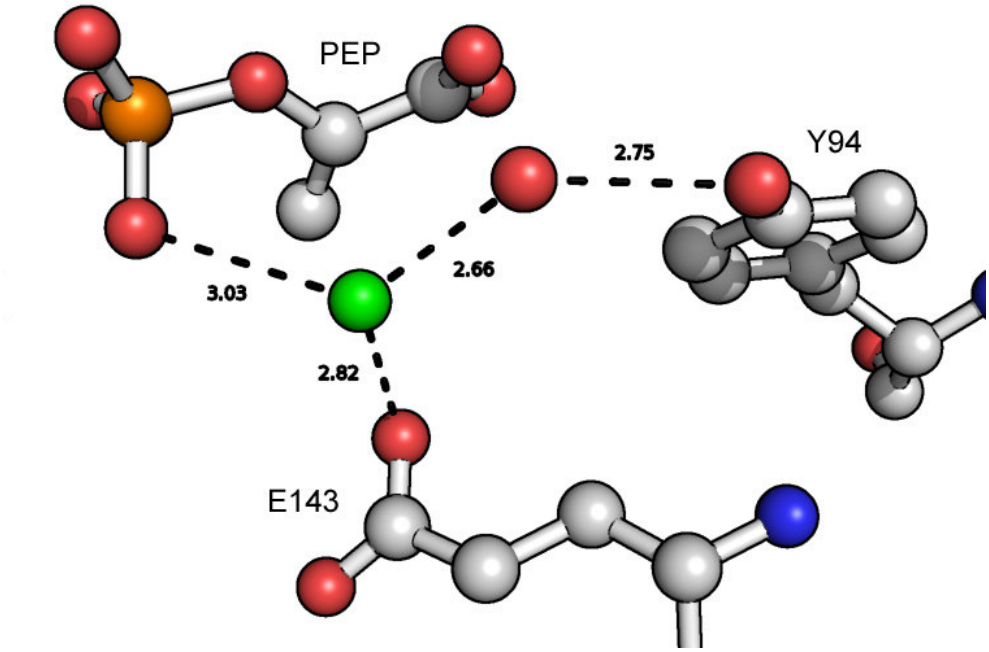

Figure 5.11: The hydrogen bonding partners of the *re*-face water molecule (green) in *E. coli* DAH7P synthase structure 1n8f[40]. Distances are indicated in angstroms.

In conclusion, the difference in interaction between (*R*)-phospholactate and (*S*)-phospholactate is complex, and potentially has contributions from transition state binding effects, as well as entropic and enthalpic effects. Based on docking of both enantiomers of phospholactate, the interactions seem to stem from the ability of the enzyme to tolerate the out of plane methyl groups in each structure. In the model, the clash of the (*S*)-isomer methyl group with the wall of the active site destabilises the enzyme-inhibitor complex relative to the corresponding (*R*)-complex. In addition to

lacking the destabilising steric interaction of (*S*)-phospholactate, the displacement of a structurally conserved water in the modelled interactions of (*R*)-phospholactate and cyclopropane 3.5 with DAH7P synthase may provide an additional increase in binding affinity for these compounds.

5.3: Future directions from phospholactates 3.3, 3.4 and cyclopropane 3.5

The results of our studies of phospholactates 3.3, 3.4 and cyclopropane 3.5can be used to design new molecules to inhibit DAH7P synthase. These molecules can be used to further map the interaction of DAH7P synthase with inhibitors, as well as being used as PEP-mimicking portions of extended molecules such as those described in Chapter 4.

An interesting comparision to both cyclopropane 3.5 and (*R*)-and (*S*)-phospholactate would be the geminal dimethyl compound 5.1 (Figure 5.12). It possesses the ability to form the destabilising steric methyl-proline interaction predicted in the modelled (*S*)-phospholactate-enzyme complex; and the potentially stabilising methyl group displacement of water proposed in the modelled (*R*)-phospholactate complex. The binding affinity of this compound may cast light on the relative importance of each effect in inhibitor binding.

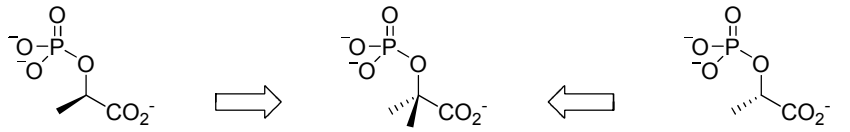

Figure 5.12: Simple analogue 5.1

One way to increase the affinity of similar molecules to DAH7P synthase would be to not only utilise the proposed water-displacement effect of the (*R*)-configured phospholactate 3.3, but build in an additional polar interaction of the molecule with the *re*-face water pocket by functionalising the methyl group. Both 5.2 and 5.3 (Figure 5.13) could be expected to fulfill this criterion. The compound 5.2 is (*R*)-2-phosphoglycerate; its interaction with *A. aeolicus* KDO8P synthase has been

investigated crystallographically[68]; but no inhibition constant has been reported. Interestingly, in the *A. aeolicus* KDO8P synthase-phosphoglycerate complex the displacement of the *re*-face water from its pocket by the 3-hydroxyl group that is postulated here was in fact observed. The phosphate and carboxylate groups of phosphoglycerate 5.2 were also observed to occupy the corresponding PEP phosphate and carboxylate sites in the enzyme, as predicted for (*R*)-phospholactate 3.3.

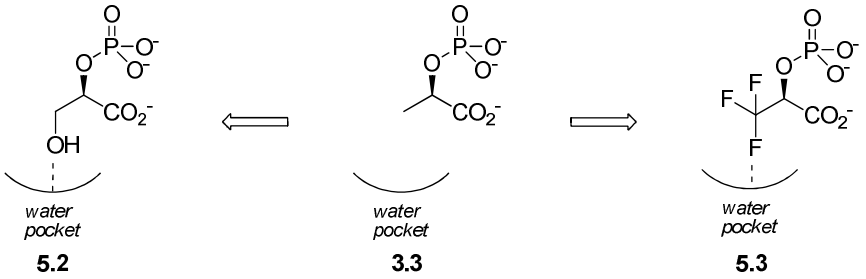

5.2 **3.3** **5.3**

Figure 5.13: Possible methods of further exploiting the proposed (*R*)-methyl/water pocket interaction

The information gained from studying the interaction of phospholactate could also be used to design higher-affinity multivalent molecules. In order for the hydrocarbon linker to occupy the same position as the PEP methylene group, it needs to replace the methine proton of (*R*)-phospholactate. Based on this rationale, the (*S*)-isomer 5.4 (n = 1) will be of interest (Figure 5. 14). The extended compound 5.5 (n=2) may be of utility in the study of inhibition of KDO8P synthase, and its additional flexibility may allow it to also be a potent DAH7P synthase inhibitor.

The molecules are potentially accessible from a Darzens-like approach as employed in Chapter Four; the chiral 2-hydroxyl group could be generated by catalytic asymmetric reduction of an α-ketoester. The efficencies of various chiral reducing agents in the asymmetric reduction of α-ketoesters have been recently investigated.[181] Alternatively, many other methods are also available to generate similar substructures, including both asymmetric transition-metal[33] and organic catalysts.[182]

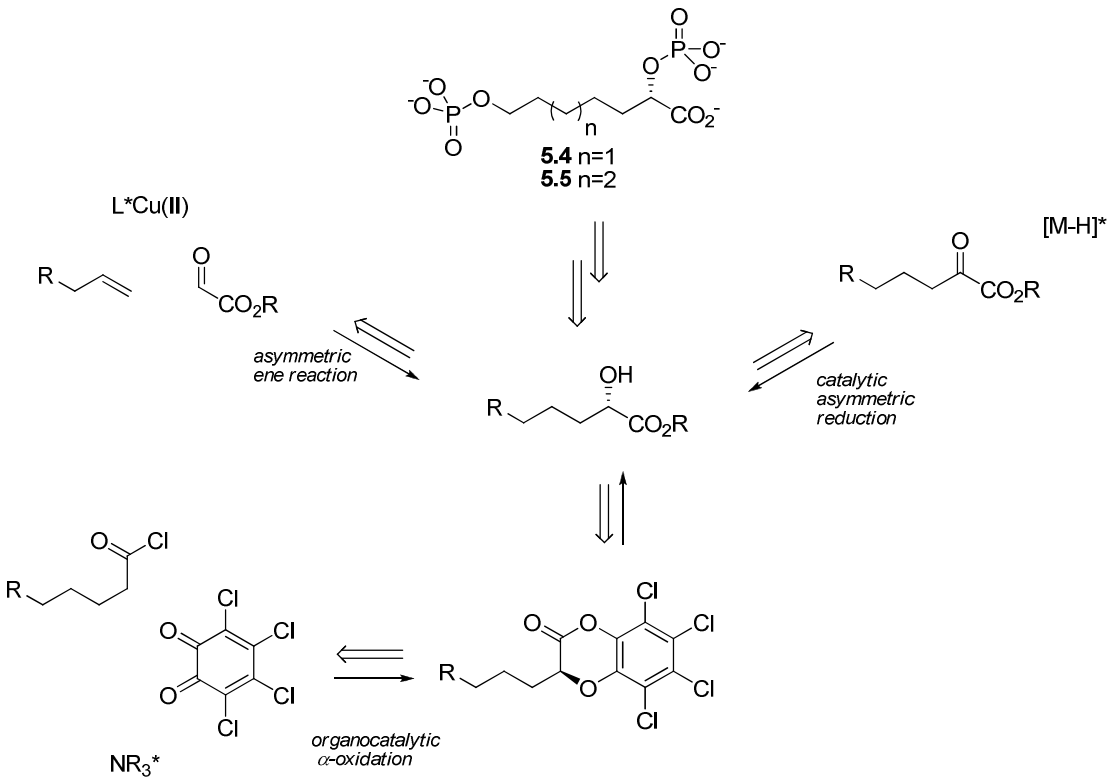

Figure 5. 14: A possible multivalent version of (*R*)-phospholactate; and suggested catalytic sources of chirality. While 5.4 would give the same length as DAH7P, extension to 5.5 may give improved binding in addition to activity against KDO8P synthase.

5.4: Vinyl phosphonates 3.12 and 3.15

The most potent single site molecule in this study, (*E*)-vinyl phosphonate 3.12, binds considerably more strongly than that previously determined for the isosteric phosphonate analogue of PEP 3.10, and only slightly less than PEP itself (Figure 5.15).[94, 95] This result is astounding, and reinforces the utility of locking the movement of rotatable bonds in inhibitor design, in order to obtain an entropic binding advantage.

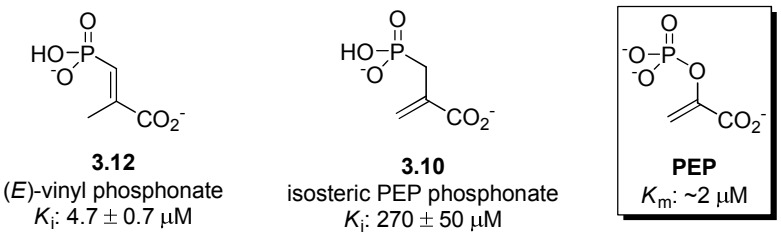

Figure 5.15: The effect of conformational restriction on enzyme inhibition

The binding of vinyl phosphonate 3.12 was investigated by docking the compound to *E. coli* DAH7P synthase using Glide. As predicted, the binding of (*E*)-vinyl phosphonate 3.12 mimics that of PEP, with the phosphonate occupying the PEP phosphate sites. However, only one carboxylate oxygen occupies the PEP carboxylate pocket; and the whole molecule is twisted toward the E4P site (Figure 5.16). The origin of the twisting effect is unclear, but may be derived from the extended planarity over the vinyl phosphonate-C2-C3 system, since in the crystallographically determined conformations of enzyme bound PEP there is a slight (~15°) dihedral twist in the corresponding P-O-C2-C3 system, which allows a slight shortening of the carboxylate-phosphate distance.

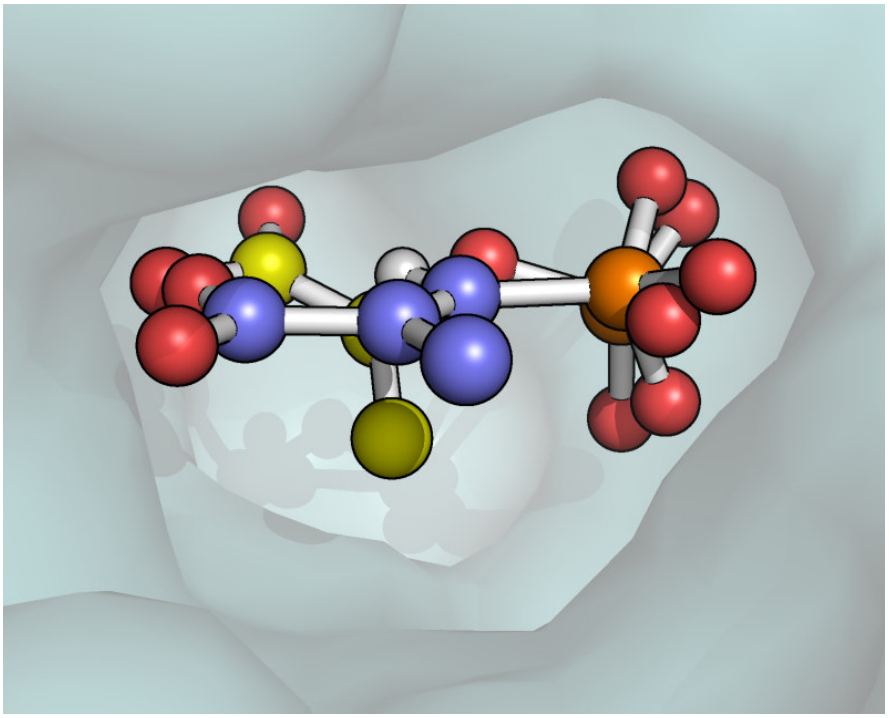

Figure 5.16:The highest-scored docked conformation of (*E*)-vinyl phosphonate 3.12 (blue carbons) and the crystallographically determined binding of PEP (yellow carbons) to *E. coli* DAH7P synthase (1n8f). Oxygen atoms are in red, phosphate in orange and hydrogen atoms in white. The solvent accessible surface of the active site is indicated. Methyl hydrogen atoms of phosphonate 3.12 removed for clarity

Whether this difference exists in the actual system is unclear. The similarity in binding affinity between PEP and vinyl phosphonate 3.12 is suggestive of them sharing a very similar binding mode, perhaps even more similar than suggested by the docking result. There also must some flexibility in the shape of the PEP site, since based on the solvent accessible surface in the crystal structure it is not possible to remove PEP from its site without clashes with the walls of the active site. Therefore, it

is likely an "induced-fit" mechanism operates during PEP binding, in which the shape of the PEP site deforms in the presence of PEP in order to provide an optimum fit. This same process may operate during the binding of vinyl phosphonate 3.12, allowing it to bind with the observed high affinity. This possibility is another that could be investigated by X-ray crystallography.

5.5: Future directions from vinyl phosphonates 3.12 and 3.15

The strong binding of vinyl phosphonate 3.12 could allow it to be used as an inert substitute for PEP, and allow the structure of the enzyme-3.12-E4P ternary complex to determined under catalytically valid conditions. This structure could greatly improve our understanding of the mechanism of DAH7P synthase.

The vinyl phosphonate 3.12 is already a strong inhibitor, and as we saw with trifluoromethyl analogue 3.15 further modification may hinder binding. One possibility for increased affinity would be to produce the vinyl fluoride 5.6 (
Figure 5.17). The fluorine atom should decrease the pK_{a2} of the neighbouring phosphonate, allowing it to better mimic PEP. Whether the fluorine atom also interferes with binding will be of interest. Vinyl fluoride 5.6 is presumably accessible by HWE reaction of fluorobisphosphonate 5.7, itself prepared by fluorination of bisphosphonate 5.8.

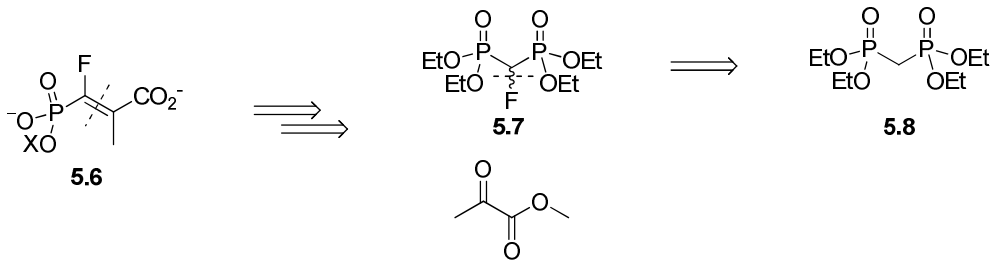

Figure 5.17: Vinyl fluoride 5.6 and a suggested route for its synthesis

5.6: Comparision between phosphoenolpyruvate and sulfoenolpyruvate

The failure of SEP 3.20 to inhibit or act as a substrate of DAH7P synthase was an unexpected finding, given the close similarity in structure between SEP 3.20 and PEP.

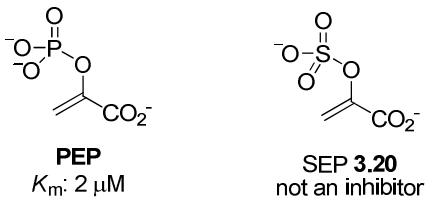

Figure 5. 18: PEP and SEP 3.20

In order to gain further understanding of possible reasons for the failure of SEP 3.20 to inhibit DAH7P synthase, the interaction of SEP and *E. coli* DAH7P synthase was modelled by docking. The best model (glide score: -2.44) displayed an overall similar location to PEP in the active site, with the SEP sulfate group in a similar position to the PEP phosphate group and the SEP carboxylate group in a similar position to the PEP carboxylate group (Figure 5.19)

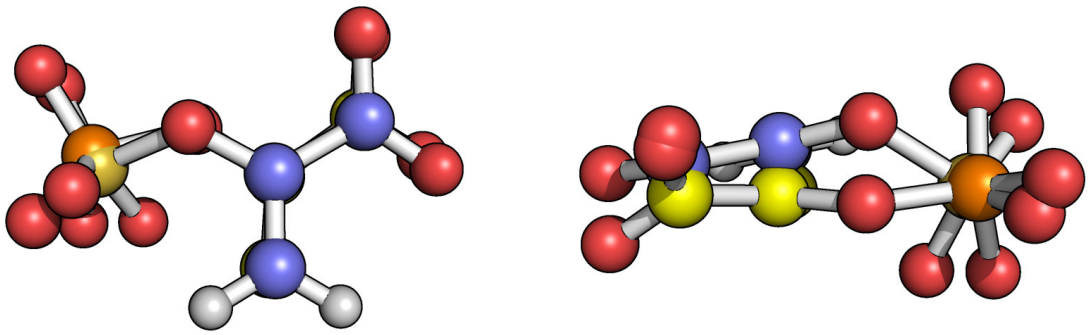

Figure 5.19; A comparison of the modelled position of SEP 3.20 (pale blue/ red/ gold corresponding to carbon/ oxygen/ sulfur respectively) and the crystallographically determined position of PEP (yellow/ red/ orange corresponding to carbon/ oxygen/ phosphate respectively) in 1n8f.pdb[27]

However unlike PEP, SEP 3.20 displayed a large dihedral twist across the enol ester carbon oxygen bond. This twist appears to be introduced due to steric clashes between a sulfate oxygen atom and the SEP methylene group (Figure 5.20).

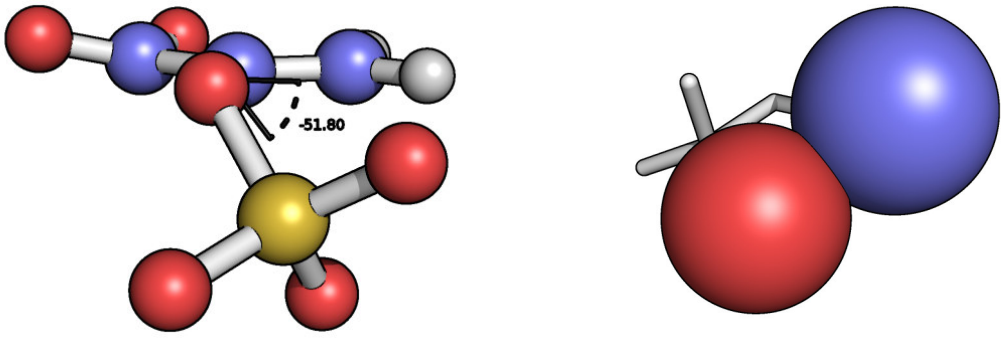

Figure 5.20: Left: the large dihedral angle present in the modelled conformation of SEP. Right: the clash between the sulfate oxygen (red) and the methylene carbon C3 (blue). Spheres are drawn at each atom's van der Waals radii.

The corresponding dihedral angle in the crystallographically determined PEP-enzyme complex 1n8f[27] is 13.2°, which allows PEP to adopt a relatively planar geometry in the active site. The best model (glide score: -2.44) of the SEP-enzyme complex has a dihedral angle of 51.8°, and the only other model produced by Glide (glide score -2.31) has dihedral angle of 32.5°. Manual manipulation of the dihedral to a more PEP-like value results in very unfavourable levels of van der Waals overlap (greater than 25% overlap of radii) between the sulfate oxygen and the methylene group at dihedral angles less than 29°.

In order for SEP to gain a good fit to the same site as PEP, it must adopt a similar conformation to that of PEP. As the enol ester dihedral angle approaches 13° however, the sulfate group encounters increasing steric repulsion from its interaction with the methylene group, which prevents the molecule from adopting the same conformation as PEP. Thus the decrease overall energy available from more closely fitting the conformation of PEP is countered by the increasing steric repulsion as the enol ester dihedral is forced flat. This places a limit on allowable conformations of SEP in the SEP-enzyme complex, making the potentially more tightly bound PEP-like conformations inaccessible. This would manifest itself as a decreased ability for SEP to bind to DAH7P synthase relative to PEP.

Another factor that was hypothesised to limit the binding of SEP was the difference in charge state. The sulfate group of SEP is only capable of adopting a -1 charge, while the phosphate group of PEP can adopt a -2 charge. Based on this difference, one

would expect qualitatively a difference in binding affinity between SEP and PEP due to decreased charge (or Coulombic) interactions. This difference would be difficult to quantitate experimentally without contribution from other factors, but it can be measured relatively easily in the modelled interactions of PEP and SEP, where the individual components of the binding energy are calculated seperately. In order to investigate the effect of charge state on the lack of interaction between SEP and DAH7P synthase, the Coulombic and hydrogen bonding energies (E_{coul} and E_{hbond} respectively) of calculated PEP-DAH7P synthase and SEP-DAH7P synthase complexes were compared (Figure 5.21).

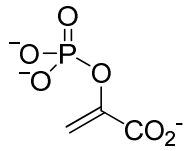

PEP
K_m: 2 μM

Glide score: -3.47

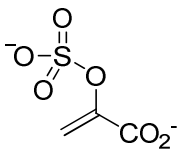

SEP 3.xx
not an inhibitor

Glide score: -2.44

model	SEP/ kJ mol^{-1}	PEP/ kJ mol^{-1}	ΔE/ kJ mol-1
E_{hbond}	-2.33	-2.29	-0.03
E_{coul}	-91.29	-149.91	58.62

Figure 5.21: A comparision between the hydrogen bonding and Coulombic components of the ligand enzyme interaction in calculated SEP and PEP DAH7P synthase complexes.

As be seen in Figure 5.21, while there is little differences in the contributions of hydrogen bonding to the interaction of each ligand with the receptor, there is a large difference in the contributions of charge interactions. The differences in charge state lead ultimately to greater than 58 kJ mol^{-1} difference in Coulombic interaction energy between the two complexes. This large energy difference will be reflected in the apparent affinities of SEP and PEP to the enzyme.

In conclusion, while the large difference in affinities between PEP and SEP 3.20 remains a surprising result, the use of molecular modeling techniques has identified that both differences in charge state and subtle differences in geometry may be in part responsible for the differences in affinity between SEP and PEP in DAH7P synthase binding.

5.7: Metal interacting inhibitors 3.17 and 3.25

The use of compounds that interfere with the metal coordination site is also of interest. As was seen in Chapter Three, the incorporation of a metal ligand at C3 of PEP (as in cyanoPEP 3.17) is capable of stopping the compound from being a substrate, presumably due to the cyano group blocking the coordination of the E4P carbonyl, and stopping Lewis acid catalysis. In addition, the metal chelator fosmidomycin was also able to inhibit DAH7P synthase relatively strongly, presumably also by metal coordination (Figure 5.22).

3.17
K_i: < 75 μM

3.25
K_i: 35 μM

Figure 5.22: Inhibitors potentially exploiting metal interaction

The binding of cyanoPEP 3.17 to DAH7P synthase was investigated by docking studies. The highest scoring dock of cyanoPEP 3.17 to *E. coli* DAH7P synthase gave a model with an overall similar binding to that of PEP, with the phosphate and carboxylate groups occupying their respective sites Figure 5.23. However, the plane of the alkene has been distorted toward the metal, allowing the cyano group to coordinate the metal atom as designed. The cyano nitrogen atom occupies a very similar position to that of the metal-coordinated *si*-face water in the crystal structure (and hence the carbonyl oxygen of E4P in the active ternary complex).

The calculated manganese-nitrogen distance (2.92 Å) is slightly longer than that in the known complex hexa(acetonitrile)mangenese(II) triflate, which has a manganese-nitrogen distance of 2.11 Å.[183]

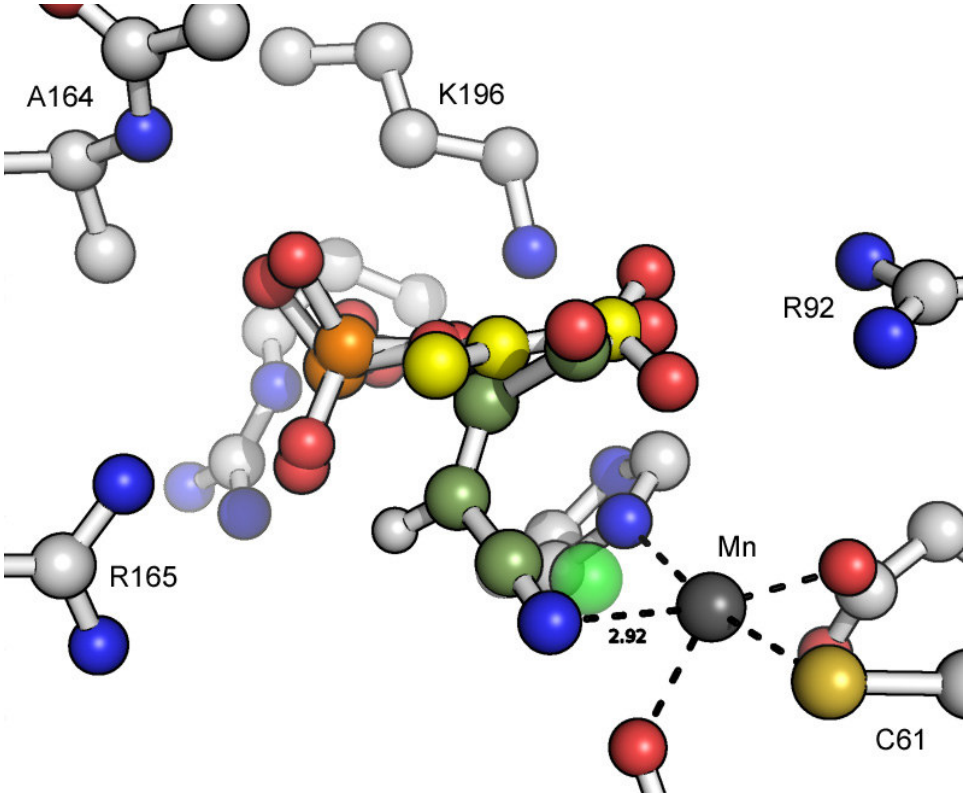

Figure 5.23: Comparison of the calculated binding position of cyanoPEP 3.17 (khaki carbons) with that of PEP (yellow carbons) in the crystallographically determined enzyme-PEP complex 1n8f[27]. Note the similar positions of the cyanide nitrogen atom with the oxygen of the crystal structure *si*-face water (transparent green sphere, drawn at 30% van der Waals radius). The cyanide nitrogen-manganese distance is indicated in angstroms

These findings can be used to inform future work on both DAH7P synthase and KDO8P synthase. As was discussed in Chapter One, the mechanism of DAH7P synthase and KDO8P synthase have been recently postulated to differ in their mode of aldehyde activation; while DAH7P synthases employ Lewis acid catalysis, KDO8P synthases are thought to employ protic acid catalysis. Based on this proposition, one might expect cyanoPEP 3.17 to be a substrate of KDO8P synthase, since it lacks a Lewis acid activation to interfere with, although there are also obvious steric and electronic differences between PEP and cyanoPEP 3.17. The interaction of this compound with metallo-KDO8P synthases will be of particular interest, since the metal has been postulated to perform a non-catalytic role in these enzymes.

The binding of fosmidomycin 3.25 to DAH7P synthase was also investigated by docking studies. Solution conformers of the minimised structure of fosmidomycin (in its phosphonate monoanion and hydroxamate ion state) were generated, and

representative conformers lacking an intramolecular hydroxamate-phosphonate hydrogen bond were docked to *E. coli* DAH7P synthase.

Surprisingly, the highest scoring model (glide score: -6.95) shows a non-coordinating role for the hydroxamate group (Figure 5.24). This group, rather than forming a complex with the metal ion, forms part of a bidentate interaction with arginine R234 of the PEP phosphate binding pocket. The monoanionic phosphonate in turn binds to the PEP carboxylate binding pocket, with the hydrocarbon chain of fosmidomycin forming a hydrophobic interaction with proline P98, in the same manner as PEP's C3 is observed to do.

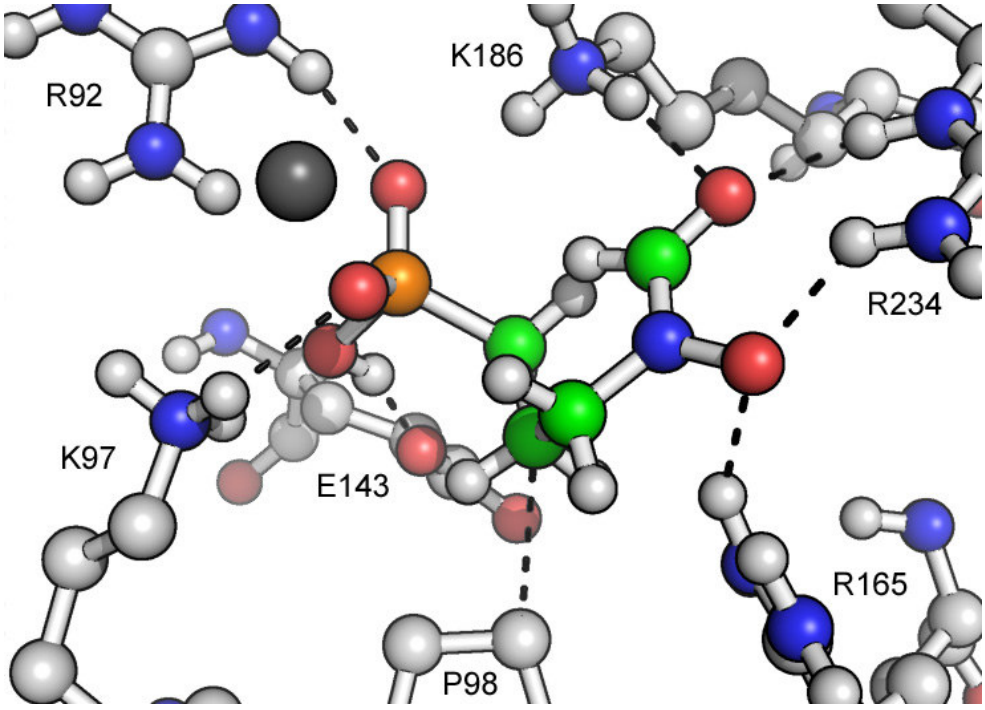

Figure 5.24: The highest scoring model of the fosmidomycin-*E. coli* DAH7P synthase complex. Note the reversal of the usual phosphoryl binding affinty; while K97 and R92 form a carboxylate site for PEP, they bind the phosphonate of fosmidomycin (green carbons, orange phosphate) in this structure. The PEP phosphate site formed in part by R234 and R165 now binds the hydroxamate moiety of fosmidomycin. No interaction of fsomidomycin with the manganese atom (grey) is present in the model

This non-metal binding role for the fosmidomycin hydroxamate group is an interesting proposition. It has been discovered in this work that the inhibition of DAH7P synthase by fosmidomycin is sensitive to the metal ions used (Chapter Three), with the strength of inhibition following the series Fe(II), Mn(II) > Co(II). While this would appear to suggest a role for the metal in the interaction of

fosmidomycin with DAH7P synthase, it may instead reflect the formation of enzyme free metal-fosmidomycin complexes *in situ*, which would lower the concentration of fosmidomycin in the cuvette. The stabilities of the relevant enzyme free metal-fosmidomycin complexes have not been measured, however the stabilities of metal complexes with another hydroxamate ligand, desferrioxamine B, have been measured and found to correspond well to the Irving-Williams series.[184] Based on this series, the relative stabilities of fosmidomycin-metal complexes should have the form Mn(II)<Fe(II)<Co(II). Thus the metal ions that are predicted to give the least stable complexes give the strongest inhibition of DAH7P synthase; which may indicate the metal dependancy of inhibition is simply due to decreases in free fosmidomycin concentration by complex formation. However, while the Irving-Williams series mainly reflects electrostatic effects, unusual geometries (such as the Jahn-Teller distortion present in six coordinate copper(II) complexes) are known to influence the relative positions of metals in the series.[184] Thus the series may not be easily applicable to the unusual distorted trigonal bipyrimidal geometries present in DAH7P synthase-metal complexes.

A lower scoring model fosmidomycin conformation (glide score: -5.87), has the phosphonate occupying the PEP phosphate pocket, and while the hydroxamate is not directly interacting with the metal ion, it falls close to it. Rotation of the C3-C4 bond would put the hydroxamate carbonyl oxygen within 2.9 Å of the manganese atom (Figure 5.25).

This rotation in the model would move the hydroxamate away from its interaction with arginine R92, but toward its other interaction partners lysine K97 and K186, which may be able to compensate for the loss of interaction with R92.

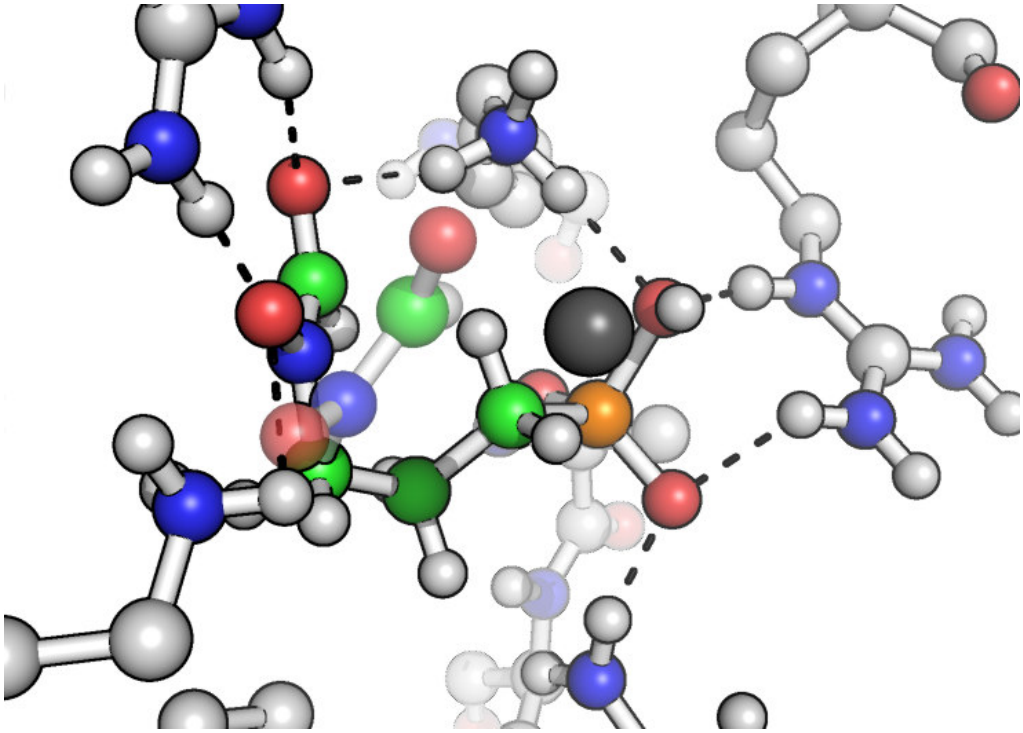

Figure 5.25: A lower scoring model of the fosmidomycin-enzyme complex. Fosmidomycin (green carbons) is shown in the models calculated position; the transparent portion indicates the position of the hydroxamate portion of the molecule after manual rotation of the C3-C4 bond to allow close approach to the manganese atom (grey).

It is of note that preliminary studies of fosmidomycin inhibition with metal independent and metal dependent KDO8P synthases show little to no inhibition. These enzymes have the same relative distance between the PEP carboxylate and phosphate pockets, yet an increased distance between the PEP phosphate pocket and the metal ion site is present in KDO8P synthase. This difference in enzyme structure may allow the elucidation of the mechanism of fosmidomycin inhibition of DAH7P synthase. The differing metal ion position would make it harder for the short hydrocarbon chain of fosmidomycin to span the distance between the phosphate pocket and metal ion, rendering the relative inhibition by fosmidomycin weakened for KDO8P synthase if the role of the hydroxamate group is to act as a metal coordinating group. Likewise, the similar positions of the carboxylate and phosphate pockets should lead to similar inhibition potencies in both DAH7P synthase and KDO8P synthase if the role of the hydroxamate group is to mimic the PEP carboxylate or phosphate groups.

In summary, there are two possible mechanisms of inhibition of DAH7P synthase by fosmidomycin. One mechanism involves the hydroxamate group binding to the PEP phosphate or carboxylate pocket by hydrogen bonding and ionic interactions. This mechanism is directly supported by computational models. The other mechanism involves interaction the fosmidomycin hydroxamate group with the DAH7P synthase metal ion cofactor. This mechanism is not directly supported by computational methods, however conformation of fosmidomycin required is similar conformations deemed possible by conformational methods. Indirect support from this mechanism is provided by the metal-binding behaviour of fosmidomycin in its natural target enzyme DXR, as well as inhibition metal dependency studies and preliminary studies of related enzymes.

5.8: Future Directions for metal binding inhibitors

These findings lead to a number of future directions for research into the interaction of fosmidomycin and DAH7P synthase. Given the known efficacy of fosmidomycin as an antibiotic and antimalarial drug; fosmidomycin might form a useful starting point for creating antibiotic and antimalarial drugs active against DAH7P synthase.

A starting point for this research will be to better characterise the interaction between fosmidomycin and DAH7P synthase, using techniques such as X-ray crystallography to determine to bound conformation of fosmidomycin, and confirm or disprove the proposed metal-coordination mechanism of action.

Improved compounds can then be designed from this information. Restricting the conformation of rotatable bonds to their active conformation can reduce the entropic cost of binding, and as shown in this work can result in large increases in binding affinity. Accordingly, restricting the allowable conformations of the chain of fosmidomycin may give more potent analogues.

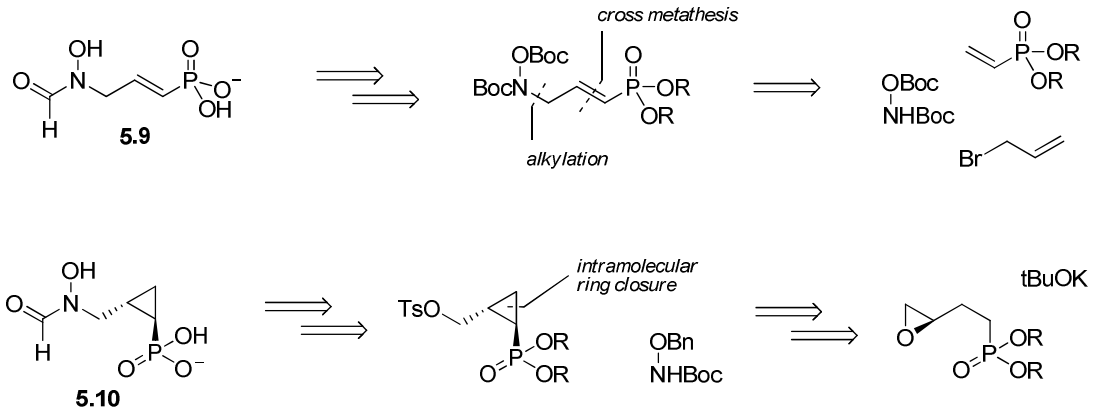

Figure 5.26: Possible conformationally restricted forms of fosmidomycin, and suggested routes of preparation

If it is found fosmidomycin binds to the enzyme through interaction with PEP phosphate site and the enzyme metal ion (Figure 5.25), then the conformation of the backbone will resemble the arrangement in (*E*)-vinyl phosphonate 5.9 (Figure 5.26), consequently 5.9 should display improved DAH7P synthase inhibition.

Likewise, if fosmidomycin binds without interaction with the metal (Figure 5.24), then its backbone will resemble the *trans*-cyclopropane 5.10 (Figure 5.26). Consequently, 5.10 should be able to inhibit DAH7P synthase more strongly than fosmidomycin, by preorganising the phosphonate and hydroxamate in space. Interestingly, cyclopropane 5.10 has been prepared in both racemic and enantiopure *trans* forms as part of studies into the natural fosmidomycin target DXR, and has been reported to strongly interfere with the growth of malarial parasite *P. falciparum.*[185]

Potent inhibitors may also be accessible by including functional groups in the chain that interact with the active site to allow the compound to more quickly adopt its active conformation. Possible ways to achieve this are by introducing a group to bind at the PEP carboxylate site or at the distal E4P phosphate site (or both), in a similar manner to the compounds designed in Chapter Four (Figure 5.27).

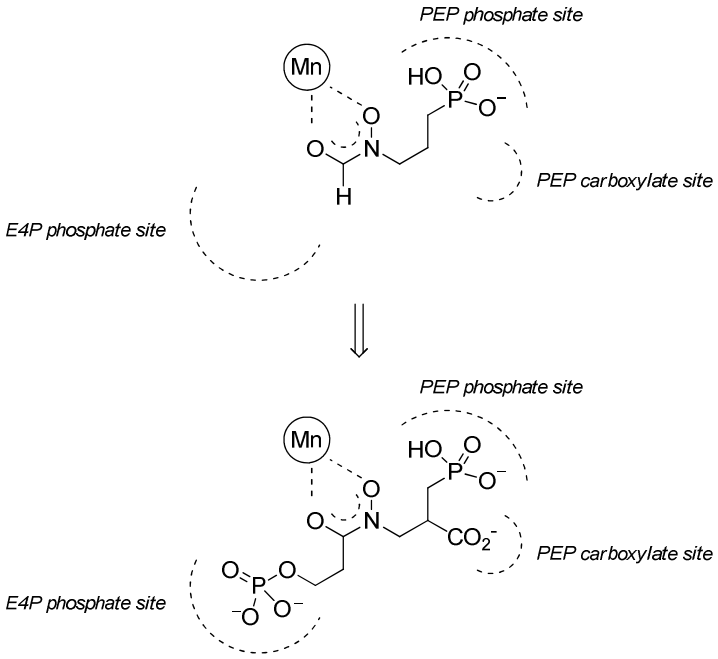

Figure 5.27: Extension of fosmidomycin to compounds making multiple enzyme contacts

The addition of an E4P phosphate mimicking portion is a potentially general addition to any of the constrained fosmidomycin-type molecules in Figure 5.26.

In addition to the future directions described above, any of the small PEP molecules in Chapter Three of this work could be investigated in their effects against both metallo and non-metallo KDO8P synthases; any differences in inhibitory potential may illuminate subtle mechanistic differences between the types of enzymes.

5.9: Multivalent inhibitors

Taken together, the results presented in Chapter Four of our attempts to increase potency by simply extending compounds to contact the E4P phosphate site are illuminating (Figure 5.28).

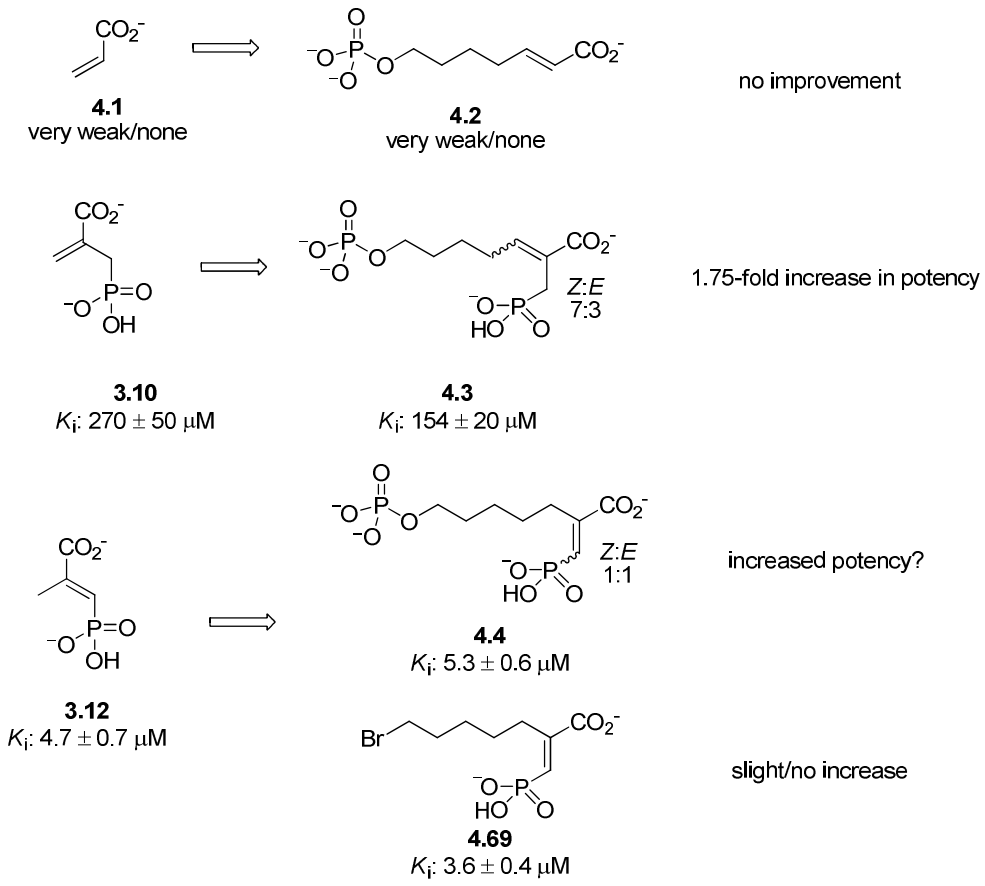

Figure 5.28: Overview of the results of Chapter Four

A number of key points are illustrated by this diagram. The comparison between acrylic acid and acrylate 4.2 show that the introduction of a terminal phosphate group is not capable of rendering an otherwise uninhibitory compound capable of inhibiting DAH7P synthase. This finding reinforces the necessity of a group mimicking the phosphate group of PEP in order to produce binding.

Comparing isosteric phosphonate 3.10 with its extended form 4.3 shows that the design rationale was correct, and that by adding a distal phosphate group a considerable increase in binding can be produced.

The results of extending vinyl phosphonate 3.12 to 4.4 are less straightforward, due to the unfortunate propensity of vinyl phosphonate 4.4 to undergo isomerisation to an ~1:1 mixture of (*E*) and (*Z*)-vinyl phosphonates on deprotection. However arguably an increase in potency is observed on extension; since the desired (*E*)-phosphonate is at half the concentration of the total vinyl phosphonate concentration, assuming no

competition between the (*E*) and (*Z*)-forms for the active site leads to an inhibition constant of ~2.7 μM. This analysis assumes the (*Z*)-isomer is comparatively inactive. This is likely to be a reasonable assumption based on the inactivity of both acrylate 4.2 and the corresponding shortened (*Z*)-vinyl phosphonate (Figure 5.29).

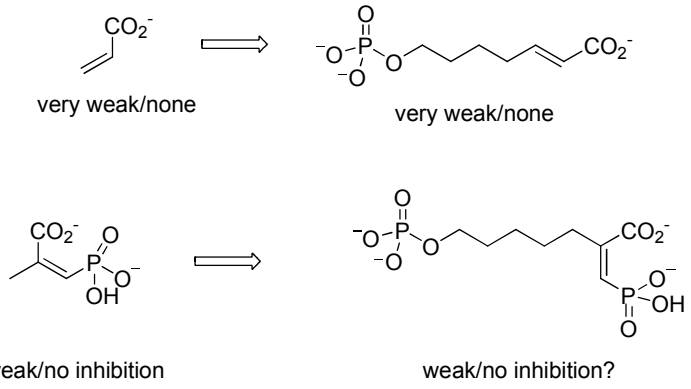

Figure 5.29: The rationale behind the proposed relative inactivity of (*Z*)-4.4

The origin of the increased potency in the extended compound is due to the phosphate group rather than the hydrocarbon linker. This is demonstrated by the bromide 4.69, which has a slight to no increase in inhibitory potency relative to parent compound 3.12. While non-covalent interactions between proteins and the halogens are known (the so called "halogen-bond"[186]), these are evidently not strong enough in this case to significantly increase the potency of bromide 4.69 relative to the parent 3.12.

5.10: Future directions for multivalent compounds

There still remain areas of investigation with these compounds. Due to its potency and stability, the extended isosteric phosphonate 4.3 will be a good basis for further investigations. Now that the potency of such compounds is established, attempts could be made to resolve the effects alkene geometry of inhibition by 4.3. Ideally it might be possible separate the different alkene isomers of 4.3, by chromatographic techniques such as silver-ion flash chromatography or preparative HPLC. Alternatively, the comparative affinities of (*Z*) and (*E*)-4.4 could be inferred by changing the relative proportion of each in the mixture. Accordingly, the proportions of alkenes in the mixture may be able to be changed by photochemical isomerisation, or by the selective destruction of one isomer by chemical resolution. Some variation in isomer

ratios may be introduced by modifying the protecting groups in phosphonylation reaction, by our proposed model (Chapter Four) larger carboxylate ester groups combined with smaller phosphite ester groups should lead to greater (*Z*)-selectivity.

The extended isosteric phosphonate 4.4 will also provide a useful scaffold to study the effect of other functionality on inhibition by DAH7P synthase. For example, will the addition of hydroxyl groups to the hydrocarbon chain in 4.4 result in increased potency, or will it lead to the complex slow binding behaviour observed with amine 2.3? The necessary compound (Figure 5.30) should be able to be prepared by substituting a protected D-*arabino* aldehyde (Chapter Two) for the simpler straight chain aldehyde used to prepare 4.3.

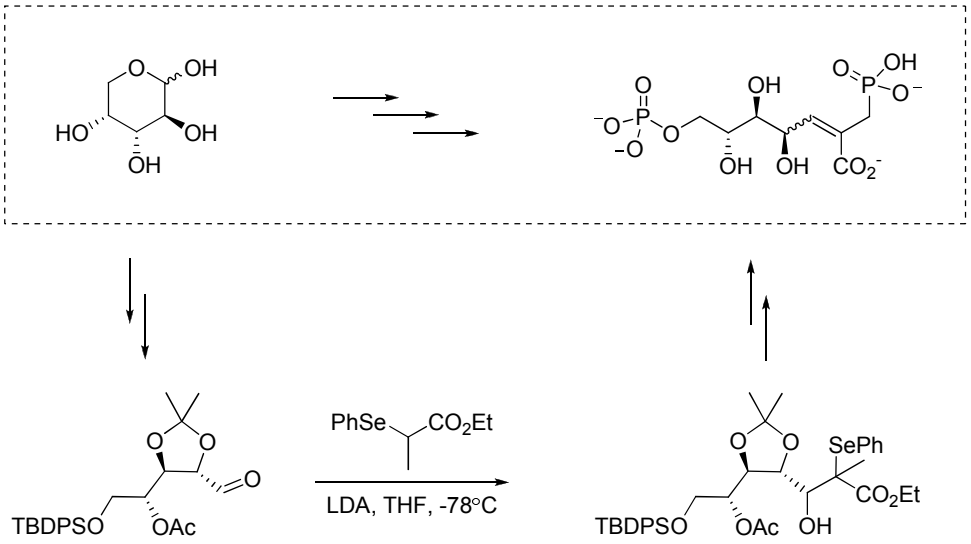

Figure 5.30: A hydroxylated form of extended isoteric phosphonate 4.4

Likewise, the influence of having metal ligands such as cyano or hydroxamate groups on the hydrocarbon linker could be investigated.

All of the syntheses in Chapter Four suffer from poor chemoselectivity of the final phosphate deprotection step; all with yields <20% and requiring expensive and time-consuming preparative anion-exchange chromatography to isolate the desired molecule from the reaction mixtures. It seems the unhindered nature of a primary phosphate group in these compounds (perhaps unsurprisingly) leads to poor

selectivity between removal of the ethyl protecting groups and cleavage of the desired C7-phosphate bond.

A number of protecting groups have been devised for phosphate groups[76]. However phosphate protecting groups are comparatively poorly investigated when compared to carboxyl ester groups, and for complex syntheses there are comparatively few precendented options. Commonly used groups such as phenyl- and benzyl phosphates are cleaved by hydrogenolysis, conditions which are not compatible with alkene containing molecules such as those in Chapter Four. In addition, the hydrogenolysis reaction can be non-trivial, especially for more complex phenyl phosphates.

Groups cleaved by reductive elimination, such as 2,2,2-trichloroethyl esters, were also excluded from use in this work; due to concerns over the susceptibility of electron deficient olefins (such as those in Chapter Four) to radical polymerisation. However, further investigation may result in suitably mild deprotection conditions allowing their use, although the careful removal of residual metal ions after deprotection will be required before assays with metal-dependent enzymes such as DAH7P synthase.

A possibility is the use of groups which are cleaved by β-elimination, such as 2-cyanoethyl and 2-(*p*-nitrophenyl)ethyl esters. These are traditionally cleaved chemoselectively by elimination with bases such as DBU[76], leading to the free phosphate and acrylonitrile or *p*-nitrostyrene respectively. Occasionally trimethylsilyl chloride is also included, to improve the rate of the second deprotection. The 2-cyanoethyl ester in particular has found considerable use in nucleoside chemistry, which shares similar problems of chemoselective deprotection. A similar group cleaved under even more specific conditions is the 2-(trimethylsilyl)ethyl ester[76], which is cleaved by nucleophilic fluoride sources to trimethylsilyl fluoride, ethylene and the desired phosphate. This group has been rarely applied in phosphate chemistry, and further experimentation may be required to elucidate suitable deprotection conditions. In addition, this group is expensive, and careful synthetic planning may be required to avoid selectivity problems with the use of synthetically valuable *tert*-butyldimethylsilyl and *tert*-butyldiphenylsilyl hydroxyl protecting groups.

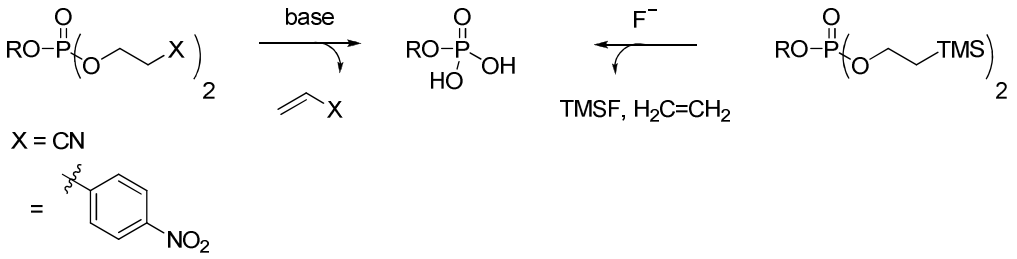

Figure 5.31: Possible improved phosphorus protecting groups for the synthesis of complex phosphorylated molecules

Further investigation of these and related groups in the synthesis of complex phosphates such as those in this work would potentially lead to greater selectivity during deprotection, and ultimately ease access to these and related molecules.

5.11: Summary

During this project, the inhibition of DAH7P synthase was investigated. A number of new inhibitors of DAH7P synthase have been prepared during this work and new strategies to achieve DAH7P synthase inhibition explored. Based on the results of this exploration, new directions for the inhibition of DAH7P synthase have been suggested, and it is hoped this work will lead to the future development of more potent DAH7P synthase inhibitors.

Chapter Six: Experimental

6.1 General Experimental

6.1.1 Solvents and Reagents

Solvents and reagents were dried by standard methods[187] where required prior to use. Tetrahydrofuran, 1,2-dimethoxyethane and diethyl ether were freshly distilled from sodium wire/ benzophenone. Dichloromethane, diisopropylamine and acetonitrile were freshly distilled from calcium hydride. Toluene was freshly distilled from sodium. Dimethylsulfoxide (DMSO) was dried azeotropically by distilling out ~25% of the volume of the undried DMSO, this fraction was discarded and the remaining DMSO distilled and stored over dried 4Å molecular sieves until further use[188]. Allyl alcohol and isopropyl alcohol were dried over 4Å molecular sieves, then distilled and stored over 4Å molecular sieves. Methanol was dried in analogous manner but using 3Å molecular sieves. Hexane was distilled from calcium hydride. Triethyl phosphite was distilled from sodium wire. Diisopropylethylamine, pyridine, diethyl oxalate and 2,6-lutidine were distilled from calcium hydride and stored over 4Å molecular sieves. Diethyl(azodicarboxylate) was cautiously vacuum distilled behind a safety shield, and stored at -20°C. Oxalyl chloride was stored frozen at -20°C. Acetic anhydride, acetyl chloride and 3-bromopyridine were distilled from calcium hydride. Benzaldehyde was vacuum distilled. Cyclohexylamine was distilled from potassium hydroxide. Cerium(III) chloride heptahydrate, diethyl chlorophosphate, magnesium powder, DBU, sodium borohydride and sodium cyanoborohydride were obtained from commercial sources, and once opened stored in a desiccator over silica. Commercial trimethylsilyl bromide was stored over fresh copper shavings in a desiccator once opened. Methyl acrylate, *n*-butyllithium solution, diisobutylaluminum hydride solution and lithium acetylide ethylenediamine complex were stored sealed at 4°C. Sodium bis(trimethylsilyl)amide solution, Grubbs first- and second-generation catalysts, Hoveyda-Grubbs first- and second-generation catalysts were stored individually sealed under argon, in a desiccator over silica. Grubbs phosphine-free catalyst was prepared as previously described[139]. The butyl Otera transesterification catalyst was prepared as previously described for the methyl analogue[132]. 2-

Iodoxybenzoic acid (IBX) was prepared by oxidation of 2-iodobenzoic acid with Oxone® as previously described[189]. Dess-Martin periodinane was prepared by acetylation of IBX with hot acetic anhydride and toluenesulfonic acid as previously described[190]. 2-(Bromomethyl)acrylic acid was prepared as previously described[191] from 2,2-bis(hydroxylmethyl) diethyl malonate[192], and dried *in vacuo* over phosphorus pentoxide prior to use in Mitsunobu reactions. Trifluoroacetic anhydride was prepared by distillation of trifluoroacetic acid from phosphorus pentoxide. (*Z*)-1,4-Diacetoxybutene was prepared by acetylation of the corresponding diol with acetic anhydride, and vacuum distilled prior to use. Ethereal hydrogen chloride was prepared by saturation of anhydrous diethyl ether with a stream of hydrogen chloride gas, prepared by reaction of ammonium chloride and concentrated sulfuric acid and dried by bubbling through further concentrated sulfuric acid. Potassium isopropoxide solutions for Darzens reactions were freshly prepared from dry isopropanol and potassium metal. Imidazole was recrystallised from distilled hexanes, and stored in a dessicator over silica. *N*-bromosuccinimide was recrystallised from water, dried over phosphorus pentoxide, and stored in the dark at 4°C. *N*-methylmorpholine *N*-oxide was recrystallised from acetone, and dried over phosphorus pentoxide under vacuum. Methyl iodide was distilled, and stored in the dark at 4°C over fresh copper shavings. Commerical Dowex resins were washed well with 1.2 M hydrochloric acid until the filtrate ran colourless; then washed with water until the filtrate ran neutral to pH paper, then air-dried before use. Dowex resins in their potassium form were prepared by washing the acidic resin well with 10% w/v potassium hydroxide, then with water until the filtrate ran neutral to pH paper, then air-dried. All other reagents were obtained from commercial sources, and used as received.

Commercial solutions of *n*-butyllithium were quantified as required by a modification of a literature procedure[193]; by titration against a known quantity of menthol in tetrahydrofuran, using catalytic 2,2'-bipyridine as an indicator under argon. Commercial sodium bis(trimethylsilyl)amide was quantified as required by a modification of a literature procedure[194], by titration with a known concentration of menthol in tetrahydrofuran, using pre-generated 2,2'-bipyridine-butyllithium adduct as an indicator under argon. In each case the concentration was taken from a mean of three concordant results.

6.1.2 Chromatography

TLC was carried out on Merck Silica Gel 60 F254 aluminum-backed sheets, and visualized under UV (254 nm), followed routinely by staining with basic aqueous potassium permanganate and heating in a stream of hot air. In some situations staining with acidified ethanolic ninhydrin (amines), acidified ethanolic vanillin (general), ethanolic phosphomolybdic acid (general) or ethanolic 2,4-dinitrophenylhydrazine (α-ketoesters) was advantageous. Flash chromatography was carried out on silica gel, 230-400 mesh. Chromatographic hexane, dichloromethane and ethyl acetate were distilled prior to use from calcium hydride; analytical grade diethyl ether, acetonitrile and methanol was used as supplied.

Anion exchange chromatography was carried out on Pharmacia SourceQ® resin, utilising a Biorad Biologic® FPLC pump, quad-wavelength detector and automated fraction collection system at 4°C.

Preparative HPLC was carried out with Waters 600 controller and Waters 2487 dual-wavelength detector, on a Rainin Instruments Dynamax® Microsorb® normal phase 21 x 250 mm column. Filtered analytical grade dichloromethane and methanol were used for HPLC.

6.1.3 Reactions and Work-ups

All reactions were carried out under an inert atmosphere of dry argon or nitrogen, unless otherwise stated. Microwave irradiations were performed in a domestic 1600 W microwave oven, modified to include a reflux condenser and inert gas source. Crude organic extracts were dried with anhydrous magnesium sulfate followed by filtration, unless otherwise stated. Evaporations were carried out on a rotary evaporator, preferably with a bath temperature of less than 40^{o}C.

6.1.4 Phosphate Assay for detection of products

The Lanzetta reagent was prepared fresh, by the following preparation:

3 parts 0.045% w/v malachite green oxalate in water
1 part 4.2% w/v ammonium molybdate in 4M HCl
0.1 parts 1.5% v/v Triton X-100

The reagents were mixed in the dark, stirred for 30 minutes and filtered through a 0.45 μm filter before use. For phosphate detection, two assays were carried out. The first determines the fractions that contain inorganic phosphate, the second fractions containing phosphate monoesters. In the first, 100 μL of sample is mixed with 700 μL of Lanzetta reagent, incubated for 20 minutes, then the absorbance determined at 630 nm . For the second, 300 μL of the sample is mixed with 10 μL calf alkaline phosphatase solution (10 units /mL, in 4 mM $MgCl_2$), and incubated for 2.5 hours. A 100 μL digest sample is mixed with 700 μL of Lanzetta reagent, incubated for 20 minutes, then the absorbance determined at 630 nm.

6.1.5 NMR Spectroscopy

NMR spectroscopy was carried out at the Institute of Fundamental Sciences, Massey University on a Bruker Avance® 400 MHz or Bruker Avance® 500 MHz NMR spectrometer, utilising a quadnuclei $^{1}H/^{13}C/^{19}F/^{31}P$ or $^{1}H/^{13}C$ inverse detection probe respectively; or at the Department of Chemistry, University of Canterbury on a Varian UNITY 300 MHz or Varian INOVA 500 MHz NMR spectrometer, utilising a standard $^{1}H/^{13}C$ probe or inverse detection $^{1}H/^{13}C$ probe respectively. ^{1}H and ^{13}C spectra are referenced to external tetramethylsilane; ^{31}P NMR spectra are referenced to external 85% phosphoric acid.

^{31}P NMR concentration determinations are performed relative to a known approximately equimolar quantity of potassium dihydrogen phosphate. Effects arising from different relaxation times were checked for prior to determination; and ^{1}H-coupled spectra were collected to avoid signal artifacts arising from NOE from the ^{1}H decoupling pulse.

6.1.6 Mass Spectrometry

High-resolution mass spectroscopy was carried out either by the Department of Chemistry at the University of Auckland, on a VG-7070 high-resolution mass spectrometer (electron ionisation, chemical ionisation, fast atom bombardment techniques); or by the Department of Chemistry at the University of Canterbury on a Micromass LCT spectrometer (positive and negative ion electrospray ionisation techniques). Unless otherwise noted, high resolution mass spectral data (HRMS) reported for compounds refers to positive ion electrospray ionisation data.

6.1.7 UV-Visible and IR Spectrometry

UV-Visible spectrophotometry was carried out on a Varian Cary® One UV-Visible spectrophotometer, in stoppered quartz cells. The temperature was continously controlled at 298 K by the use of a jacketed multicell holder, connected to an external Varian Peltier temperature controller filled with either water or ethylene glycol.
FTIR spectroscopy was conducted on a Shimadzu FTIR-8201 PC Spectrometer, either by diffuse reflectance in potassium bromide suspensions (solids) or as films between sodium chloride plates, cast from chloroform (oils).

6.1.8 Enzyme Assays

Enzyme activity was monitored by UV-Visible spectrophotometry, following the decrease in absorbance at 232 nm as the enol alkene of PEP is consumed. DAHP synthase inhibitor assays were conducted with recombinant *E. coli* DAH7P synthase (phenylalanine-repressed isozyme), which was prepared as previously described, diluted to ~2 mg mL^{-1} and stored at -80°C until required. Enzyme solutions were thawed and centrifuged (14 000 rpm/ 2 minutes) prior to use, and stored on ice during use.
The BTP buffer utilised for both activity measurements and stock solution preparation was prepared by dissolving sufficient bis-tris-propane free base in MilliQ water to give a 50 mM solution, then adjusting the pH to 6.8 with hydrochloric acid. The resulting mixture was treated with Chelex® resin for two hours, then filtered through a 0.2 μm membrane and stored at 4°C until required. Stock solutions of PEP and E4P

were prepared from monopotassium-PEP (Sigma) and sodium-E4P (Sigma) respectively, in buffer. Solutions were treated with Chelex® resin for 2 hours, and filtered through a 0.2 μm filter and stored until further use. PEP solutions were stored frozen at -20°C; to avoid problems with concentration-dependent oligomerisation E4P solutions were stored at 4°C. Stock solutions of manganese(II) sulfate, cobalt(II) chloride and iron(II) sulfate were prepared in MilliQ water at 10 mM; and were filtered through a 0.2 μm membrane and stored at 4°C until use. Inhibitor solutions were prepared in BTP buffer, and treated with Chelex® resin and filtered through a 0.2 μm filter before use.

Inhibition constants were measured by enzyme assay. Cuvettes containing PEP, E4P, manganese(II) sulfate and inhibitor in BTP buffer at 25°C were initiated by the addition of ~2 μg enzyme, the initial rate of reaction was determined by linear least-squares fitting of the change in absorbance with time. Collected initial rate data at given inhibitor and substrate concentrations were converted to positive values, and globally fitted by multivariable non-linear least squares regression using Grafit® to the Michaelis-Menten equation modified for competitive inhibition:

$$v = \frac{V_{\max}[S]}{K_m\left(1+\frac{[I]}{K_i}\right)+[S]}$$

where v = initial rate;

V_{max} = maximum rate

[S] = competitive substrate concentration

K_m = Michaelis constant in the absence of inhibitor

[I] = inhibitor concentration

K_i = inhibition constant

6.1.9 Computational Methods

All molecular modelling experiments were conducted with the Schrödinger Suite 2005. Ligands were built using Maestro, and were energy-minimised with Macromodel 9.0 using the OPLS2005 force field. Conformational searches were used

to establish representative initial ligand conformations for docking. These searches were carried out with Macromodel 9.0, by the MCMM method using a GB/SA water model and the OPLS2005 force field, with 3000 steps for the search and up to 5000 iterations for the minimisation of each structure. The minimisation was stopped with the default gradient confergence threshold of $\delta = 0.05$ kJ mol^{-1} $Å^{-1}$. The default Polak-Ribiere conjugate gradient method was used for all minimisations.

The docking grid was generated from chain A of the *E. coli* DAH7P synthase structure 1n8f.pdb, using the protein preparation function of Glide. The centre of grid was defined as the PEP ligand observed in the crystal structure, and was generated by Glide using the default settings.

The docking of flexible ligands into the grid was performed with Glide utilising the following parameters: OPLS2005 force field, extra precision mode, 9000 poses per ligand for the initial docking run, scoring window for keeping initial poses:5000, 1000 best poses per ligand kept for energy minimisation, energy minimisation with a distance dependent dielectric constant of 2 and a maximum of 5000 conjugate steps. The 10 highest scoring poses for each ligand were output for evalution.

6.2 Experimental Procedures

6.2.1: Experimental for Chapter Two

D-arabinose diethyl dithioacetal

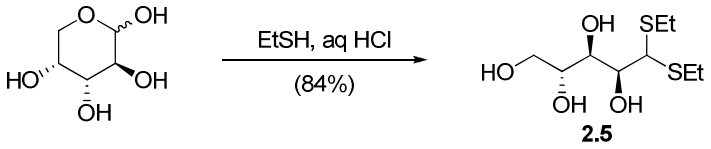

2.5

To a stirred solution of D-arabinose (10.00 g, 66.6 mmol) in aqueous 6M HCl solution (100 mL) was added ethanethiol (12.0 mL, 162 mmol). After three hours stirring at room temperature, the reaction was cooled to 4°C for two hours, and the crystalline product collected by filtration. The product was recrystallised from ethanol, and the crystals washed with a small quantity of cold hexane to give D-arabinose diethyl dithioacetal 2.5 (14.31g, 84%) as white plates. mp: 127-130°C; R_f (60% ethyl acetate/hexane): 0.14; ^{1}H NMR (400 MHz, d_4-MeOH) δ ppm. 4.08 (d, J = 9.2 Hz, 1H, H1), 4.00 (d, J = 8.5 Hz, 1H, H3), 3.87 (d, J = 9.4 Hz, 1H, H2), 3.82 (dd, J = 11.2 Hz, 3.1 Hz, 1H, H5'), 3.67 (m, 1H, H4), 3.59 (dd, J = 10.9 Hz, 5.1 Hz, 1H, H5), 2.69 (4H, m, $SC\underline{H}_2CH_3$), 1.23 (6H, m, $SCH_2C\underline{H}_3$),^{13}C NMR (101 MHz, d_4-MeOH) δ ppm 72.1 (C4), 71.7 (C3), 71.0 (C2), 64.1 (C5), 55.1 (C1), 24.3 ($S\underline{C}H_2CH_3$), 13.8 (app d, $SCH_2\underline{C}H_3$),

2,3:4,5-Di-O-isopropylidene-D-arabinose diethyl dithioacetal

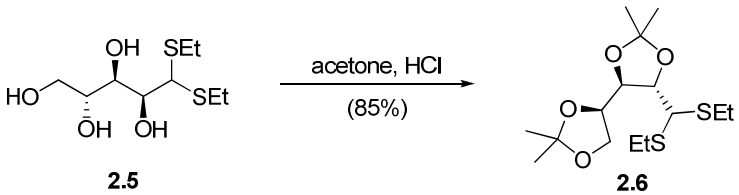

2.5 **2.6**

To a stirred solution of polyol 2.5 (1.217 g, 4.77 mmol) in acetone (35 mL) was added concentrated hydrochloric acid (600 μL), and the mixture was stirred under a drying tube for 5 hours. The solution was dried, filtered through a plug of anhydrous potassium carbonate and evaporated. Flash chromatography (20% ether/hexane) gave

diisopropylidene acetal 2.6 as a colourless oil (1.363g, 85%) with data as reported in the literature[195]. R_f (40% ether/hexane) 0.76, ^{1}H NMR (400 MHz, $CDCl_3$) δ ppm: 4.30 (m, 1H, H2), 4.14 (m, 1H, H5'), 4.08 (m, 2H, H3 & H4), 4.04 (d, J = 2.7 Hz, 1H, H1), 3.97 (dd, J = 8.4, 4.3 Hz, 1H, H5), 2.74 (m , 6H, 2x $SC\underline{H}_2CH_3$), 1.45 (s, 3H, $C\underline{Me}_2$), 1.42 (s, 3H, $C\underline{Me}_2$), 1.38 (s, 3H, $C\underline{Me}_2$), 1.30 (s, 3H, $C\underline{Me}_2$), 1.27 (m, 6H, 2x $SCH_2C\underline{H}_3$) ^{13}C NMR (101 MHz, $CDCl_3$) δ ppm 110.2 ($\underline{C}Me_2$), 109.7 ($\underline{C}Me_2$), 84.4 (C2), 79.1 (C4), 77.1 (C3), 67.8 (C5), 52.4 (C1), 27.3 ($C\underline{Me}_2$), 27.1 ($C\underline{Me}_2$), 26.6 ($C\underline{Me}_2$), 25.2 (app d, $S\underline{C}H_2CH_3$), 24.9 ($C\underline{Me}_2$), 14.4 (app d, $SCH_2\underline{C}H_3$), HRMS (EI): Required for $C_{15}H_{28}O_4S_2$: 336.14290; Found 336.14258

Ethyl 2-(((4*S*,4'*R*,5*R*)-2,2,2',2'-tetramethyl-4,4'-bi(1,3-dioxolan)-5-yl) methylamino) acetate – Mercury Route

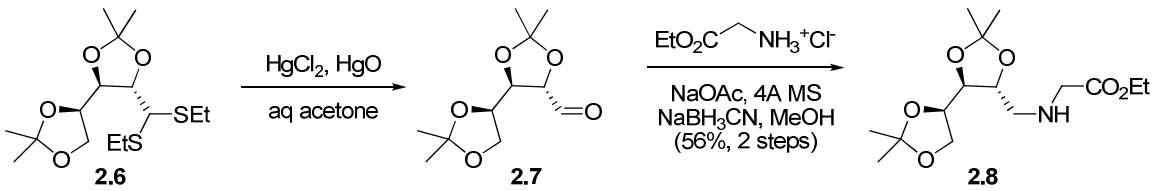

To a vigorously solution of dithioacetal 2.6 (3.496 g, 10.4 mmol) in acetone (40.5 mL) and water (4.5 mL) was added red mercury(II) oxide (5.643 g, 26.0 mmol) and mercury(II) chloride (7.074 g, 26.0 mmol). After 22 hours, the suspension was filtered through celite, and evaporated. The residue was suspended in chloroform (60 mL), filtered, and washed with 1M aqueous potassium iodide (4x 60 mL), 50% saturated sodium thiosulfate (2x 60 mL), brine (60 mL), dried and evaporated. (NB: the celite, chloroform precipitate and KI washes contain mercury compounds, and should be disposed of accordingly).

The resulting yellow oil (2.067 g, 8.98 mmol, assuming pure aldehyde) was dissolved in methanol (36 mL), and anhydrous sodium acetate (1.483 g, 18.1 mmol), ethyl glycinate hydrochloride (1.253 g, 8.98 mmol) and activated 4Å molecular sieves (9.023 g) were each added, and the mixture stirred under nitrogen for 45 minutes. Sodium cyanoborohydride (1.142 g, 18.2 mmol) was added, and stirred for 16 hours. The mixture was then filtered through celite, and the celite washed with methanol. The filtrate was evaporated, the residue dissolved in 60 mL chloroform, washed with 50% saturated potassium carbonate (2x 60 mL), brine (60 mL), dried and evaporated.

Flash chromatography (40% ethyl acetate/hexane) gave secondary amine 2.8 as a colourless oil (1.767 g, 54% over two steps). R_f (80% ethyl acetate/hexane) 0.56; ^{1}H NMR (400 MHz, $CDCl_3$) δ ppm 4.18 (q, J =: 7.2 Hz, 2H, $CO_2C\underline{H}_2CH_3$), 4.11 (m, 1H, H5'), 4.04 (m, 2H, H2 & H4), 3.93 (dd, *J* = 8.5 Hz, 5.1 Hz, 1H, H5), 3.67 (t, *J* = 8.1 Hz, 1H, H3), 3.45 (d, *J* = 3.4 Hz, 2H, $NC\underline{H}_2CO_2Et$), 2.97 (dd, *J* = 12.2 Hz, 3.4 Hz, 1H, H1), 2.77 (dd, *J* = 12.3 Hz, 6.8 Hz, 1H, H1), 1.95 (br s, N<u>H</u>), 1.35 (s, 2x $C\underline{Me}_2$, 6H), 1.35 (s, 3H, $C\underline{Me}_2$), 1.33 (s, 3H, $C\underline{Me}_2$), 1.27 (app q, *J* = 3.4 Hz, 3H, $CO_2CH_2C\underline{H}_3$) ^{13}C NMR (101 MHz, $CDCl_3$) δ ppm 171.1 ($\underline{C}O_2CH_2CH_3$), 109.6 ($\underline{C}Me_2$), 109.3 ($\underline{C}Me_2$), 80.2 (C2), 79.2 (C3), 77.1 (C4), 67.8 (C5), 60.3 ($CO_2\underline{C}H_2CH_3$), 51.5 (C1), 51.1 ($N\underline{C}H_2CO_2Et$), 27.2 ($C\underline{Me}_2$), 26.9 ($C\underline{Me}_2$), 26.6 ($C\underline{Me}_2$), 25.2 ($C\underline{Me}_2$), 14.2 ($CO_2CH_2\underline{C}H_3$), HRMS (FAB, *m*-nitrobenzyl alcohol matrix): Required for $C_{15}H_{27}NO_6$: 318.19166; Found 318.19139

Ethyl 2-(((4*S*,4'*R*,5*R*)-2,2,2',2'-tetramethyl-4,4'-bi(1,3-dioxolan)-5-yl)methylamino) acetate – Iodine Route

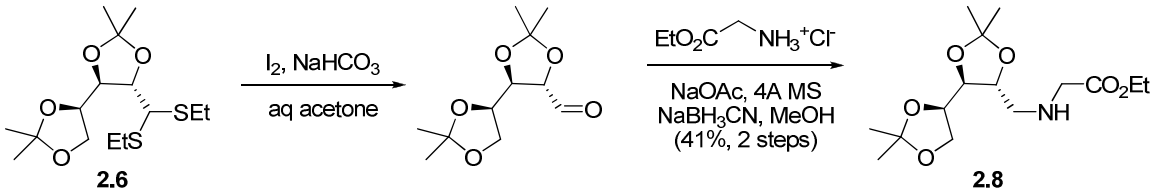

To a vigorously solution of dithioacetal 2.6 (1.610 g, 4.79 mmol) in acetone (33 mL) was added water (750 μL, 41.7 mmol), sodium hydrogen carbonate (1.780 g, 21.2 mmol) and iodine (2.658 g, 10.5 mmol) and the dark mixture stirred overnight. Saturated aqueous sodium thiosulfate was added until the stirred brown solution became colourless, and the solution volume was reduced by around a third on a rotary evaporator. Brine was added to give a volume of 50 mL, and the solution was extracted with ethyl acetate (4x 40 mL). The combined organic fractions were washed with brine, dried and evaporated. The resulting yellow oil (1.791 g, 7.78 mmol, assuming pure aldehyde) was dissolved in methanol (20 mL), and anhydrous sodium acetate (0.840 g, 10.2 mmol), ethyl glycinate hydrochloride (0.701 g, 5.02 mmol) and activated 4Å molecular sieves (5.076 g) were added, and stirred under nitrogen for 30 minutes, then sodium cyanoborohydride (0.642 g, 10.2 mmol) was added, and stirred

for 17 hours. The mixture was then filtered through celite, and the celite plug washed with methanol. The filtrate was evaporated, dissolved in chloroform (30 mL) and water (10 mL), the organic layer separated, and the aqueous washed with further chloroform (30 mL). The combined organic layers were washed with saturated aqueous potassium carbonate (60 mL), brine (60 mL), dried and evaporated. Flash chromatography (40% ethyl acetate/hexane) gave secondary amine 2.8 as a colourless oil (0.654 g, 41% over two steps), with analytical data identical to that reported above.

Diethyl hydroxymethylphosphonate[78]

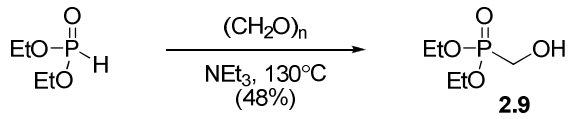

2.9

To stirred diethyl phosphite (6.44 mL, 50.5 mmol) in a 25 mL round bottom flask under nitrogen (a large flask is required to contain the foam produced in the reaction) was added finely ground paraformaldehyde (1.56 g, 52.0 mmol as CH_2O) and dry triethylamine (0.70 mL, 5.02 mmol), and the flask (with condenser) was placed in a 120°C oil bath, and stirred for 4 hours (caution: reaction can initiate violently), then cooled to room temperature and evaporated at 80°C (rotary evaporator) to remove excess formaldehyde. Dichloromethane (20 mL) was added, and the organic layer was washed with saturated ammonium chloride (2x 20 mL), saturated potassium carbonate (2x 20 mL), dried and evaporated to give phosphonate alcohol 2.9 (4.094 g, 48%) as a colourless oil, approximately 85% pure by ^{31}P NMR, which was used without further purification. Key data: ^{1}H NMR (400 MHz, CDCl3) δ ppm 4.71 (br, 1H, $PCH_2O\underline{H}$), 4.03 (app p, *J* = 7.0 Hz, 4H, $POC\underline{H}_2CH_3$), 3.79 (d, 2H, *J* = 6.1 Hz, $PC\underline{H}_2OH$), 1.22 (t, 6H, *J* = 7.1 Hz, $POCH_2C\underline{H}_3$); ^{13}C NMR (101 MHz, $CDCl_3$) δ ppm 62.9 (d, *J* = 6.7 Hz, $PO\underline{C}H_2CH_3$), 57.1 (d, *J* = 162.8 Hz, $P\underline{C}H_2OH$), 16.8 (d, *J* = 5.7 Hz, $POCH_2\underline{C}H_3$); ^{31}P NMR (162 MHz, ^{1}H-decoupled, $CDCl_3$) δ ppm -25.7 ($\underline{P}CH_2OH$).

(Diethoxyphosphonyl)methyl trifluoromethanesulfonate[79]

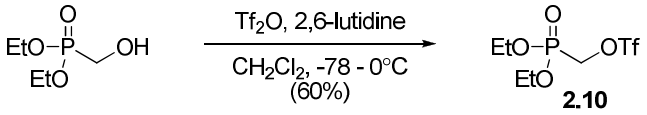

To a stirred solution of alcohol 2.9 (2.01 g, 11.94 mmol) and dry 2,6-lutidine (1.70 mL, 30.6 mmol) in dry dichloromethane (20 mL) under nitrogen at –78°C was added triflic anhydride (2.30 mL, 13.7 mmol), and stirring was continued for 1.5 hours, over which time the cold-bath was allowed to warm to –20°C. The cold bath was replaced with an ice-bath, and stirring continued for another 1.5 hours. The brown reaction mixture was poured into diethyl ether (150 mL), and cooled to –20°C for 1 hour, the crystallised lutidinium triflate filtered, and the filtrate was washed with water (3x 150 mL), 1.2M HCl solution (2x 150 mL), brine (150 mL), dried and evaporated to give triflate 2.10 (2.141 g, 60%) as a yellow oil, which was ~80% pure by ^{19}F NMR spectroscopy, and was used as such without further purification. Key data: ^{1}H NMR (400 MHz, $CDCl_3$) δ ppm 4.57 (d, 2H, *J* = 8.7 Hz, $PC\underline{H}_2OTf$), 4.18 (app p, *J* = 7.0 Hz, 4H, $POC\underline{H}_2CH_3$), 1.35 (t, *J* = 7.0 Hz, 6H, $POCH_2C\underline{H}_3$ ^{13}C NMR (101 MHz, $CDCl_3$) δ ppm 118.9 (d, *J* = 318.3 Hz, $OS(O)_2\underline{C}F_3$), 66.7 (d, *J* = 169.2 Hz, $P\underline{C}H_2OTf$), 64.6 (d, *J* = 6.5 Hz, $PO\underline{C}H_2CH_3$), 16.6 (d, *J* = 5.3 Hz, $POCH_2\underline{C}H_3$);); ^{31}P NMR (162 MHz, ^{1}H-decoupled, $CDCl_3$) δ ppm -13.5 ($\underline{P}CH_2OTf$); ^{19}F NMR (376 MHz, $CDCl_3$) δ ppm -79.32 ($OS(O)_2C\underline{F}_3$).

Ethyl 2-(((diethoxyphosphonyl)methyl)(((4*S*,4'*R*,5*R*)-2,2,2',2'-tetramethyl-4,4'-bi(1,3-dioxolan)-5-yl)methyl)amino)acetate

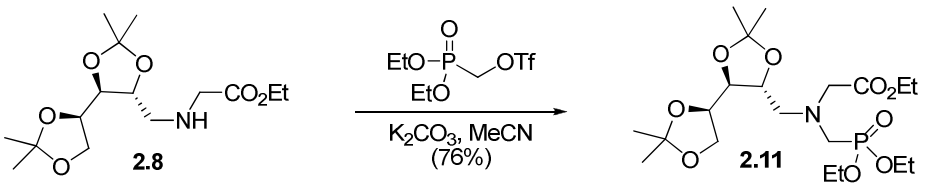

To a stirred solution of secondary amine 2.8 (299 mg, 0.941 mmol) in dry acetonitrile (7 mL) under argon was added anhydrous potassium carbonate (502 mg, 3.63 mmol) and triflate 2.10 (271 mg, 0.722 mmol at 80%), and stirring was continued for 4

hours. The suspension was filtered, the filtrate evaporated and suspended in chloroform (25 mL) with the aid of a sonicator. The chloroform phase was washed with 2% w/v sodium hydroxide (25 mL), and the aqueous phase extracted with further chloroform (25 mL). The combined organic extracts were washed with brine (50 mL), dried and evaporated. Flash chromatography (step-gradient, 200 mL 40% ethyl acetate/hexane, then 60% ethyl acetate/hexane) gave tertiary amine 2.11 as a colourless syrup (258 mg, 76%). R_f (10% methanol/chloroform) 0.88. ^{1}H NMR (400 MHz, $CDCl_3$) δ ppm 4.09 (m, 7H, H5', 2x P(O)OC$\underline{H}_2$CH$_3$ & CO$_2$C$\underline{H}_2$CH$_3$), 3.99 (m, 2H, H2 & H4), 3.86 (dd, 1H, *J* = 8.4 Hz, 5.3 Hz, H5), 3.68 (dd, 2H, *J* = 24.8 Hz; 17.9 Hz, NC$\underline{H}_2$P), 3.26 (dd, 2H, *J* = 9.7 Hz, 1.7 Hz, NC$\underline{H}_2$CO$_2$Et), 3.09 (br d, 1H, *J* = 14.2 Hz, H1'), 2.92 (dd, 1H, *J* = 14.0 Hz, 7.2 Hz, H1), 1.34 (s, 3H, C$\underline{Me}_2$), 1.31 (s, 3H, C$\underline{Me}_2$), 1.27 (m, 12H, 2x C$\underline{Me}_2$, 2x P(O)OCH$_2$C$\underline{H}_3$), 1.21 (t, 3H, *J* = 7.2 Hz, CO$_2$CH$_2$C$\underline{H}_3$); ^{13}C NMR (101 MHz, $CDCl_3$) δ ppm 109.6, (C$\underline{Me}_2$), 109.4 (C$\underline{Me}_2$), 80.5 (C2), 78.9 (C3), 77.0 (C4), 67.6 (C5), 61.9 (app dd, 2x P(O)OC$\underline{H}_2$CH$_3$), 60.2 (CO$_2$C$\underline{H}_2$CH$_3$), 58.3 (d, *J* = 10.3 Hz, C1), 55.8 (d, *J* = 3.7 Hz, NC$\underline{H}_2$CO$_2$Et), 50.3 (d, *J* = 160.1 Hz, NC$\underline{H}_2$P), 27.1 (C$\underline{Me}_2$), 26.9 (C$\underline{Me}_2$), 26.6, (C$\underline{Me}_2$), 25.2 (C$\underline{Me}_2$), 16.5 (d, *J* = 5.5 Hz, P(O)OCH$_2$C$\underline{H}_3$), 14.3 (CO$_2$CH$_2$C$\underline{H}_3$); ^{31}P NMR (162 MHz, $CDCl_3$, ^{1}H-coupled) δ ppm 25.2, (sept, *J* = 8.8 Hz, CH$_2$P(O)OEt) HRMS: Required $C_{20}H_{38}NO_9P$: 467.22842 Found: 467.22834.

(2*S*,3*R*,4*R*)-5-(*Tert*-butyldiphenylsilyloxy)-1,1-bis(ethylthio)pentane-2,3,4-triol

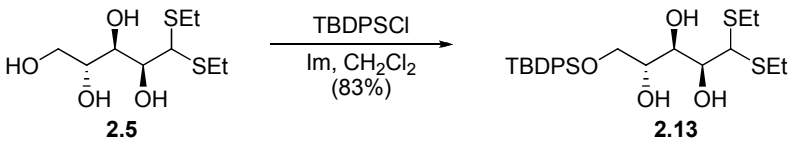

2.5 **2.13**

To a vigorously stirred solution of 2.5 (0.660 g, 2.59 mmol) in dry dichloromethane (20 mL) under nitrogen was added imidazole (0.361 g, 5.30 mmol), the solution was cooled to 0°C, and *tert*-butyl diphenylchlorosilane (0.70 mL, 2.73 mmol) was added dripwise. The solution was allowed to warm to room temperature; after 23 hours the solution was evaporated, and the residue taken up in chloroform (25 mL). The chloroform solution was washed with water (3x 25 mL) and dried and evaporated. Flash chromatography (25% ethyl acetate/ hexane) gave 2.13 as an oil, that solidifies to a waxy white solid on standing under high vacuum (1.07 g, 83%). R_f (25% ethyl

acetate/ hexane): 0.33; ^{1}H NMR (400 MHz, $CDCl_3$) δ ppm 7.66 (m, 4H, $\underline{Ph}_2Si$), 7.38 (m, 6H,$\underline{Ph}_2Si$), 4.06 (m, 2H, H1 & H4), 3.84 (m, 3H, H5,H5'& H2), 3.76 (dd, *J* = 7.3 Hz, 4.7 Hz, 1H, H3), 2.67 (m, 4H, $SC\underline{H}_2CH_3$), 1.25 (t, *J* = 7.4 Hz, 6H, $SCH_2C\underline{H}_3$), 1.04 (s, 9H, $\underline{Me}_3CSi$); ^{13}C NMR (101 MHz, $CDCl_3$) δ ppm 136.0 ($\underline{Ph}_2Si$), 133.4 ($\underline{Ph}_2Si$); 130.3 ($\underline{Ph}_2Si$); 128.2 ($\underline{Ph}_2Si$); 72.8 (C3), 70.8, 70.4, (C2, C4), 65.1 (C5), 56.1 (C1), 27.3 ($C\underline{Me}_3$); 26.0 ($S\underline{C}H_2CH_3$), 23.9 ($S\underline{C}H_2CH_3$), 15.0 (s, $SCH_2\underline{C}H_3$), 14.9 ($SCH_2\underline{C}H_3$); HRMS (EI, positive ion) calculated for $C_{25}H_{38}O_4SiS_2$ 494.198082, found 494.196335.

(2*S*,3*R*,4*R*)-5-(*Tert*-butyldiphenylsilyloxy)-1,1-bis(ethylthio)pentane-2,3,4-triyl triacetate

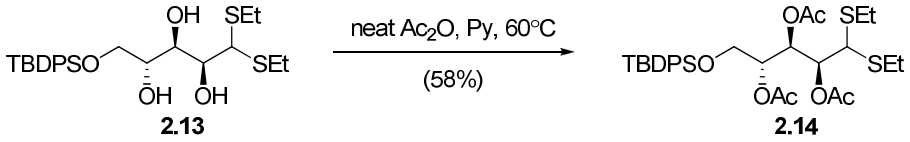

2.13 **2.14**

To a stirred solution of triol 2.13 (1.116 g, 2.26 mmol) in pyridine (15 mL) was added acetic anhydride (10 mL) and a catalytic quantity of DMAP. The mixture was heated to 60°C, and after 16 hours the mixture was cooled to 0°C, and methanol (20 mL) was added dropwise, the mixture stirred for 30 minutes then concentrated to approximately 20 mL. The residue was diluted with diethyl ether (40 mL), and extracted with 1.2M HCl solution (3x 60 mL), 10% w/v sodium hydroxide (2x 60 mL), water (2x 60 mL), brine (60 mL), dried and evaporated. The residue was separated by flash chromatography (40% diethyl ether/hexane) to give triacetate 2.14 (0.814 g, 58%) as a colourless oil. R_f (25% ethyl acetate/hexane) 0.55; ^{1}H NMR (400 MHz, $CDCl_3$) δ ppm 7.61 (m, 4H, Ph_2Si), 7.36 (m, 6H, Ph_2Si), 5.82 (dd, *J* = 7.7, 2.6 Hz, 1H, H3), 5.28 (dd, *J* = 7.9, 2.7 Hz, 1H, H2), 5.08 (m, 1H, H4), 3.85 (d, *J* = 7.9 Hz, 1H, H1), 3.68 (m, 2H, H5H5'), 2.59 (m, 2x $SC\underline{H}_2CH_3$), 2.06 (s, 3H, $C(O)C\underline{H}_3$), 1.99 (s, 3H, $C(O)C\underline{H}_3$), 1.97 (s, 3H, $C(O)C\underline{H}_3$), 1.18 (m, 2x $SCH_2C\underline{H}_3$), 1.00 (s, 9H, $\underline{Me}_3CSi$); ^{13}C NMR: (101 MHz, $CDCl_3$) δ ppm 170.4 ($\underline{C}(O)CH_3$), 170.3 ($\underline{C}(O)CH_3$), 169.9 ($\underline{C}(O)CH_3$), 136.1 ($\underline{Ph}_2Si$), 133.4 ($\underline{Ph}_2Si$), 130.1 (Ph_2Si), 128.2 (Ph_2Si), 71.7 (C4), 71.3 (C2), 70.1 (C3), 62.7 (C5), 52.6 (C1), 27.0 ($\underline{Me}_3CSi$), 25.4 ($S\underline{C}H_2CH_3$), 25.3 ($S\underline{C}H_2CH_3$), 21.3 (2x $C(O)\underline{C}H_3$), 21.4 ($C(O)\underline{C}H_3$), 19.6 ($Me_3\underline{C}Si$), 14.6 ($SCH_2\underline{C}H_3$), 14.5 ($SCH_2\underline{C}H_3$).

2,3 -O-isopropylidene-D-arabinose diethyl dithioacetal

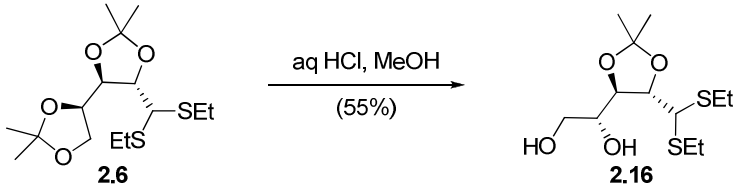

To a solution of diacetonide 2.6 (1.506 g, 4.19 mmol) in methanol (10 mL) was added a 1M aqueous HCl solution (1 mL, 1 mmol), and the resulting solution was stirred at 50°C. After 45 minutes the solution was neutralised by the addition of saturated aqueous sodium bicarbonate solution, and the solvent evaporated. The resulting residue was suspended in dichloromethane and water, filtered to remove precipitated tetraol 2.5, the organic phase separated, and the aqueous phase extracted with dichloromethane. The combined organic phases were dried and evaporated, and the resulting oil separated by flash chromatography (40% ethyl acetate/hexane) to give recovered starting diacetonide 2.6 (96.6 mg, 6%) and diol 2.16 (689.5 mg, 55%) with spectral data as reported in the literature[195]. R_f (40% ethyl acetate / hexane): 0.29; ^{1}H NMR (400 MHz, $CDCl_3$) δ ppm 4.32 (dd, *J* = 6.9 Hz, 3.7 Hz, 1H, H2), 4.08 (t, *J* = 7.2 Hz, 1H, H3), 4.02 (d, *J* = 3.7 Hz, 1H, H1), 3.81 (dd, *J* = 11.2, 3.2 Hz , 1H, H5'), 3.74 (m, 1H, H4), 3.67 (dd, *J* = 11.2, 5.7 Hz 1H, H5), 3.15 (br s, 2H, C4O<u>H</u> & C5O<u>H</u>), 2.72 (m, 4H, 2x S<u>C</u>H$_2$CH$_3$), 1.44 (s, 3H, C<u>Me</u>$_2$), 1.36 (s, 3H, C<u>Me</u>$_2$), 1.26 (t *J* = 7.3 Hz, 3H, SCH$_2$C<u>H</u>$_3$), 1.25 (t, *J* = 7.3 Hz, 3H, SCH$_2$<u>CH</u>$_3$); ^{13}C NMR (101 MHz, $CDCl_3$) δ ppm 110.1 (<u>C</u>Me$_2$), 83.3 (C2), 79.2 (C3), 73.1 (C4), 64.0 (C5), 53.2 (C1), 27.3 (C<u>Me</u>$_2$), 27.1 (C<u>Me</u>$_2$), 25.4 (S<u>C</u>H$_2$CH$_3$), 25.1 (S<u>C</u>H$_2$CH$_3$), 14.4 (2x SCH$_2$<u>CH</u>$_3$); HRMS (EI): Required for $C_{12}H_{24}O_4S_2$: 296.11160; Found: 296.11143.

2,3-O-isopropylidene-4-(O-acetyl) -5-*(tert*-butyldiphenylsilyloxy) D-arabinose diethyl dithioacetal

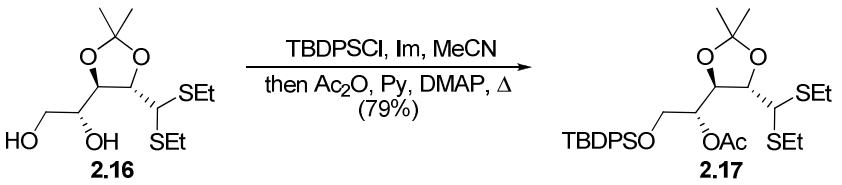

To a solution of diol 2.16 (689.5 mg, 2.33 mmol) in acetonitrile (21 mL) at 0°C under argon was added imidazole (329.8 mg, 4.84 mmol) and *tert*-butyldiphenylsilyl

chloride (630 μL, 2.42 mmol). The solution was stirred overnight, and the temperature was slowly allowed to rise to room temperature by melting of the ice-bath. Acetic anhydride (1.5 mL, 15.9 mmol), dry pyridine (3 mL, 37.2 mmol) and 4-(dimethylamino)pyridine (154 mg, 1.26 mmol) were added, and the solution brought to reflux under argon. After 3 hours at reflux, the solution was cooled and methanol (5 mL) was added, after 10 minutes solution was evaporated. The residue was taken up in dichloromethane (25 mL), washed with saturated ammonium chloride (3x 25 mL), saturated sodium bicarbonate solution (1x 25 mL), saturated sod ium chloride solution (1x 25 mL), dried and evaporated. The residue was separated by flash chromatography (20% diethyl ether/ hexane) to give arabinose derivative 2.17 (1.054g, 79%) as a colourless oil, with spectral data as reported in the literature[195]. R_f (40% ether/ hexane): 0.70; ^{1}H NMR (400 MHz, $CDCl_3$) δ ppm 7.65 (d, *J* = 7.0 Hz, 4H, Si$\underline{Ph}_2$), 7.38 (m, 6H, Si$\underline{Ph}_2$), 5.11 (m, 1H, H4), 4.40 (t, *J* = 6.9 Hz, 1H, H3), 4.29 (m, 1H, H2), 3.92 (dd, *J* = 11.3, 3.56 Hz, 1H, H5'), 3.84 (m, 2H, H1 & H5), 2.69 (m, 4H, 2x S$\underline{CH}_2CH_3$), 2.04 (s, 3H, OC(O)$\underline{Me}$), 1.43 (s, 3H, $\underline{Me}_2C$), 1.31 (s, 3H, $\underline{Me}_2C$), 1.24 (t, *J* = 7.4Hz, 6H, 2x $SCH_2C\underline{H}_3$), 1.04 (s, 9H, $\underline{Me}_3C$); ^{13}C NMR (101 MHz, $CDCl_3$) δ ppm 170.0 (O$\underline{C}$(O)Me), 135.6 (d, *J* = 2.8 Hz, PhSi), 133.2 (PhSi), 129.8 (*J* = 5.1 Hz, PhSi), 127.7 (d, *J* = 1.5 Hz, PhSi), 110.6 ($\underline{C}Me_2$), 82.7 (C2), 77.1 (C3), 74.7 (C4), 62.7 (C5), 53.5 (C1), 27.2 ($\underline{Me}_2C$), 27.2 ($\underline{Me}_2C$), 26.7 ($\underline{Me}_3C$), 25.3 (S$\underline{CH}_2CH_3$), 25.1 (S$\underline{CH}_2CH_3$), 21.1 (OC(O)$\underline{Me}$), 19.2 ($Me_3\underline{C}$), 14.4 (2x $SCH_2\underline{CH}_3$); HRMS (FAB, m-nitrobenzyl alcohol matrix): Required for $C_{30}H_{45}O_5SiS_2$: 577.24777; Found: 577.24678.

Ethyl 2-(((4*R*,5*S*)-5-((*R*)-1-acetoxy-2-(*tert*-butyldiphenylsilyloxy)ethyl)-2,2-dimethyl-1,3-dioxolan-4-yl)methylamino)acetate

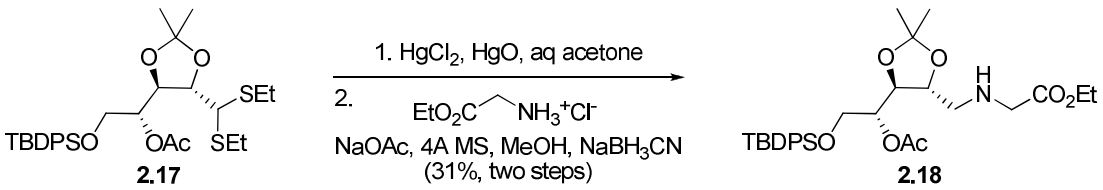

To a vigorously solution of dithioacetal 2.17 (238.3 mg, 0.413 mmol) in acetone (1.58 mL) was added water (175 μL), red mercury(II) oxide (209.2 mg, 0.966 mmol) and mercury(II) chloride (288.3 mg, 1.062 mmol). After 15 hours, the suspension was

filtered through celite, and the filtrate evaporated. The residue was resuspended in chloroform (20 mL), filtered, and washed with 1M aqueous potassium iodide (2x 20 mL), 50% saturated aqueous sodium thiosulfate solution (20 mL), brine (20 mL), dried and evaporated. (NB: the celite, chloroform precipitate and KI washes contain mercury compounds, and should be disposed of accordingly).

The resulting yellow oil (129.2 mg, 0.275 mmol assuming pure aldehyde) was dissolved in methanol (1.2 mL), and anhydrous sodium acetate (46.9 mg, 0.572 mmol), ethyl glycinate hydrochloride (38.6 mg, 0.277 mmol) and activated 4A molecular sieves (277 mg) were added, and stirred under nitrogen for 50 minutes, then sodium cyanoborohydride (43.9 mg, 0.699 mmol) was added, and stirred for 15 hours. The mixture was then filtered through celite, and the celite plug washed with methanol. The filtrate was evaporated, dissolved in dichloromethane and saturated sodium bicarbonate solution, the organic phase was separated, and the aqueous phase washed with dichloromethane. The combined organic phases were washed with brine, dried and evaporated. Flash chromatography (50% ethyl acetate/ hexane) gave secondary amine 2.18 (72.1 mg, 31% over two steps) as a colourless oil. R_f (40% ethyl acetate/ hexane): 0.33; ^{1}H NMR (400 MHz, $CDCl_3$) δ ppm 7.67 (dm, J = 7.2 Hz, 4H, Si$\underline{Ph}_2$), 7.40 (m, 6H, Si$\underline{Ph}_2$), 5.10 (m, 1H, H4), 4.20 (q, J = 7.2 Hz, 2H, $CO_2C\underline{H}_2CH_3$), 4.07 (dt, J = 7.5, 2.8 Hz, 1H, H2), 4.00 (m, 1H, H3), 3.87 (m, 2H, H5H5'), 3.43 (s, 2H, $N\underline{C}H_2CO_2Et$), 2.87 (dd, J = 12.3, 3.0 Hz, 1H, H1'), 2.74 (dd, J = 12.4, 7.3 Hz, 1H, H1), 2.06 (s, 3H, OC(O)$\underline{Me}$), 1.86 (br s, N$\underline{H}$), 1.40 (s, 3H, $\underline{Me}_2C$), 1.33 (s, 3H, $\underline{Me}_2C$), 1.28 (t, J = 7.2 Hz, 3H, $CO_2CH_2C\underline{H}_3$), 1.05 (s, 9H, $\underline{Me}_3C$); ^{13}C NMR (101 MHz, $CDCl_3$) δ ppm 172.2 ($\underline{C}O_2CH_2CH_3$), 170.1, (O$\underline{C}$(O)Me), 135.6 (d, J = 4.4 Hz, PhSi), 133.2 (*p*-PhSi), 129.8 (d, J = 5.9 Hz, PhSi), 127.7 (d, J = 2.5 Hz, PhSi), 109.6 ($Me_2\underline{C}$), 78.5 (C2), 76.5 (C3), 74.4 (C4), 62.8 (C5), 60.7 ($CO_2\underline{C}H_2CH_3$), 52.0 (C1), 51.0 ($N\underline{C}H_2CO_2Et$), 27.2 ($\underline{Me}_2C$), 26.8 ($\underline{Me}_2C$), 26.7 ($\underline{Me}_3C$), 21.0 (OC(O)$\underline{Me}$), 19.2 ($Me_3\underline{C}$), 14.2 $CO_2CH_2\underline{C}H_3$; HRMS (FAB$^+$, m-nitrobenzyl alcohol matrix): Required for $C_{30}H_{44}NO_7Si$: 558.28871; Found: 558.28856.

Ethyl 2-((((4*R*,5*S*)-5-((*R*)-1-acetoxy-2-(*tert*-butyldiphenylsilyloxy)ethyl)-2,2-dimethyl-1,3-dioxolan-4-yl)methyl)((diethoxyphosphonyl)methyl)amino)acetate

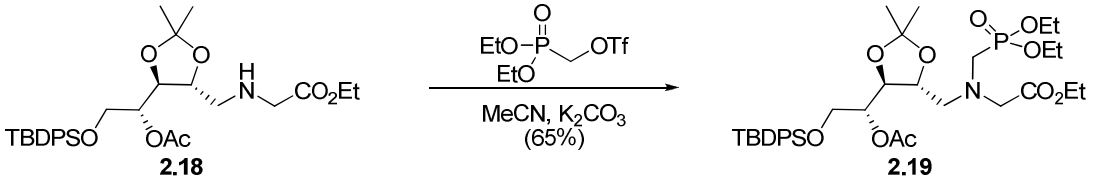

To a stirred solution of secondary amine 2.18 (136 mg, 0.244 mmol) in dry acetonitrile (1.8 mL) under argon was added anhydrous potassium carbonate (133.2 mg, 0.964 mmol) and fresh diethyl phosphonomethyl triflate (80.7 mg, 0.215 mmol at 80%). After 18 hours stirring, the solution was filtered through a celite plug, and the filtrate evaporated. The residue was resuspended in chloroform (25 mL) and saturated aqueous sodium bicarbonate solution (10 mL), the organic phase separated, washed with brine (10 mL), dried and evaporated. The residue was separated by column chromatography (60% ethyl acetate/hexane) to give tertiary amine 2.19 (90.1 mg, 65%) as a colourless oil. R_f (40% ethyl acetate/hexane): 0.17; ^{1}H NMR (400 MHz, $CDCl_3$) δ ppm 7.61 (dm, *J* = 7.0 Hz, 4H, Si$\underline{Ph}_2$), 7.35 (m, 6H, Si$\underline{Ph}_2$), 5.03 (m, 1H, H4), 4.08 (m, 7H, H2 & $CO_2\underline{CH}_2CH_3$ & 2x P(O)O$\underline{CH}_2CH_3$), 3.83 (m, 3H, H3 & H5H5'), 3.67 (dd, 2H, *J* =, 36.4, 18.0 Hz, N$\underline{CH}_2$P), 3.24 (m, 2H, N$\underline{CH}_2CO_2$Et), 2.96 (m, 2H, H1H1'), 2.03 (s, 3H, OC(O)$\underline{Me}$), 1.32 (s, 3H, $\underline{Me}_2$C), 1.27 (m, 9H, 2x P(O)OCH$_2\underline{CH}_3$ and $\underline{Me}_2$C), 1.22 (t, *J* = 7.2 Hz, 3H, $CO_2CH_2\underline{CH}_3$), 1.00, (s, 9H, $\underline{Me}_3$C); ^{13}C NMR (101 MHz, $CDCl_3$) δ ppm 171.1 (d, *J* = 1.46 Hz, $\underline{C}O_2CH_2CH_3$), 170.2 (O$\underline{C}$(O)Me), 135.6 (d, *J* = 3.2 Hz, PhSi), 133.2 (PhSi), 129.7 (d, *J* = 5.2 Hz, PhSi), 127.7 (d, *J* = 2.7 Hz, PhSi), 109.7, $Me_2\underline{C}$, 79.0, (C2), 76.2 (C3), 74.5 (C4), 62.9 (C5), 62.0 (dd, *J* = 7.0 Hz, 2x P(O)O$\underline{CH}_2CH_3$), 60.2, $CO_2\underline{CH}_2CH_3$, 58.5 (d, *J* = 11.1 Hz, C1), 55.7 (d, *J* = 4.9 Hz, N$\underline{CH}_2CO_2$Et), 50.0 (d, *J* = 160.4 Hz, N$\underline{CH}_2$P), 27.1 ($\underline{Me}_2$C), 26.8 ($\underline{Me}_2$C), 26.7 ($\underline{Me}_3$C), 21.0 (OC(O)$\underline{Me}$), 19.2 ($Me_3\underline{C}$), 16.5 (P(O)OCH$_2\underline{C}H_3$), 16.4 (P(O)OCH$_2\underline{C}H_3$), 14.2 ($CO_2CH_2\underline{CH}_3$); ^{31}P NMR (162 MHz, $CDCl_3$, ^{1}H-decoupled) δ ppm: 24.6 (NCH$_2\underline{P}$); HRMS (FAB, *m*-nitrobenzyl alcohol matrix): Required for $C_{35}H_{55}NO_{10}PSi$: 708.33329; Found: 708.33263.

Ethyl 2-((((4*R*,5*S*)-5-((*R*)-1-acetoxy-2-hydroxyethyl)-2,2-dimethyl-1,3-dioxolan-4-yl)methyl)((diethoxyphosphonyl)methyl)amino)acetate

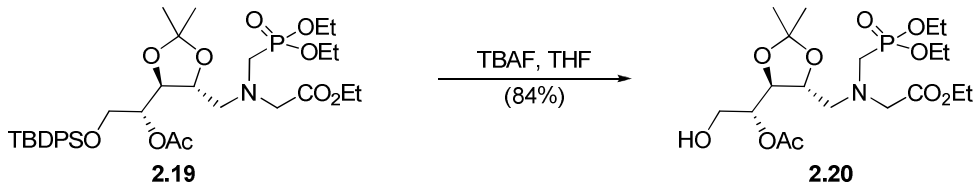

To a stirred solution of TBDPS ether 2.19 (90.0 mg, 0.127 mmol) in dry THF (1.9 mL) under argon was added a 1M THF solution of tetrabutylammonium fluoride (0.33 mL, 0.33 mmol). The brown solution was stirred for 1.75 hours, then evaporated. The residue was immediately purified by flash chromatography (50% ethyl acetate/hexane till silyl fluoride byproduct elutes, then 100% ethyl acetate) to give alcohol 2.20 (49.2 mg, 82%) as a colourless oil. R_f (100% ethyl acetate): 0.30, ^{1}H NMR (400 MHz, $CDCl_3$) δ ppm 4.81 (br s, 1H, C5-O<u>H</u>), 4.39 (dd, *J* = 11.5 Hz and 2.3 Hz, 1H, H5'), 4.13 (m, 8H, 2x P(O)O<u>CH$_2$</u>CH$_3$ & CO$_2$<u>CH$_2$</u>CH$_3$ & H2 & H5), 3.85 (t, *J* = 8.5 Hz, 1H, H3); 3.78 (m, 1H, H4), 3.66 (dd, 2H, *J* = 29.8 Hz, 18.0 Hz , N<u>C</u>H$_2$P), 3.13 (m, 4H, H1H1', NC<u>H$_2$</u>CO$_2$Et), 2.09 (s, 3H, OC(O)<u>Me</u>), 1.33 (m, 12H, 2x P(O)OCH$_2$<u>CH$_3$</u> and 2x <u>Me$_2$</u>C), 1.21 (t, *J* = 7.2 Hz, 3H, CO$_2$CH$_2$<u>CH$_3$</u>), ^{13}C NMR (101 MHz, $CDCl_3$) δ ppm 171.3 (O<u>C</u>(O)Me), 171.1 (<u>C</u>O$_2$CH$_2$CH$_3$), 109.1 (Me$_2$<u>C</u>), 80.9 (C2), 77.6 (C3), 71.9 (C4), 66.7 (C5), 62.3 (app dd, *J* = 7.3 Hz, 2.8 Hz, 2x P(O)O<u>C</u>H$_2$CH$_3$), 60.6 (CO$_2$<u>C</u>H$_2$CH$_3$), 57.6 (d, *J* = 4.6 Hz, N<u>CH$_2$</u>CO$_2$Et), 57.4 (d, *J* = 10.2 Hz, C1), 51.3 (d, *J* = 164.0 Hz, N<u>C</u>H$_2$P), 27.0 (<u>Me$_2$</u>C), 26.8 (<u>Me$_2$</u>C), 21.0, OC(O)<u>Me</u>, 16.4 (app dd, *J* = 5.3 Hz, 2x P(O)OCH$_2$<u>C</u>H$_3$), 14.2 (CO$_2$CH$_2$<u>C</u>H$_3$); ^{31}P NMR (162 MHz, $CDCl_3$, ^{1}H-decoupled) δ ppm 24.2 (NCH$_2$<u>P</u>); HRMS (FAB, *m*-nitrobenzyl alcohol matrix), Required for $C_{19}H_{37}NO_{10}P$: 470.21551; Found: 470.21604.

Ethyl 2-((((4*R*,5*S*)-5-((*R*)-1-acetoxy-2-(diethoxyphosphoryl)ethyl)-2,2-dimethyl-1,3-dioxolan-4-yl)methyl)((diethoxyphosphonyl)methyl)amino)acetate

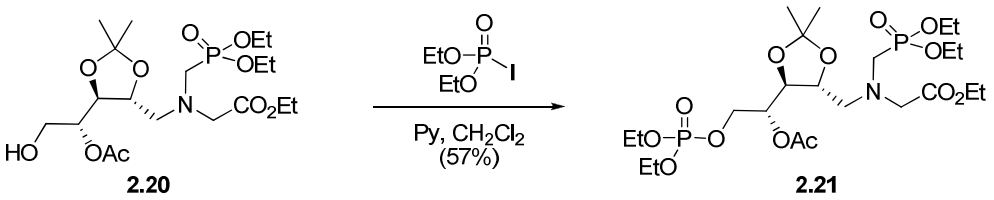

To a stirred solution of triethyl phosphite (43 μL, 0.25 mmol) in dry dichloromethane (0.8 mL) at 0°C under argon was added iodine (56.0 mg, 0.22 mmol). Stirring was continued for 5 minutes, over which time the brown colour of iodine disappeared. The resulting solution of diethylphosphoryl iodide was added dripwise (syringe pump) over 15 minutes to a solution of alcohol 2.20 (50.9 mg, 0.108 mmol) and pyridine (66 μL, 0.819 mmol) in dry dichloromethane (4.2 mL) under argon. After all the diethylphosphoryl iodide solution had been added, the solution was stirred for a further 25 minutes, then 50% saturated aqueous potassium carbonate (6 mL) and dichloromethane (10 mL) were added. After 5 minutes vigorous stirring the organic layer was separated, the aqueous phase extracted with dichloromethane (10 mL). The combined organic layers were washed with brine (10 mL), dried and evaporated. The residue was separated by flash chromatography (100% ethyl acetate) to give phosphate 2.21 (37.3 mg, 57%) as a colourless oil. R_f (100% ethyl acetate): 0.30, ^{1}H NMR (400 MHz, $CDCl_3$) δ ppm 4.40 (dd, *J* = 11.6 Hz, 2.4 Hz, 1H, H5'), 4.26 (app p, *J* = 7.3 Hz, 4H, OP(O)OC$\underline{H}_2$CH$_3$), 4.14 (m, 8H, 2x P(O)OC$\underline{H}_2$CH$_3$ & CO$_2$C$\underline{H}_2$CH$_3$ & H2 & H5), 3.86 (t, *J* = 7.8 Hz, 1H, H3), 3.79 (m, 1H, H4), 3.67 (dd, *J* = 32.3, 18.0 Hz, 2H, NC$\underline{H}_2$P), 3.18 (m, 3H, NC$\underline{H}_2$CO$_2$Et, H1'), 3.06 (dd, 1H, *J* = 14.8, 4.0 Hz, H1), 2.10 (s, 3H, OC(O)$\underline{Me}$), 1.36 (m, 18H, 4x P(O)O$\underline{CH}_2$CH$_3$ and 2x $\underline{Me}_2$C), 1.36 (m, 18H, 4x P(O)OCH$_2\underline{C}$H$_3$ and 2x $\underline{Me}_2$C), 1.28 (t, *J* = 7.3 Hz, 3H, CO$_2$CH$_2$C$\underline{H}_3$); ^{13}C NMR (101 MHz, $CDCl_3$) δ ppm 171.3 (O$\underline{C}$(O)Me), 171.1 (d, *J* = 8.1 Hz, NCH$_2\underline{C}$O$_2$Et), 109.1 ($Me_2\underline{C}$), 80.9 (C2), 77.6 (C3), 71.9 (C4), 66.7 (C5), 65.2 (app t, *J* = 2.8 Hz, OP(O)O$\underline{C}$H$_2$CH$_3$), 62.3 (app dd, *J* = 6.9 Hz, 3.0 Hz, CH$_2$P(O)O$\underline{C}$H$_2$CH$_3$), 60.6 (CO$_2\underline{C}$H$_2$CH$_3$), 57.6 (d, *J* = 3.6 Hz, N$\underline{C}$H$_2$CO$_2$Et), 57.4 (d, *J* = 11.0 Hz, C1), 51.3 (d, *J* = 163.9 Hz, N$\underline{C}$H$_2$P), 27.0 ($\underline{Me}_2$C), 26.8 ($\underline{Me}_2$C), 21.0 (OC(O)$\underline{Me}$), 16.5 (t, *J* = 5.0 Hz, 2x CH$_2$P(O)OCH$_2\underline{C}$H$_3$), 16.0 (t, *J* = 3.6 Hz, 2x OP(O)OCH$_2\underline{C}$H$_3$), 14.3 (CO$_2$CH$_2\underline{C}$H$_3$); ^{31}P NMR (162 MHz, $CDCl_3$, ^{1}H-decoupled) δ ppm -13.2,(O$\underline{P}$(O)OEt); 24.1, (NCH$_2\underline{P}$); HRMS (FAB, *m*-nitrobenzyl alcohol matrix): Required for $C_{23}H_{36}NO_{13}P_2$: 606.24444, Found: 606.24369.

Ammonium 2-((phosphonomethyl) ((2*R*,3*S*,4*R*)- 2,3,4-trihydroxy-5-(phospho)pentyl)amino)acetate

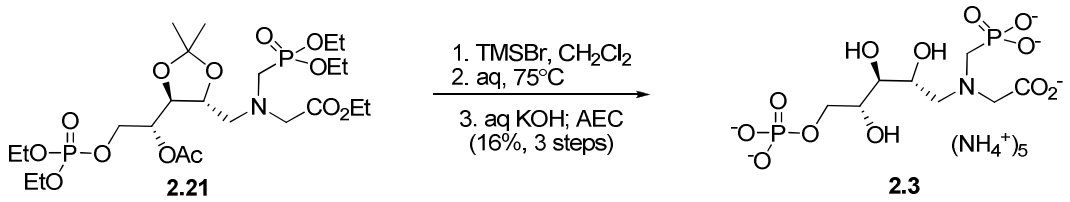

2.21 **2.3**

To a stirred solution of phosphate triester 2.21 (31.9 mg, 52.7 μmol) in dry acetonitrile (750 μL) under argon at 4°C was added triethylamine (73 μL, 0.53 mmol) and trimethylsilyl bromide (56 μL, 0.42 mmol). The resulting tan suspension was stirred for 19 hours, then further portions of triethylamine (35 μL, 0.25 mmol) and trimethylsilyl bromide (25 μL, 0.19 mmol) were added. Stirring was continued for 4 hours, then water (1 mL) was added, and the brown suspension stirred vigorously for 30 minutes, then extracted with chloroform (3x 2.5 mL). The aqueous solution was briefly placed under vacuum on a rotary evaporator at room temperature to remove volatiles, then stirred at 75°C for two hours. The pH of the solution was adjusted to 13 with 10% aqueous KOH, then stirred at 75°C for one hour. The solution was cooled, and the volatiles again removed on a rotary evaporator. The solution was diluted to 2 mL with water, centrifugally filtered through a 0.2 μm filter and purified by anion-exchange chromatography (0 – 500 mM ammonium bicarbonate). The fractions containing product (at ~125 mM ammonium bicarbonate) were lyophilised to give the target molecule 2.3 (7 mg, 16%). ^{1}H NMR (D_2O, pD 13, COSY) δ ppm 4.16 (H2), 4.11 (H5'), 4.03 (H5), 3.95 (H4 or H3), 3.71 (H3 or H4), 3.61 (NCH<u>H</u>'CO_2H), 3.32 (NC<u>H</u>H'CO_2H), 3.02 (H1'), 2.80 (NCH<u>H</u>'P), 2.79,(H1), 2.68 (NC<u>H</u>H'P); ^{13}C NMR (101 MHz, D_2O, pD 13) δ ppm 180.5 ($NCH_2\underline{C}O_2H$), 71.2 (C3), 70.8 (d, J =: 6.7 Hz, C5), 67.2 (C2), 65.9 (d, *J* = 4.4 Hz, $N\underline{C}H_2CO_2H$), 60.7 (d, *J* = 6.5 Hz, C4), 59.1 (d, *J* = 8.4 Hz, C1), 52.6 (d, *J* = 140.8 Hz, $N\underline{C}H_2P$); ^{31}P NMR: (162 MHz, D_2O, pD 13, ^{1}H-coupled) 16.7 (t, *J* = 10.8 Hz, $CH_2\underline{P}(O)(O^-)_2$), 4.9 (t, *J* = 6.0 Hz, $CH_2O\underline{P}(O)(O^-)_2$).

6.2.2 Experimental for Chapter Three

Methyl 2-(diethoxyphosphoryloxy)propanoate

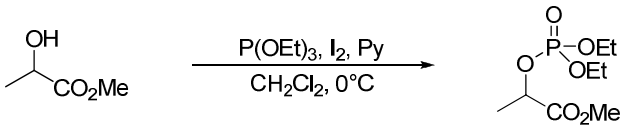

A solution of triethylphosphite (0.860 mL, 5.01 mmol) in dichloromethane (12 mL) under nitrogen was cooled to 0°C, and iodine (1.159 g, 4.57 mmol) was added. The solution was stirred until the characteristic brown iodine colour had been discharged (~ 5 minutes). The resulting solution of diethylphosphoryl iodide was added dripwise over 15 minutes to (*S*)-methyl lactate (400.1 mg, 3.843 mmol) in pyridine (2.5 mL) and dichloromethane (60 mL) at 0°C under nitrogen. Once addition was complete the mixture was stirred for 1 hour, then quenched with saturated aqueous sodium bicarbonate solution (20 mL), and stirred vigorously for 5 minutes. The organic phase was separated, and washed with 1.2 M aqueous hydrochloric acid (2x 75 mL), saturated aqueous sodium bicarbonate solution (75 mL), and brine (75 mL), dried and evaporated. Flash chromatography (50% ethyl acetate/hexane) gave the phosphate ester (615.9 mg, 67%). R_f (50% ethyl acetate/hexane): 0.34; ^{1}H NMR (400 MHz, $CDCl_3$) δ ppm 4.83 (qd, *J* = 14.1, 7.0 Hz, 1H, H2), 4.17-3.99 (m, 4H, POC$\underline{H}_2$CH$_3$), 3.70 (s, 3H, CO$_2\underline{Me}$), 1.48 (d, *J* = 6.9 Hz, 3H, H3), 1.27 (dt, *J* = 7.1, 3.3 Hz, 6H, POC$\underline{H}_2$CH$_3$); ^{13}C NMR (101 MHz, $CDCl_3$) δ ppm 171.0 (d, *J* = 5.2 Hz, C1), 71.6 (d, *J* = 5.2 Hz, C2), 64.2 (d, *J* = 6.0 Hz, PO$\underline{C}$H$_2$CH$_3$), 64.0 (d, *J* = 6.0 Hz, PO$\underline{C}$H$_2$CH$_3$), 52.4 (CO$_2\underline{Me}$), 19.2 (d, *J* = 5.4 Hz, C3), 16.0 (app dd, *J* = 6.9, 1.0 Hz, 2x PO$\underline{C}$H$_2$CH$_3$); ^{31}P NMR (162 MHz, $CDCl_3$) δ ppm -2.0 (C2O$\underline{P}$OEt); $[\alpha]_D^{20}$ = -18.3°.
Treatment of (*R*)-methyl lactate (400.6 mg, 3.85 mmol) under the same conditions gave the corresponding (*R*)-phosphoester (475.6 mg, 51%), with identical spectral data except $[\alpha]_D^{20}$ = +18.5°.

Tris(cyclohexylammonium) 2-(phosphoryl)propanoate

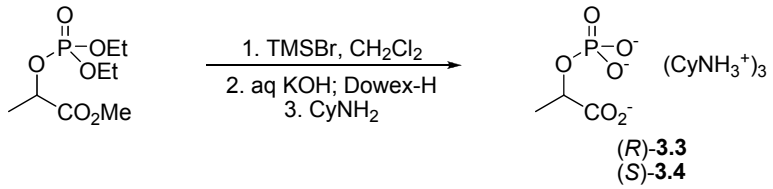

(*R*)-**3.3**
(*S*)-**3.4**

To a solution of (*R*)-phosphoester (470.5 mg, 1.96 mmol) in dichloromethane (15 mL) under nitrogen was added trimethylsilyl bromide (1.55 mL, 11.7 mmol), and the mixture was stirred overnight then evaporated. The residue was dissolved in 10% w/v aqueous potassium hydroxide, stirred for five minutes then extracted with dichloromethane (3x 2 mL) and the organic phases discarded. The aqueous phase was passed through a short column of Dowex-50X8 H^+-form, eluted with water (20 mL), neutralised with cyclohexylamine and lyophilised to give a white powder, (757.3 mg). Analysis of the solid (^{1}H NMR) showed the hydrolysis of the carboxylate ester was incomplete, so a portion of the solid (474.2 mg) was treated with 10% w/v aqueous potassium hydroxide (4 mL) for two hours, the mixture was extracted with dichloromethane (3x 2 mL) and the organic phases discarded. After treatment with Dowex-50X8 H^+-form and cyclohexylamine and lyophillisation, (*R*)-phospholactate tris(cyclohexylammonium salt) 3.3 was obtained as a white solid (361.7 mg, 63%), containing ~20% lactate due to neighbouring group assisted hydrolysis. ^{1}H NMR (500 MHz, D_2O) δ ppm 4.3-4.2 (app p, *J* = 7.3 Hz, 1H, H2-OP), 3.1-2.9 (q, *J* = 7.0 Hz, 0.25H, H2-OH), 1.9-1.7 (m, $CyNH_3^+$), 1.7-1.6 (m, $CyNH_3^+$), 1.6 (d, *J* = 6.9 Hz, 3H, C3), 1.5 (dm, *J* = 12.8 Hz, $CyNH_3^+$), 1.2-1.1 (m, $CyNH_3^+$), 1.0 (m, $CyNH_3^+$); ^{13}C NMR (75 MHz, D_2O) δ ppm 181.5 (d, *J* = 6.4 Hz, C1), 71.9 (d, *J* = 5.0 Hz, C2), , 50.5 ($CyNH_3^+$), 30.5 ($CyNH_3^+$), 24.5 ($CyNH_3^+$), 24.0 ($CyNH_3^+$), 20.3 (d, *J* = 3.1 Hz, C3), lactate 182.6 (C1), 68.6 (C2), 20.2 (C3); ^{31}P NMR (121 MHz, D_2O) δ ppm 2.1 (C2O<u>P</u>); 2.0 (Pi). $[\alpha]^{20}_{365\ nm}$: +2.6°; ESI-MS, (negative ion, 20% AcOH matrix): required for $C_3H_6O_6P^-$: 168.9902, found 168.9904.

In a similar manner the (*S*)-isomer 3.4 was prepared, with the spectral data in accordance with that above, except $[\alpha]^{20}_{365\ nm}$: -2.9°; and ESI-MS, (negative ion, 20% AcOH matrix): required for $C_3H_6O_6P^-$: 168.9902, found 168.9909.

Methyl 1-(diethoxyphosphoryl)cyclopropanecarboxylate

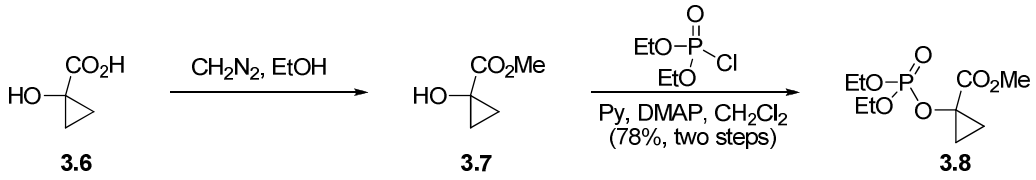

3.6 **3.7** **3.8**

A solution of diazomethane (freshly prepared from Diazald® by the manufacturers directions) in diethyl ether was added dropwise from a flame-polished pipette behind a safety shield to a solution of 1-hydroxy 1-carboxylcyclopropane (206 mg, 2.018 mmol) in ethanol (2 mL) at 0°C, until TLC (50% ethyl acetate/hexane) indicated the absence of free acid. Nitrogen was bubbled thorough the solution to remove excess diazomethane, and the solution was evaporated.

The crude methyl ester (291.8 mg) was dissolved in dichloromethane (20 mL) under nitrogen, and pyridine (0.980 mL, 12.1 mmol) and DMAP (51.2 mg, 0.419 mmol) were added, followed by diethyl chlorophosphate (0.875 mL, 6.05 mmol). The mixture was stirred overnight, then quenched with saturated aqueous sodium bicarbonate solution (10 mL) and stirred vigorously for 15 minutes. The organic phase was separated, and the aqueous phase extracted with dichloromethane (20 mL). The combined organic phases were washed with saturated ammonium chloride solution (2x 30 mL) and brine (30 mL), dried and evaporated. Flash chromatography (100% ethyl acetate) gave phosphate ester 3.8 as a colourless oil (396.8 mg, 78%). R_f (80% ethyl acetate/hexane): 0.13; ^{1}H NMR (500 MHz, $CDCl_3$) δ ppm 4.21-4.13 (m, 4H, POC$\underline{H}_2$CH$_3$), 4.07-3.99 (m, 3H, CO$_2$$\underline{Me}$), 1.30 (t, J = 7.2 Hz, 6H, POCH$_2$C$\underline{H}_3$), 1.26 (dt, J = 7.1, 0.8 Hz, 2H, H3-phosphoryl face), 1.17 (t, J = 7.1 Hz, 2H, H3-carboxyl face); ^{13}C NMR (126 MHz, $CDCl_3$) δ ppm 171.2 (C1), 65.3 (app t, J = 3.0 Hz, 2x PO$\underline{C}$H$_2$CH$_3$), 63.7 (d, J = 5.9 Hz, C2), 60.5 (CO$_2$$\underline{Me}$), 16.3 (d, J = 6.7 Hz, C3), 16.1 (t, J = 3.6 Hz, 2x PO$\underline{C}$H$_2$CH$_3$). HRMS, required for $C_9H_{18}O_6P$ 253.0841, found 253.0843.

Ammonium 1-(phosphoryl)cyclopropanecarboxylate

3.8 **3.5**

To a solution of ester 3.8 (312.5 mg, 1.24 mmol) in dichloromethane (12 mL) under nitrogen was added trimethylsilyl bromide (0.980 mL, 7.42 mmol), and the mixture stirred overnight. The mixture was evaporated, and the residue dissolved in 10% w/v aqueous potassium hydroxide (5 mL) and stirred for 3 hours. The mixture was extracted with dichloromethane (3x 5 mL), and the organic extracts discarded. The aqueous phase was loaded onto a column of Dowex-50X8 H^+-form (20 x 70 mm), and eluted with water (45 mL). The filtrate was neutralised with cyclohexylamine, and lyophilised.

A portion (200 mg) of crude product was recrystallised from methanol/acetone (crystallised at -80°C/ 2 hours), and the collected material (61 mg) was purified by anion-exchange chromatography (Source Q, 0-1M ammonium bicarbonate). The product was located by treatment of the fractions with the Lanzetta reagent, and the active fractions lyophilised to give a crude preparation of cyclopropane 3.5 (5.2 mg). The mixture contained only one phosphorus species by ^{31}P NMR, and appeared mostly desired product by ^{13}C NMR but some impurities were observed in the ^{1}H NMR spectrum. Key data[91]: ^{1}H NMR (300 MHz, D_2O) δ ppm 1.2 (app t, J = 10.8 Hz, H3); ^{13}C NMR (75 MHz, D_2O) δ ppm 164.5 (C1), 50.5 (C2), 24.0 (C3), ^{31}P NMR (121 MHz, D_2O) δ ppm 0.7 (C2O<u>P</u>).

Methyl 3-(diethoxyphosphonyl)-2-methylacrylate

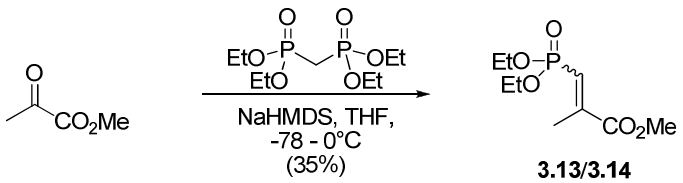

3.13/3.14
E/*Z*
46:54

To a solution of tetraethyl methylene bisphosphonate (820 μL, 3.30 mmol) in tetrahydrofuran (4 mL) under nitrogen at -78°C was added a 0.846 M solution of sodium bis(trimethylsilyl)amide in tetrahydrofuran (3.6 mL, 3.05 mmol), and the mixture was stirred for 30 minutes, and allowed to come to -35°C over this time. The cold bath was replaced with an ice bath, and technical grade methyl pyruvate (96%, 290 μL, 3.08 mmol) was added dropwise. The mixture was stirred for 2.5 hours, and quenched with saturated potassium dihydrogen phosphate (5 mL). The tetrahydrofuran was removed on a rotary evaporator, and the residue extracted with ethyl acetate (5x 10 mL).The combined organic phases were washed with brine (50 mL), dried and evaporated. Flash chromatography (60% ethyl acetate/hexane) gave pure (*E*)-3.13 (116.3 mg, 16%) and (*Z*)-3.14 (137.1 mg, 24%), which contained ~10% (*E*)-isomer by NMR.

(*E*)-isomer: R_f (60% ethyl acetate/hexane): 0.25; ^{1}H NMR (500 MHz, $CDCl_3$) δ ppm 6.64 (dq, *J* = 16.0, 1.2 Hz, 1H, H3'), 4.11-4.04 (dq, *J* = 7.8, 7.1 Hz, 4H, C3'POC$\underline{H}_2$CH$_3$), 3.76 (s, 3H, CO$_2\underline{Me}$), 2.23 (dd, *J* = 3.6, 1.3 Hz, 3H, H3), 1.30 (t, *J* = 7.1, 6H, C3'POCH$_2$C$\underline{H}_3$); ^{13}C NMR (75 MHz, $CDCl_3$) δ ppm 167.1 (d, *J* = 29.3 Hz, C1), 147.1 (d, *J* = 9.0 Hz, C2), 125.5 (d, *J* = 185.9 Hz, C3'), 62.2 (d, *J* = 5.6 Hz, C3'PO$\underline{C}$H$_2$CH$_3$), 52.9 (s, CO$_2\underline{Me}$), 16.6 (d, *J* = 6.4 Hz, C3'POCH$_2\underline{C}$H$_3$), 16.0 (d, *J* = 6.3 Hz, C3); ^{31}P NMR (121 MHz, $CDCl_3$) δ ppm 13.0 (C3'$\underline{P}$OCH$_2$CH$_3$). HRMS, required for $C_9H_{18}O_5P$ 237.0892, found 237.0885.

(*Z*)-isomer: R_f (60% ethyl acetate/hexane): 0.10; ^{1}H NMR (500 MHz, $CDCl_3$) δ ppm 5.72 (dq, *J* = 14.7, 1.4 Hz, 1H), 4.10-3.98 (m, 4H, C3'POC$\underline{H}_2$CH$_3$), 3.76 (s, 3H, CO$_2\underline{Me}$), 2.04 (app t, *J* = 1.4 Hz, 3H, H3), 1.26 (t, *J* = 7.1 Hz, 6H, C3'POCH$_2$C$\underline{H}_3$); ^{13}C NMR (75 MHz, $CDCl_3$) δ ppm 168.3 (d, *J* = 9.4 Hz, C1), 149.6 (d, *J* = 3.1 Hz, C2), 120.7 (d, *J* = 188.6 Hz, C3), 62.2 (d, *J* = 5.6 Hz, C3'PO$\underline{C}$H$_2$CH$_3$), 52.6 (s, CO$_2\underline{Me}$), 22.7 (d, *J* = 20.5 Hz, C3), 16.5 (d, *J* = 6.5 Hz, C3'POCH$_2\underline{C}$H$_3$); ^{31}P NMR (121 MHz, $CDCl_3$) δ ppm 13.8 (C3'$\underline{P}$OCH$_2$CH$_3$).

Tris(cyclohexylammonium) (*E*)-2-methyl-3-phosphonatoacrylate

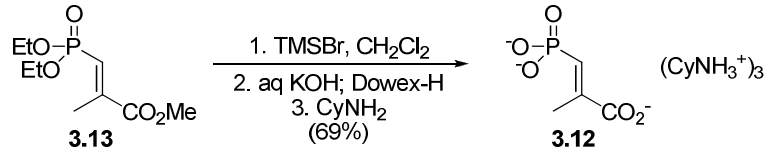

3.13 **3.12**

To a solution of ester 3.13 (116.3 mg, 0.492 mmol) in dichloromethane (3.8 mL) under nitrogen was added trimethylsilyl bromide (390 μL, 2.95 mmol), and the mixture was stirred overnight then evaporated. The residue was dissolved in 10% w/v aqueous potassium hydroxide (2 mL), stirred for five minutes then extracted with dichloromethane (3x 2 mL) and the organic phases discarded. The aqueous phase was passed through a short column of Dowex-50X8 H^+-form (10 x 80 mm), eluted with water (30 mL), neutralised with cyclohexylamine and lyophilised to give a white powder (328.8 mg). Analysis of this powder by NMR showed only the presence of the desired product 3.12, and ^{31}P NMR quantitation showed the powder was 48% pure (69% yield), the balance presumably being inorganic cyclohexylammonium salts and/or waters of hydration.

^{1}H NMR (500 MHz, D_2O) δ ppm 6.19 (dd, *J* = 14.6, 1.2 Hz, 1H, H3'), 3.10-2.88 ($CyNH_3^+$), 1.87 (dd, *J* = 2.9, 1.2 Hz, 3H, H3), 1.85-1.78 (m, $CyNH_3^+$), 1.67-1.59 (m, $CyNH_3^+$), 1.48 (dm, *J* = 12.8 Hz, $CyNH_3^+$), 1.24-1.09 (m, $CyNH_3^+$), 1.01 (ddm, *J* = 22.2, 10.1 Hz, $CyNH_3^+$); ^{13}C NMR (75 MHz, D_2O) δ ppm 178.4 (d, *J* = 22.5 Hz, C1), 144.7 (d, *J* = 4.2 Hz, C2), 131.2 (d, *J* = 165.9 Hz, C3'), 50.5 ($CyNH_3^+$), 30.5 ($CyNH_3^+$), 24.5 ($CyNH_3^+$), 24.0 ($CyNH_3^+$), 16.4 (d, *J* = 6.5 Hz, C3); ^{31}P NMR (121 MHz, D_2O, ^{1}H-decoupled) δ ppm 9.8 (C3'P); ^{31}P NMR (121 MHz, D_2O, ^{1}H-coupled) δ ppm 9.8 (d, *J* = 14.9 Hz, C3'PO_3^{2-}). ESI-MS, (negative ion, 20% AcOH matrix). required for $C_4H_6O_5P^-$: 164.9953; found: 164.9948.

(*Z*)-Methyl 3-(diethoxyphosphonyl)-2-(trifluoromethyl)acrylate

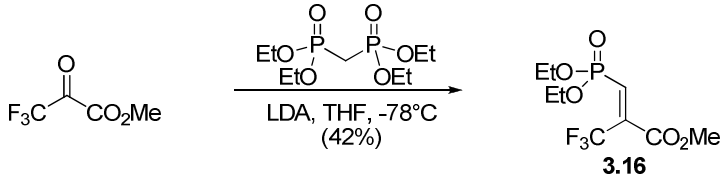

3.16

A stirred solution of diisopropylamine (340 µL, 2.41 mmol) in tetrahydrofuran (20 mL) was cooled to -78°C under nitrogen, and a 1.6 M solution of n-butyllithium in hexanes (1.38 mL, 2.21 mmol) was added. After 30 minutes, tetraethyl methylene bisphosphonate (620 µL, 2.49 mmol) was added, the mixture was stirred for 20 minutes before methyl 3,3,3-trifluoropyruvate (200 µL, 1.96 mmol) was added. The mixture was stirred for ten minutes, then brought to 0°C and stirred for 2.5 hours. The reaction was quenched with saturated aqueous potassium dihydrogen phosphate (5 mL), and the tetrahydrofuran removed on a rotary evaporator. The residue was partitioned between dichloromethane (20 mL) and water (10 mL), the aqueous phase was separated and extracted with further dichloromethane (10 mL). The combined organic phases were washed with 10% w/v sodium hydroxide (2x 10 mL), 1.2 M hydrochloric acid (10 mL) and brine (10 mL). The organic phase was dried and evaporated. Flash chromatography (60 % ethyl acetate/hexane) gave phosphonate 3.16 as an oil (238.3 mg, 42%). R_f (60% ethyl acetate/hexane): 0.32; ^{1}H NMR (500 MHz, $CDCl_3$) δ ppm 6.47 (d, *J* = 9.3 Hz, 1H, H3'), 4.21-4.06 (m, 4H, $POC\underline{H}_2CH_3$), 3.82 (s, 3H, $CO_2\underline{Me}$), 1.28 (app dd, *J* = 14.9, 7.7 Hz, 6H, $POCH_2C\underline{H}_3$); ^{13}C NMR (75 MHz, $CDCl_3$) δ ppm 170.9 (C1), 128.1 (dd, *J* = 185.0, 5.4 Hz, C3'), 62.9 (d, *J* = 5.8 Hz, $PO\underline{C}H_2CH_3$), 53.2 (d, *J* = 0.9 Hz, $CO_2\underline{Me}$), 16.1 (d, *J* = 6.0 Hz, $POCH_2\underline{C}H_3$); ^{31}P NMR (121 MHz, $CDCl_3$) δ ppm 9.8 (C3'$\underline{P}$).

Tris(cyclohexylammonium) (*Z*)-3-phosphonato-2-(trifluoromethyl)acrylate

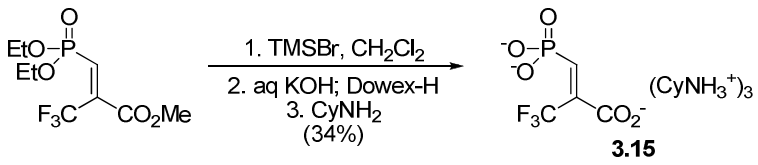

3.15

Deprotection of ester 3.16 (283.3 mg, 0.821 mmol), by the method described for 3.13 gave free phosphonate 3.15 as a white powder (583.5 mg). The powder gave only the expected signals for 3.15 by NMR, however the cyclohexylamine signals integrated to give a higher value than expected. Quantitation by ^{31}P NMR showed the powder was 25% product 3.15 (34% yield), the balance presumably being inorganic cyclohexylammonium salts and/or waters of hydration. ^{1}H NMR (300 MHz, D_2O) δ ppm 6.75 (d, *J* = 6.2 Hz, H3'), 3.21-2.89 (m, $CyNH_3^+$), 2.02-1.75 (m, $CyNH_3^+$), 1.75-

1.59 (m, $CyNH_3^+$), 1.52 (dm, J = 12.2 Hz, $CyNH_3^+$), 1.21 (m, $CyNH_3^+$) ^{13}C NMR (75 MHz, D_2O) δ ppm 142.2 (dd, J = 153.1, 3.1 Hz, C3'), 50.6 ($CyNH_3^+$), 30.5 ($CyNH_3^+$), 24.5 ($CyNH_3^+$), 24.0 ($CyNH_3^+$); ^{31}P NMR (121 MHz, D_2O) δ ppm 4.6 (overlapping dq, J = 7.5, 2.4 Hz, $F_3CCC(H)\underline{P}$);. HRMS (ESI, negative ion, 20% AcOH matrix): required for $C_4H_3O_5F_3P$: 218.9670, found 218.9670.

Potassium 1-cyano-3-ethoxy-3-oxoprop-1-en-2-olate[101]

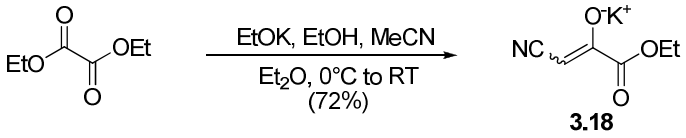

3.18

Finely cut potassium metal (2.495 g, 63.8 mmol) was slowly added in small portions to a mixture of ethanol (16 mL) and diethyl ether (11.5 mL) under argon, once the initially vigorous reaction slowed the mixture was sonicated until all of the metal had reacted. The resulting solution of potassium ethoxide was cooled to 0°C under nitrogen, and diethyl oxalate (4.3 mL, 31.7 mmol) was added. The heterogeneous mixture was stirred for 30 minutes, then acetonitrile (1.7 mL, 32.6 mmol) was added, the ice bath was removed and the mixture stirred at room temperature for 1 hour. Diethyl ether (15 mL) was added, the solid yellow residue was suspended with vigorous stirring and filtered, and the solid washed well with cold diethyl ether. The solid was dried under high vacuum overnight to give potassium enolate 3.18 as a lemon yellow solid (4.080 g, 72%), which was not further purified. mp: >200°C; ^1H NMR (500 MHz, d_4-methanol) δ ppm 4.34-4.06 (m, 2H, $CO_2C\underline{H}_2CH_3$), 3.78-3.65 (app t, J = 4.2 Hz, 0.5H, H3-enol geometry A), 3.62-3.55 (app t, J = 4.2 Hz, 0.5H, H3-enol geometry B), 1.41-1.23 (m, 3H, $CO_2CH_2CH_3$) ^{13}C NMR (126 MHz, d_4-methanol) δ ppm 169.9 (C1 isomer A), 166.6 (C1 isomer B), 133.7, 122.1, 72.1, 60.7 ($CO_2\underline{C}H_2CH_3$), 13.1 ($CO_2CH_2\underline{C}H_3$).

Ethyl 3-cyano-2-(diethoxyphosphoryl)acrylate – NMR optimised procedure

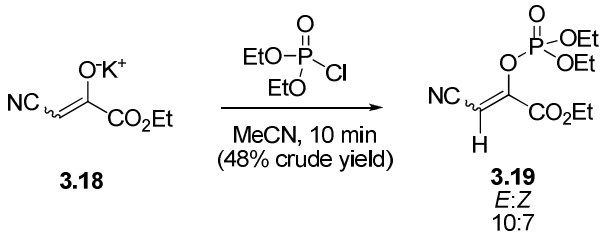

To a stirred mixture of enolate 3.18 (540.1 mg, 3.02 mmol) and acetonitrile (15 mL) under argon was added diethyl chlorophosphate (460 μL, 3.17 mmol). The mixture was stirred for ten minutes, then poured into diethyl ether (150 mL). The diethyl ether solution was washed with 0.6 M aqueous hydrochloric acid (2x 30 mL), then with 1:3 saturated aqueous sodium bicarbonate solution:water (4x 50 mL) and brine (50 mL). The organic phase was dried and evaporated to give crude unstable enol phosphate 3.19 (400.8 mg, 48%) as a 60:40 (*E*):(*Z*) mixture, containing other phosphoryl species, which was not purified further but used in the same day for the next step. Key data: ^{1}H NMR (400 MHz, $CDCl_3$) δ ppm 6.07 (d, *J* = 1.6 Hz, 0.6H, *E*-H3), 6.00 (d, *J* = 2.0 Hz, 0.4H, *Z*-H3), 4.02 (app p, *J* = 7.2 Hz, 4H, $OPO\underline{C}H_2CH_3$), ^{13}C NMR (101 MHz, $CDCl_3$) δ ppm 159.7 (C1), 152.4 (C1), 113.2 (*Z*-C3<u>C</u>N), 112.7 (d, *J* = 2.6 Hz, *E*-C3<u>C</u>N), 95.6 (d, *J* = 7.0 Hz, C3), 94.5 (d, *J* = 4.4 Hz, C3), 16.0 (app t, *J* = 6.8 Hz, $POCH_2\underline{C}H_3$), 13.9 ($CO_2CH_2\underline{C}H_3$), 13.9 ($CO_2CH_2\underline{C}H_3$); ^{31}P NMR (162 MHz, $CDCl_3$) δ ppm -7.9 (*Z*-C2O<u>P</u>), -8.3 (*E*-C2O<u>P</u>).

Cyclohexylammonium (*E*)-3-(cyano)phosphoenolpyruvate

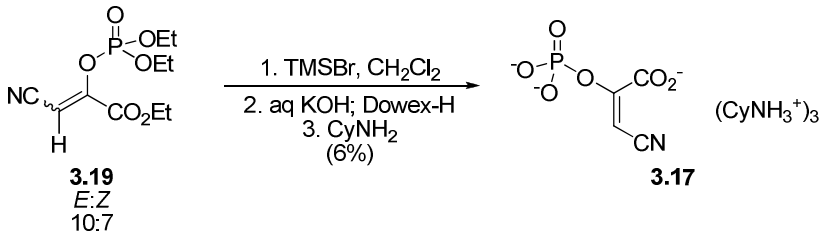

To a solution of ester 3.19 (400.8 mg, 1.45 mmol) in dichloromethane (14 mL) under nitrogen was added trimethylsilyl bromide (1.4 mL, 10.6 mmol), and the mixture was stirred overnight. The mixture was evaporated, and 10% w/v potassium hydroxide (6

mL) was added, and the mixture was sat for 5 minutes. The mixture was extracted with dichloromethane (3 x 10 mL), and the organic phases discarded. The aqueous phase was passed through a short column of Dowex-50X8 H^+-form (10 x 60 mm), and eluted with water (20 mL). The filtrate was neutralised with cyclohexylamine, and lyophilised. Recrystallisation of the tan powder from methanol/diethyl ether gave a white solid identified as cyanophosphoenolpyruvate cyclohexylammonium salt 3.17 (84.8 mg, 6%), by comparison with known spectral data[101]. ^{1}H NMR (400 MHz, D_2O) δ ppm 5.52 (d, J = 1.8 Hz, *E*-H3), 3.05-2.91 (m, $CyNH_3^+$), 1.93-1.72 (m, $CyNH_3^+$), 1.74-1.54 (m, $CyNH_3^+$), 1.48 (dm, J = 12.7 Hz, $CyNH_3^+$), 1.28-1.07 (m, $CyNH_3^+$), 1.08-0.93 (m, $CyNH_3^+$).

Ethyl 3-bromo-2-hydroxypropanoate[104]

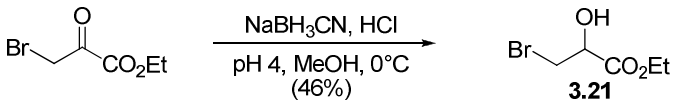

A solution of technical grade ethyl bromopyruvate (≥70%, 3.25 mL, 18.1 mmol) in methanol (12 mL) was slowly transferred by cannula into a solution of sodium cyanoborohydride (1.779 g, 28.3 mmol) in methanol (16 mL) under argon at 0°C, the bromopyruvate flask was washed with further methanol (4 mL), and the washings transferred by cannula into the cyanoborohydride flask. A catalytic quantity of bromocresol green was added, and the blue solution was treated with an ethereal solution of hydrogen chloride dropwise until solution was yellow. The mixture was stirred for 3 hours, then evaporated. The residue was partitioned between saturated ammonium chloride solution (25 mL) and diethyl ether (25 mL), the aqueous phase was separated and extracted with diethyl ether (5x 30 mL). The combined organic extracts were washed with brine (20 mL), dried and evaporated. The yellow oily residue was mixed with diethyl ether (20 mL), and cooled to -78°C under nitrogen for 2.5 hours. The resulting white crystalline bromolactate 3.21 (1.1468 g) was collected by filtration. The mother liquor was evaporated, the semi-solid residue dissolved in a minimum quantity of diethyl ether, and allowed to crystallise at -80°C overnight to give a second crop of bromolactate 3.21 (1.187 g), giving a total yield of bromolactate 3.21 of 2.338 g (46%). mp: 39-44°C; R_f (80% ethyl acetate/hexane): 0.12; ^{1}H NMR

(500 MHz, $CDCl_3$) δ ppm 4.50 (t, *J* = 3.4 Hz, 1H), 4.38-4.23 (m, 2H, $CO_2C\underline{H}_2CH_3$), 3.70 (dq, *J* = 10.7, 3.5 Hz, 2H, $CHC\underline{H}_2Br$), 2.96 (br s, 1H, C3O<u>H</u>), 1.33 (t, *J* = 7.1 Hz, 3H, $CO_2CH_2C\underline{H}_3$), ^{13}C NMR (75 MHz, $CDCl_3$) δ ppm 171.8 (C1), 70.0 (C2), 62.8 ($CO_2\underline{C}H_2CH_3$), 35.4 (C3), 14.5 ($CO_2CH_2\underline{C}H_3$); HRMS, Required for $C_5H_{10}O_3Br$: 196.9813, Found: 196.9805.

Pyridinium ethyl 3-bromo-2-(sulfo)propanoate[104]

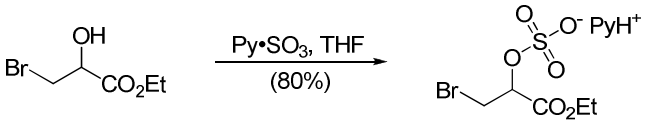

3.21 **3.22**

To a solution of technical grade pyridine-sulfur trioxide complex (49-50% as SO_3, 297 mg, 1.84 mmol as SO_3) in tetrahydrofuran (3 mL) under argon was added bromolactate 3.21 (336.6 mg, 1.71 mmol) in tetrahydrofuran (2 mL). The mixture was stirred overnight, and then the tetrahydrofuran carefully evaporated on a rotary evaporator (bath ≤30°C) until the first signs evaporation had ceased. The semi-solid residue was diluted with chloroform, and sat at -20°C for 2 hours. The resulting precipitate of excess pyridine-sulfur trioxide complex was separated by centrifugation, and the supernatant carefully evaporated to give unstable pyridinium sulfate 3.22 (489 mg, 80%), as a pale yellow syrup, containing <15% unsulfated starting material by NMR. ^1H NMR (500 MHz, $CDCl_3$) δ ppm 10.80 (br s, $Py\underline{H}^+$), 9.06 (br s, 2H, Py-H2), 8.58-8.44 (m, 1H, Py-H4), 8.07 (m, 2H, Py-H3), 5.24 (t, *J* = 4.0 Hz, 1H, H2), 4.37-4.10 (m, 2H, $CO_2C\underline{H}_2CH_3$), 3.89 (dd, *J* = 10.8, 4.3 Hz, 1H, H3a), 3.79 (dd, *J* = 10.8, 3.7 Hz, 1H, H3b), 1.28 (t, *J* = 7.1 Hz, 3H, $CO_2CH_2C\underline{H}_3$). ^{13}C NMR (75 MHz, $CDCl_3$) δ ppm 169.0 (C1), 146.5 (br, Py-C4), 142.7 (br, 2xPy-C2), 127.7 (br, 2xPy-C3), , 74.5 (C2), 62.3 ($CO_2\underline{C}H_2CH_3$), 32.5 (C3), 14.4 ($CO_2CH_2\underline{C}H_3$); HRMS (electrospray, negative ion) required for $C_5H_8O_6SBr^-$: 274.9225, found 274.9232.

Potassium sulfoenolpyruvate[104]

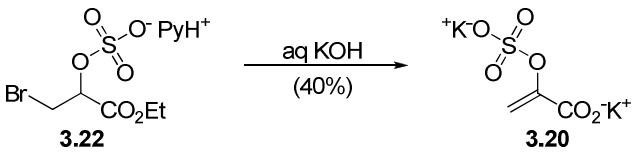

3.22 **3.20**

A mixture of pyridinium sulfate 3.22 (461.3 mg, 1.30 mmol) and water (420 μL) was stirred vigorously while 1M aqueous potassium hydroxide was added in portions (10 portions, 420 μL per portion, added at accurately timed 2 minute intervals). Once all of the potassium hydroxide had been added, the yellow solution was stirred for 1 hour. The reaction was worked up at 4°C due to the poor stability of SEP 3.20 to acidic conditions. The yellow solution was loaded onto a short column (10 x 80 mm) of Dowex-50X4 H^+-form, and the column was quickly eluted with water into an ice-cooled flask until an elutate pH of ~6 (approximately 25-30 mL). The combined elutate was neutralised with saturated aqueous barium hydroxide, lyophilised, and the pale yellow solid collected. The crude solid was mixed with water (25 mL), and filtered through a 0.2 μm membrane filter and the filtrate diluted with absolute ethanol (220 mL) and sat at 4°C overnight. The majority of the mother liquor was discarded, and the precipitated solid was suspended in ~60 mL of mother liquor and the solid collected by centrifugation (8000x *g*, 3 minutes, 4°C). The supernatant was discarded, and the solid resuspended in absolute ethanol (10 mL) and again the solid was collected by centrifugation and the supernatant discarded. The ethanol suspension/centrifugation process was repeated twice more, and the collected fine solid was dried under high vacuum for one hour. Analysis of the solid by FTIR (diffuse reflectance, KBr solid suspension) indicated it was the barium salt of SEP (1377, 1288, 1263 cm^{-1} sulfate S=O asymmetric, symmetric and symmetric stretches; 1585, 1421 cm^{-1} carboxylate symmetric and asymmetric stretches; 1211, 1640(d) cm^{-1} enol C-O and C=C stretches). The barium salt of SEP was dissolved in the minimum volume of water (~12 mL), and loaded onto a column of Dowex-50X4 K^+-form (14 x 90 mm), and the column eluted with water (35 mL). The combined elutates were lyophilised to give potassium sulfoenolpyruvate 3.20 as a fine white powder (126.5 mg, 40%). ^{1}H NMR (300 MHz, D_2O) δ ppm 5.65 (d, *J* = 2.0 Hz, 1H, H3*Z*), 5.40 (d, *J* = 2.0 Hz, 1H, H3*E*); ^{13}C NMR (75 MHz, D_2O) δ ppm 169.3 (C1), 149.3 (C2), 107.6

(C3); HRMS (electrospray, negative ion): required for $C_3H_3O_6S^-$: 166.9650; found 166.9649.

2-Aminothiazole-4-carboxylic acid

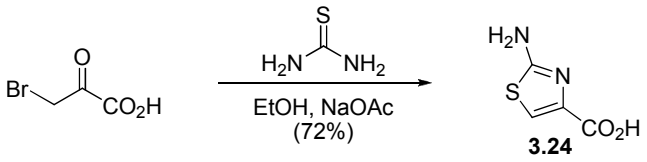

3.24

To a stirred solution of bromopyruvic acid (503.6 mg, 3.02 mmol) in absolute ethanol (20 mL) was added thiourea (233.2 mg, 3.06 mmol), and the solution was stirred vigorously for 30 minutes. The ethanol was evaporated, and the residue suspended in water (10 mL). Solid sodium acetate was added until a pH of 5 was reached, and the suspension was cooled to 4°C for twenty minutes. The precipitated solid was collected and dried to give thiazole 3.24 as a white solid (316 mg, 72%). ^{1}H NMR (300 MHz, d_6-DMSO) δ ppm 7.48 (s, 1H, H3), 7.28 (br s, 2H, CN$\underline{H}_2$); ^{13}C NMR (75 MHz, d_6-DMSO) δ ppm 168.9 (C1), 163.2 (C4), 143.7 (C2), 117.4 (C3), FTIR (diffuse reflectance, KBr solid suspension) cm^{-1}: 3530, 3279, 2800, 1844, 1652, 1599, 1570.

6.4 Experimental for Chapter Four

Diethyl hex-5-enyl phosphate

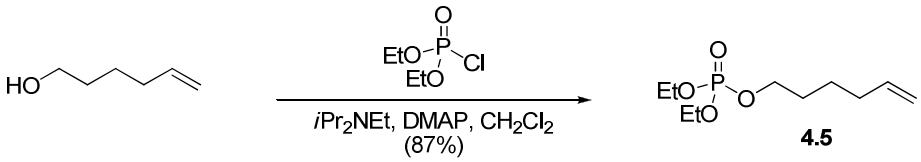

4.5

To a stirred solution of hex-5-en-1-ol (0.36 mL, 3.02 mmol) in dichloromethane (15 mL) under nitrogen was added DMAP (73.1 mg, 0.598 mmol) and diisopropylethylamine (1.04 mL, 5.97 mmol); followed by diethyl chlorophosphate (0.65 mL, 4.50 mmol). After stirring overnight, additional dichloromethane (15 mL) and saturated aqueous sodium bicarbonate solution (15 mL) were added, and the mixture stirred vigorously for twenty minutes. The organic phase was separated, and washed sequentially with equal volumes of 1.2M HCl solution and brine, dried and evaporated. Flash chromatography (40% ethyl acetate/hexane) afforded 4.5 as a colourless oil (619.4 mg, 87%). R_f (40% ethyl acetate/hexane): 0.25; ^{1}H NMR (500 MHz, $CDCl_3$) δ ppm; 5.76 (tdd, *J* = 16.9, 10.2, 6.7, Hz, 1H, H2), 4.98 (ddd, *J* = 17.1, 3.1, 1.6 Hz, 1H, H1E), 4.93 (tdd, *J* = 10.2, 2.1, 1.1 Hz, 1H, H1Z), 4.08 (app qd, *J* = 9.0, 7.4 Hz, 6H, H6 & POC$\underline{H}_2$CH$_3$), 2.06 (ddt, *J* = 14.3, 7.3, 1.2 Hz, 2H, H3), 1.67 (app td, *J* = 14.9, 6.7 Hz, 2H, H5), 1.46 (app p, *J* = 7.7 Hz, 2H, H4), 1.31 (dt, *J* = 7.1, 0.9 Hz, 6H, POCH$_2$C$\underline{H}_3$), ^{13}C NMR (75 MHz, $CDCl_3$) δ ppm 138.2 (C2), 114.8 (C1), 67.3 (d, *J* = 6.0 Hz, PO$\underline{C}$6), 63.6 (d, *J* = 5.7 Hz, PO$\underline{C}$H$_2$CH$_3$), 33.1 (C3), 29.6 (d, *J* = 6.9 Hz, POC6$\underline{C}$5), 24.6 (C4), 16.1 (d, *J* = 6.7 Hz, POCH$_2\underline{C}$H$_3$); ^{31}P NMR (121 MHz, $CDCl_3$, ^{1}H decoupled) δ ppm -0.3 (O$\underline{P}$OCH$_2$CH$_3$); HRMS, required for $C_{10}H_{22}O_4P$ 237.1256, found 237.1245.

Methyl 7-(diethoxyphosphoryloxy)hept-2-enoate

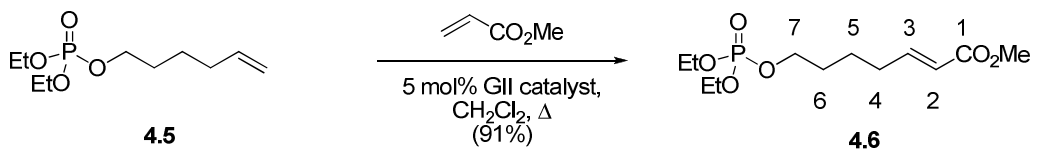

4.5 **4.6**

To a solution of alkene 4.5 (235.6 mg, 0.997 mmol) and methyl acrylate (180 μL, 2.00 mmol) in dichloromethane (5 mL) was added Grubbs second generation catalyst (42.3 mg, 50 μmol, 5 mol%). The mixture was deoxygenated by purging three cycles of vacuum/argon, then refluxed overnight under argon. After 20 hours, the reaction was cooled, DMSO (180 μL, ~50 catalyst equivalents) was added and stirring continued at room temperature overnight. Evaporation and flash chromatography (60% ethyl acetate/hexane), followed by the addition of further dichloromethane (5 mL) and DMSO (180 μL), stirring overnight and a second round of flash chromatography (50% ethyl acetate/hexane) gave acrylate 4.6 as a pale yellow oil (268 mg, 91%). R_f (60% ethyl acetate/hexane): 0.26; ^{1}H NMR (500 MHz, $CDCl_3$) δ ppm 6.91-6.85 (m, 1H, H3), 5.77 (app ddd, *J* = 15.7, 2.5, 1.3 Hz, 1H, H2), 4.08-4.00 (m, 4H, POC$\underline{H}_2$CH$_3$), 3.98 (dt, *J* = 10.5, 6.5 Hz, 2H, H7), 3.66 (app dd, *J* = 3.2, 1.1 Hz, 3H, $CO_2\underline{Me}$), 2.23-2.14 (m, 2H, H4), 1.68-1.61 (m, 2H, H6), 1.56-1.46 (m, 2H, H5), 1.27 (td, *J* = 7.0, 4.0 Hz, 6H, POCH$_2$C$\underline{H}_3$); ^{13}C NMR (126 MHz, $CDCl_3$) δ ppm 167.1 (C1), 148.9 (C3), 121.5 (C2), 67.3 (d, *J* = 5.9 Hz, C7), 64.0 (d, *J* = 5.9 Hz, PO$\underline{C}$H$_2$CH$_3$), 51.6 ($CO_2\underline{Me}$), 31.7 (C4), 29.8 (d, *J* = 7.0 Hz, C6), 24.1 (C5), 16.3 (d, *J* = 6.6 Hz, POCH$_2\underline{C}$H$_3$); ^{31}P NMR (121 MHz, $CDCl_3$, ^{1}H-coupled) δ ppm -0.4 (sept, *J* = 7.6 Hz, C7O$\underline{P}$); HRMS, Required for $C_{12}H_{24}O_6P$: 295.1311, Found: 295.1297.

7-(Phospho)hept-2-enoate, potassium salt

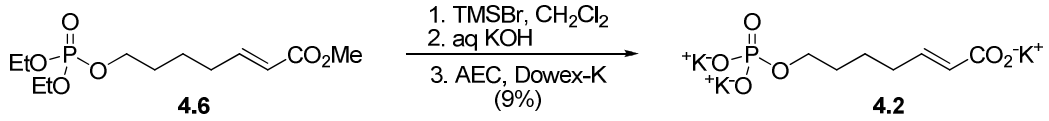

To a solution of ester 4.6 (134 mg, 0.455 mmol) in dichloromethane (3.5 mL) under nitrogen was added trimethylsilyl bromide (360 μL, 2.73 mmol) dropwise, the mixture was then stirred overnight. The reaction was quenched with methanol (1 mL) and evaporated. The residue was dissolved in 10% w/v aqueous potassium hydroxide (4 mL), and stirred vigorously for three hours. After three hours the aqueous phase was extracted with dichloromethane (3x 3 mL), and the organic phases discarded. The aqueous phase was passed through a short column of Dowex-50X8 (H^+-form, 10 x 50 mm), the filtrate was collected and the column washed with water (15 mL). The combined aqueous extracts were lyophilised, and separated by preparative anion-

exchange chromatography, (SourceQ® resin, 4°C, 0 to 1M ammonium bicarbonate gradient elution, product elutes at 180 mM ammonium bicarbonate). The product fractions were lyophilised, redissolved in water (1 mL), passed through a short column of Dowex-50X8 (H^+-form, to quench any residual ammonium bicarbonate) then thorough a column of Dowex-50X8 (K^+-form). The filtrate was lyophilised to give phosphate 4.2 as an off-white powder (14.4 mg, 9%), containing <20% residual ethyl groups (NMR). ^{1}H NMR (500 MHz, D_2O, presat) δ ppm 6.49 (td, *J* = 14.2, 6.9 Hz, 1H, H3), 5.68 (d, *J* = 15.7 Hz, 1H, H2), 3.60 (app dd, *J* = 12.5, 6.6 Hz, 2H, H7), 2.05 (dd, *J* = 13.7, 7.0 Hz, H4), 1.46 (app sext, *J* = 7.1 Hz 2H, H6), 1.35 (app p, *J* = 7.4 Hz , 2H, H5); ^{13}C NMR (126 MHz, D_2O, HSQC-DEPT135) δ ppm 145.7 (C2), 126.1 (C3), 64.3 (C7), 31.2 (C4) , 29.9 (C6), 24.3 (C5), ^{31}P NMR (121 MHz, D_2O, ^{1}H-decoupled): 4.2 (br s, C7O<u>P</u>).

Hex-5-enyl 2-(bromomethyl)acrylate

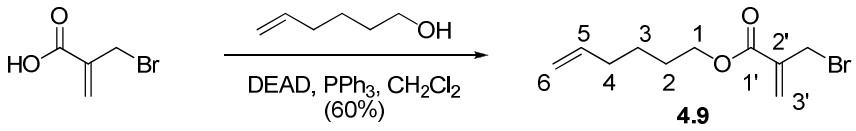

4.9

To a stirred solution of acid (1.6484 g, 9.99 mmol) in diethyl ether (15 mL) at 0°C under nitrogen was added distilled diethylazodicarboxylate (1.58 mL, 10.0 mmol). In another flask, a solution of hex-5-enyl alcohol (1.08 mL, 8.99 mmol) and triphenylphosphine (2.624 g, 10.0 mmol) in diethyl ether (10 mL) was prepared, the solution was transferred to a dropping funnel and added dropwise to the vigorously stirred acid/DEAD solution. The funnel was washed with further diethyl ether (5 mL), the washings were also added dropwise to the acid flask. The resulting mixture was stirred vigorously overnight; the ice bath was allowed to melt during this time. The suspension was filtered through a short plug of silica (1 x 5 cm), the precipitate washed well with diethyl ether (2x 20 mL), and the combined filtrates evaporated. Pentane (50 mL) was added to the residue, the precipitated triphenylphosphine oxide was removed by filtration, and the filtrate evaporated and purified by flash chromatography (5% diethyl ether/hexane) to afford ester 4.9 as a colourless oil (1.3345 g, 60%). R_f (5% diethyl ether/hexane): 0.36; ^{1}H NMR (500 MHz, $CDCl_3$) δ ppm 6.32 (d, *J* = 0.7 Hz, 1H, H3'E), 5.94 (d, *J* = 0.8 Hz, 1H, H3'Z), 5.80 (tdd, *J* =

16.9, 10.2, 6.7, Hz, 1H, H5), 5.02 (ddd, *J* = 17.1, 3.4, 1.6 Hz, 1H, H6Z), 4.97 (tdd, *J* = 10.2, 2.0, 1.1, Hz, 1H, H6E), 4.22 (t, *J* = 6.6 Hz, 2H, H1), 4.18 (d, *J* = 0.8 Hz, 2H, C$\underline{H}_2$Br), 2.10 (dd, *J* = 14.3, 7.2 Hz, 1H, H4), 1.72 (td, *J* = 14.8, 6.7 Hz, 2H, H2), 1.50 (m, 2H, H3); ^{13}C NMR (126 MHz, $CDCl_3$) δ ppm 165.1 (C1'), 138.5 (C2'), 137.8 (C5), 129.3 (C3'), 115.2 (C6), 65.5 (C1), 33.5 (C4), 29.6 (C$\underline{H}_2$Br), 28.2 (C2), 25.4, (C3).

Allyl 2-(bromomethyl)acrylate

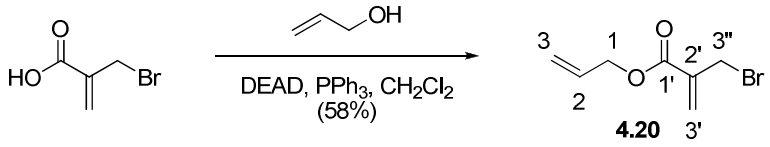

By a similar method as used for 4.9 but using allyl alcohol (190 μL, 2.79 mmol) gave ester 4.20 (332.6 mg, 58%) after flash chromatography (10% diethyl ether/hexane). R_f (10% diethyl ether/hexane): 0.39; ^{1}H NMR (500 MHz, $CDCl_3$) δ ppm 6.36 (dd, *J* = 1.2, 0.8 Hz, 1H, H3'*E*), 6.01-5.91 (m, 2H, H3'*Z*, H2), 5.37 (dm, *J* = 17.2 Hz, 1H, H3E), 5.27 (dtd, *J* = 10.4, 2.3, 1.2 Hz, 1H, H3Z), 4.71 (dm, *J* = 5.6 Hz, 2H, H1), 4.19 (dd, *J* = 1.7, 0.8 Hz, 2H, H3''); ^{13}C NMR (75 MHz, $CDCl_3$) δ ppm 164.7 (C1), 137.6 (C2'), 132.0 (C2), 129.6 (C3'), 118.7 (C3), 66.1 (C1), 29.5 (C3'').

Acetoxyhept-5-enyl 2-(bromomethyl)acrylate

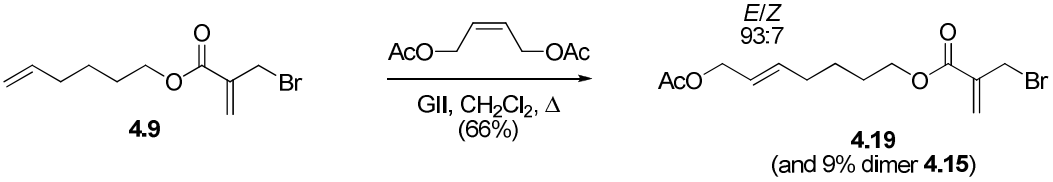

To a solution of diene 4.9 (123.5 mg, 0.500 mmol) in dichloromethane (1 mL) was added diacetoxy-(*Z*)-butene (115 μL, 0.721 mmol). The resulting olefin solution was added *via* syringe to a solution of Grubbs second generation catalyst (11.7 mg, 13.8 μmol, 2.8 mol %) in dichloromethane (1 mL) under argon, and the syringe washed with further dichloromethane (0.5 mL). The combined solutions were degassed (3x cycles of vacuum/ argon), and refluxed overnight under argon. After 23 hours heating

ceased, the reaction was quenched with DMSO (100 μL) and stirred overnight. Flash chromatography (10% diethyl ether/hexane) gave hindered diene 4.19 (99.4 mg, 66%), as an unseparated 93:7 *E*:*Z* mixture of isomers.. R_f (10% diethyl ether/hexane): 0.49; ^{1}H NMR (500 MHz, $CDCl_3$) δ ppm 6.30 (s, 1H, H3'E), 5.92 (s, 1H, H3'Z), 5.73 (tdd, *J* = 15.4, 7.4, 0.7 Hz, 1H, H5), 5.56 (tdd, 15.4, 6.5, 0.9 Hz, 1H, H6), 4.48 (d, *J* = 6.4 Hz, 2H, H7), 4.19 (t, *J* = 6.5 Hz, 2H, H1), 4.15 (s, 2H, C$\underline{H}_2$Br), 2.09 (app q, *J* = 7.2, 7.1 Hz, 2H, H4), 2.03 (s, 3H, C(O)C$\underline{H}_3$), 1.68 (dq, *J* = 10.3 Hz, 6.73 Hz, 2H, H2), 1.49 (app quintet, *J* = 7.6 Hz, 2H, H3), distinct Z isomer signals: 6.35 (s, 0.08H, Z-H3'Z), 5.95 (s, 0.08H, Z- H3'E), 4.59 (d, *J* = 6.7 Hz, 0.16H, Z-H7), 4.26 (s, 0.16H, Z-C$\underline{H}_2$Br); ^{13}C NMR (126 MHz, $CDCl_3$) δ ppm 171.1 (O$\underline{C}$(O)CH_3), 165.1 (C1'), 137.8 (C2'), 135.8 (C5), 129.3 (C3'), 124.7, (C6) 65.4 (C7 and C1), 32.0 (C4), 29.6 ($\underline{C}H_2$Br), 28.3 (C3), 25.5 (C2), 21.3 (C(O)$\underline{C}H_3$). HRMS; required for $C_{13}H_{20}O_4Br$ 319.0545, found 319.0537.

Summary of unsuccessful RCM reactions*

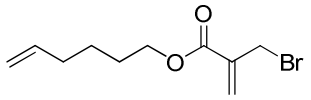

4.9

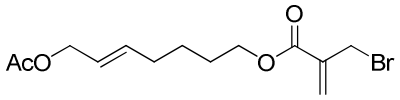

4.19

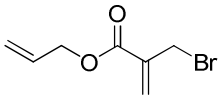

4.20

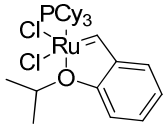

HGI

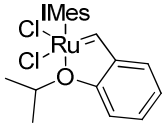

HGII

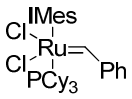

GII

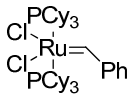

GI

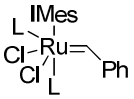

GPF

L=

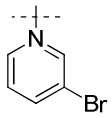

IMes=

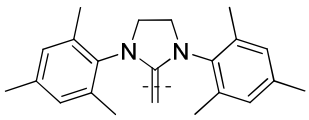

Diene	[diene]	Catalyst	Notes
4.20	20 mM	GII	
4.19	0.67 mM	GII	
4.19	0.67 mM	GII	+ 10 mol% Ti(O*i*Pr)$_4$
4.20	5 mM	GII	+ 10 mol% Ti(O*i*Pr)$_4$
4.20	6 mM	GPF	
4.19	3 mM	GII	+ 10 mol% Ti(O*i*Pr)$_4$, diene slow addition (10 hrs)
4.20	2 mM	GI	Diene, catalyst slow addition (8 hrs)
4.9	7 mM	GII	Toluene, 80°C
4.9	46 mM	HGI	

4.9	111 μM	GII	Toluene, reflux
4.9	2 mM	GII	Diene, catalyst slow addition
4.9	20 mM	GII	+ 25 mol% $Ti(OiPr)_4$
4.9	5 mM	GII	
4.9	23 mM	GII	
4.9	19 mM	GII	2x 10 min microwave heating, 2x 2 mol% catalyst
4.9	2 mM	GI	+ 15 mol% $Ti(OiPr)_4$, diene slow addition
4.9	2.6 mM	HGII	

* Standard parameters: refluxed all reactants with conventional heating, overnight in dichloromethane under argon. Deviations from these parameters are noted.

Key data for Metathesis Byproducts

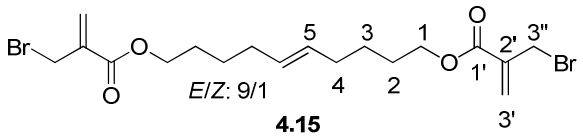

4.15

oil; R_f (20% diethyl ether/hexane): 0.40; ^{1}H NMR (500 MHz, $CDCl_3$) δ ppm major *E* isomer: 6.31 (s, 0.9H, H3'*E*), 5.92 (s, 0.9H, H3'*Z*), 5.39 (ddd, *J* = 5.2, 3.7, 1.4 Hz, 0.9H, *E*-H5), 4.19 (m, 2H, both isomers H1), 4.16 (s, H3''), 2.01 (m, 2H, both isomers H4), 1.68 (app td, *J* = 14.7, 6.7 Hz, 2H, both isomers H2); 1.48-1.40 (m, 2H, H3) distinct (*Z*)-isomer signals: 6.36 (s, 0.1H, H3'*E*), 5.95 (s, 0.1H, H3'*Z*), 5.36 (t, *J* = 4.6 Hz, 0.1H, *Z*-H5), 4.27 (s, 0.2H, H3''); ^{13}C NMR (126 MHz, $CDCl_3$): 130.4 (C5), 129.2 (C3'), 65.6 (C1), 32.0 (C4), 29.8 (C3''), 28.1 (C4), 25.9 (C3); HRMS, required for $C_{18}H_{27}O_4Br_2$ 465.0276, found 465.0254.

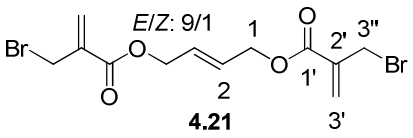

4.21

white solid, mp: 60-62°C; R_f (20% diethyl ether/hexane): 0.24; ^{1}H NMR (500 MHz, $CDCl_3$) δ ppm major *E* isomer: 6.35 (s, 1H, H3'*E*), 5.98 (s, 1H, H3'*Z*), 5.97-5.93 (m, 1H, H2), 4.74 (dd, *J* = 2.8, 1.3 Hz, 1H, H3''), 4.19 (d, *J* = 0.4 Hz, 1H, H1); distinct (*Z*)-isomer signals: 6.42 (s, 0.1H), 6.01 (s, 0.1H), 5.89-5.83 (m, 0.1H), 4.85 (dd, *J* = 4.0, 1.0 Hz, 0.2H), 4.29 (d, *J* = 0.7 Hz, 0.2H); ^{13}C NMR (75 MHz, $CDCl_3$) δ ppm

164.7 (C1'), 137.5 (C2'), 129.8 (C3'), 128.1 (C2), 64.8 (C1), 29.5 (C3''). HRMS (electrospray, Cs^+ matrix) required for $C_{12}H_{14}O_4CsBr_2$: 512.8313, found 512.8326 ($M\text{-}Cs^+$).

5-(*Tert*-butyldimethylsilyloxy)pentan-1-ol

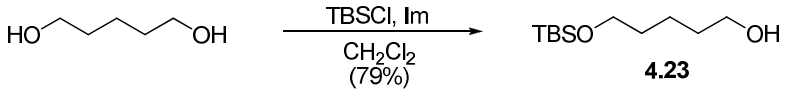

To a solution of imidazole (2.862g, 42.0 mmol) in dichloromethane (200 mL) was added pentane-1,5-diol (6.3 mL, 60.0 mmol); The suspension was stirred vigorously at 0°C under nitrogen as a solution of *tert*-butyldimethylsilyl chloride (3.018 g, 20.0 mmol) in dichloromethane (50 mL) was added dripwise over approximately one hour. The resulting solution was stirred vigorously overnight, the ice bath being allowed to thaw over this time. Water (150 mL) was added, and the organic phase was separated and washed with further water (2x 150 mL), saturated ammonium chloride solution (150 mL), and brine (150 mL); the solution was dried and evaporated. Flash chromatography (40% ethyl acetate/hexane) gave monoprotected diol 4.23 as a colourless oil (3.4345g, 79%) with spectral data in accordance with the literature[196]. R_f (20% ethyl acetate/hexane): 0.29; ^{1}H NMR (500 MHz, $CDCl_3$) δ ppm 3.57 (app t, 4H, J = 6.6 Hz, H1&H5), 1.51 (m, H2&H4), 1.36 (m, 2H, H3), 0.84 (d, 9H, J = 1.3 Hz, $\underline{Me}_3CSi$), 0.00 (d, 6H, J = 1.3 Hz, $\underline{Me}_2Si$),; ^{13}C NMR (75 MHz, $CDCl_3$) δ ppm 63.1 (C1), 62.5 (C5), 32.4 (C2), 32.3 (C4), 25.9 ($\underline{Me}_3CSi$), 21.9 (C3), 18.3 ($Me_3\underline{C}Si$).

5-(*Tert*-butyldimethylsilyloxy)pentanal *via* IBX oxidation

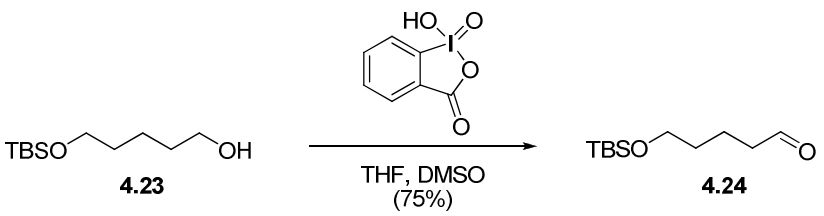

To a vigorously stirred solution of alcohol 4.23 (3.4345 g, 15.73 mmol) in tetrahydrofuran (66 mL) and dimethylsulfoxide (10 mL, 140. 7 mmol) was added 2-

iodoxybenzoic acid (6.627 g, 23.6 mmol), and the mixture was stirred overnight. The mixture was filtered through celite, evaporated and the residue diluted with diethyl ether (250 mL). The liquid was decanted from the precipitate, and washed with water (2x 200 mL) and brine (200 mL), dried and evaporated. The residue was loaded onto a short plug of silica and eluted with 10% ethyl acetate/hexane. Evaporation of product fractions gave aldehyde 4.24 as a pale yellow oil (2.554g, 75%) with spectral data in accordance with the literature[197]. R_f (20% ethyl acetate/hexane): 0.71; ^{1}H NMR (500 MHz, $CDCl_3$) δ ppm 9.74 (t, *J* = 1.76 Hz, 1H, H1), 3.60 (t, *J* = 6.21 Hz, 2H, H5), 2.43 (dt, *J* = 7.35, 1.76 Hz, 2H, H2), 1.72-1.63 (m, 2H, H3), 1.57-1.49 (m, 2H, H4), 0.86 (s, 9H, $\underline{Me}_3CSi$), 0.02 (s, 6H, $\underline{Me}_2Si$); ^{13}C NMR (75 MHz, $CDCl_3$): 202.5 (C1), 62.5 (C5), 43.6 (C2), 32.0 (C4), 25.9 ($\underline{Me}_3CSi$), 18.6 (C3), 18.3 ($Me_3\underline{C}Si$).

Ethyl 2-(hydroxy(phenyl)methyl)acrylate[146]

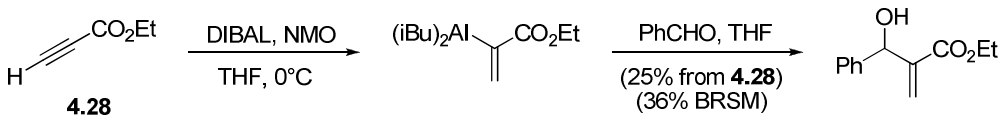

A vigorously stirred suspension of *N*-methylmorpholine *N*-oxide (234.7 mg, 2.00 mmol) in tetrahydrofuran (3.8 mL) under nitrogen was cooled to 0°C, and diisobutylaluminium hydride (20 wt% in toluene, 1.25 mL, 1.5 mmol) was added dropwise. The suspension became a solution on DIBAL addition, and a small amount of effervescence was observed. After 45 minutes, ethyl propiolate 4.28 (102 μL, 1.01 mmol) was added, and stirring continued for one hour. To the resulting solution of vinyl alane was added benzaldehyde (120 μL, 1.18 mmol), the ice bath was removed and the mixture stirred for five hours at room temperature. The mixture was cooled to 0°C, and saturated aqueous citric acid (5 mL) was added dropwise with vigorous stirring, after five minutes ethyl acetate (10 mL) was added. The organic phase was separated, and the aqueous phase was extracted with further ethyl acetate (2x 10 mL). The combined organic phases were washed with saturated aqueous sodium bicarbonate solution (10 mL) and brine (10 mL), dried and evaporated. Flash chromatography (10% ethyl acetate/hexane) gave recovered benzaldehyde (39 mg) and the desired acrylate (52.8 mg, 25%); with spectral data in accordance with that published.

5-(*Tert*-butyldiphenylsilyloxy)pentan-1-ol

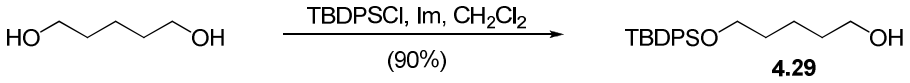

By the same method as for 4.23; using *tert*-butyldiphenylsilyl chloride (2.60 mL, 10.1 mmol) gave the corresponding mono-TBDPS protected alcohol 4.29 (3.126 g, 90%) after flash chromatography (20% ethyl acetate/hexane) with spectral data in accordance with the literature[198]. R_f (20% ethyl acetate/hexane): 0.36; ^{1}H NMR (500 MHz, $CDCl_3$) δ ppm 7.68 (m, 4H, *o*-SiArH), 7.46-7.34 (m, *m*,*p*-SiArH), 3.69 (dt, *J* = 6.29, 0.82 Hz, 2H, H5), 3.62 (dt, *J* = 6.52, 1.40 Hz, 2H, H1), 1.66-1.51 (m, 6H, H2, H3, H4), 1.07 (t, *J* = 1.12 Hz, 9H, $\underline{Me}_3CSi$); ^{13}C NMR (126 MHz, $CDCl_3$) δ ppm 135.8 (ArSi), 134.3 (ArSi), 129.8 (ArSi), 127.9 (ArSi), 64.1 (C5), 63.2(C1), 32.7 (C4), 32.5 (C2), 27.1 ($\underline{Me}_3CSi$), 22.3 (C3), 19.5 ($Me_3\underline{C}Si$); HRMS: Required for $C_{21}H_{31}O_2Si$: 343.2093, Found: 343.2080.

5-(*Tert*-butyldiphenylsilyloxy)pentanal

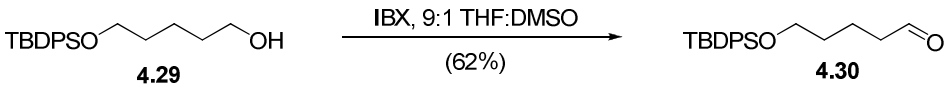

By the same method as for 4.24; using TBDPS-alcohol 4.29 (1.3721 g, 4.01 mmol) after flash chromatography (10% ethyl acetate/hexane) gave aldehyde 4.30 (850.7 mg, 62%) with spectral data in accordance with the literature[199]. R_f (20% ethyl acetate/hexane): 0.73; ^{1}H NMR (500 MHz, $CDCl_3$) δ ppm 9.76 (t, *J* = 1.76 Hz, 1H, H1), 7.71-7.65 (m, 4H, *o*-SiArH), 7.46-7.37 (m, 6H, *m*,*p*-SiArH), 3.69 (t, *J* = 6.17 Hz, 2H, H5), 2.42 (dt, *J* = 7.36, 1.76 Hz, 2H, H2), 1.80-1.70 (m, 2H, H3), 1.65-1.57 (m, 2H, H4), 1.07 (s, 9H, $\underline{Me}_3CSi$); ^{13}C NMR (126 MHz, $CDCl_3$) δ ppm 202.9 (C1), 135.8 (ArSi), 134.1 (ArSi), 129.8 (ArSi), 127.9 (ArSi), 63.5 (C5), 43.8 (C2), 32.1 (C4), 27.1($\underline{Me}_3CSi$), 19.4 ($Me_3\underline{C}Si$), 18.8 (C3); HRMS: Required for $C_{21}H_{29}O_2Si$: 341.1937, Found: 341.1936.

Ethyl 7-(tert-butyldiphenylsilyloxy)-3-hydroxy-2-methyleneheptanoate

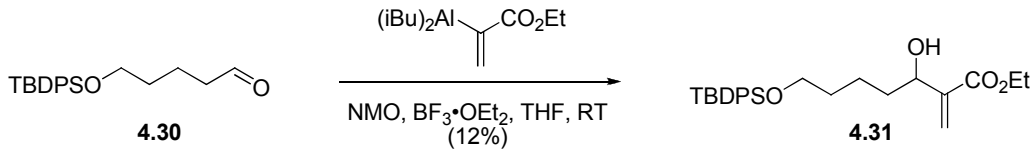

4.30 **4.31**

A solution of vinyl alane was prepared from ethyl propiolate 4.28 as described above for ethyl 2-(hydroxy(phenyl)methyl)acrylate. Aldehyde 4.30 (416.2 mg, 1.22 mmol) followed by boron trifluoride - diethyl ether complex (150 µL, 1.22 mmol) were added dropwise at 0ºC, then the pale yellow mixture was stirred at room temperature for four hours, before quenching and workup as above for ethyl 2-(hydroxy(phenyl)methyl)acrylate. Flash chromatography (15% ethyl acetate/hexane) gave aliphatic acrylate 4.31 (52.9 mg, 12%), contaminated with a small amount of aldehyde 4.30. R_f (20% ethyl acetate/hexane): 0.36; ^{1}H NMR (500 MHz, $CDCl_3$) δ ppm 7.75-7.64 (m, 4H, SiArH), 7.46-7.36 (m, 6H, SiArH), 6.24 (d, *J* = 1.07 Hz, 1H, H3'E), 5.79 (t, *J* = 1.07, Hz, 1H, H3'Z), 4.41 (dd, *J* = 7.14, 5.66 Hz, 1H, H3), 4.25 (q, *J* = 7.14 Hz, 2H, $CO_2C\underline{H}_2CH_3$), 3.70 (t, *J* = 6.35 Hz, 2H, H7), 2.96 (br s, 1H, C3O<u>H</u>), 1.73-1.59 (m, H4, H6), 1.49-1.42 (m, H5), 1.08 (s, 9H, $\underline{Me}_3CSi$), 1.32 (t, *J* = 7.12, 3H, $CO_2CH_2C\underline{H}_3$); ^{13}C NMR (126 MHz, $CDCl_3$) δ ppm 166.9 (C1), 142.9 (C2), 135.9 (ArSi), 134.3 (ArSi), 129.8 (ArSi) , 127.9 (ArSi), 125.0 (C3'), 72.0 (C3), 64.1 (C5), 61.1 ($CO_2\underline{C}H_2CH_3$), 36.2 (C2), 32.6 (C4) , 27.2 ($\underline{Me}_3CSi$), 22.4 (C5), 19.5, ($Me_3\underline{C}Si$), 14.4 ($CO_2CH_2\underline{C}H_3$).

Methyl 2-bromoacrylate[149]

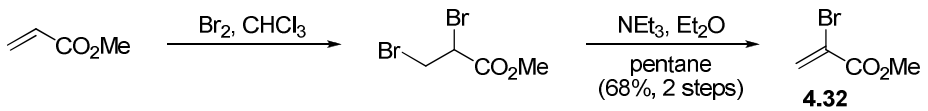

4.32

To a stirred solution of methyl acrylate (22.0 mL, 0.244 mol) in chloroform (100 mL) was added bromine (12.5 mL, 0.243 mol) dropwise over twenty minutes. After stirring for 3 hours the mixture was evaporated, and the residue diluted with diethyl ether (150 mL) and pentane (150 mL). The mixture was stirred vigorously as triethylamine (35 mL, 0.251 mol) was added dropwise, and after three hours the

suspension was filtered, and the precipitate washed with pentane (200 mL). The combined filtrates were washed with water (150 mL), dried and evaporated. The residue was vacuum distilled (65-75°C/ 48 mmHg) to give methyl 2-bromoacrylate (27.301 g, 68%) as a colourless oil. ^{1}H NMR (500 MHz, $CDCl_3$) δ ppm 6.95 (app t, *J* = 1.5 Hz, 1H), 6.26 (app t, *J* = 1.5 Hz, 1H), 3.82 (d, 3H, *J* = 1.5 Hz), ^{13}C NMR (126 MHz, $CDCl_3$) δ ppm 162.7 ($\underline{C}O_2Me$), 131.1 ($C=\underline{C}H_2$), 121.2 ($\underline{C}Br$), 53.7 ($CO_2\underline{Me}$).

Methyl 3-(dimethylamino)propanoate

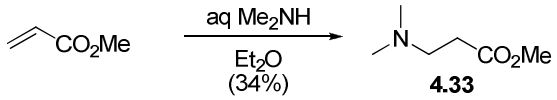

4.33

To a vigorously stirred mixture of 40% aqueous methylamine (7 mL, 55.3 mmol as Me_2NH) and diethyl ether (20 mL) was added methyl acrylate (4.5 mL, 50.0 mmol) dropwise. Once the initial exothermic reaction subsided the mixture was brought to reflux. After 3 hours the mixture was cooled, diluted with further diethyl ether (50 mL) and dried with sodium sulfate. The sodium sulfate was washed with further diethyl ether (100 mL), and the combined extracts were evaporated. Kugelrohr distillation (70°C/high vacuum) gave methyl 3-(dimethylamino)propanoate 4.33 (2.258g, 34%). The compound was stored over 4Å molecular sieves at 4°C. ^{1}H NMR (500 MHz, d_4-MeOH) δ ppm 5.05 (s, 3H, $CO_2\underline{Me}$), 4.02 (t, *J* = 7.2 Hz, 2H, $C\underline{H}_2NMe_2$), 3.89 (t, *J* = 7.2 Hz, 2H, $C\underline{H}_2CO_2Me$), 3.62 (s, 6H, $\underline{Me}_2N$); ^{13}C NMR (126 MHz, $CDCl_3$) δ ppm 32.9 ($\underline{C}H_2CO_2Me$), 45.4 ($\underline{Me}_2N$), 51.8 ($CO_2\underline{Me}$), 54.9 ($\underline{C}H_2NMe_2$), 173.0 ($\underline{C}O_2Me$).

5-(Tetrahydro-2H-pyran-2-yloxy)pentan-1-ol

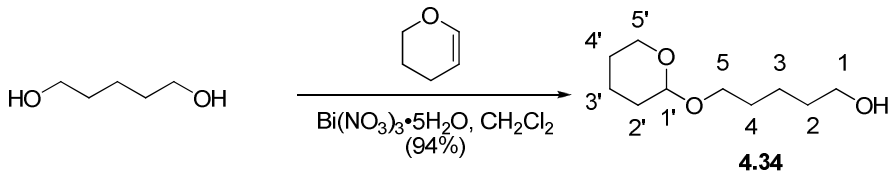

4.34

To a vigorously stirred suspension of 1,5-pentanediol (6.2728 g, 60.2 mmol) in dichloromethane (40 mL) was added dihydropyran (1.80 mL, 19.7 mmol) and finely

ground bismuth(III) nitrate pentahydrate (484.3 mg, 0.998 mmol, 5 mol%). After 2.5 hours the mixture was filtered through a plug of 1:1 chromatographic silica:celite, and the plug eluted with dichloromethane (50 mL fractions). The fractions containing product were combined and evaporated to give THP diethyl ether 4.34 (3.5061 g, 94%) with spectral data in accordance with the literature[200]. R_f (40% ethyl acetate/hexane): 0.25; ^{1}H NMR (500 MHz, $CDCl_3$) δ ppm 4.54 (dd, *J* = 4.28, 2.84 Hz, 1H, H1'), 3.83 (ddd, *J* = 11.06, 7.67, 3.34 Hz, 1H, H5'a), 3.72 (td, *J* = 9.65, 6.72, Hz, 1H, H5a), 3.60 (t, *J* = 6.58 Hz, 2H, H1), 3.50-3.43 (m, 1H, H5'b), 3.37 (td, *J* = 9.65, 6.5 Hz, 1H, H5b), 2.12 (br s, 1H, C1O<u>H</u>), 1.84-1.75 (m, 1H, H3'a), 1.72-1.64 (m, 1H, H2'a), 1.64-1.45 (m, 8H, H2, H4, H2'b, H3'b, H4'), 1.45-1.37 (m, 2H, H3); ^{13}C NMR (126 MHz, $CDCl_3$) δ ppm 98.8 (C1'), 67.4 (C5), 62.6 (C1), 62.3 (C5'), 32.4 (C2) , 30.6 (C2'), 29.3 (C4), 25.4 (C4'), 22.4 (C3), 19.6 (C3'a).

5-(Tetrahydro-2H-pyran-2-yloxy)pentanal *via* buffered Dess-Martin periodinane

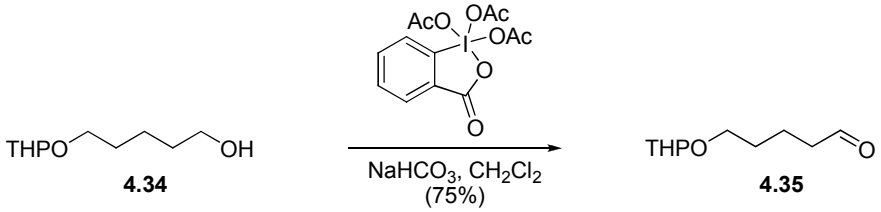

To Dess-Martin periodinane (2.757g, 6.5 mmol) in dichloromethane (30 mL) was added in small portions sodium bicarbonate solution (845.3 mg, 10.06 mmol) followed by alcohol 4.34 (205 mg, 1.09 mmol) in dichloromethane (1 mL). After 4.5 hours the mixture was poured into diethyl ether (100 mL), filtered through celite, washed with saturated aqueous sodium bicarbonate solution (50 mL) and brine (50 mL), dried and evaporated. Flash chromatography (20% ethyl acetate/hexane) afforded aldehyde 4.35 (152.8 mg, 75%) with spectral data in accordance with the literature[201]; R_f (40% ethyl acetate/hexane): 0.67; ^{1}H NMR (500 MHz, $CDCl_3$) δ ppm 9.75 (t, *J* = 1.7 Hz, 1H, H1), 4.54 (dd, *J* = 4.2, 2.7 Hz, 1H, H1'), 3.90-3.78 (m, 1H, H5'a), 3.73 (td, *J* = 9.7, 6.4 Hz, 1H, H5a), 3.51-3.42 (m, 1H, H5'b), 3.37 (td, *J* = 9.7, 6.2 Hz, 1H, H5b), 2.46 (dt, *J* = 7.3, 1.6 Hz, 1H, H2), 1.80-1.43 (m, 10H, H3, H4, H2', H3' H4'); ^{13}C NMR (126 MHz, $CDCl_3$); 99.1 (C1'), 67.2 (C5), 62.6 (C5'), 43.7 (C2), 30.9 (C2'), 29.1 (C4), 25.5 (C4'), 19.9 (C3'), 19.3 (C3).

5-(Tetrahydro-2H-pyran-2-yloxy)pentanal via Swern oxidation

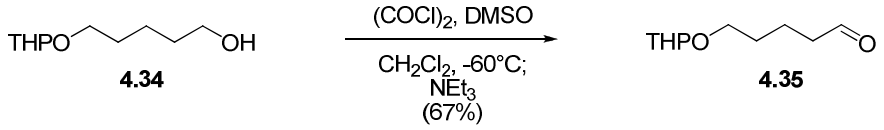

A solution of oxalyl chloride (1.95 mL, 22.7 mmol) in dichloromethane (50 mL) was cooled to -60°C (dry ice/ chloroform, monitored with a thermocouple) under nitrogen, and DMSO (3.2 mL, 45. 1 mmol) in dichloromethane (10 mL) was added dropwise from a pressure equalised dropping funnel. Once all of the DMSO solution had been added, stirring was continued at -60°C for five minutes, the funnel was charged with alcohol 4.34 (3.5061 g, 18.62 mmol) in dichloromethane (19 mL) and the alcohol solution was added dropwise to the oxidant solution. Once all of the alcohol had been added, the solution was stirred for 30 minutes, then brought to -20°C. Neat triethylamine (12.5 mL, 89.7 mmol), was then added dropwise; once addition was complete the mixture was stirred for 20 minutes then brought to room temperature. Diethyl ether (100 mL) was added, and the solution washed with saturated ammonium chloride solution (50 mL), saturated sodium bicarbonate solution (100 mL), and brine (100 mL). The solution was dried and evaporated, and flash chromatography (20% ethyl acetate/hexane) gave aldehyde 4.35 as a colourless oil (2.334 g, 67%), with spectral data as reported above.

Methyl-3-hydroxy-2-methylene-7-(tetrahydro-2H-pyran-2-yloxy)heptanoate

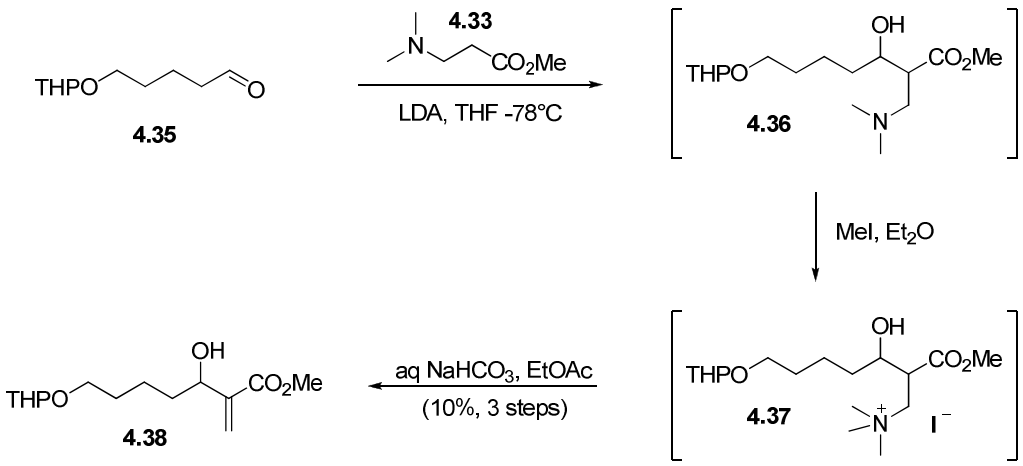

A solution of diisopropylamine (980 μL, 7.04 mmol) in tetrahydrofuran (20 mL) was cooled to -78°C under nitrogen, and a 1.6M solution of *n*-butyllithium in hexanes (4.0 mL, 6.4 mmol) was added dropwise. The mixture was stirred at -78°C for ten minutes, then brought to 0°C for thirty minutes, then cooled back to -78°C. A solution of aminoester 4.33 (707 mg, 5.39 mmol) in tetrahydrofuran (2 mL) was slowly added, and the solution stirred for 15 minutes. To the resulting enolate solution was added a solution of aldehyde 4.35 (999.5 mg, 5.37 mmol) in tetrahydrofuran (2 mL), the solution was stirred for twenty minutes then quenched with saturated sodium carbonate (10 mL) and allowed to come to room temperature. The mixture was diluted with water (10 mL), the organic phase separated and the aqueous phase extracted with chloroform (2x 25 mL). The organic extracts were dried separately over sodium sulfate, and evaporated to give a pale yellow oil (1.165 g). This oil was immediately dissolved in diethyl ether (10 mL) and excess methyl iodide (5 mL) was added. The mixture was stirred in the dark for 2 hours, and diluted with pentane (30 mL). The solution was carefully decanted from the resulting sticky residue, and the residue was washed in the same flask with further pentane (30 mL). Ethyl acetate (10 mL) and saturated aqueous sodium bicarbonate solution (10 mL) were added, and the heterogeneous mixture stirred vigorously for five hours. The mixture was diluted with dichloromethane (50 mL), the aqueous phase was separated and washed with further dichloromethane (2x 30 mL). The combined dichloromethane phases were washed with brine (30 mL – an emulsion initially formed, which slowly separates over 15-20 minutes), dried and evaporated. Flash chromatography (30% ethyl acetate/hexane) gave acrylate 4.38 (144.7 mg, 10% over three steps). In similar experiments the yields were erratic, ranging from 17% on a 0.82 mmol scale to 1.1% on 12.5 mmol scale. R_f (33% ethyl acetate/hexane): 0.38; ^{1}H NMR (500 MHz, $CDCl_3$) δ ppm 6.20 (d, J = 0.88 Hz, 1H, alkene H-E), 5.79 (s, 1H, alkene H-Z), 4.55 (s, 1H, H1'), 4.39 (dd, J = 7.04, 5.61 Hz, 1H, H3), 4.12-4.06 (m, 2H, $CO_2C\underline{H}_2CH_3$), 3.83 (t, J = 9.94 Hz, 1H, H5'a), 3.72 (dd, J = 6.79, 2.64 Hz, 1H, H7a), 3.47 (dd, J = 5.82, 5.39 Hz, 1H, H5'b), 3.37 (td, J = 10.91, 7.32 Hz, 1H, H7b), 2.77 (br s, 1H, C3O$\underline{H}$), 1.80 (dd, J = 17.93, 9.47 Hz, 1H, H3'a), 1.73-1.35 (m, 11H, H4, H5, H6, H2', H3b' H4'), 1.23 (m, 3H, $CO_2CH_2C\underline{H}_3$); ^{13}C NMR (126 MHz, $CDCl_3$) δ ppm 171.4 (C1), 142.8 (C2), 125.189 (term. alkene C), 99.2 (C1'), 71.7 (C3), 67.7 (C7), 62.6 (C5'), 60.6 ($CO_2\underline{C}H_2CH_3$), 36.3 (C4), 31.0 (C4'), 29.7 (C6), 25.7 (C2'), 21.3 (C5), 19.9 (C3'), 14.4 ($CO_2CH_2\underline{C}H_3$); HRMS; required for $C_{14}H_{25}O_5$ 273.1702, found 273.1699.

(±)-Ethyl 2-(phenylselanyl)propanoate

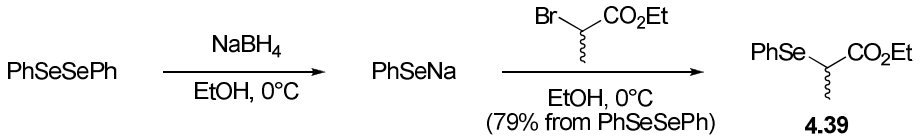

To a solution of diphenyl diselenide (3.747 g, 12.0 mmol) in absolute ethanol (90 mL) at 0°C, under a calcium chloride drying tube as a gas outlet, was added in small portions sodium borohydride (1.364 g, 36.1 mmol) over 45 minutes. Once all of the borohydride had been added, stirring was continued for a further 30 minutes. To the resulting colourless solution of phenylselenylsodium was added a solution of (±)-ethyl 2-bromopropionate (3.9 mL, 30.0 mmol) in absolute ethanol (20 mL) dropwise over 15 minutes and the mixture stirred for 1 hour. Water (50 mL) was added, and the mixture was concentrated to remove ethanol on a rotary evaporator in a fumehood. To the residue was added further water (25 mL) and diethyl ether (100 mL), and the mixture was stirred vigorously and filtered through a plug of celite. The organic phase was separated, and washed with brine (50 mL), dried over sodium sulfate for one hour, filtered and evaporated. The residue was filtered through a silica plug (55 x 55 mm), and eluted with 100 mL portions of 10% diethyl ether/hexane. Evaporation of the fractions containing product gave masked acrylate reagent 4.39 (4.877 g, 79%) as a near colourless oil, with spectral data in accordance with the literature.[160] R_f (10% diethyl ether/hexane): 0.5; ^{1}H NMR (500 MHz, $CDCl_3$) δ ppm 7.61 (m, 2H, *m*-ArH), 7.36-7.25 (m, 3H, *o*, *p*-ArH), 4.09 (dq, *J* = 7.12, 1.67 Hz, 2H, $CO_2C\underline{H}_2CH_3$), 3.77 (dq, *J* = 7.14, 1.61 Hz, 1H, H2), 1.55 (dd, *J* = 7.14, 1.68 Hz, 3H, H3), 1.17 (dd, *J* = 7.12, 1.61 Hz, 3H, $CO_2CH_2C\underline{H}_3$); ^{13}C NMR (126 MHz, $CDCl_3$) δ ppm 173.4 (C1), 135.6 (*m*-ArSe C), 128.9 (*o*-ArSe C), 128.4 (*p*-ArSe C), 127.8 (*i*-ArSe C), 60.9 ($CO_2\underline{C}H_2CH_3$), 37.3 (C2), 17.6 ($CO_2CH_2\underline{C}H_3$), 13.9 (C3); HRMS, required for $C_{11}H_{15}O_2{}^{80}Se$ 259.0237, found 259.0247.

Ethyl 7-(*tert*-butyldiphenylsilyloxy)-3-hydroxy-2-methyl- 2-(phenylselanyl)heptanoate

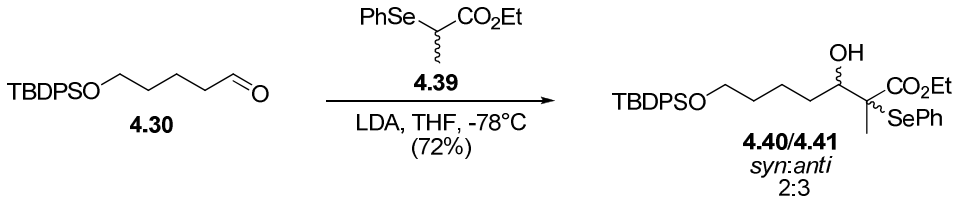

To a stirred solution of diisopropylamine (1.14 mL, 8.42 mmol) in tetrahydrofuran (65 mL) at -78°C under nitrogen was added dropwise a 1.42M solution of *n*-butyllithium in hexanes (5.5 mL, 7.81 mmol). After 45 minutes, selenyl ester 4.39 (2.337 g, 9.09 mmol) in tetrahydrofuran (5 mL) was added, and the mixture was stirred for one hour. To the resulting enolate solution was added aldehyde 4.30 (2.203 g, 6.47 mmol) in tetrahydrofuran (5 mL) dropwise. After 1.5 hours the solution was quenched with saturated ammonium chloride solution (50 mL) and the mixture allowed to come to room temperature. Enough water was added to dissolve the precipitate, and the organic phase was separated. The aqueous phase was extracted with diethyl ether (2x 50 mL), and the combined organic phases were washed with brine (50 mL) dried and evaporated. Flash chromatography (5% ethyl acetate/hexane until excess selenide 4.39 elutes, then 10% ethyl acetate/hexane) afforded the product as cleanly separated *syn*-4.40 (1.098 g, 28%) and *anti*-4.41(1.690 g, 44%) adducts.

syn adduct 4.40: R_f (10% ethyl acetate/hexane): 0.46; ^{1}H NMR (500 MHz, $CDCl_3$) δ ppm 7.67 (dm, J= 7.0 Hz, 4H, *m*-HArSi), 7.62 (dm, *J* = 6.9 Hz, 2H, *m*-HArSe), 7.46-7.35 (m, 7H, *o*,*p*-HArSi, *p*-HArSe), 7.35-7.30 (t, *J* = 7.3 Hz, 2H *o*-HArSe), 4.15-4.03 (m, 2H, $CO_2C\underline{H}_2CH_3$), 3.91 (dd, *J* = 9.7, 1.3 Hz, 1H, H3), 3.66 (dt, *J* = 6.2, 1.2 Hz, 2H, H7), 2.92 (br s, 1H, C3O<u>H</u>), 1.72-1.52 (m, 4H, H4, H6), 1.44, (m, 2H, H5), 1.41 (d, J= 1.1 Hz, 3H, H3'), 1.38-1.26 (m, 2H, H3), 1.12 (dt, *J* = 7.1, 2.0 Hz, 3H, $CO_2CH_2C\underline{H}_3$), 1.05 (d, *J* = 1.3 Hz, 9H); ^{13}C NMR (75 MHz, $CDCl_3$): 173.4 (C1), 138.3 (ArSi), 135.8 (ArSi), 134.3 (ArSe), 129.8 (ArSe), 129.7 (ArSi), 129.2 (ArSe), 129.1 (ArSe), 127.9 (ArSi), 73.2 (C3), 64.1 (C7), 61.3 ($CO_2\underline{C}H_2CH_3$), 57.9 (C2), 32.7 (C6), 32.0 (C5), 27.2 ($\underline{Me}_3CSi$), 23.4 (C4), 19.5 ($Me_3\underline{C}Si$), 17.3 ($CO_2CH_2\underline{C}H_3$), 14.1 (C3'); HRMS required for $C_{32}H_{43}O_4{}^{80}SeSi$: 599.2096, found 599.2121.

anti adduct 4.41: R_f (10% ethyl acetate/hexane): 0.26; ^{1}H NMR (500 MHz, $CDCl_3$) δ ppm 7.70 (dm, J = 6.4 Hz, 4H *m*-HArSi), 7.58 (dm, J = 7.6 Hz, 2H, *m*-HArSe), 7.46-7.36 (m, 7H, *o*,*p*-HArSi, *p*-HArSe), 7.31 (t, J = 7.6 Hz, 2H, *o*-HArSe), 4.12 (qt, J = 7.1, 1.5 Hz, 2H, $CO_2C\underline{H}_2CH_3$), 3.87 (dd, J = 10.1 Hz, 1.1 Hz, 1H, H3), 3.70 (dt, J = 6.0, 1.5 Hz, 2H, H7), 2.79 (br s, 1H, C3O<u>H</u>), 1.89 (m, 1H, H4a), 1.79-1.56 (m, 3H, H4b), 1.44, (m, 2H, H5), 1.42 (s, 3H, H3'), 1.22 (dt, J = 7.1, 1.0 Hz, 3H, $CO_2CH_2C\underline{H}_3$), 1.07 (s, 9H, $\underline{Me}_3CSi$); ^{13}C NMR (75 MHz, $CDCl_3$): 174.3 (C1), 138.4 (ArSi), 135.9 (ArSi), 134.3 (ArSe), 129.8 (ArSe), 129.6 (ArSi), 129.0 (ArSe), 127.9 (ArSi), 127.0 (ArSe), 75.7 (C3), 64.1 (C7), 61.5 ($CO_2\underline{C}H_2CH_3$), 55.1 (C2), 32.7 (C6), 31.6 (C5), 27.2 ($\underline{Me}_3CSi$), 23.5 (C4), 19.5 ($Me_3\underline{C}Si$), 18.5 ($CO_2CH_2\underline{C}H_3$), 14.3 (C3'); HRMS required for $C_{32}H_{43}O_4{}^{80}SeSi$: 599.2096, found 599.2087.

Ethyl 7-(*tert*-butyldiphenylsilyloxy)-3-hydroxy-2-methyleneheptanoate

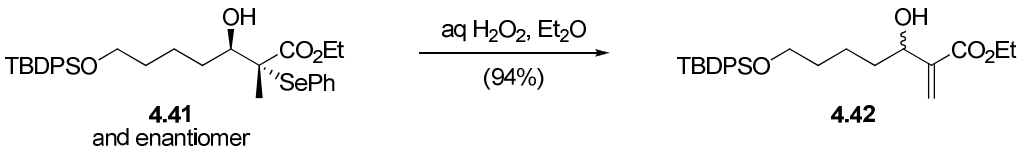

To a solution of *anti*-selenide 4.41 (1.690 g, 2.83 mmol) in diethyl ether (60 mL) and water (15 mL) was added an excess of 50% w/w aqueous hydrogen peroxide (1.5 mL). The biphasic mixture was stirred vigorously for 2.5 hours, then water (20 mL) was added, the organic phase was separated and the aqueous phase was extracted with diethyl ether (40 mL). The combined organic phases were washed with brine (50 mL), dried and evaporated to give acrylate 4.42 as a pale yellow oil (1.175 g, 94%). R_f (20% ethyl acetate/hexane): 0.38; ^{1}H NMR (500 MHz, $CDCl_3$) δ ppm: 7.69 (d, J = 7.8 Hz, 4H, *m*-HArSi), 7.45-7.39 (m, 1H, *o*,*p*-HArSi), 6.24 (d, J = 0.8 Hz, 1H, H3'E), 5.78 (app t, J = 0.9 Hz, 1H, H3'Z), 4.40 (t, J = 6.4 Hz, 1H, H3), 4.25 (q, J = 7.1 Hz, 2H, $CO_2C\underline{H}_2CH_3$), 3.69 (t, J = 6.4 Hz, 2H, H7), 2.65 (br s, 1H, C3O<u>H</u>), 1.73-1.50 (m, 5H, H5, H6, H4a), 1.50-1.38 (m, 1H, H4b), 1.33 (t, J = 7.1 Hz, 3H, $CO_2CH_2C\underline{H}_3$), 1.07 (s, 9H, $\underline{Me}_3CSi$); ^{13}C NMR (75 MHz, $CDCl_3$): 166.9 (C1), 142.9 (C2), 135.9 (ArSi), 134.3 (ArSi), 129.8 (ArSi), 128.6 (ArSi), 125.0 (C3'), 72.1 (C3), 64.1 (C7), 61.1 ($CO_2\underline{C}H_2CH_3$), 36.2 (C5), 32.6 (C6), 27.2 ($\underline{Me}_3CSi$), 22.4 (C4), 19.5 ($Me_3\underline{C}Si$), 14.4 ($CO_2CH_2C\underline{H}_3$). HRMS, required for $C_{26}H_{37}O_4Si$: 441.2461, found 441.2477.

Ethyl 3-acetoxy-7-(*tert*-butyldiphenylsilyloxy)-2-methyleneheptanoate

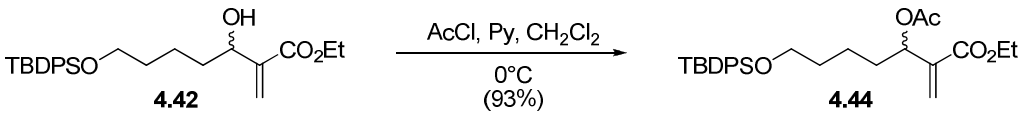

A solution of alcohol 4.42 (1.175 g, 2.67 mmol) in dichloromethane (25 mL) was cooled to 0°C under nitrogen, and pyridine (430 μL, 5.34 mmol) and acetyl chloride (380 μL, 5.37 mmol) were added. The mixture was stirred for three hours, then evaporated. Immediate purification of the residue by flash chromatography gave acetate 4.44 as a colourless oil (1.197 g, 93%). R_f (20% ethyl acetate/hexane): 0.45; ^{1}H NMR (500 MHz, $CDCl_3$) δ ppm 7.66 (dm, *J* = 6.5 Hz, 4H, ArSi), 7.46-7.35 (m, 6H, ArSi), 6.28 (d, *J* = 1.6 Hz, 1H, H3'E), 5.74 (app t, *J* = 1.1 Hz, 1H, H3'Z), 5.67-5.60 (app t, *J* = 3.7 Hz, 1H, H3), 4.23 (qtd, *J* = 10.7, 7.0, 3.6 Hz, 2H, $CO_2C\underline{H}_2CH_3$), 3.66 (dt, *J* = 6.2, 2.4 Hz, 2H, H7), 2.07 (d, *J* = 2.8 Hz, 3H, O<u>Ac</u>), 1.82-1.73 (m, 1H, H4a) 1.73-1.34 (m, 5H, H4b, H5, H6), 1.30 (dt, *J* = 7.2, 2.7 Hz, 3H, $CO_2C\underline{H}_2CH_3$), 1.05 (d, *J* = 2.6 Hz, 9H); ^{13}C NMR (75 MHz, $CDCl_3$) δ ppm 170.2 (O<u>C</u>(O)Me), 165.5 (C1), 140.7 (C2), 135.8 (ArSi), 134.3 (d, *J* = 1.2 Hz, *i*ArSi), 129.8 (ArSi), 127.9 (ArSi), 125.0 (C3'), 72.0 (C3), 63.8 (C7), 61.1 ($CO_2\underline{C}H_2CH_3$), 34.3 (C4), 32.4 (C6), 27.1 ($\underline{Me}_3CSi$), 21.9 (C5), 21.3 (OC(O)<u>Me</u>), 19.5 ($Me_3\underline{C}Si$), 14.4 ($CO_2CH_2C\underline{H}_3$); HRMS, required for $C_{28}H_{39}O_5Si$: 483.2567, found 483.2568.

Ethyl 2-((diethoxyphosphonyl)methylene)-7-(*tert*-butyldiphenylsilyl)hept-2-enoate

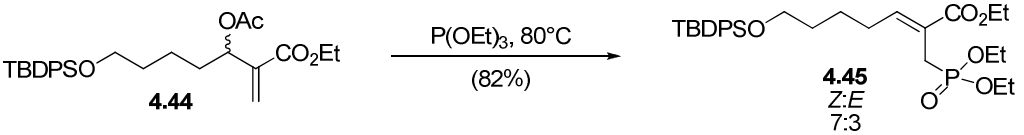

A stirred mixture of acetate 4.44 (1.047 g, 2.17 mmol) and excess triethylphosphite (1 mL, 5.83 mmol) was sealed in a resealable Carius tube, and heated behind a safety shield to 80°C. After 3.5 hours, the tube was cooled to room temperature, and vigorously stirred under high vacuum overnight. The viscous residue was dissolved in a small quantity of ethyl acetate, transferred to a round bottom flask and evaporated.

Flash chromatography (60% ethyl acetate/hexane) gave phosphonate 4.45 as a colourless oil (1.002 g, 82%), as an unseparated mixture of (*Z*)- and (*E*)-isomers (7:3 by ^{1}H and ^{31}P NMR spectroscopy). R_f (60% ethyl acetate/hexane): 0.31; ^{1}H NMR (500 MHz, $CDCl_3$) δ ppm 7.66 (app dd, *J* = 6.8, 1.1 Hz, 4H, *Z*&*E*-ArSi), 7.45-7.34 (m, 6H, *Z*&*E*-ArSi), 6.91 (app q, *J* = 6.9 Hz, 0.7H, *Z*-H3), 6.12 (app dd, *J* = 13.0, 7.0 Hz, 0.3H, *E*-H3), 4.22 (m, 2H, *Z*&*E*-$CO_2C\underline{H}_2CH_3$), 4.07 (app p, *J* = 7.1 Hz, 4H, P(O)$OC\underline{H}_2CH_3$), 3.70-3.62 (m, 2H, *Z*&*E*-H7), 2.96 (d, *J* = 22.1 Hz, 1.5H, *Z*-$C\underline{H}_2P$), 2.88 (d, *J* = 21.2 Hz, 0.6H, *E*-$C\underline{H}_2P$), 2.56-2.47 (app p, J= 6.4. Hz, 0.6H, *E*-H4), 2.32-2.21 (dt, *J* = 12.0, 6.9 Hz, 1.5H, *Z*-H4), 1.65-1.48 (m, 4H, *Z*&*E*-H5, H6), 1.35-1.22 (m, 9H, P(O)$OCH_2C\underline{H}_3$ & $CO_2CH_2C\underline{H}_3$), 1.04 (app dd, *J* = 2.8, 0.7 Hz, 9H, $\underline{Me}_3CSi$). ^{13}C NMR (75 MHz, $CDCl_3$) δ ppm 167.0 (d, *J* = 2.7 Hz, *Z*-C1), 166.9 (d, *J* = 2.5 Hz, *E*-C1), 147.1 (d, *J* = 10.6 Hz, *E*-C3), 146.1 (d, *J* = 10.3 Hz, *Z*-C3), 135.8 (*Z*,*E* ArSi), 134.2 (*Z*,*E* ArSi), 129.8 (*Z*,*E* ArSi) 127.9 (*Z*-ArSi), 127.8 (*E*-ArSi), 123.4 (d, *J* = 11.6 Hz, *Z*-C2), 122.9 (d, *J* = 10.7 Hz, *E*-C2), 63.9 (*E*-C7), 63.8 (*Z*-C7), 62.2 (d, *J* = 6.7 Hz, P(O)$O\underline{C}H_2CH_3$), 61.2 (*Z*- $CO_2CH_2\underline{C}H_3$), 60.8 (*E*- $CO_2CH_2\underline{C}H_3$), 32.6 (*E* -C6), 32.5 (*Z*-C6), 31.4 (d, *J* = 139.9 Hz, *E*-$\underline{C}H_2P$), 29.9 (d, *J* = 2.7 Hz, *E*-C4), 29.3 (d, *J* = 2.8 Hz, *Z*-C4), 27.1 ($\underline{Me}_3CSi$), 25.8 (d, *J* = 3.1 Hz, *E*-C5), 25.2 (d, *J* = 140.4 Hz, *Z*-$\underline{C}H_2P$), 25.1 (d, *J* = 2.7 Hz, *Z*-C5), 19.5 ($Me_3\underline{C}Si$), 16.6 (d, *J* = 6.3 Hz, P(O)$OCH_2\underline{C}H_3$), 14.5 ($CO_2CH_2\underline{C}H_3$); ^{31}P NMR (121 MHz, $CDCl_3$) δ ppm 27.2 (*Z*-$CH_2\underline{P}$), 27.0 (*E*-$CH_2\underline{P}$); HRMS; required for $C_{30}H_{46}O_6PSi$ 561.2801, found 561.2787.

Ethyl 2-((diethoxyphosphonyl)methylene)-7-hydroxyhept-2-enoate

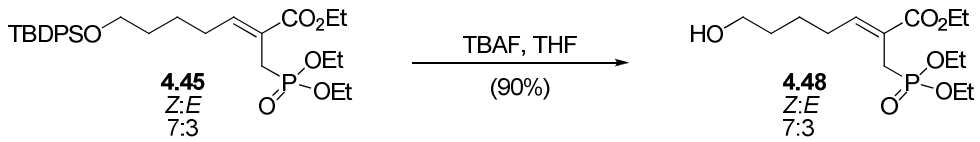

To a stirred solution of phosphonate 4.45 (993.6 mg, 1.77 mmol) in tetrahydrofuran (20 mL) was added a 1M solution of tetrabutylammonium fluoride in tetrahydrofuran (3.60 mL, 3.6 mmol). After two hours the reaction seemed to have stopped before completion (TLC), a further portion of TBAF (0.6 mL, 0.6 mmol) was added. After one hour the mixture was evaporated, and immediately purified by flash chromatography (100% acetonitrile). Evaporation of the solvent gave alcohol 4.48 as a colourless oil (515.7 mg, 90%). R_f (100% acetonitrile): 0.20; ^{1}H NMR (500 MHz,

$CDCl_3$) δ ppm 6.90 (dd, *J* = 13.8, 7.3 Hz, 0.7H, *Z*-H3), 6.12 (dd, *J* = 13.0, 7.4 Hz, 0.3H, *E*-H3), 4.22-4.11 (m, 2H, *Z*&*E*-$CO_2C\underline{H}_2CH_3$), 4.02 (app p, *J* = 7.2 Hz, 4H, P(O)$OC\underline{H}_2CH_3$), 3.64-3.55 (m, 2H, *Z*&*E*-H7), 2.94 (d, *J* = 22.1 Hz, 1.8H, *Z*-$C\underline{H}_2P$), 2.82 (d, *J* = 21.2 Hz, 0.7H, *E*-$C\underline{H}_2P$), 2.55-2.45 (m, 0.9H, *E*-H4), 2.32-2.22 (m, 1.8H, *Z*-H4), 1.60-1.46 (m, 4H, *Z*&*E*-H5&H6), 1.32-1.19 (m, 9H, P(O)$OCH_2C\underline{H}_3$ & $CO_2CH_2C\underline{H}_3$). ^{13}C NMR (75 MHz, $CDCl_3$) δ ppm 166.9 (*Z*-C1), 147.4 (d, *J* = 10.6 Hz, *E*-C3), 146.2 (d, *J* = 10.2 Hz, *Z*-C3), 123.1 (d, *J* = 11.2 Hz, *Z*-C2), 122.7 (d, *J* = 10.6 Hz, *E*-C2), 62.1 (d, *J* = 18.8 Hz, P(O)$O\underline{C}H_2CH_3$), 62.3 (*Z*-C7), 62.2 (*E*-C7), 61.2 (*Z*-$CO_2\underline{C}H_2CH_3$), 60.9 (*E*-$CO_2\underline{C}H_2CH_3$), 32.3 (*E*,*Z*-C6), 31.2 (d, *J* = 140.0 Hz, *E*-$\underline{C}H_2P$), 29.7 (d, *J* = 2.9 Hz, *E*-C4), 29.1 (d, *J* = 2.9 Hz, *Z*-C4), 25.5 (d, *J* = 3.3 Hz, *E*-C5), 24.9 (d, *J* = 140.8 Hz, *Z*-$\underline{C}H_2P$), 24.8 (d, *J* = 3.2 Hz, *Z*-C5), 16.6 (d, *J* = 6.2 Hz, *E*-P(O)$OCH_2\underline{C}H_3$), 16.6 (d, *J* = 6.2 Hz , *Z*-P(O)$OCH_2\underline{C}H_3$), 14.5 (s, *Z*- $CO_2CH_2\underline{C}H_3$), 14.5 (s, *E*- $CO_2CH_2\underline{C}H_3$); HRMS, required for $C_{14}H_{28}O_6P$: 323.1624, found 323.1630.

Ethyl 2-((diethoxyphosphonyl)methyl)-7-(diethoxyphosphoryl)hept-2-enoate

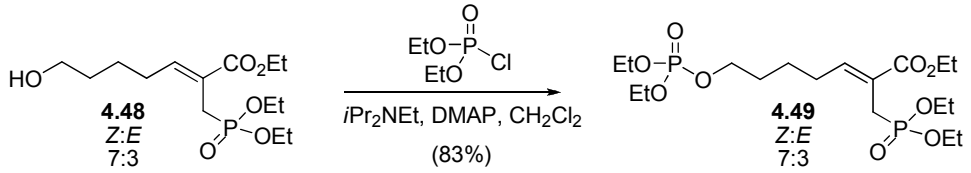

To a solution of alcohol 4.48 (184 mg, 0.571 mmol) in dichloromethane (3 mL) under nitrogen was added diisopropylethylamine (200 μL, 1.15 mmol) and DMAP (14.1 mg, 115 μmol). To this mixture was added diethyl chlorophosphate (130 μL, 0.900 mmol), and the mixture stirred overnight. The mixture was added to dichloromethane (5 mL) and saturated aqueous sodium bicarbonate solution (5 mL), and stirred vigorously for twenty minutes. The organic phase was separated, and the aqueous phase extracted with dichloromethane (5 mL). The combined organic phases were extracted with saturated ammonium chloride solution (5 mL), and the aqueous phase was back-extracted with further dichloromethane (5 mL). The combined dichloromethane phases were dried and evaporated. Flash chromatography (5% methanol/ dichloromethane) afforded phosphate 4.49 (218.5 mg, 83%) as a pale yellow oil. R_f (5% methanol/ dichloromethane): 0.58; ^{1}H NMR (500 MHz, $CDCl_3$) δ ppm 6.86 (dd, *J* = 13.5, 7.3 Hz, 0.7H, *Z*-H3), 6.08 (dd, *J* = 12.9, 7.4 Hz, 0.3H, *E*-H3), 4.30-4.13 (m,

2H, *Z*&*E*-$CO_2C\underline{H}_2CH_3$), 4.12-3.95 (m, 10H, $CH_2P(O)OC\underline{H}_2CH_3$, $OP(O)OC\underline{H}_2CH_3$, H7), 2.94 (d, *J* = 22.1 Hz, 1.8H, *Z*-$C\underline{H}_2P$), 2.84 (d, *J* = 21.3 Hz, 0.7H, *E*-$C\underline{H}_2P$), 2.52 (dq, *J* = 7.4, 5.2 Hz, 0.7H, *E*-H4), 2.29 (dq, *J* = 7.4, 5.0 Hz, 2H, *Z*-H4), 1.78-1.62 (m, 2H, H6), 1.59-1.48 (m, 2H, H5), 1.37-1.21 (m, 15H, $CH_2P(O)OCH_2C\underline{H}_3$, $OP(O)OCH_2C\underline{H}_3$, $CO_2CH_2C\underline{H}_3$); ^{13}C NMR (75 MHz, $CDCl_3$) δ ppm 166.9 (d, *J* = 2.8 Hz, C1), 146.3 (d, *J* = 10.4 Hz, *E*-C3), 145.2 (d, *J* = 10.4 Hz, *Z*-C3), 123.8 (d, *J* = 11.5 Hz, *z*-C2), 123.3 (d, *J* = 10.6 Hz, *E*-C2), 67.5 (d, *J* = 6.2 Hz, *E*-$\underline{C}$7OP), 67.4 (d, *J* = 5.9 Hz, *Z*-$\underline{C}$7OP), 63.9 (d, *J* = 5.8 Hz), 63.9-63.7 (m, *E*&*Z*-$CH_2P(O)O\underline{C}H_2CH_3$), 62.2 (d, *J* = 6.7 Hz, *E*&*Z*-$OP(O)O\underline{C}H_2CH_3$), 61.2 (*Z*-$CO_2\underline{C}H_2CH_3$), 60.9 (*E*-$CO_2\underline{C}H_2CH_3$), 31.3 (d, *J* = 140.0 Hz, *E*-$\underline{C}H_2P$), 30.2 (d, *J* = 7.0 Hz, *Z*-C6), 30.1 (d, *J* = 6.9 Hz, *E*-C6), 29.5 (d, *J* = 2.2 Hz, *E*-C4), 29.0 (d, *J* = 2.7 Hz, *Z*-C4), 25.4 (d, *J* = 3.2 Hz, *E*-C5), 25.1 (d, *J* = 140.4 Hz, *Z*-$\underline{C}H_2P$), 24.7 (d, *J* = 2.8 Hz, *Z*-C5), 16.6 (d, *J* = 6.4 Hz, $CH_2P(O)OCH_2\underline{C}H_3$), 16.4 (d, *J* = 6.7 Hz, $OP(O)OCH_2\underline{C}H_3$), 14.5 ($CO_2CH_2\underline{C}H_3$), ^{31}P NMR (121 MHz, $CDCl_3$) δ ppm 27.0 (*E*-$CH_2\underline{P}$), 26.8 (*Z*-$CH_2\underline{P}$),-0.3 (*E*&*Z*-C7O$\underline{P}$); HRMS, required for $C_{18}H_{37}O_9P_2$: 459.1913, found 459.1913.

Potassium 2-phosphonylmethyl-7-phosphorylhept-2-enoate

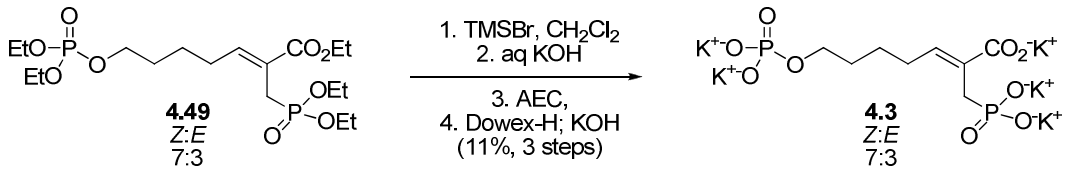

Ester 4.49 (100.7 mg, 0.220 mmol) was stirred in dichloromethane (1.2 mL) under nitrogen, and trimethylsilyl bromide (120 μL, 0.909 mmol) was added. The mixture was stirred overnight, then quenched with methanol (1 mL).The mixture was evaporated, and the residue dissolved in 10% w/v potassium hydroxide (1 mL), and the mixture stirred vigorously for 3 hours. The mixture was extracted with dichloromethane (3x 2mL), and the organic extracts discarded. The mixture was passed through a short column of Dowex-50X8 H^+-form (10 x 50 mm), and eluted with water (20 mL). The solution was neutralised with 10% w/v sodium hydroxide, and lyophilised. The residue was separated by preparative anion exchange chromatography (SourceQ® resin, 4°C, 0 to 1M ammonium bicarbonate gradient elution, product elutes at 220 mM ammonium bicarbonate). The product fractions

were lyophilised, redissolved in water (1 mL), passed through a short column of Dowex-50X8 (H^+-form, to quench any residual ammonium bicarbonate) then thorough a column of Dowex-50X8 (K^+-form). The filtrate was lyophilised to give inhibitor 4.3 (12 mg, 11%) as a mixture of (*Z*) and (*E*) isomers (65:35), with <4% residual ethylation. ^{1}H NMR (500 MHz, D_2O) δ ppm 5.89 (app p, *J* = 7.3 Hz, 0.7H, *Z*-H3), 5.11 (dd, *J* = 11.4, 7.2 Hz, 0.4H, *Z*-H3), 3.33 (dd, *J* = 12.5, 6.6 Hz, 1.4H, *Z*-H7OP), 3.12 (app t, *J* = 6.7 Hz, 0.7H, *E*-H7OP), 2.24 (dd, *J* = 20.6, 3.0 Hz, 1.5H, *Z*-CH_2P), 2.03 (d, *J* = 19.4 Hz, 0.5H, *E*-CH_2P), 1.82 (app dq, *J* = 7.5, 4.1 Hz, 1.5H, *Z*-H4), 1.74 (app dq, *J* = 7.3, 4.0 Hz, 0.5H, *E*-H4), 1.51-1.43 (m, 0.7H, *E*-H6), 1.25-0.96 (m, 3.7H, *Z*-H6, *Z*-H5, *E*-H5); ^{13}C NMR (126 MHz, D_2O, HSQC-DEPT135) δ ppm 137.4 (*Z*-C3), 130.3 (*E*-C3), 64.3 (*Z*-C7OP), 60.4, 35.4 (*E*-C7OP), 34.9 (d, *J* = 134 Hz, *E*-CH_2P), 31.8 (*E*-C6), 29.9 (*Z*-C6), 29.2 (d, *J* = 152 Hz, *Z*-CH_2P), 28.6 (*E*-C4), 27.7 (*Z*-C4), 26.7 (*E*-C5), 24.7 (*Z*-C6 and/or *Z*-C5); ^{31}P NMR (121 MHz, D_2O) δ ppm 19.7 (*Z*-C3'P), 18.3 (*E*-C3'-P), 3.9 (*E*&*Z*-C7OP); HRMS (electrospray, negative ion): required for $C_8H_{15}O_9P_2^-$: 317.0191; found 317.0203.

(5-Bromopentyloxy)(*tert*-butyl)diphenylsilane

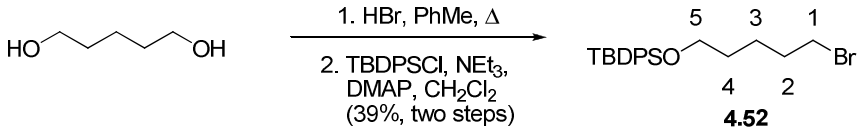

4.52

To a mixture of 1,5-pentanediol (1.044 g, 10.0 mmol) and toluene (30 mL) was added 48% aqueous HBr (1.33 mL, 12 mmol), and the biphasic mixture was refluxed under nitrogen for 9 hours. The cooled mixture was diluted with diethyl ether (75 mL), and washed with 10% w/v aqueous sodium hydroxide (75 mL), brine (75 mL) and 3M pH 7 potassium phosphate buffer (75 mL), dried and evaporated. The residue (1.107 g, 6.2 mmol assuming pure alcohol) was diluted with dichloromethane (32 mL) and cooled to 0°C under nitrogen. DMAP (76.8 mg, 0.629 mmol), TBDPSCl (1.91 mL, 7.45 mmol) and triethylamine (2.60 mL, 18.7 mmol) were added, and the mixture was stirred overnight, the ice bath being allowed to melt over this time. The mixture was then quenched with ammonium chloride solution (20 mL), the organic phase was separated and washed with further saturated ammonium chloride solution (20 mL), saturated aqueous sodium bicarbonate solution (20 mL), brine (20 mL). The solution

was dried and evaporated, and the residue purified by filtration through a short silica plug, eluting with 33% chloroform/hexane to give bromide 4.52 (1.572 g, 39%) with spectral data in accordance with the literature.[202] R_f (10% chloroform/hexane): 0.26; ^{1}H NMR (400 MHz, $CDCl_3$) δ ppm 7.64 (dm, *J* = 6.3 Hz, 4H, ArSi), 7.44-7.32 (m, 6H, ArSi), 3.64 (t, *J* = 6.1 Hz, 2H, H5), 3.36 (t, *J* = 6.9 Hz, 2H, H1), 1.92-1.76 (m, 2H, H2), 1.63-1.42 (m, 4H, H3, H4), 1.03 (s, 9H, $\underline{Me}_3CSi$); ^{13}C NMR (101 MHz, $CDCl_3$) δ ppm 135.6 (ArSi), 134.0 (ArSi), 129.6 (ArSi), 127.6 (ArSi), 63.6 (C5), 33.9 (C1), 32.5 (C2), 31.6 (C4), 26.9 ($\underline{Me}_3CSi$), 24.6 (C3), 19.2 ($Me_3\underline{C}Si$).

Tert-butyl(hept-6-ynyloxy)diphenylsilane

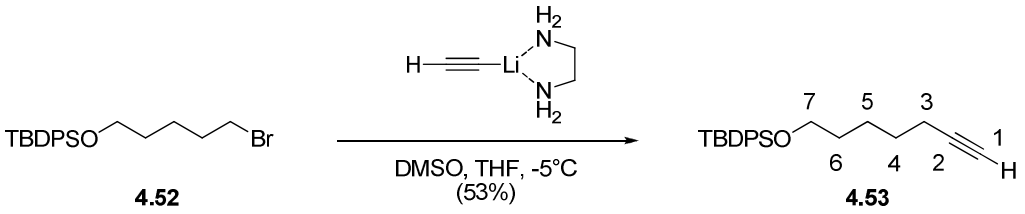

To a mixture of lithium acetylide-ethylenediamine complex (379.1 mg, 4.12 mmol), DMSO (2.4 mL) and tetrahydrofuran (0.5 mL) at -5°C was added bromide 4.52 (813.3 mg, 2.01 mmol) in tetrahydrofuran (0.5 mL) dropwise over thirty minutes. After 1.5 hours the reaction was quenched with saturated ammonium chloride solution (15 mL) and water (3 mL). The mixture was extracted with 50% diethyl ether/hexane (3x 20 mL), the combined organic phases were well washed with brine (2x 50 mL), dried and evaporated. Flash chromatography (15% chloroform/hexane) gave alkyne 4.53 (370.1 mg, 53%), with spectral data in accordance with the literature.[202] R_f (10% chloroform/hexane): 0.26; ^{1}H NMR (400 MHz, $CDCl_3$) δ ppm 7.64 (dm, *J* = 7.9 Hz, 4H, ArSi), 7.44-7.31 (m, 6H, ArSi), 3.64 (t, *J* = 6.3 Hz, 2H, H7), 2.15 (dt, *J* = 6.7, 6.7, 2.5 Hz, 2H, H3), 1.90 (t, *J* = 2.6 Hz, 1H, H1), 1.61-1.38 (m, 6H, H4, H5, H6), 1.03 (s, 9H, $\underline{Me}_3CSi$); ^{13}C NMR (101 MHz, $CDCl_3$) δ ppm 135.6 (ArSi), 134.1 (ArSi), 129.5 (ArSi), 127.6 (ArSi), 84.6 (C2), 68.168 (C1), 63.7 (C7), 32.0 (C6), 28.2 (C4), 26.9 ($\underline{Me}_3CSi$), 25.0 (C5), 19.2 ($Me_3\underline{C}Si$), 18.4 (C3).

(7-Bromohept-6-ynyloxy)(*tert*-butyl)diphenylsilane

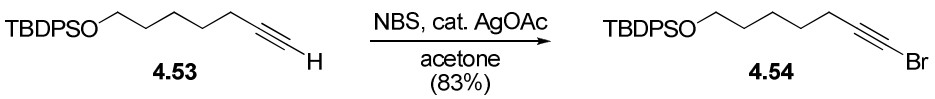

To a solution of alkyne 4.53 (192.7 mg, 0.545 mmol) in acetone (3.1 mL) in the dark was added recrystallised *N*-bromosuccinimide (138.2 mg, 0.776 mmol) and silver(I) acetate (37.2 mg, 0.223 mmol). The mixture was stirred in the dark for 1.5 hours, then filtered through a celite plug, and the plug washed with diethyl ether (20 mL). The filtrate was washed with water (2x 20 mL), brine (20 mL), dried, filtered through a silica plug, and eluted with further diethyl ether (20 mL). The filtrate was evaporated to give alkynyl bromide 4.54 as a colourless oil (195 mg, 83%). R_f (10% chloroform/hexane): 0.49; ^{1}H NMR (400 MHz, $CDCl_3$) δ ppm 7.65 (dm, J = 7.7 Hz, 4H, ArSi), 7.42-7.33 (m, 6H, ArSi), 3.65 (t, J = 6.2 Hz, 2H, H7), 2.17 (t, J = 6.6 Hz, 2H, H3), 1.62-1.40 (m, 6H, H4, H5, H6), 1.04 (s, 9H, $\underline{Me}_3CSi$); ^{13}C NMR (101 MHz, $CDCl_3$) δ ppm 135.6 (ArSi), 134.1 (ArSi), 129.5 (ArSi), 127.6 (ArSi), 80.3 (C2), 65.8 (C1), 63.6 (C7), 32.0 (C6), 28.0 (C4), 26.9 ($\underline{Me}_3CSi$), 25.0 (C5), 19.7 ($Me_3\underline{C}Si$), 19.2 (C3).

Methyl 7-(tert-butyldiphenylsilyloxy)-2-oxoheptanoate

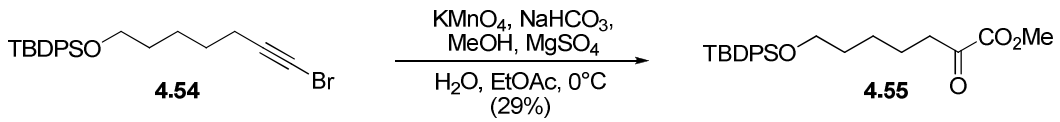

To a solution of alkynyl bromide 4.54 (367.2 mg, 0.855 mmol) in methanol (13 mL) and ethyl acetate (13 mL) at 0°C was added a solution of magnesium sulfate (258.4 mg, 2.15 mmol) and sodium bicarbonate solution (60.8 mg, 0.724 mmol) in water (13 mL). Further ethyl acetate (13 mL) was added, the mixture was stirred for 10 minutes then potassium permanganate (541.0 mg, 3.42 mmol) was added in small portions over 5 minutes. The resulting dark purple solution was stirred for 6 hours, filtered through celite, and the celite washed with ethyl acetate (30 mL). The filtrate organic phase was separated, and the aqueous phase extracted with ethyl acetate (30 mL). The combined organic phases were washed with brine until no more purple colouration

was extractable from the organic phase into the brine (5 x 30 mL). The organic phase was then dried and evaporated. Flash chromatography gave α-ketoester 4.55 as a colourless oil (102 mg, 29%). R_f (20% diethyl diethyl ether/hexane): 0.34; ^{1}H NMR (400 MHz, $CDCl_3$) δ ppm 7.64 (app dd, J = 7.8, 1.5 Hz, 4H, ArSi), 7.44-7.32 (m, 6H, ArSi), 3.84 (s, 3H, $CO_2\underline{Me}$), 3.64 (t, J = 6.3 Hz, 2H, H7), 2.80 (t, J = 7.3 Hz, 2H, H3), 1.68-1.49 (m, 4H, H4, H6), 1.44-1.34 (m, 2H, H5), 1.02 (s, 9H, $\underline{Me}_3CSi$); ^{13}C NMR (101 MHz, $CDCl_3$) δ ppm 194.2 (C2), 161.6 (C1), 135.6 (ArSi), 134.0 (ArSi), 129.6 (ArSi), 127.6 (ArSi), 63.6 (C7), 52.9 ($CO_2\underline{Me}$), 39.3 (C3), 32.2 (C6), 26.9 ($\underline{Me}_3CSi$), 25.3 (C5), 22.7 (C4), 19.2 ($Me_3\underline{C}Si$).

Ethyl 2-oxohept-6-enoate

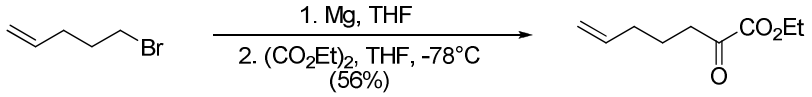

A vigorously stirred portion of magnesium turnings (0.7859 g, 32.3 mmol) was strongly heated (heat gun) under high vacuum, and allowed to cool under nitrogen. Tetrahydrofuran (2.5 mL) and a small crystal of iodine was added. The mixture was heated to reflux for thirty seconds, and the pale grey-green mixture allowed to cool to room temperature. A solution of 5-pentenyl 1- bromide (2.228 g, 15.0 mmol) in tetrahydrofuran (2.5 mL) was prepared in a separate dry flask, and approximately half of this mixture was added to the magnesium turnings suspension. The mixture was brought to reflux for 2 minutes, and the remaining bromide solution added dropwise over 5 minutes. The reaction was stirred without external heating for 1.5 hours, over which time a dark grey suspension forms. The suspension was diluted with tetrahydrofuran (10 mL), and added slowly to a solution of diethyl oxalate (2.467 g, 16.7 mmol) in THF (25 mL) under nitrogen at -78°C. A further portion of dry THF (5 mL) was used to rinse the magnesium turnings; this solution was also slowly added to the diethyl oxalate solution. The solution was stirred for 30 minutes at -78°C, and then the heterogeneous suspension was warmed to -10°C, where it was stirred for a further 30 minutes. The now homogenous solution was quenched with saturated aqueous ammonium chloride solution (10 mL), and concentrated on a rotary evaporator. The residue was diluted with water (50 mL) and chloroform (50 mL), and

the organic phase separated. The aqueous phase was extracted with a further 50 mL of chloroform, and the combined chloroform fractions washed with brine (100 mL), dried and evaporated. Purification of the residue by flash chromatography (10% ether/ hexane) gave ethyl 2-oxohept-6-enoate as a colourless oil (1.424 g, 56%). R_f (20% diethyl ether/hexane): 0.55; ^{1}H NMR (500 MHz, $CDCl_3$) δ ppm 5.77 (tdd, *J* = 16.9, 10.2, 6.8, Hz, 1H, H6), 5.10-4.93 (m, 2H, H7*E*, H7*Z*), 4.33 (q, *J* = 7.1 Hz, 2H, $CO_2C\underline{H}_2CH_3$), 2.85 (t, *J* = 7.3 Hz, 2H, H3), 2.12 (app q, *J* = 7.1 Hz, 2H, H5), 1.76 (app p, *J* = 7.3 Hz, 2H, H4), 1.38 (t, *J* = 7.2 Hz, 3H, $CO_2CH_2C\underline{H}_3$) ^{13}C NMR (126 MHz, $CDCl_3$) δ ppm 194.5 (C2), 161.2 (C1), 137.5 (C6), 115.7 (C7), 62.4 ($CO_2\underline{C}H_2CH_3$), 38.4 (C3), 32.8 (C5), 22.1(C4), 14.0 ($CO_2CH_2\underline{C}H_3$).

Isopropyl dichloroacetate

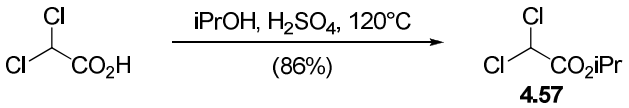

4.57

A mixture of dichloroacetic acid (80 mL, 0.970 mol) and isopropanol (25 mL, 327 mmol) was stirred vigorously as concentrated sulfuric acid (550 μL) was added, then the mixture was heated to 120°C overnight under a condenser and drying tube. The mixture was cooled to room temperature, and diluted with dichloromethane (100 mL). The mixture was vigorously stirred as calcium carbonate was added in portions, until the mixture became too thick to stir. The mixture was filtered and the calcium salts washed well with chloroform, the filtrate was still acidic (pH paper) so saturated aqueous sodium bicarbonate solution was added cautiously until pH~6. The organic phase was separated and the aqueous phase diluted with an equal volume of brine and washed with chloroform (25 mL). The combined organic phases were dried over sodium sulfate and evaporated, the residue was purified by vacuum distillation (112-118°C/160 mmHg) to give isopropyl dichloroacetate 4.57 as a colourless oil (47.866 g, 86%). ^{1}H NMR (500 MHz, $CDCl_3$) δ ppm 5.89 (s, 1H, $C\underline{H}Cl_2$), 5.10 (sept, 1H, *J* = 6.3 Hz, $OC\underline{H}Me_2$), 1.32 (d, 6H, *J* = 6.3 Hz, $OCH\underline{Me}_2$); ^{13}C NMR (126 MHz, CDCl3) δ ppm 164.2 ($\underline{C}O_2iPr$), 72.1 ($\underline{C}HCl_2$), 64.8 ($O\underline{C}HMe_2$), 21.6 ($OCH\underline{Me}_2$).

Isopropyl 7-(*tert*-butyldiphenylsilyloxy)-2-oxoheptanoate

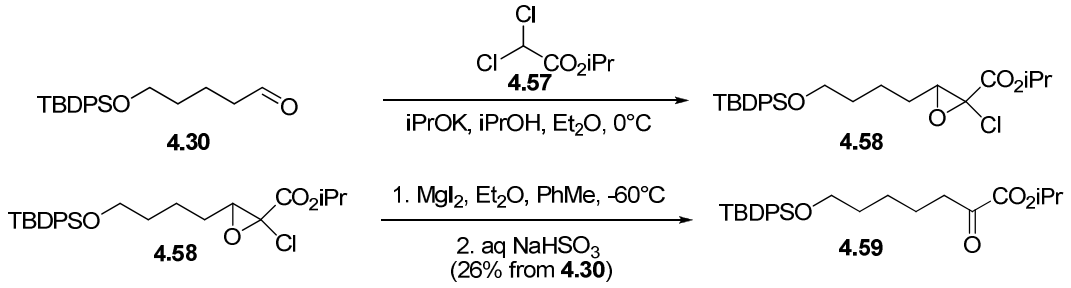

A solution of isopropyl dichloroacetate (2.349 g, 13.7 mmol) in isopropanol (13.5 mL) was stirred under nitrogen at 0°C as a 1M isopropanol solution of potassium isopropoxide (freshly prepared from potassium metal, 13.5 mL, 13.5 mmol) was added dropwise. A solution of aldehyde 4.30 (2.330g, 6.84 mmol) in diethyl ether (5 mL) was added slowly from a syringe, and the flask and syringe were washed with further diethyl ether (8 mL). After 1.5 hours the mixture was poured into diethyl ether (120 mL), and water (50 mL). The organic phase was separated and the aqueous phase was extracted with additional diethyl ether (100 mL). The combined organic phases were washed with water (50 mL) and brine (50 mL), dried and evaporated. The resulting crude chloroepoxide (2.873 g) was stored at -20°C before being used (on the same day) for the next step.

Concurrently, powdered (-50 mesh) magnesium metal (301 mg, 12.4 mmol) was suspended in diethyl ether (40 mL), iodine (1.531 g, 6.05 mmol) was added, the mixture was refluxed under argon in the dark for three hours, and the resulting solution of anhydrous magnesium iodide (over excess magnesium) allowed to cool to room temperature in the dark.

Crude chloroepoxide 4.58 (2.873 g) was dissolved in toluene (24 mL) and diethyl ether (96 mL) and the mixture was stirred and cooled to -60°C under argon. The magnesium iodide solution was carefully added by cannula dropwise to the chloroepoxide solution, care must be taken to avoid clogging the cannula with the excess magnesium powder. After 3.5 hours the bath had warmed to -20°C, the dark solution was quenched with water (50 mL) and filtered. The organic phase was separated, and the aqueous phase extracted with diethyl ether (2x 50 mL). The combined organic phases were washed with brine (50 mL), dried and evaporated. The crude iodoketone (2.794 g) can be stored in the dark at -20°C at this point if required.

The crude iodoketone was dissolved in diethyl ether (100 mL), and treated with commerical 40% sodium hydrogen sulfite solution (50 mL) The solution rapidly becomes dark, then colourless with a crystalline precipitate. After 5 minutes, a minimum volume of 1:1 water : saturated aqueous sodium bicarbonate solution was added to dissolve the precipitate, the organic phase separated and the aqueous phase extracted with diethyl ether (2x 50 mL). The combined organic phases were washed with brine (50 mL), dried and evaporated. Two rounds of flash chromatography (10% ethyl acetate/hexane, then 5% ethyl acetate/hexane) afforded α-ketoester 4.59 as a colourless oil (770.9 mg, 26%). R_f (20% ethyl acetate/hexane): 0.55; ^{1}H NMR (500 MHz, $CDCl_3$) δ ppm 7.70 (dm, *J* = 6.5 Hz, 4H, ArSi), 7.48-7.37 (m, 6H, ArSi), 5.16 (app oct, *J* = 6.3 Hz, 1.0 Hz, 1H, $Me_2C\underline{H}OR$), 3.70 (t, *J* = 6.3 Hz, 2H, H7), 2.83 (t, *J* = 7.4 Hz, 2H, H3), 1.69-1.56 (m, 4H, H4, H6), 1.49-1.41 (m, 2H, H5), 1.37 (dd, *J* = 6.3, 0.8 Hz, 1H, $\underline{Me}_2CHOR$), , 1.10-1.08 (app d, *J* = 2.4 Hz, 9H, $\underline{Me}_3CSi$); HRMS, required for $C_{26}H_{37}O_4Si$: 441.2461, found 441.2480.

Distinct enolate signals, 5.69 (t, *J* = 7.69 Hz, enol H3), 2.26 (app q, *J* = 7.4 Hz, 7.2 Hz, enol H4) 1.34 (dd, *J* = 6.2 Hz, *i*Pr ester); ^{13}C NMR (126 MHz, $CDCl_3$) δ ppm 195.2 (C1), 161.2 (C1), 135.8 (ArSi), 134.2 (ArSi), 129.8 (ArSi), , 127.9 (ArSi), , 70.7 ($Me_2\underline{C}HOR$), 63.8 (C7), 39.5 (C3), 32.5 (C6), 27.1 ($\underline{Me}_3CSi$), 25.5 (C5), 23.0 (C4), 21.9 ($\underline{Me}_2CHOR$), 19.5 ($Me_3\underline{C}Si$), distinct enol signals 165.2 (C1), 140.3 (C2), 114.0 (C3), 70.1 ($Me_2\underline{C}HOR$), 34.9 (H6), 31.9 (C4), 22.0 ($\underline{Me}_2CHOR$).

Isopropyl 7-(*tert*-butyldiphenylsilyloxy)-2-(diethoxyphosphonomethenyl) heptanoate

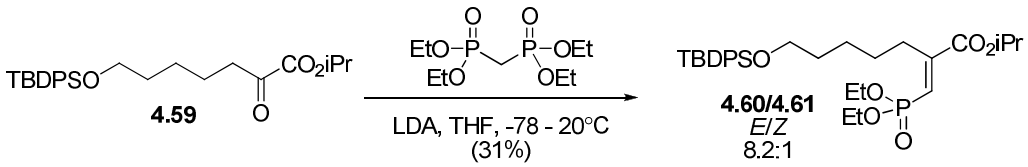

Diisopropylamine (43 μL, 0.31 mmol) in tetrahydrofuran (2.5 mL) under nitrogen was stirred and cooled to -78°C, and a 1.42 M solution of *n*-butyllithium in hexanes (195 μL, 0.277 mmol) was added, the resulting mixture was warmed to room temperature for 20 minutes, then returned to -78°C. Tetraethyl methylene bisphosphonate (75 μL, 0.30 mmol) was added, and the mixture stirred for 30 minutes, then α-ketoester 4.59

(110.7 mg, 0.251 mmol) in tetrahydrofuran (1 mL) was added, and the mixture was stirred for 45 minutes at -78°C, then for 2 hours at room temperature. The reaction was quenched with saturated potassium dihydrogen phosphate (3 mL), and the tetrahydrofuran removed under vacuum. The precipitated salts were dissolved in the minimum volume of water, dichloromethane (5 mL) was added, and the aqueous phase was separated and washed with dichloromethane (3x 5 mL). The combined organic extracts were dried and evaporated. Flash chromatography (40% ethyl acetate/hexane) gave the desired (*E*)-vinylphosphonate 4.60 (41.1 mg, 28%) and the undesired (*Z*)-vinylphosphonate 4.61 (5 mg, 3%).

(*E*)-isomer: R_f (40% ethyl acetate/hexane): 0.48; ^{1}H NMR (500 MHz, $CDCl_3$) δ ppm 7.67 (app dd, *J* = 7.8, 1.5 Hz, 4H), 7.45-7.34 (m, 6H, ArSi), 6.59 (d, *J* = 16.7 Hz, 1H, H3'), 5.08 (sept., *J* = 6.2 Hz, 1H, $Me_2C\underline{H}OR$), 4.12 (app p, *J* = 7.4 Hz, 4H, $CP(O)OC\underline{H}_2CH_3$), 3.66 (t, *J* = 6.5 Hz, 2H, H7), 2.72 (dt, *J* = 6.2, 2.0 Hz, 2H, H3), 1.69-1.53 (m, 2H, H6), 1.53-1.38 (m, 4H, H4, H5), 1.33 (t, *J* = 7.1 Hz, 6H, $CP(O)OCH_2C\underline{H}_3$), 1.28 (d, *J* = 6.3 Hz, 6H, $\underline{Me}_2CHOR$), 1.05 (s, 9H, $\underline{Me}_3CSi$); ^{13}C NMR (126 MHz, $CDCl_3$) δ ppm 166.0 (d, *J* = 29.1 Hz, C1), 152.8 (d, *J* = 9.4 Hz, C2), 135.8 (ArSi), 134.3 (ArSi), 129.7 (ArSi), 127.8 (ArSi), 124.1 (d, *J* = 187.1 Hz, C3'), 69.5 ($Me_2\underline{C}HOR$), 64.1 (C7), 62.2 (d, *J* = 5.8 Hz, $CP(O)O\underline{C}H_2CH_3$), 34.2 (s,1C), 32.7 (C6), 30.0 (d, *J* = 5.9 Hz, C3), 29.4 (d, *J* = 2.4 Hz, C4), 27.1 ($\underline{Me}_3CSi$), 26.2 (C5), 21.9 ($\underline{Me}_2CHOR$), 19.4 ($Me_3\underline{C}Si$), 16.6 (d, *J* = 6.4 Hz, $CP(O)OCH_2\underline{C}H_3$), ^{31}P NMR (121 MHz, $CDCl_3$, ^{1}H-decoupled) δ ppm 16.1 ($C\underline{P}(O)OEt$); ^{31}P NMR (121 MHz, $CDCl_3$, ^{1}H-coupled) δ ppm 16.1 (sept, *J* = 7.7 Hz, $HC\underline{P}(O)OEt$); HRMS, required for $C_{31}H_{48}O_6SiP$ 575.2958, found 575.2929.

(*Z*)-isomer: R_f (40% ethyl acetate/hexane): 0.24; ^{1}H NMR (500 MHz, $CDCl_3$) δ ppm 7.65 (dd, *J* = 7.9, 1.5 Hz, 4H, ArSi), 7.44-7.34 (m, 6H, ArSi), 5.62 (td, *J* = 14.9, 1.3 Hz, 1H, H3'), 5.14 (sept., *J* = 6.3, Hz, 1H, $Me_2C\underline{H}OR$), 4.14-4.04 (m, 4H, $CP(O)OC\underline{H}_2CH_3$), 3.65 (t, *J* = 6.4 Hz, H7), 2.36 (dt, *J* = 7.4, 1.1 Hz 2H, H3), 1.61-1.50 (m, 2H, H6), 1.50-1.37 (m, 4H, H4, H5), 1.31 (t, *J* = 7.0 Hz, 6H, $CP(O)OCH_2C\underline{H}_3$), 1.31 (d, *J* = 6.1 Hz, 6H, $\underline{Me}_2CHOR$), 1.04 (s, 9H, $\underline{Me}_3CSi$); ^{13}C NMR (126 MHz, $CDCl_3$) δ ppm 167.7 (d, *J* = 9.7 Hz, C1), 155.1 (d, *J* = 3.1 Hz, C2), 135.8 (ArSi), 134.2 (ArSi), 129.8 (ArSi), 127.8 (ArSi), 117.3 (d, *J* = 187.9 Hz, C3'), 69.5 ($Me_2\underline{C}HOR$), 63.9 (s, C7), 62.1 (d, *J* = 5.6 Hz, $CP(O)O\underline{C}H_2CH_3$), 36.4 (d, *J* = 19.0 Hz, C3), 32.4 (C5), 27.1 ($\underline{Me}_3CSi$), 27.1 (C4), 25.5 (C6), 21.9 ($\underline{Me}_2CHOR$), 19.4 ($Me_3\underline{C}Si$), 16.5 (d, *J* = 6.4 Hz, $CP(O)OCH_2\underline{C}H_3$); ^{31}P NMR (121 MHz, $CDCl_3$, ^{1}H-

decoupled) δ ppm 14.7 (C<u>P</u>(O)OEt); ^{31}P NMR (121 MHz, $CDCl_3$, ^{1}H-coupled) δ ppm 14.7 (sept, *J* = 7.8 Hz, HC<u>P</u>(O)OEt); HRMS, required for $C_{31}H_{48}O_6SiP$ 575.2958, found 575.2933.

(*E*)-Isopropyl 7-hydroxy-2-(diethoxyphosphonomethenyl)heptanoate

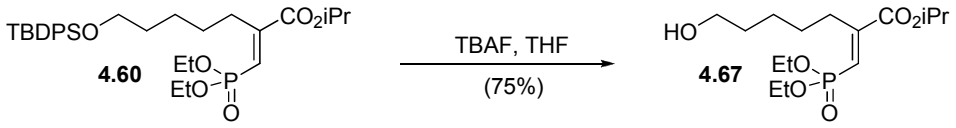

To a stirred solution of silyl compound 4.60 (114.2 mg, 0.200 mmol) in tetrahydrofuran (2 mL) was added a 1M solution of TBAF in tetrahydrofuran (400 μL, 0.40 mmol). After 3.5 hours, the solution was evaporated, and flash chromatography of the residue (100% acetonitrile) afforded alcohol 4.67 as a pale yellow oil (49.8 mg, 75%). R_f (100% acetonitrile): 0.46; ^{1}H NMR (500 MHz, $CDCl_3$) δ ppm 6.52 (dd, *J* = 16.3, 3.3 Hz, 1H, H3'), 5.04 (app sext, *J* = 5.8 Hz, 1H), 4.12-4.02 (m, 4H), 3.57 (dd, *J* = 10.9, 6.0 Hz, 2H, H7), 2.69 (br s, 2H, H3), 2.53 (br s, 1H, C7O<u>H</u>), 1.60-1.51 (m, 2H, H6), 1.51-1.35 (m, 4H, H4, H5), 1.30 (m, 6H, CP(O)OCH$_2$C<u>H</u>$_3$), 1.25 (m, 6H, <u>Me</u>$_2$CHOR); ^{13}C NMR (75 MHz, $CDCl_3$) δ ppm 165.6 (d, *J* = 29.5 Hz, C1), 152.4 (d, *J* = 9.9 Hz, C2), 123.8 (d, *J* = 186.8 Hz, C3'), 69.2 (Me$_2$<u>C</u>HOR), 62.3 (C7), 61.9 (d, *J* = 5.9 Hz, CP(O)O<u>C</u>H$_2$CH$_3$), 32.1 (C6), 29.4 (d, *J* = 6.0 Hz, C3), 28.8 (d, *J* = 2.3 Hz, C4), 25.6 (C5), 21.6 (<u>Me</u>$_2$CHOR), 16.2 (d, *J* = 6.5 Hz, CP(O)OCH$_2$<u>C</u>H$_3$); ^{31}P NMR (121 MHz, $CDCl_3$, ^{1}H-decoupled) δ ppm 15.9 (C<u>P</u>(O)OEt); ^{31}P NMR (121 MHz, $CDCl_3$, ^{1}H-coupled) δ ppm 15.9 (sept, *J* = 8.0 Hz, HC<u>P</u>(O)OEt); HRMS; required for $C_{15}H_{30}O_6P$: 337.1780; found: 337.1783.

(*E*)-Isopropyl 7-(diethoxyphosphoryl)-2-(diethoxyphosphonomethenyl) heptanoate

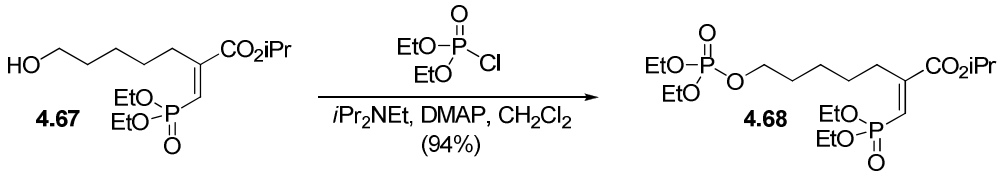

To a stirred solution of alcohol 4.67 (49.8 mg, 0.148 mmol) in dichloromethane (1 mL) was added diisopropylethylamine (52 μL, 0.30 mmol) and DMAP (2.6 mg, 21 μmol). Diethyl chlorophosphate (33 μL, 0.23 mmol) was added, and the mixture was stirred overnight under nitrogen. The reaction was quenched with saturated aqueous sodium bicarbonate solution (1 mL), and stirred vigorously for 30 minutes. The mixture was diluted with dichloromethane (3 mL), the aqueous phase was separated and extracted with further dichloromethane (3x 3 mL). The combined organic extracts were washed with saturated ammonium chloride solution, and the aqueous phase back-extracted with dichloromethane (3 mL). The combined organic phases were dried and evaporated. The residue was purified by flash chromatography (5% methanol/ dichloromethane) to give phosphate ester 4.68 (65.5 mg, 94%). R_f (5% methanol/ dichloromethane): 0.41; ^{1}H NMR (500 MHz, $CDCl_3$) δ ppm 6.5 (d, *J* = 16.3 Hz, 1H, H3'), 5.0 (sept, *J* = 6.1 Hz, 1H, $Me_2C\underline{H}OR$), 4.1-4.0 (app sext, 8H, $CP(O)O\underline{C}H_2CH_3$, $OP(O)O\underline{C}H_2CH_3$), 3.9 (app q, *J* = 6.7 Hz, 2H, H7), 2.66 (t, *J* = 6.5 Hz, 2H, H3), 1.63 (app p, *J* = 7.0 Hz, 2H, H6), 1.5-1.3 (m, 4H, H4, H5), 1.3 (app q, *J* = 6.9 Hz, 12H, $CP(O)OCH_2\underline{C}H_3$, $OP(O)OCH_2\underline{C}H_3$), 1.2 (d, *J* = 6.3 Hz, 6H, $\underline{Me}_2CHOR$); ^{13}C NMR (75 MHz, $CDCl_3$) δ ppm 165.5 (d, *J* = 29.1 Hz, C1), 152.0 (d, *J* = 9.8 Hz, C2), 124.1 (d, *J* = 186.3 Hz, C3'), 69.2 ($Me_2\underline{C}HOR$), 67.3 (d, *J* = 6.0 Hz, C7), 63.5 (d, *J* = 5.9 Hz, $OP(O)O\underline{C}H_2CH_3$), 61.8 (d, *J* = 5.8 Hz, $CP(O)O\underline{C}H_2CH_3$), 29.9 (d, *J* = 7.0 Hz, C6), 29.3 (d, *J* = 5.9 Hz, C3), 28.7 (d, *J* = 2.3 Hz, C4), 25.4 (C5), 21.6 ($\underline{Me}_2CHOR$), 16.3 (d, *J* = 6.4 Hz, $XP(O)OCH_2\underline{C}H_3$), 16.0 (d, *J* = 6.5 Hz, $XP(O)OCH_2\underline{C}H_3$); ^{31}P NMR (121 MHz, $CDCl_3$, ^{1}H-decoupled) δ ppm 15.9 ($CP(O)OCH_2\underline{C}H_3$), -0.4 ($OP(O)OCH_2\underline{C}H_3$), ^{31}P NMR (121 MHz, $CDCl_3$, ^{1}H-coupled) δ ppm 15.9 (app sept, *J* = 8.1 Hz, $CP(O)OCH_2\underline{C}H_3$); -0.4 (app sept, *J* = 7.5 Hz, $OP(O)OCH_2\underline{C}H_3$). HRMS; required for $C_{19}H_{39}O_9P_2$ 473.2069, found 473.2047.

(*E*,*Z*)-Potassium 7-(phosphoryl)-2-(phosphonomethenyl)heptanoate

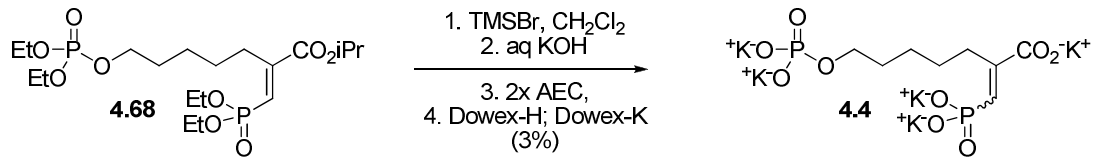

To a solution of ester 4.68 (47.8 mg, 101 μmol) in dichloromethane (1.4 mL) was added trimethylsilyl bromide (135 μL, 1.02 mmol), and the mixture was stirred overnight under nitrogen. The reaction was quenched with methanol (1 mL) and evaporated. The residue was dissolved in 10% w/v potassium hydroxide (2 mL), and stirred vigorously for two hours. The mixture was extracted with dichloromethane (3x 2 mL), and the organic extracts discarded. The solution was passed through a column of Dowex-50X8 H^+-form (10 x 90 mm), and eluted with water (30 mL). The solution was neutralised with 10% w/v sodium hydroxide, and lyophilised. The residue was separated by preparative anion exchange chromatography (two rounds, SourceQ® resin, 4°C, 0 to 1M ammonium bicarbonate gradient elution, product elutes at 250 mM ammonium bicarbonate). The product fractions were lyophilised, redissolved in water (1 mL), passed through a short column of Dowex-50X8 (H^+-form, to quench any residual ammonium bicarbonate) then thorough a column of Dowex-50X8 (K^+-form). The filtrate was lyophilised to give inhibitor 4.4 (1.7 mg, 3%) as a 1:1 mixture of (*E*) and (*Z*) isomers. The bromide side product 4.69 was also isolated from the chromatography step (eluting at 140 mM ammonium bicarbonate) as its tris(ammonium) salt (16.4 mg, 47%).

Inhibitor 4.4: ^{1}H NMR (500 MHz, D_2O, presat) δ ppm 6.58 (d, *J* = 11.9 Hz, 1H, *Z*-H3'), 5.91 (d, *J* = 14.7 Hz, 1H, *E*-H3'), 4.02 (t, *J* = 6.9 Hz, 2H, *Z*-H7'), 3.35 (t, *J* = 6.8 Hz, 2H, *E*-H7'), 2.49 (t, *J* = 6.7 Hz, 2H, H3), 2.43 (t, *J* = 6.1, 2H, H3), 1.75-1.66 (app p, *J* = 6.7 Hz, 2H, *Z*-H6), 1.60-1.51 (app p, *J* = 6.6 Hz, 2H, *E*-H6), 1.32-1.21 (m, 8H, *E*,*Z*-H4, *E*,*Z*-H5); ^{13}C NMR (126 MHz, D_2O, HSQC-DEPT135) δ ppm 137.8 (d, *J* = 142.7 Hz, *Z*-C3'), 127.1 (d, *J* = 160.5 Hz, *E*-C3'), 66.2 (*Z*-C7), 35.3 (*E*-C7), 31.9 (*Z*-C6), 29.8 (C3), 28.4 (C3), 27.9 (*E*-C6), 27.7 (C4s), 25.4 (C5s); ^{31}P NMR (121 MHz, D_2O) δ ppm 9.9 (*Z*- C3'PO_3), 7.3 (*Z*- C3'$\underline{P}O_3$), -3.7 (C7O$\underline{P}O_3$), -4.4 (C7O$\underline{P}O_3$).

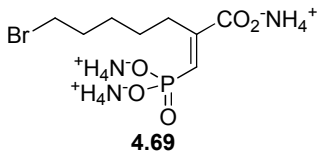

4.69

Bromide 4.69: ^{1}H NMR (500 MHz, D_2O) δ ppm 6.55 (d, *J* = 14.7 Hz, 1H, *Z*-H3'), 3.40 (t, *J* = 6.8 Hz, 2H, H7), 2.51 (t, *J* = 5.8 Hz, 2H, H3), 1.83-1.71 (app p, *J* = 6.5 Hz, 2H, H6), 1.39-1.34 (m, 4H, H4, H5); ^{13}C NMR (126 MHz, D_2O) δ ppm 172.2 (d,

J = 25.6 Hz, C1), 146.8 (d, *J* = 6.5 Hz, C2), 131.5 (d, *J* = 172.6 Hz, C3'), 35.2 (C7), 32.0 (C6), 29.1 (d, *J* = 6.2 Hz, C3), 27.6 (d, *J* = 2.1 Hz, C4), 27.5 (C5); ^{31}P NMR (121 MHz, D_2O) δ ppm 9.5 (*Z*- C3'PO_3);. HRMS (ESI, negative ion, 20% AcOH matrix) required for $C_8H_{13}O_5BrP^-$ 298.9684, found 298.9687.

References

1. Abell, C., Enzymology and molecular biology of the shikimate pathway. *Comprehensive Natural Products Chemistry* **1999,** 1, 573-607.
2. Dubeler, A.; Krastel, P.; Floss, H. G.; Zeeck, A., Biosynthesis of the antibiotic echinosporin by a novel branch of the shikimate pathway. *Eur. J. Org. Chem.* **2002**, (6), 983-987.
3. Kolappan, S.; Zwahlen, J.; Zhou, R.; Truglio, J. J.; Tonge, P. J.; Kisker, C., Lysine 190 is the catalytic base in MenF, the menaquinone-specific isochorismate synthase from *Escherichia coli*: Implications for an enzyme family. *Biochemistry* **2007,** 46, (4), 946-953.
4. Dahm, C.; Muller, R.; Schulte, G.; Schmidt, K.; Leistner, E., The role of isochorismate hydroxymutase genes entC and menF in enterobactin and menaquinone biosynthesis in *Escherichia coli*. *Biochimica et Biophysica Acta, General Subjects* **1998,** 1425, (2), 377-386.
5. Roberts, C. W.; Roberts, F.; Lyons, R. E.; Kirisits, M. J.; Mui, E. J.; Finnerty, J.; Johnson, J. J.; Ferguson, D. J. P.; Coggins, J. R.; Krell, T.; Coombs, G. H.; Milhous, W. K.; Kyle, D. E.; Tzipori, S.; Barnwell, J.; Dame, J. B.; Carlton, J.; McLeod, R., The shikimate pathway and its branches in apicomplexan parasites. *J. Infect. Dis.* **2002,** 185, (Suppl. 1), S25-S36.
6. Coggins, J. R.; Abell, C.; Evans, L. B.; Frederickson, M.; Robinson, D. A.; Roszak, A. W.; Lapthorn, A. P., Experiences with the shikimate-pathway enzymes as targets for rational drug design. *Biochem. Soc. Trans.* **2003,** 31, (3), 548-552.
7. Ducati, R. G.; Basso, L. A.; Santos, D. S., Mycobacterial shikimate pathway enzymes as targets for drug design. *Curr. Drug Targets* **2007,** 8, (3), 423-435.
8. Sassetti, C. M.; Boyd, D. H.; Rubin, E. J., Genes required for mycobacterial growth defined by high density mutagenesis. *Mol. Microbiol.* **2003,** 48, (1), 77-84.
9. Chandran, S. S.; Yi, J.; Draths, K. M.; Von Daeniken, R.; Weber, W.; Frost, J. W., Phosphoenolpyruvate Availability and the Biosynthesis of Shikimic Acid. *Biotechnol. Prog.* **2003,** 19, (3), 808-814.
10. Abrecht, S.; Harrington, P.; Iding, H.; Karpf, M.; Trussardi, R.; Wirz, B.; Zutter, U., The synthetic development of the anti-influenza neuraminidase inhibitor oseltamivir phosphate (Tamiflu): A challenge for synthesis & process research. *Chimia* **2004,** 58, (9), 621-629.
11. Schonbrunn, E.; Eschenburg, S.; Shuttleworth, W. A.; Schloss, J. V.; Amrhein, N.; Evans, J. N. S.; Kabsch, W., Interaction of the herbicide glyphosate with its target enzyme 5-enolpyruvylshikimate 3-phosphate synthase in atomic detail. *Proc. Natl. Acad. Sci. U. S. A.* **2001,** 98, (4), 1376-1380.
12. Bode, R.; Melo, C.; Birnbaum, D., Enzymological basis for glyphosate action in Candida maltosa. *Biochemie und Physiologie der Pflanzen* **1984,** 179, (9), 775-83.
13. Baerson, S. R.; Rodriguez, D. J.; Tran, M.; Feng, Y.; Biest, N. A.; Dill, G. M., Glyphosate-resistant goosegrass. Identification of a mutation in the target enzyme 5-enolpyruvylshikimate-3-phosphate synthase. *Plant Physiol.* **2002,** 129, (3), 1265-1275.
14. Ogino, T.; Garner, C.; Markley, J. L.; Herrmann, K. M., Biosynthesis of aromatic compounds: carbon-13 NMR spectroscopy of whole *Escherichia coli* cells. *Proc. Natl. Acad. Sci. U. S. A.* **1982,** 79, (19), 5828-32.

15. DeLeo, A. B.; Sprinson, D. B., Mechanism of 3-deoxy-D-*arabino*heptulosonate-7-phosphate (DAHP) synthetase. *Biochem. Biophys. Res. Commun.* **1968,** 32, (5), 873-7.
16. Stephens, C. M.; Bauerle, R., Analysis of the metal requirement of 3-deoxy-D-arabino-heptulosonate-7-phosphate synthase from *Escherichia coli*. *J. Biol. Chem.* **1991,** 266, (31), 20810-17.
17. Webby, C. J.; Baker, H. M.; Lott, J. S.; Baker, E. N.; Parker, E. J., The Structure of 3-Deoxy-D-*arabino*-heptulosonate 7-phosphate Synthase from *Mycobacterium tuberculosis* Reveals a Common Catalytic Scaffold and Ancestry for Type I and Type II Enzymes. *J. Mol. Biol.* **2005,** 354, (4), 927-939.
18. Webby, C. J.; Patchett, M. L.; Parker, E. J., Characterization of a recombinant type II 3-deoxy-D-*arabino*-heptulosonate-7-phosphate synthase from *Helicobacter pylori*. *Biochem. J.* **2005,** 390, (1), 223-230.
19. Schofield, L. R.; Patchett, M. L.; Parker, E. J., Expression, purification, and characterization of 3-deoxy-D-arabino-heptulosonate 7-phosphate synthase from Pyrococcus furiosus. *Protein Expression Purif.* **2004,** 34, (1), 17-27.
20. Wu, J.; Howe, D. L.; Woodard, R. W., Thermotoga maritima 3-Deoxy-D-arabino-heptulosonate 7-Phosphate (DAHP) Synthase: The ancestral eubacterial dahp synthase? *J. Biol. Chem.* **2003,** 278, (30), 27525-27531.
21. Wu, J.; Sheflyan, G. Y.; Woodard, R. W., Bacillus subtilis 3-deoxy-D-arabino-heptulosonate 7-phosphate synthase revisited: resolution of two long-standing enigmas. *Biochem. J.* **2005,** 390, (2), 583-590.
22. Onderka, D. K.; Floss, H. G., Steric course of the chorismate synthetase reaction and the 3-deoxy-D-*arabino*-heptulosonate 7-phosphate (DAHP) synthetase reaction. *J. Am. Chem. Soc.* **1969,** 91, (21), 5894-6.
23. DeLeo, A. B.; Dayan, J.; Sprinson, D. B., Purification and kinetics of tyrosine-sensitive 3-deoxy-D-arabino-heptulosonic acid 7-phosphate synthetase from *Salmonella*. *J. Biol. Chem.* **1973,** 248, (7), 2344-53.
24. Pietersma, A. L. PhD thesis, Massey University, 2007.
25. Shumilin, I. A.; Kretsinger, R. H.; Bauerle, R. H., Crystal structure of phenylalanine-regulated 3-deoxy-D-arabino-heptulosonate-7-phosphate synthase from Escherichia coli. *Structure (London)* **1999,** 7, (7), 865-875.
26. Wagner, T.; Shumilin, I. A.; Bauerle, R.; Kretsinger, R. H., Structure of 3-Deoxy-D-*arabino*-heptulosonate-7-phosphate Synthase from *Escherichia coli*: Comparison of the Mn^{2+}*2-Phosphoglycolate and the Pb^{2+}*2-Phosphoenolpyruvate Complexes and Implications for Catalysis. *J. Mol. Biol.* **2000,** 301, (2), 389-399.
27. Shumilin Igor, A.; Bauerle, R.; Kretsinger Robert, H., The high-resolution structure of 3-deoxy-D-arabino-heptulosonate-7-phosphate synthase reveals a twist in the plane of bound phosphoenolpyruvate. *Biochemistry* **2003,** 42, (13), 3766-76.
28. Shumilin, I. A.; Bauerle, R.; Wu, J.; Woodard, R. W.; Kretsinger, R. H., Crystal structure of the reaction complex of 3-deoxy-D-arabino-heptulosonate-7-phosphate synthase from Thermotoga maritima refines the catalytic mechanism and indicates a new mechanism of allosteric regulation. *J. Mol. Biol.* **2004,** 341, (2), 455-466.
29. Schofield, L. R.; Anderson, B. F.; Patchett, M. L.; Norris, G. E.; Jameson, G. B.; Parker, E. J., Substrate Ambiguity and Crystal Structure of *Pyrococcus furiosus* 3-Deoxy-D-*arabino*-heptulosonate-7-phosphate Synthase: An Ancestral 3-Deoxyald-2-ulosonate-phosphate Synthase? *Biochemistry* **2005,** 44, (36), 11950-11962.
30. Wang, J.; Duewel, H. S.; Woodard, R. W.; Gatti, D. L., Structures of *Aquifex aeolicus* KDO8P Synthase in Complex with R5P and PEP, and with a Bisubstrate

Inhibitor: Role of Active Site Water in Catalysis. *Biochemistry* **2001,** 40, (51), 15676-15683.
31. Sundaram, A. K.; Woodard, R. W., Probing the Stereochemistry of *E. coli* 3-Deoxy-D-*arabino*-heptulosonate 7-Phosphate Synthase (Phenylalanine-Sensitive)-Catalyzed Synthesis of KDO 8-P Analogues. *J. Org. Chem.* **2000,** 65, (19), 5891-5897.
32. Palomo, C.; Oiarbide, M.; Garcia, J. M., The aldol addition reaction: an old transformation at constant rebirth. *Chem.--Eur. J.* **2002,** 8, (1), 36-44.
33. Evans, D. A.; Tregay, S. W.; Burgey, C. S.; Paras, N. A.; Vojkovsky, T., C2-Symmetric Copper(II) Complexes as Chiral Lewis Acids. Catalytic Enantioselective Carbonyl-Ene Reactions with Glyoxylate and Pyruvate Esters. *J. Am. Chem. Soc.* **2000,** 122, (33), 7936-7943.
34. Du, S.; Plat, D.; Belakhov, V.; Baasov, T., First Nonenzymic Synthesis of Kdo8P through a Mechanism Similar to That Suggested for the Enzyme Kdo8P Synthase. *J. Org. Chem.* **1997,** 62, (4), 794-804.
35. Walker, G. E.; Dunbar, B.; Hunter, I. S.; Nimmo, H. G.; Coggins, J. R., Evidence for a novel class of microbial 3-deoxy-D-*arabino*-heptulosonate-7-phosphate synthase in *Streptomyces coelicolor* A3(2), *Streptomyces rimosus* and *Neurospora crassa*. *Microbiology (Reading, U. K.)* **1996,** 142, (8), 1973-1982.
36. Jensen, R. A.; Xie, G.; Calhoun, D. H.; Bonner, C. A., The correct phylogenetic relationship of KdsA (3-deoxy-D-manno-octalosonate 8-phosphate synthase) with one of two independently evolved classes of AroA (3-deoxy-D-arabino-heptulosonate 7-phosphate synthase). *J. Mol. Evol.* **2002,** 54, (3), 416-423.
37. Wierenga, R. K., The TIM-barrel fold: a versatile framework for efficient enzymes. *FEBS Lett.* **2001,** 492, (3), 193-198.
38. Shumilin, I., A.; Bauerle, R.; Kretsinger Robert, H., The high-resolution structure of 3-deoxy-D-*arabino*-heptulosonate-7-phosphate synthase reveals a twist in the plane of bound phosphoenolpyruvate. *Biochemistry* **2003,** 42, (13), 3766-76.
39. Ahn, M.; Pietersma, A. L.; Schofield, L. R.; Parker, E. J., Mechanistic divergence of two closely related aldol-like enzyme-catalysed reactions. *Org. Biomol. Chem.* **2005,** 3, (22), 4046-4049.
40. Konig, V.; Pfeil, A.; Braus, G. H.; Schneider, T. R., Substrate and Metal Complexes of 3-Deoxy-D-*arabino*-heptulosonate-7-phosphate Synthase from *Saccharomyces cerevisiae* Provide New Insights into the Catalytic Mechanism. *J. Mol. Biol.* **2004,** 337, (3), 675-690.
41. Buergi, H. B.; Dunitz, J. D.; Lehn, J. M.; Wipff, G., Stereochemistry of reaction paths at carbonyl centers. *Tetrahedron* **1974,** 30, (12), 1563-72.
42. Kona, F.; Xu, X.; Martin, P.; Kuzmic, P.; Gatti, D. L., Structural and Mechanistic Changes along an Engineered Path from Metallo to Nonmetallo 3-Deoxy-D-*manno*-octulosonate 8-Phosphate Synthases. *Biochemistry* **2007,** 46, (15), 4532-4544.
43. Li, Y.; Evans, J. N. S., The hard-soft acid-base principle in enzymic catalysis: dual reactivity of phosphoenolpyruvate. *Proc. Natl. Acad. Sci. U. S. A.* **1996,** 93, (10), 4612-4616.
44. Keen, K.; Parker, E. J., *Personal communication*.
45. Williamson, R. M.; Pietersma, A. L.; Jameson, G. B.; Parker, E. J., Stereospecific deuteration of 2-deoxyerythrose 4-phosphate using 3-deoxy-D-arabino-heptulosonate 7-phosphate synthase. *Bioorg. Med. Chem. Lett.* **2005,** 15, (9), 2339-2342.

46. Bondinell, W. E.; Vnek, J.; Knowles, P. F.; Sprecher, M.; Sprinson, D. B., Mechanism of 5-enolpyruvylshikimate 3-phosphate synthetase. *J. Biol. Chem.* **1971,** 246, (20), 6191-6.
47. Eschenburg, S.; Kabsch, W.; Healy, M. L.; Schoenbrunn, E., A New View of the Mechanisms of UDP-N-Acetylglucosamine Enolpyruvyl Transferase (MurA) and 5-Enolpyruvylshikimate-3-phosphate Synthase (AroA) Derived from X-ray Structures of Their Tetrahedral Reaction Intermediate States. *J. Biol. Chem.* **2003,** 278, (49), 49215-49222.
48. Hedstrom, L.; Abeles, R., 3-Deoxy-D-manno-octulosonate-8-phosphate synthase catalyzes the carbon-oxygen bond cleavage of phosphoenolpyruvate. *Biochem. Biophys. Res. Commun.* **1988,** 157, (2), 816-20.
49. Sundaram, A. K.; Pitts, L.; Muhammad, K.; Wu, J.; Betenbaugh, M.; Woodard, R. W.; Vann, W. F., Characterization of N-acetylneuraminic acid synthase isoenzyme 1 from *Campylobacter jejuni*. *Biochem. J.* **2004,** 383, (1), 83-89.
50. Bravo, I. G.; Garcia-Vallve, S.; Romeu, A.; Reglero, A., Prokaryotic origin of cytidylyltransferases and α-ketoacid synthases. *Trends Microbiol.* **2004,** 12, (3), 120-128.
51. Gunawan, J.; Simard, D.; Gilbert, M.; Lovering, A. L.; Wakarchuk, W. W.; Tanner, M. E.; Strynadka, N. C. J., Structural and Mechanistic Analysis of Sialic Acid Synthase NeuB from *Neisseria meningitidis* in Complex with Mn^{2+}, Phosphoenolpyruvate, and N-Acetylmannosaminitol. *J. Biol. Chem.* **2005,** 280, (5), 3555-3563.
52. Duewel, H. S.; Woodard, R. W., A metal bridge between two enzyme families. 3-Deoxy-D-*manno*-octulosonate-8-phosphate synthase from *Aquifex aeolicus* requires a divalent metal for activity. *J. Biol. Chem.* **2000,** 275, (30), 22824-22831.
53. Li, J.; Wu, J.; Fleischhacker, A. S.; Woodard, R. W., Conversion of *Aquifex aeolicus* 3-Deoxy-D-manno-octulosonate 8-Phosphate Synthase, a Metalloenzyme, into a Nonmetalloenzyme. *J. Am. Chem. Soc.* **2004,** 126, (24), 7448-7449.
54. Shulami, S.; Furdui, C.; Adir, N.; Shoham, Y.; Anderson, K. S.; Baasov, T., A Reciprocal Single Mutation Affects the Metal Requirement of 3-Deoxy-D-manno-2-octulosonate-8-phosphate (KDO8P) Synthases from *Aquifex pyrophilus* and *Escherichia coli*. *J. Biol. Chem.* **2004,** 279, (43), 45110-45120.
55. Oliynyk, Z.; Briseno-Roa, L.; Janowitz, T.; Sondergeld, P.; Fersht, A. R., Designing a metal-binding site in the scaffold of *Escherichia coli* KDO8PS. *Protein Eng., Des. Sel.* **2004,** 17, (4), 383-390.
56. Duewel, H. S.; Radaev, S.; Wang, J.; Woodard, R. W.; Gatti, D. L., Substrate and metal complexes of 3-deoxy-D-manno-octulosonate-8-phosphate synthase from *Aquifex aeolicus* at 1.9-angstrom resolution. Implications for the condensation mechanism. *J. Biol. Chem.* **2001,** 276, (11), 8393-8402.
57. Kohen, A.; Jakob, A.; Baasov, T., Mechanistic studies of 3-deoxy-D-manno-2-octulosonate-8-phosphate synthase from *Escherichia coli*. *Eur. J. Biochem.* **1992,** 208, (2), 443-9.
58. Li, Z.; Sau, A. K.; Shen, S.; Whitehouse, C.; Baasov, T.; Anderson, K. S., A Snapshot of Enzyme Catalysis Using Electrospray Ionization Mass Spectrometry. *J. Am. Chem. Soc.* **2003,** 125, (33), 9938-9939.
59. Liang, P.-H.; Kohen, A.; Baasov, T.; Anderson, K. S., Catalytic mechanism of Kdo8P synthase. Pre-steady-state kinetic analysis using rapid chemical quench flow methods. *Bioorg. Med. Chem. Lett.* **1997,** 7, (19), 2463-2468.
60. Li, Z.; Sau, A. K.; Furdui, C. M.; Anderson, K. S., Probing the role of tightly bound phosphoenolpyruvate in *Escherichia coli* 3-deoxy-D-*manno*-octulosonate 8-

phosphate synthase catalysis using quantitative time-resolved electrospray ionization mass spectrometry in the millisecond time range. *Anal. Biochem.* **2005,** 343, (1), 35-47.
61. Staub, M.; Denes, G., Kinetic study on the inactivation of 3-deoxy-D-*arabino*-heptulosonate-7-phosphate synthase by bromopyruvate. *Biochimica et Biophysica Acta, Enzymology* **1967,** 139, (2), 519-21.
62. Rubin, J. L.; Gaines, C. G.; Jensen, R. A., Enzymological basis for herbicidal action of glyphosate. *Plant Physiol.* **1982,** 70, (3), 833-9.
63. Ganson, R. J.; Jensen, R. A., The essential role of cobalt in the inhibition of the cytosolic isozyme of 3-deoxy-D-*arabino*-heptulosonate-7-phosphate synthase from *Nicotiana silvestris* by glyphosate. *Arch. Biochem. Biophys.* **1988,** 260, (1), 85-93.
64. Forlani, G.; Lejczak, B.; Kafarski, P., The herbicidally active compound *N*-2-(6-methylpyridyl)aminomethylenebisphosphonic acid inhibits *in vivo* aromatic biosynthesis. *J. Plant Growth Regul.* **1999,** 18, (2), 73-79.
65. Cromartie, T. H.; Fisher, K. J.; Grossman, J. N., The Discovery of a Novel Site of Action for Herbicidal Bisphosphonates. *Pestic. Biochem. Physiol.* **1999,** 63, (2), 114-126.
66. Grison, C.; Petek, S.; Finance, C.; Coutrot, P., Synthesis and antibacterial activity of mechanism-based inhibitors of KDO8P synthase and DAH7P synthase. *Carbohydr. Res.* **2005,** 340, (4), 529-537.
67. Sheffer-Dee-Noor, S.; Belakhov, V.; Baasov, T., Insight into the catalytic mechanism of KDO8P synthase. Synthesis and evaluation of the isosteric phosphonate mimic of the putative cyclic intermediate. *Bioorg. Med. Chem. Lett.* **1993,** 3, (8), 1583-8.
68. Xu, X.; Wang, J.; Grison, C.; Petek, S.; Coutrot, P.; Birck, M. R.; Woodard, R. W.; Gatti, D. L., Structure-based design of novel inhibitors of 3-deoxy-D-*manno*-octulosonate 8-phosphate synthase. *Drug Des. Discovery* **2003,** 18, (2-3), 91-99.
69. Du, S.; Faiger, H.; Belakhov, V.; Baasov, T., Towards the development of novel antibiotics: synthesis and evaluation of a mechanism-based inhibitor of Kdo8P synthase. *Bioorg. Med. Chem.* **1999,** 7, (12), 2671-2682.
70. Belakhov, V.; Dovgolevsky, E.; Rabkin, E.; Shulami, S.; Shoham, Y.; Baasov, T., Synthesis and evaluation of a mechanism-based inhibitor of KDO8P synthase. *Carbohydr. Res.* **2004,** 339, (2), 385-392.
71. Asojo, O.; Friedman, J.; Adir, N.; Belakhov, V.; Shoham, Y.; Baasov, T., Crystal Structures of KDOP Synthase in Its Binary Complexes with the Substrate Phosphoenolpyruvate and with a Mechanism-Based Inhibitor. *Biochemistry* **2001,** 40, (21), 6326-6334.
72. Singh, V.; Evans, G. B.; Lenz, D. H.; Mason, J. M.; Clinch, K.; Mee, S.; Painter, G. F.; Tyler, P. C.; Furneaux, R. H.; Lee, J. E.; Howell, P. L.; Schramm, V. L., Femtomolar Transition State Analogue Inhibitors of 5'-Methylthioadenosine/S-Adenosylhomocysteine Nucleosidase from *Escherichia coli*. *J. Biol. Chem.* **2005,** 280, (18), 18265-18273.
73. White, J. D.; Jensen, M. S., Cyclopropane-Containing Eicosanoids of Marine Origin. Biomimetic Synthesis of Constanolactones A and B from the Alga Constantinea simplex. *J. Am. Chem. Soc.* **1995,** 117, (23), 6224-33.
74. Koelln, O.; Redlich, H.; Frank, H., Trimethylenedithioacetals of carbohydrates; Part 2. D-Arabinose, D-glucose, and D-mannose propane-1,3-diyldithioacetals and their isopropylidene derivatives. *Synthesis* **1995**, (11), 1383-8.

75. Burghardt, T. E., Developments in the deprotection of thioacetals. *Journal of Sulfur Chemistry* **2005,** 26, (4-5), 411-427.
76. Greene, T. W.; Wuts, P. G. M., *Protective Groups in Organic Synthesis*. 3rd ed.; John Wiley and Sons: 1999.
77. Texier-Boullet, F.; Foucaud, A., Synthesis of 1-hydroxyalkanephosphonic esters on alumina. *Synthesis* **1982**, (11), 916.
78. Kluge, A. F., Diethyl [[(2-tetrahydropyranyl)oxy]methyl]phosphonate. *Org. Synth.* **1986,** 64, 80-4.
79. Creary, X.; Underiner, T. L., Stabilization demands of diethyl phosphonate substituted carbocations as revealed by substituent effects. *J. Org. Chem.* **1985,** 50, (12), 2165-70.
80. Mohri, K.; Suzuki, K.; Usui, M.; Isobe, K.; Tsuda, Y., A convenient synthesis of tertiary amines by alkylation of secondary amines with alkyl halides in the presence of potassium hydride and triethylamine. *Chem. Pharm. Bull.* **1995,** 43, (1), 159-61.
81. Fadel, A.; Yefsah, R.; Salaun, J., Anhydrous iron(III) chloride dispersed on silica gel. III. A convenient and mild reagent for deacetalization in dry medium. *Synthesis* **1987**, (1), 37-40.
82. Vijayasaradhi, S.; Singh, J.; Singh Aidhen, I., An efficient, selective hydrolysis of terminal isopropylidene acetal protection by $Zn(NO_3)_2.6H_2O$ in acetonitrile. *Synlett* **2000**, (1), 110-112.
83. Xiao, X.; Bai, D., An efficient and selective method for hydrolysis of acetonides. *Synlett* **2001**, (4), 535-537.
84. Wessel, H. P.; Iversen, T.; Bundle, D. R., Acid-catalyzed benzylation and allylation by alkyl trichloroacetimidates. *J. Chem. Soc., Perkin Trans. 1* **1985**, (11), 2247-50.
85. Lanzetta, P. A.; Alvarez, L. J.; Reinach, P. S.; Candia, O. A., An improved assay for nanomole amounts of inorganic phosphate. *Anal. Biochem.* **1979,** 100, (1), 95-7.
86. Morrison, J. F., The slow-binding and slow, tight-binding inhibition of enzyme-catalyzed reactions. *Trends Biochem. Sci.* **1982,** 7, (3), 102-5.
87. Madsen, H. E. L.; Christensen, H. H.; Gottlieb-Petersen, C., Stability constants of copper(II), zinc, manganese(II), calcium, and magnesium complexes of N-(phosphonomethyl)glycine (glyphosate). *Acta Chem. Scand., Ser. A* **1978,** A32, (1), 79-83.
88. Glass, R. L., Metal complex formation by glyphosate. *J. Agric. Food Chem.* **1984,** 32, (6), 1249-53.
89. Nowak, T.; Mildvan, A. S., Stereoselective interactions of phosphoenolpyruvate analogs with phosphoenolpyruvate-utilizing enzymes. *J. Biol. Chem.* **1970,** 245, (22), 6057-64.
90. Lineweaver, H.; Burk, D., Determination of enzyme dissociation constants. *J. Am. Chem. Soc.* **1934,** 56, 658-66.
91. O'Leary, M. H.; DeGooyer, W. J.; Dougherty, T. M.; Anderson, V., 1-Hydroxycyclopropane carboxylic acid phosphate: a potent inhibitor of enzymes metabolizing phosphoenolpyruvate. *Biochem. Biophys. Res. Commun.* **1981,** 100, (3), 1320-5.
92. Kulinkovich, O. G., The Chemistry of Cyclopropanols. *Chem. Rev. (Washington, DC, U. S.)* **2003,** 103, (7), 2597-2632.
93. Wiberg, K. B., Bent Bonds in Organic Compounds. *Acc. Chem. Res.* **1996,** 29, (5), 229-34.
94. Cumming, H. MSc thesis, University of Canterbury, 2007.

95. Parker, E. J. PhD thesis, University of Cambridge.
96. Thompson, S. K.; Heathcock, C. H., Effect of cation, temperature, and solvent on the stereoselectivity of the Horner-Emmons reaction of trimethyl phosphonoacetate with aldehydes. *J. Org. Chem.* **1990,** 55, (10), 3386-8.
97. Blanchette, M. A.; Choy, W.; Davis, J. T.; Essenfeld, A. P.; Masamune, S.; Roush, W. R.; Sakai, T., Horner-Wadsworth-Emmons reaction: use of lithium chloride and an amine for base-sensitive compounds. *Tetrahedron Lett.* **1984,** 25, (21), 2183-6.
98. Berger, S.; Braun, S., *200 and More NMR Experiments*. 2nd ed.; Wiley-VCH: 2004.
99. Romanenko, V. D.; Kukhar, V. P., Fluorinated Phosphonates: Synthesis and Biomedical Application. *Chem. Rev. (Washington, DC, U. S.)* **2006,** 106, (9), 3868-3935.
100. Kumadaki, I., Steric effect of a trifluoromethyl group based on the results of ene reaction of trifluoromethyl carbonyl compounds. *Rev. Heteroat. Chem.* **1993,** 9, 181-204.
101. Wirsching, P.; O'Leary, M. H., (*E*)-3-Cyanophosphoenolpyruvate, a new inhibitor of phosphoenolpyruvate-dependent enzymes. *Biochemistry* **1985,** 24, (26), 7602-6.
102. Durst, H. D., Crown ether catalysis. "Naked" anions as reactive intermediates in the synthesis of phenacyl esters. *Tetrahedron Lett.* **1974**, (28), 2421-4.
103. Cymerman Craig, J.; Bergenthal, M. D.; Fleming, I.; Harley-Mason, J., Synthesis of alkynes from enol esters. *Angew. Chem., Int. Ed. Engl.* **1969,** 8, (6), 429-37.
104. Peliska, J. A.; O'Leary, M. H., Sulfuryl transfer catalyzed by pyruvate kinase. *Biochemistry* **1989,** 28, (4), 1604-11.
105. Parker, E. J.; Bulloch, E. M. M.; Jameson, G. B.; Abell, C., Substrate Deactivation of Phenylalanine-Sensitive 3-Deoxy-D-arabino-heptulosonate 7-Phosphate Synthase by Erythrose 4-Phosphate. *Biochemistry* **2001,** 40, (49), 14821-14828.
106. Skarzynski, T.; Mistry, A.; Wonacott, A.; Hutchinson, S. E.; Kelly, V. A.; Duncan, K., Structure of UDP-N-acetylglucosamine enolpyruvyl transferase, and enzyme essential for the synthesis of bacterial peptidoglycan, complexed with substrate UDP-N-acetylglucosamine and the drug fosfomycin. *Structure (London)* **1996,** 4, (12), 1465-1474.
107. Sperry, J. B.; Wright, D. L., Furans, thiophenes and related heterocycles in drug discovery. *Curr. Opin. Drug Discovery Dev.* **2005,** 8, (6), 723-740.
108. Okuhara, M.; Kuroda, Y.; Goto, T.; Okamoto, M.; Terano, H.; Kohsaka, M.; Aoki, H.; Imanaka, H., Studies on new phosphonic acid antibiotics. III. Isolation and characterization of FR-31564, FR-32863 and FR-33289. *J. Antibiot.* **1980,** 33, (1), 24-8.
109. Mine, Y.; Kamimura, T.; Nonoyama, S.; Nishida, M.; Goto, S.; Kuwahara, S., *In vitro* and *in vivo* antibacterial activities of FR-31564, a new phosphonic acid antibiotic. *J. Antibiot.* **1980,** 33, (1), 36-43.
110. Rohmer, M.; Seemann, M.; Horbach, S.; Bringer-Meyer, S.; Sahm, H., Glyceraldehyde 3-phosphate and pyruvate as precursors of isoprenic units in an alternative non-mevalonate pathway for terpenoid biosynthesis. *J. Am. Chem. Soc.* **1996,** 118, (11), 2564-6.

111. Eisenreich, W.; Bacher, A.; Arigoni, D.; Rohdich, F., Biosynthesis of isoprenoids via the non-mevalonate pathway. *Cell. Mol. Life Sci.* **2004,** 61, (12), 1401-1426.
112. Kuzuyama, T.; Shimizu, T.; Takahashi, S.; Seto, H., Fosmidomycin, a specific inhibitor of 1-deoxy-D-xylulose 5-phosphate reductoisomerase in the nonmevalonate pathway for terpenoid biosynthesis. *Tetrahedron Lett.* **1998,** 39, (43), 7913-7916.
113. Koppisch, A. T.; Fox, D. T.; Blagg, B. S. J.; Poulter, C. D., E. coli MEP synthase: Steady-state kinetic analysis and substrate binding. *Biochemistry* **2002,** 41, (1), 236-243.
114. Yajima, S.; Hara, K.; Iino, D.; Sasaki, Y.; Kuzuyama, T.; Ohsawa, K.; Seto, H., Structure of 1-deoxy-D-xylulose 5-phosphate reductoisomerase in a quaternary complex with a magnesium ion, NADPH and the antimalarial drug fosmidomycin. *Acta Crystallogr., Sect. F: Struct. Biol. Cryst. Comm.* **2007,** F63, (6), 466-470.
115. Wong, U.; Cox, R. J., The chemical mechanism of D-1-deoxyxylulose-5-phosphate reductoisomerase from *Escherichia coli*. *Angew. Chem., Int. Ed.* **2007,** 46, (26), 4926-4929.
116. Jomaa, H.; Wiesner, J.; Sanderbrand, S.; Altincicek, B.; Weidemeyer, C.; Hintz, M.; Turbachova, I.; Eberl, M.; Zeidler, J.; Lichtenthaler, H. K.; Soldati, D.; Beck, E., Inhibitors of the nonmevalonate pathway of isoprenoid biosynthesis as antimalarial drugs. *Science (Washington, D. C.)* **1999,** 285, (5433), 1573-1576.
117. Roberts, F.; Roberts, C. W.; Johnson, J. J.; Kyle, D. E.; Krell, T.; Coggins, J. R.; Coombs, G. H.; Milhous, W. K.; Tzipori, S.; Ferguson, D. J. P.; Chakrabarti, D.; McLeod, R., Evidence for the shikimate pathway in apicomplexan parasites. *Nature (London)* **1998,** 393, (6687), 801-805.
118. Mammen, M.; Chio, S.-K.; Whitesides, G. M., Polyvalent interactions in biological systems: implications for design and use of multivalent ligands and inhibitors. *Angew. Chem., Int. Ed.* **1998,** 37, (20), 2755-2794.
119. Chatterjee, A. K.; Choi, T.-L.; Sanders, D. P.; Grubbs, R. H., A General Model for Selectivity in Olefin Cross Metathesis. *J. Am. Chem. Soc.* **2003,** 125, (37), 11360-11370.
120. Scholl, M.; Ding, S.; Lee, C. W.; Grubbs, R. H., Synthesis and Activity of a New Generation of Ruthenium-Based Olefin Metathesis Catalysts Coordinated with 1,3-Dimesityl-4,5-dihydroimidazol-2-ylidene Ligands. *Org. Lett.* **1999,** 1, (6), 953-956.
121. Ahn, Y. M.; Yang, K.; Georg, G. I., A Convenient Method for the Efficient Removal of Ruthenium Byproducts Generated during Olefin Metathesis Reactions. *Org. Lett.* **2001,** 3, (9), 1411-1413.
122. Cossy, J.; BouzBouz, S.; Hoveyda, A. H., Cross-metathesis reaction. Generation of highly functionalized olefins from unsaturated alcohols. *J. Organomet. Chem.* **2001,** 624, (1-2), 327-332.
123. Mattes, H.; Benezra, C., Double-headed haptens with pyrocatechol (poison ivy-like) and methylene lactone functional groups: a search for skin-tolerance inducers. *J. Med. Chem.* **1987,** 30, (1), 165-8.
124. Reisch, J.; Kamal, G. M.; Gunaherath, B., Natural products chemistry. Part 124. Revised structure and synthesis of a new acridone alkaloid, hallacridone from Ruta graveolens tissue cultures. *J. Chem. Soc., Perkin Trans. 1* **1989**, (5), 1047-51.
125. Csuk, R.; Schroder, C.; Hutter, S.; Mohr, K., Enantioselective Dreiding-Schmidt reactions: asymmetric synthesis and analysis of α-methylene-γ-butyrolactones. *Tetrahedron: Asymmetry* **1997,** 8, (9), 1411-1429.

126. Volonterio, A.; Zanda, M., Domino condensation/aza-Michael/O-> N acyl migration of carbodiimides with activated α,β-unsaturated carboxylic acids to form hydantoins. *Tetrahedron Lett.* **2003,** 44, (47), 8549-8551.
127. Coste, J.; Campagne, J.-M., Esterification of carboxylic acids by BOP or PyBOP. *Tetrahedron Lett.* **1995,** 36, (24), 4253-6.
128. Kendhale, A.; Gonnade, R.; Rajamohanan, P. R.; Sanjayan, G. J., Isotactic N-alkyl acrylamide oligomers assume self-assembled sheet structure: first unequivocal evidence from crystal structures. *Chem. Commun. (Cambridge, U. K.)* **2006**, (26), 2756-2758.
129. Brass, S.; Chan, N.-S.; Gerlach, C.; Luksch, T.; Boettcher, J.; Diederich, W. E., Synthesis of 2,3,4,7-tetrahydro-1H-azepines as privileged ligand scaffolds for the design of aspartic protease inhibitors via a ring-closing metathesis approach. *J. Organomet. Chem.* **2006,** 691, (24-25), 5406-5422.
130. Otera, J.; Yano, T.; Kawabata, A.; Nozaki, H., Novel distannoxane-catalyzed transesterification and a new entry to α,β-unsaturated carboxylic acids. *Tetrahedron Lett.* **1986,** 27, (21), 2383-6.
131. Otera, J.; Ioka, S.; Nozaki, H., Distannoxane as reverse micelle-type catalyst: novel solvent effect on reaction rate of transesterification. *J. Org. Chem.* **1989,** 54, (17), 4013-14.
132. Otera, J.; Danoh, N.; Nozaki, H., Novel template effects of distannoxane catalysts in highly efficient transesterification and esterification. *J. Org. Chem.* **1991,** 56, (18), 5307-11.
133. But, T. Y. S.; Toy, P. H., The Mitsunobu reaction: origin, mechanism, improvements, and applications. *Chemistry--An Asian Journal* **2007,** 2, (11), 1340-1355.
134. Fuerstner, A.; Dierkes, T., Concise Synthesis of (*S*,*S*)-(+)-Dehydrohomoancepsenolide. *Org. Lett.* **2000,** 2, (16), 2463-2465.
135. Michaut, A.; Rodriguez, J., Selective construction of carbocyclic eight-membered rings by ring-closing metathesis of acyclic precursors. *Angew. Chem., Int. Ed.* **2006,** 45, (35), 5740-5750.
136. Schwab, P.; France, M. B.; Ziller, J. W.; Grubbs, R. H., A series of well-defined metathesis catalysts - synthesis of $[RuCl_2(:CHR')(PR_3)_2]$ and their reactions. *Angew. Chem., Int. Ed. Engl.* **1995,** 34, (18), 2039-41.
137. Kingsbury, J. S.; Harrity, J. P. A.; Bonitatebus, P. J., Jr.; Hoveyda, A. H., A Recyclable Ru-Based Metathesis Catalyst. *J. Am. Chem. Soc.* **1999,** 121, (4), 791-799.
138. Garber, S. B.; Kingsbury, J. S.; Gray, B. L.; Hoveyda, A. H., Efficient and Recyclable Monomeric and Dendritic Ru-Based Metathesis Catalysts. *J. Am. Chem. Soc.* **2000,** 122, (34), 8168-8179.
139. Love, J. A.; Morgan, J. P.; Trnka, T. M.; Grubbs, R. H., A practical and highly active ruthenium-based catalyst that effects the cross metathesis of acrylonitrile. *Angew. Chem., Int. Ed.* **2002,** 41, (21), 4035-4037.
140. Fuerstner, A.; Langemann, K., Total Syntheses of (+)-Ricinelaidic Acid Lactone and of (-)-Gloeosporone Based on Transition-Metal-Catalyzed C-C Bond Formations. *J. Am. Chem. Soc.* **1997,** 119, (39), 9130-9136.
141. Krafft, M. E.; Song, E.-H.; Davoile, R. J., Intramolecular Morita-Baylis-Hillman adducts via sequential MBH and ring-closing-metathesis reactions. *Tetrahedron Lett.* **2005,** 46, (37), 6359-6362.
142. Lee, K. Y.; Gowrisankar, S.; Kim, J. N., Baylis-Hillman reaction and chemical transformations of Baylis-Hillman adducts. *Bull. Korean Chem. Soc.* **2005,** 26, (10), 1481-1490.

143. Basavaiah, D.; Pandiraraju, S., Nucleophilic addition of triethyl phosphite to acetates of the Baylis-Hillman adducts: stereoselective synthesis of (E)- and (Z)-allylphosphonates. *Tetrahedron* **1996,** 52, (6), 2261-8.
144. Basavaiah, D.; Rao, K. V.; Reddy, R. J., The Baylis-Hillman reaction: a novel source of attraction, opportunities, and challenges in synthetic chemistry. *Chem. Soc. Rev.* **2007,** 36, (10), 1581-1588.
145. Frigerio, M.; Santagostino, M.; Sputore, S.; Palmisano, G., Oxidation of Alcohols with o-Iodoxybenzoic Acid in DMSO: A New Insight into an Old Hypervalent Iodine Reagent. *J. Org. Chem.* **1995,** 60, (22), 7272-6.
146. Ramachandran, P. V.; Rudd, M. T.; Burghardt, T. E.; Reddy, M. V. R., Vinylalumination for the Synthesis of Functionalized Allyl Alcohols, Vinylepoxides, and α-Alkylidene-β-hydroxy-γ-lactones. *J. Org. Chem.* **2003,** 68, (24), 9310-9316.
147. Tsuda, T.; Yoshida, T.; Saegusa, T., Generation of [α-(alkoxycarbonyl)vinyl]aluminum and aluminum allenolates by the hydroalumination of α,β-acetylenic carbonyl compounds and their reaction with carbonyl compounds. *J. Org. Chem.* **1988,** 53, (5), 1037-40.
148. Clive, D. L. J.; Li, Z.; Yu, M., Intramolecular Conjugate Displacement: A General Route to Hexahydroquinolizines, Hexahydroindolizines, and Related [m,n,0]-Bicyclic Structures with Nitrogen at a Bridgehead. *J. Org. Chem.* **2007,** 72, (15), 5608-5617.
149. Rachon, J.; Goedken, V.; Walborsky, H. M., Rearrangement of a bicyclic [2.2.2] system to a bicyclic [3.2.1] system. Nonclassical ions. *J. Org. Chem.* **1989,** 54, (5), 1006-12.
150. Parrish, J. D.; Shelton, D. R.; Little, R. D., Titanocene(III)-Promoted Reformatskii Additions. *Org. Lett.* **2003,** 5, (20), 3615-3617.
151. Zhu, L.; Wehmeyer, R. M.; Rieke, R. D., The direct formation of functionalized alkyl(aryl)zinc halides by oxidative addition of highly reactive zinc with organic halides and their reactions with acid chlorides, α,β-unsaturated ketones, and allylic, aryl, and vinyl halides. *J. Org. Chem.* **1991,** 56, (4), 1445-53.
152. Fuerstner, A.; Shi, N., Nozaki-Hiyama-Kishi Reactions Catalytic in Chromium. *J. Am. Chem. Soc.* **1996,** 118, (49), 12349-12357.
153. Yu, L.-C.; Helquist, P., b-Amino ester enolate as an acrylate anion equivalent for the synthesis of a-methylene esters, acids, and lactones. *J. Org. Chem.* **1981,** 46, (22), 4536-41.
154. Rouvier, E.; Giacomoni, J. C.; Cambon, A., Amines containing a second functional group. I. Reactivity of primary and secondary amines with activated olefins. *Bull. Soc. Chim. Fr.* **1971**, (5), 1717-23.
155. Khan, A. T.; Ghosh, S.; Choudhury, L. H., A highly efficient synthetic protocol for tetrahydropyranylation/depyranylation of alcohols and phenols. *Eur. J. Org. Chem.* **2005**, (22), 4891-4896.
156. Dess, D. B.; Martin, J. C., Readily accessible 12-I-5 oxidant for the conversion of primary and secondary alcohols to aldehydes and ketones. *J. Org. Chem.* **1983,** 48, (22), 4155-6.
157. Mancuso, A. J.; Huang, S.-L.; Swern, D., Oxidation of long-chain and related alcohols to carbonyls by dimethyl sulfoxide "activated" by oxalyl chloride. *J. Org. Chem.* **1978,** 43, (12), 2480-2.
158. March, J.; Smith, M. B., *March's Advanced Organic Chemistry*. 5th ed.; John Wiley and Sons: 2001.

159. Jones, D. N.; Mundy, D.; Whitehouse, R. D., Steroidal selenoxides diastereoisomeric at selenium; *syn*-elimination, absolute configuration, and optical rotatory dispersion characteristics. *J. Chem. Soc., Chem. Commun.* **1970**, (2), 86-7.
160. Arrica, M. A.; Wirth, T., Fluorinations of α-seleno carboxylic acid derivatives with hypervalent (difluoroiodo)toluene. *Eur. J. Org. Chem.* **2005**, (2), 395-403.
161. Yang, D.; Gao, Q.; Zheng, B.-F.; Zhu, N.-Y., Et_2AlCl-Promoted Asymmetric Phenylseleno Group Transfer Radical Cyclization Reactions of Unsaturated β-Hydroxy Esters. *J. Org. Chem.* **2004,** 69, (25), 8821-8828.
162. Ireland, R. E.; Willard, A. K., Stereoselective generation of ester enolates. *Tetrahedron Lett.* **1975**, (46), 3975-8.
163. Reich, H. J.; Wollowitz, S.; Trend, J. E.; Chow, F.; Wendelborn, D. F., Syn elimination of alkyl selenoxides. Side reactions involving selenenic acids. Structural and solvent effects of rates. *J. Org. Chem.* **1978,** 43, (9), 1697-705.
164. Li, L.-S.; Wu, Y.-L., An efficient method for synthesis of α-keto acid esters from terminal alkynes. *Tetrahedron Lett.* **2002,** 43, (13), 2427-2430.
165. Li, L.-S.; Wu, Y.-L., Recent progress in syntheses of higher 3-deoxy-2-ulosonic acids and their derivatives. *Curr. Org. Chem.* **2003,** 7, (5), 447-475.
166. Liu, K.-G.; Hu, S.-G.; Wu, Y.; Yao, Z.-J.; Wu, Y.-L., A straightforward synthesis of DAH (3-deoxy-D-*arabino*-hept-2-ulosonic acid) and DRH (3-deoxy-D-*ribo*-hept-2-ulosonic acid). *Journal of the Chemical Society, Perkin Transactions 1* **2002**, (16), 1890-1895.
167. Chong, J. M.; Heuft, M. A.; Rabbat, P., Solvent Effects on the Monobromination of α,ω-Diols: A Convenient Preparation of w-Bromoalkanols. *J. Org. Chem.* **2000,** 65, (18), 5837-5838.
168. Romeril, S. P.; Lee, V.; Claridge, T. D. W.; Baldwin, J. E., Synthesis of a possible structure of pyrinodemin A. *Tetrahedron Lett.* **2002,** 43, (2), 327-329.
169. Plet, J. R. H.; Porter, M. J., Synthesis of the bicyclic core of tagetitoxin. *Chem. Commun. (Cambridge, U. K.)* **2006**, (11), 1197-1199.
170. Li, L.-S.; Wu, Y.-L., Synthesis of 3-deoxy-2-ulosonic acid KDO and 4-epi-KDN, a highly efficient approach of 3-C homologation by propargylation and oxidation. *Tetrahedron* **2002,** 58, (44), 9049-9054.
171. Singh, J.; Kissick, T. P.; Mueller, R. H., Improved procedure for the one-step synthesis of α-keto esters. *Org. Prep. Proced. Int.* **1989,** 21, (4), 501-4.
172. Coutrot, P.; Legris, C., Convenient synthesis of α-keto-esters and unsymmetrical 1,2-diketones from carbonyl compounds. *Synthesis* **1975**, (2), 118-20.
173. Coutrot, P.; Grison, C.; Tabyaoui, M.; Czernecki, S.; Valery, J. M., Novel application of alkyl dihaloacetates; chain extension with an α-keto ester unit of carbohydrates. *J. Chem. Soc., Chem. Commun.* **1988**, (23), 1515-16.
174. Coutrot, P.; Grison, C.; Tabyaoui, M.; Tabyaoui, B.; Dumarcay, S., Towards a synthesis of glycidic phosphoenol pyruvic acid derivatives. *Synlett* **1999**, (6), 792-794.
175. Grison, C.; Coutrot, F.; Comoy, C.; Lemilbeau, C.; Coutrot, P., New efficient synthesis of α-hydroxy esters from carbonyl compounds via α-chloroglycidic esters. *Tetrahedron Lett.* **2000,** 41, (34), 6571-6574.
176. Evans, D. A.; Nelson, J. V.; Vogel, E.; Taber, T. R., Stereoselective aldol condensations via boron enolates. *J. Am. Chem. Soc.* **1981,** 103, (11), 3099-111.
177. Friesner, R. A.; Banks, J. L.; Murphy, R. B.; Halgren, T. A.; Klicic, J. J.; Mainz, D. T.; Repasky, M. P.; Knoll, E. H.; Shelley, M.; Perry, J. K.; Shaw, D. E.; Francis, P.; Shenkin, P. S., Glide: A new approach for rapid, accurate docking and

scoring. 1. method and assessment of docking accuracy. *J. Med. Chem.* **2004,** 47, (7), 1739-1749.
178. Lam, P. Y. S.; Jadhav, P. K.; Eyermann, C. J.; Hodge, C. N.; Ru, Y.; Bacheler, L. T.; Meek, O. M. J.; Rayner, M. M., Rational design of potent, bioavailable, nonpeptide cyclic ureas as HIV protease inhibitors. *Science (Washington, DC)* **1994,** 263, (5145), 380-4.
179. Ladbury, J. E., Just add water! The effect of water on the specificity of protein-ligand binding sites and its potential application to drug design. *Chem. Biol.* **1996,** 3, (12), 973-980.
180. Barillari, C.; Taylor, J.; Viner, R.; Essex, J. W., Classification of Water Molecules in Protein Binding Sites. *J. Am. Chem. Soc.* **2007,** 129, (9), 2577-2587.
181. Grison, C.; Coutrot, F.; Coutrot, P., New glycosyl α-hydroxyesters as key intermediates in a convenient route to glycosyl α-aminoester chirons. *Tetrahedron* **2002,** 58, (14), 2735-2741.
182. Bekele, T.; Shah, M. H.; Wolfer, J.; Abraham, C. J.; Weatherwax, A.; Lectka, T., Catalytic, Enantioselective [4 + 2]-Cycloadditions of Ketene Enolates and o-Quinones: Efficient Entry to Chiral, α-Oxygenated Carboxylic Acid Derivatives. *J. Am. Chem. Soc.* **2006,** 128, (6), 1810-1811.
183. Inada, Y.; Sugata, T.; Ozutsumi, K.; Funahashi, S., Solvation Structures and Kinetics of Solvent Exchange Reactions of the Manganese(II) Ion in Six Nitriles As Studied by X-ray Diffraction, EXAFS, and NMR Techniques. *Inorg. Chem.* **1998,** 37, (8), 1886-1891.
184. Farkas, E.; Enyedy, E. A.; Zekany, L.; Deak, G., Interaction between iron(II) and hydroxamic acids: oxidation of iron(II) to iron(III) by desferrioxamine B under anaerobic conditions. *J. Inorg. Biochem.* **2001,** 83, (2-3), 107-114.
185. Devreux, V.; Wiesner, J.; Goeman, J. L.; Van der Eycken, J.; Jomaa, H.; Van Calenbergh, S., Synthesis and biological evaluation of cyclopropyl analogues of fosmidomycin as potent *Plasmodium falciparum* growth inhibitors. *J. Med. Chem.* **2006,** 49, (8), 2656-2660.
186. Auffinger, P.; Hays, F. A.; Westhof, E.; Ho, P. S., Halogen bonds in biological molecules. *Proc. Natl. Acad. Sci. U. S. A.* **2004,** 101, (48), 16789-16794.
187. Chai, C.; Armarego, W. L. F., *Purification of Laboratory Chemicals*. 5th ed.; Butterworth-Heinemann: 2003.
188. Burfield, D. R.; Smithers, R. H., Desiccant efficiency in solvent drying. 3. Dipolar aprotic solvents. *J. Org. Chem.* **1978,** 43, (20), 3966-8.
189. Frigerio, M.; Santagostino, M.; Sputore, S., A user-friendly entry to 2-iodoxybenzoic acid (IBX). *J. Org. Chem.* **1999,** 64, (12), 4537-4538.
190. Ireland, R. E.; Liu, L., An improved procedure for the preparation of the Dess-Martin periodinane. *J. Org. Chem.* **1993,** 58, (10), 2899.
191. Ramarajan, K.; Ramalingam, K.; O'Donnell, D. J.; Berlin, K. D., Ethyl α-(bromomethyl)acrylate. (2-Propenoic acid, 2-(bromomethyl)-, ethyl ester). *Org. Synth.* **1983,** 61, 56-9.
192. Block, P., Jr., Diethyl bis(hydroxymethyl)malonate. *Org. Synth.* **1960,** 40, 27-8.
193. Lin, H.-S.; Paquette, L. A., A convenient method for determining the concentration of Grignard reagents. *Synth. Commun.* **1994,** 24, (17), 2503-6.
194. Ireland, R. E.; Meissner, R. S., Convenient method for the titration of amide base solutions. *J. Org. Chem.* **1991,** 56, (14), 4566-8.
195. Armstrong, R. W.; Teegarden, B. R., Synthesis of a-methyl 1',2'-dideoxycellobioside: a novel C-disaccharide. *J. Org. Chem.* **1992,** 57, (3), 915-22.

196. McDougal, P. G.; Rico, J. G.; Oh, Y. I.; Condon, B. D., A convenient procedure for the monosilylation of symmetric 1,n-diols. *J. Org. Chem.* **1986,** 51, (17), 3388-90.
197. Mann, S.; Carillon, S.; Breyne, O.; Marquet, A., Total synthesis of amiclenomycin, an inhibitor of biotin biosynthesis. *Chem.--Eur. J.* **2002,** 8, (2), 439-450.
198. Nemoto, H.; Shiraki, M.; Fukumoto, K., Novel Access to Neopentyl-Type Halogenated Cyclopentanoids via Olefinic Cyclobutanols. *J. Org. Chem.* **1996,** 61, (4), 1347-53.
199. Barrett, A. G. M.; Flygare, J. A., Triply convergent, stereospecific alkene formation via Peterson olefination. *J. Org. Chem.* **1991,** 56, (2), 638-42.
200. Abbenhuis, R. A. T. M.; Boersma, J.; van Koten, G., Ruthenium-Complex-Catalyzed N-(Cyclo)alkylation of Aromatic Amines with Diols. Selective Synthesis of N-(w-Hydroxyalkyl)anilines of Type PhNH(CH2)nOH and of Some Bioactive Arylpiperazines. *J. Org. Chem.* **1998,** 63, (13), 4282-4290.
201. Qiu, Y.; Li, D., Bifunctional Inhibitors of Mevalonate Kinase and Mevalonate 5-Diphosphate Decarboxylase. *Org. Lett.* **2006,** 8, (6), 1013-1016.
202. Romeril, S. P.; Lee, V.; Baldwin, J. E.; Claridge, T. D. W., On the synthesis of pyrinodemin A. Part 1. The location of the olefin. *Tetrahedron* **2005,** 61, (5), 1127-1140.